MACHINING OF NICKEL BASED SUPERALLOYS USING COATED PCBN TOOLING

by

SARMAD ALI KHAN
M.Sc. Engg., B.Sc. Engg.(Hons)

A thesis submitted to
the University of Birmingham
for the degree of
Doctor of Philosophy (PhD)

School of Mechanical Engineering
College of Engineering and Physical Sciences
University of Birmingham
November 2013

ABSTRACT

Following an extensive literature review on the machinability of nickel based superalloys with particular emphasis on the use of PCBN tooling, experimental work was undertaken in three main phases on the machinability of Inconel 718. Phases 1 and 2 involved optimisation of tool geometry, edge preparation, cutting environment and operating parameters while in Phase 3, a newly developed polycrystalline cubic boron nitride (PCBN) grade and various coating products were evaluated in high speed turning of Inconel 718. The majority of publications involved the use of uncoated and coated carbide tooling however the use of whisker reinforced ceramics was also detailed when roughing at speeds up to ~ 600 m/min. Quoted cutting speeds for carbide tooling were typically 50 - 60 m/min however in some cases this ranged up to 140 m/min. The use of PCBN tools appeared to be limited however when finishing, speeds of between 200 – 300 m/min were detailed with a corresponding tool life of ~ 5 min. Limited information involving the use of TiN coated PCBN for machining Inconel 718 was available.

Phase 1A involved preliminary experimental trials to determine the performance of an off-the-shelf PCBN tool (Amborite DBC 50). Tool life did not exceed 1.63min in any of the trials. Substantial grooving and notching was prevalent at the cutting speed of 150m/min however when cutting speed was increased to 300 and 450 m/min, rapid catastrophic fracture was observed. In Phase 1B, trials were performed to benchmark the machinability of workpiece material sourced from Mitsubishi Heavy Industries (MHI) with Rolls Royce (RR) material when employing approved operating parameters and cutting tools (PCBN/carbide inserts) used by RR in production for turning Inconel 718. Uncoated carbide inserts produced the same level of tool wear when machining the RR and the MHI alloy, therefore it was decided that the MHI workpiece material was suitable for subsequent Phase 1C and 1D experiments.

Phase 1C aimed to perform a wide ranging preliminary investigation of key output measures including tool life, productivity, cutting forces and surface roughness in order to provide baseline data for future in depth trials. A modified L36 Taguchi orthogonal array was used to investigate the effect of tool geometry (Round, C-type), edge preparation (E25, S-type), cutting environment (10bar, 100bar), surface condition (uncoated, TiAlN+TiN), cutting speed (150, 300 and 450 m/min) and feed rate (0.05, 0.10, 0.20 mm/rev). In terms

of productivity, a cutting speed of 300m/min and feed rate of 0.20mm/rev at 100bar fluid pressure was the preferred operating parameter combination. At these operating parameters, C-type inserts removed ~50% more material than corresponding round inserts and were therefore selected for future trials. The coating failed to provide any benefit in terms of tool life. This work was followed by Phase 1D in which the performance of E25 and S-type edge peripheries was evaluated at two different cutting speeds; 300m/min and 450m/min using uncoated C-type inserts both in the new and worn condition when employing 100bar cutting fluid pressure. Higher cutting forces and surface roughness was recorded with S-type geometry, therefore E25 edge preparation was selected for Phase 2 and 3 experimental work.

A bar of Inconel 718 was purchased from Superalloys International Ltd. (SI) USA for Phase 2 and 3 experimental trials involving low and medium concentration PCBN products, which in general provided similar results in terms of tool life. In Phase 2A, the effect of cutting environment, cutting speed and feed rate was assessed in terms of tool life, surface roughness and cutting forces. In terms of productivity, a cutting speed of 300m/min was preferred and workpiece surface roughness (Ra) was <0.70µm over the test duration for the trials performed at a feed rate of 0.15mm/rev. Workpiece surface integrity aspects were evaluated in Phase 2B. No significant workpiece surface damage was observed for the samples machined with new PCBN tools, however grooves, microcracks were recorded in all specimens when employing worn tools. Minimal variation in sub-surface microhardness was recorded with new tools however samples turned with worn inserts showed a rise of up to ~560$HK_{0.025}$ over a depth of 100µm. Grain elongation (15-30µm) in the cutting speed direction was evident. Phase 3A involved experimental trials to evaluate the performance of a recently developed PCBN grade and various coatings on tool life. At a cutting speed of 200m/min, BUE and fracture was observed in all trials and was detrimental to tool life for the TiSiN/TiAlN, AlCrN, CrAlN-3µm, CrAlN-5.5µm coated inserts due to poor edge integrity/coating adhesion. However when cutting speed was increased to 300 and 450m/min, no difference in tool life was recorded irrespective of the insert surface condition. Phase 3B assessed the performance of uncoated and coated inserts on workpiece surface integrity. In terms of workpiece surface damage and microstructure, results were similar to that obtained in Phase 2B. Phase 3C involved the evaluation of PCBN grades and cutting environment on residual stresses, which were compressive (up to - 443MPa) in all samples measured parallel to the feed, while results perpendicular to the feed were predominantly tensile (typically up to 320MPa). The use of worn insert

generated the highest level of sub-surface compressive residual stresses extending to a depth of ~450µm however this was limited to ~140µm when machining with new inserts.

Based on the results obtained in three phases, a cutting speed of 300m/min, feed rate of 0.15mm/rev, cutting fluid pressure of 100bar, C-type tool geometry with E25 edge configuration and CBN 170 PCBN grade was recommended as the preferred operating variables for finishing applications.

ACKNOWLEDGEMENTS

I would like to thank the following people and organisations for their advice and support during this project.

Firstly, I am indebted to my academic supervisors Dr. Sein Leung Soo (Senior Lecturer and Head of Machining Research Group) and Prof. David Keith Aspinwall for their guidance and technical support. I would also like to express my appreciation to Richard Fasham and Andrew Loat (Machining Research Group Technicians) for their assistance with experimental work and material preparation.

Colin Sage, Dr. Gregor Kappmeyer and Dr. Andrew Mantle from Rolls-Royce plc for their technical and industrial support including provision of funding, technical data and workpiece materials.

Michael Fleming, David Pearson and Dr. Rachid M'Saoubi from Seco Tools for financial and product support (inserts) together with technical advice, in particular that relating to residual stress measurement.

Dr. Peter Harden, Dr. Neels Pretorius and Dr. Wayne Leahy of Element Six for project support (financial and PCBN product) together with useful discussions and encouragement.

Dr. Allan White, University of Birmingham Statistician and Dr. Khalid Al-Ghamdi (Honorary Research Fellow) for their invaluable assistance with statistical design and analysis.

Teer Coatings and Balzers for the provision of coating products.

The School of Mechanical Engineering, University of Birmingham for a partial scholarship to undertake the research work together with experimental facilities. Additional thanks are due to my colleagues within the Machining Research Group for their insightful discussions.

I would like to acknowledge the University of Engineering and Technology (UET) Lahore for a Faculty Development Programme Scholarship, which allowed me to undertake the research.

My sincerest gratitude and appreciations are due to Dr. Richard Hood (Lecturer, School of Mechanical Engineering) and Mr Debajyoti Bhaduri (Research Fellow, School of Mechanical Engineering) for sharing their experience and knowledge over the duration of the project.

Last but certainly not least, I wish to express my love and deepest gratitude to my beloved parents, family and friends especially Dr Shafiq Irfan, Dr Shoaib Malik, Muhammad Saleem and Amir Mohammad for their endless encouragement, support, patience and love throughout this work.

TABLE OF CONTENTS

LIST OF FIGURES

LIST OF TABLES

NOMENCLATURE

γ:	Gamma phase
γ′:	Gamma prime precipitate
γ″:	Gamma double prime precipitate
δ:	Delta phase
%:	Percentage
>:	Greater than
<:	Less than
AJA:	Air jet assisted
Al:	Aluminium
Al_2O_3:	Aluminium oxide
AlCrN:	Aluminium chromium nitride
AlTiN:	Aluminium titanium nitride
Alumina:	Aluminium oxide
ANOVA:	Analysis of variance
APB:	Anti-phase boundary energy
bct:	Body central tetragonal
BUE:	Built up edge
cBN:	Cubic boron nitride
Co:	Cobalt
Cr:	Chromium
CrN:	Chromium nitride
CVD:	Chemical vapour deposition
DA:	Direct aged
DoC:	Depth of cut
2D:	Two dimensional
3D:	Three dimensional
EBSD:	Electron backscattered diffraction
EDX:	Energy dispersive X-ray analysis

E6:	Element Six
F:	Feed rate
FCC:	Face centred cubic
FCG:	Fatigue crack growth
FIB:	Focused ion beam
HCF:	High cycle fatigue
HP:	High pressure
HSM:	High speed machining
K_m:	Crater depth
K_t:	Cutting edge distance from the centre line of crater
LCF:	Low cycle fatigue
µLL:	Micro litre lubrication
MHI:	Mitsubishi Heavy Industries
Mo:	Molybdenum
MoN:	Molybdenum nitride
MoS_2:	Molybdenum disulphide
Nb:	Niobium
NbN:	Niobium nitride
NDE:	Non destructive technique
Ni:	Nickel
NJA:	Nitrogen jet assisted
PCBN:	Polycrystalline cubic boron nitride
PCD:	Polycrystalline diamond
PCR:	Percentage contribution
PM:	Powder metallurgy
PVD:	Physical vapour deposition
R^2(Adj):	Adjusted R-square
Re:	Rhenium
Ru:	Ruthenium
RR:	Rolls Royce

SBE:	Stepwise backward elimination
SEM:	Scanning electron microscope
SFE:	Stepwise forward entry
SI:	Superalloys International Ltd.
Ta:	Tantalum
TCP:	Topologically closed packed
Ti:	Titanium
TiAlN:	Titanium aluminium nitride
TiC:	Titanium carbide
TiCN:	Titanium carbon nitride
TiSiN:	Titanium silicon nitride
UTS:	Ultimate tensile strength
Vc:	Cutting speed
VN:	Notch wear
W:	Tungsten
WC:	Tungsten carbide
WL:	White layer
WN:	Tungten nitride
XRD:	X-ray diffraction
YS:	Yield strength

1. INTRODUCTION

1.1 Background to the project

Nickel based superalloys are extensively used for gas turbine applications and account for ~50% of aeroengine weight [1-5]. Figure 1 details materials used in the Rolls Royce Trent 800 engine where nickel based superalloys are employed in the hotter parts such as the combustor and turbine.

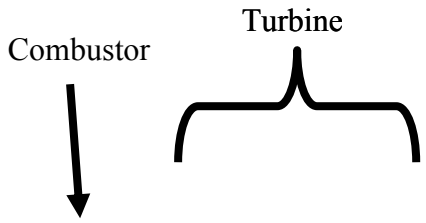

Figure 1: Usage of different materials in a Rolls-Royce Trent 800 aero engine (Courtesy of Rolls-Royce Plc)

With high strength, good hot corrosion and oxidation resistance, mechanical and thermal fatigue resistance, mechanical and thermal shock resistance, nickel based superalloys are ideally suited to high temperature applications. However, they also possess low thermal conductivity (~ 11W/mºC) [3], a greater tendency for built-up-edge (BUE) formation, a strong affinity to react with tool materials, and high localisation of cutting temperatures (≥1000ºC) at the tool tip [2] which results in exceptionally high mechanical and thermal stresses on cutting tools and the possibility of severe work hardening of the workpiece. Therefore these alloys are more demanding in terms of machinability and are

regarded as difficult-to-machine materials. Additionally, excessive tool wear necessitates frequent change in the tooling set up, hence low productivity.

Due to their favourable balance between fracture toughness and thermal shock resistance, carbide cutting tools are the most widely used tool materials for machining nickel based alloys. The ISO K group of carbides and specifically K10/K20 grades are generally recommended at cutting speeds of 20-35 m/min [5]. Therefore material removal rates are quite low and the cost of machining these alloys is very high. Even when employing hard tool coatings such as TiC or TiAlN, cutting speeds are generally limited within the range of 60-140 m/min [6-9]. Alternatives to carbide include ultra-hard PCBN tools and conventional ceramics. Due to the greater susceptibility to notch wear however, oxide ceramics such as Al_2O_3 are not suitable for machining these aero-space alloys. Furthermore, the use of mixed alumina, sialon and silicon carbide (SiC) whisker reinforced ceramics are mostly limited to roughing operations due to their unfavourable effects on surface integrity [5, 10] with cutting speeds up to 600 m/min reported [10].

Polycrystalline cubic boron nitride (PCBN) is an advanced ceramic tool material which appeared in the mid-1970's principally for the machining of hardened steels (turning, milling etc.); it can also be employed to advantage for the finish turning of some nickel based alloys. In terms of market penetration, the use of PCBN has remained small but not least because of the diversity of nickel alloys used and their wide ranging & challenging mechanical/physical properties. Over the last 15 years, the range and variety of PCBN products increased dramatically and the introduction of coated inserts provides greater scope and potential for their use. Significant benefits in terms of tool life and surface roughness have been seen with coated PCBN inserts in the machining of hardened steels and cast iron [11-16]. The key advantage/benefit associated with PCBN tooling is the possibility of enhancing productivity by employing higher cutting speeds i.e. within the range of 300-600 m/min [5]. Compared with publications concerned with machining of hardened steels and cast irons, there are relatively few papers detailing nickel alloy machining using PCBN cutting tools. This suggests that there is considerable scope and potential for a wider evaluation of uncoated/coated PCBN products, grades, tool geometries, edge preparations, and operating parameters (including cutting environments), when turning selected nickel based superalloys.

1.2 Aims and objectives of the project

The overall aim of the project was to investigate the performance of current and prototype uncoated/coated PCBN products for the turning of Inconel 718 and to establish the preferred operating parameters for finishing applications with emphasis on tool life and workpiece surface integrity analysis. Specific objectives were to

- Carry out a comprehensive literature review of previous research and published machinability data on the cutting of nickel based superalloys involving carbide, conventional ceramics and PCBN tooling.
- Survey published literature detailing uncoated and state of the art coated PCBN tooling when turning hardened steels and cast irons.
- Undertake statistically designed turning experiments to benchmark current and prototype uncoated/coated PCBN products for finishing operation and identify preferred tool geometries, edge preparations, cutting environments and operating parameters in terms of tool life, tool wear mechanisms and productivity.
- Investigate the influence of different types of edge preparation and cutting speed on workpiece surface integrity including surface roughness, surface/subsurface damage, microstructure and microhardness.
- Evaluate the performance of various types of cutting environment and cutting parameters on tool life/wear mechanisms and workpiece surface integrity.
- Investigate the effect of different PCBN grades and cutting environments on workpiece residual stress.

1.3 Industrial collaborators and funding

The research was carried out as part of a Doctor of Philosophy (PhD) degree programme. A PhD research studentship was obtained through a scholarship from the University of Engineering and Technology, Lahore, Pakistan together with a partial scholarship from the School of Mechanical Engineering, University of Birmingham, UK. The total award covered the cost of tuition fees at an international rate (12,800£/year) and a stipend of up to £9000/year, which equated to approximately £65,000 over the 3 year period. The facilities of the University of Birmingham, School of Mechanical Engineering were utilised for experimental based machinability work and analysis of results. A cash contribution of £21,000 over the 3 year period was obtained from Rolls Royce (RR) to cover project costs including travel, equipment hire, consumables, technical support and

machine maintenance over the duration of the project. The project also involved collaboration with Element Six (E6), Ireland which provided current and prototype PCBN tool materials for evaluation. Seco tools provided finished uncoated and coated PCBN inserts. Both companies contributed £2,000 cash per year over the project duration. During the course of the work, Teer Coatings Ltd. UK (now part of the Miba Group) and Balzers Oerlikon UK were contacted to provide specific coatings for comparative performance evaluation. In addition, all companies provided specialist technical knowledge and expertise in their relevant fields. See Appendix A for details of collaborators and industrial advisors.

2. LITERATURE REVIEW

2.1 Nickel based superalloys

2.1.1 Composition and microstructure

Nickel based superalloys comprise up to 75% nickel (Ni) and up to 30% chromium (Cr) which provide outstanding oxidation resistance [17]. Alloying elements are used to impart strength and to improve the microstructure. These are detailed below with key phase details.

- Gamma phase: is the main phase in which all other phases reside. It is denoted by 'γ' and consist of continuous austenitic matrix having face centred cubic (FCC) structure with significant concentration of cobalt (Co), chromium (Cr), molybdenum (Mo), ruthenium (Ru), rhenium (Re) and tungsten (W) as they all are solid solution elements [17-19].
- Gamma prime precipitate: is denoted by γ′. It contains elements including aluminium (Al), titanium (Ti) and tantalum (Ta) [17-18] with chemical formula Ni_3(Al, Ti) [2]. The gamma matrix is generally coherent with this precipitate phase [18] which is present as an intermetallic compound [2] having a spherical or cuboidal shaped structure [19] as shown Figure 2 (a). The presence of Ta can further increase the heat and creep resistance properties [2]. Inconel 718 and Inconel 706 posses greater than 4% Niobium (Nb) and are regarded as Nickel iron superalloys, gamma prime is transformed to gamma double prime, denoted by γ″. This phase exhibits a body central tetragonal (bct) structure and is expressed with a chemical formula Ni_3Nb. Precipitation of this phase at the grain boundaries increases the creep rupture properties [2]. In the overaged condition, this phase can change into an orthorhombic plate like structure called delta phase (δ) (Figure 2-b). This does not provide strength as it is not coherent with the gamma matrix, however it can be used for grain size refinement which in turn can optimise tensile and fatigue properties. Excessive formation of δ-phase during service can cause severe degradation in properties [18].

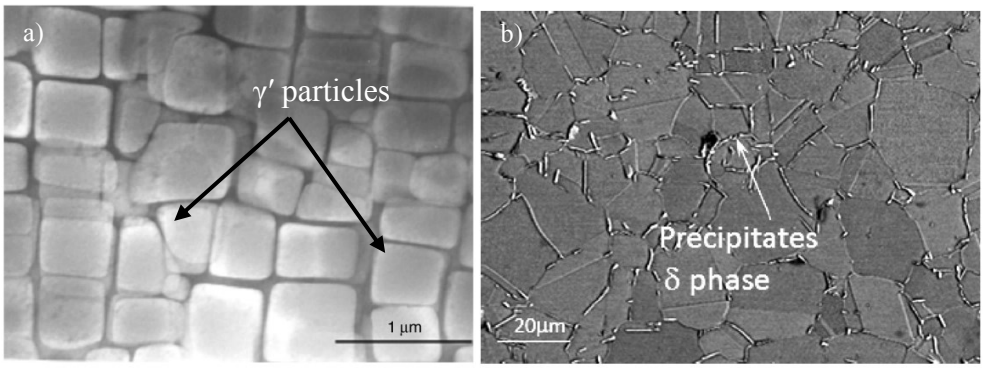

Figure 2: (a) TEM micrograph of NiCr17TiAl nickel based alloy showing gamma prime γ′ particle in gamma matrix γ [20] and (b) δ-precipitates in SEM micrograph of Inconel718 [21]

- Carbide and boride phases: Alloy composition and processing methods determine the type of carbides [18]. Common types include MC, M_6C, $M_{23}C$, M_7C_3 which are present in the microstructure as grain boundary precipitates [17], see Figure 3 which shows Nb and Ti carbides in the microstructure of Inconel 718.

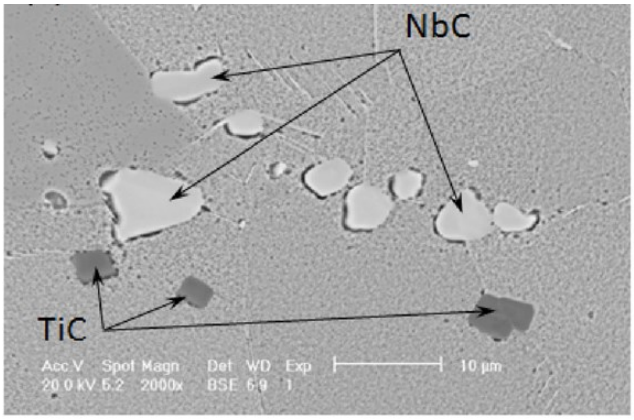

Figure 3: Carbides of Nb and Ti in the microstructure of Inconel 718 [21]

- Topologically closed packed (TCP) phases: are brittle, more prone to fracture and can deteriorate the mechanical properties of the alloy. They are generally formed when nickel alloys are exposed to elevated temperatures [1].

2.1.2 Properties

A large fraction of the turbine engine consists of nickel based superalloys due to a good combination of physical and mechanical properties [22] . Typical physical properties of nickel based superalloys are presented in Table 1.

Table 1: Typical physical properties of nickel based superalloys [17]

Property	**Typical ranges**
Density (g/cm^3)	7.92-9.21
Melting temperature (liquidus)	1290-1425ºC
Specific heat (J/KgK)	389-523
Electric resistivity (nΩ.m)	148-1380

Material density is influenced by alloying additions, larger amounts of lighter elements such as Al, Ti and Cr decreasing the density whereas heavier elements like W and Ta cause an increase [17]. Optimisation of mechanical properties is of prime interest and strongly depends on microstructure and grain size. Both static and dynamic mechanical properties are important as they may be life limiting [22]. The former involves tensile and yield strengths while creep and fatigue strength are dynamic properties.

i) Tensile properties

Nickel based superalloys posses high yield and ultimate tensile strengths at room temperature in the range of 900-1300 MPa. and 1200-1600 MPa. respectively. They can also maintain their tensile strength at high temperatures (~850ºC) [22]. Different factors including the percentage of γ′ and γ″ phases, Ti/Al ratio and grain size can significantly affect the tensile and yield strength of these alloys. A linear relationship exist between yield stress, γ′ and γ″ strengthening phases and increasing the fraction of these increase the yield stress of nickel based superalloys. For example, the yield stress of Nimonic 80A is ~550Mpa. with 20% of above mentioned phases but when this fraction is doubled as in Udimet 500, a ~46% rise in the value of yield stress is observed [18].

A second factor affecting the yield properties is the concentration of Al, Ti and Nb elements. Higher fractions of Ti+Al elements provides greater strength as shown in Figure 4 [19]. In addition, their presence causes a significant increase in the anti-phase boundary energy (APB), which is produced as a result of intersection of γ′ particles with dislocations, thus restricting the movement of dislocations and an increase in the shear strength of the material [1].

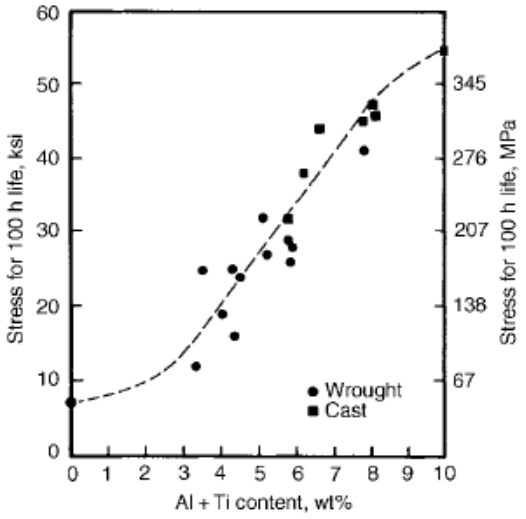

Figure 4: Stress rupture strength of wrought and cast nickel based superalloys as a function of Al + Ti content [17, 19]

Finally, grain size significantly influences the tensile and yield strength of these alloys. The change of grain size is a complex phenomenon and strongly depends on time and temperature. Overheating can change the grain size from fine to coarse provided that grains were initially fine [23]. Polycrystalline nickel alloys with fine grain size exhibit better ultimate tensile and yield strengths; see Figure 5 which highlights yield and ultimate tensile strength as a function of grain size for Udimet 720 superalloy. Here a rapid decrease in the tensile and yield strength is evident up to 150µm grain size while a further increase in the grain size to 400µm shows a marginal reduction in strength [18].

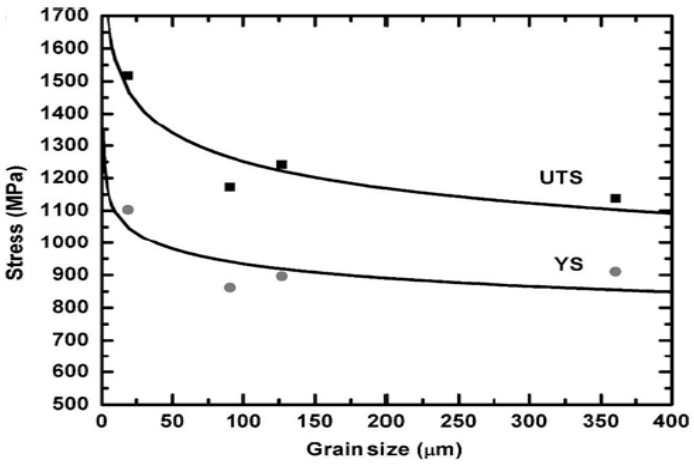

Figure 5: Effect of grain size on yield stress(YS) and ultimate tensile strength(UTS) of the Udimet 720 superalloy [18]

ii) Creep, fatigue and fatigue crack growth

A resistance to time dependent creep deformation is necessary for superalloys which experience high temperatures/stresses during service [22]. A relationship between the creep rupture life of a nickel based alloys at 982ºC is shown in Figure 6 which highlights that with an increase in the percentage of strengthening phase γ′, the creep life is subsequently increased [19].

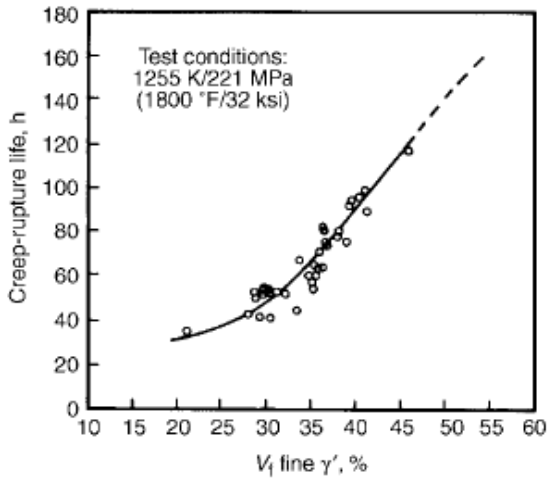

Figure 6: Creep rupture life against the volume fraction of γ′ of nickel based alloy CGDS MAR-M-200 [19]

The repeated take off and landing cycles of aircraft cause remarkable fluctuation of temperatures and stresses in the components of turbine engine which in turn can produce small localised plastic strains. Hence from an engine design perspective, low-frequency and low-cycle fatigue (LCF) is of great concern. High-cycle fatigue (HCF) occurs at much higher frequency (generally in the kHz range) in the engine components as a result of engine vibrations and airflow between different parts of the turbine. These repeated loading and unloading cycles may result in microscopic cracks which cause sudden fracture of components, therefore resistance to fatigue crack growth (FCG) of a material is of paramount importance, specifically for turbine disk materials. Processing methods introduce certain inclusions and pores which may initiate FCG [22]. Fatigue crack growth can be classified into three main stages; In the first stage, short cracks develop which grow to the longer ones in the following stage and finally fracture occurs in stage 3 [24].

With respect to grain size of the materials, the LCF life of nickel alloys is generally better with fine grain size but optimum creep and resistance to fatigue crack growth are obtained when the grain size is large as shown in Figure 7. Therefore in order to obtain a

balance in these properties, a compromise is required [18]. As a solution to this problem, a dual microstructure variant of RR 1000 has been developed by Rolls Royce (RR) for use in high pressure turbine disc applications. Grain sizes are different in different parts of a component as a result of solution heat treatment in one particular part allowing the grains to grow to a required size, other parts are covered using refractory caps. For example, in order to optimise the yield stress and LCF, grain size of the bore of a disc was reduced to <10µm while for optimum resistance to dwell fatigue crack growth and creep strain, an average grain size of 30-50µm was developed in the rim and diaphragm [10].

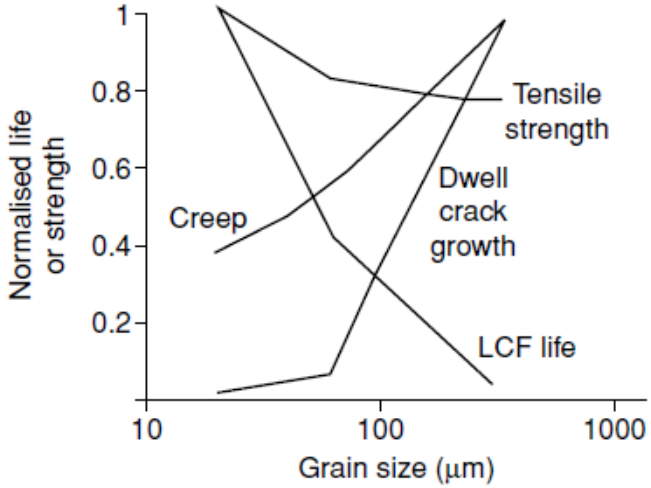

Figure 7: Important properties of turbine disc alloys with respect to the variation in the grain size [18]

For optimum creep life and low cycle fatigue, the presence of carbide precipitates at grain boundaries is necessary [18] but their shape change can cause a degradation in properties [17].

2.1.3 Industrial applications

Superalloys have been developed with specific properties that relate to their applications. The consumption of superalloys in the aerospace industry accounts for approximately ~70% with the rest utilised in chemical, structural and medical applications, see Figure 8 (a) [3]. Figure 8 (b) highlights the fact that use of composites in aero engines has increased dramatically over a past decade due to their low density and good stiffness, however nickel based superalloys are still the most widely used material in aircraft engines, currently accounting for ~40% of engine weight followed by titanium [2].

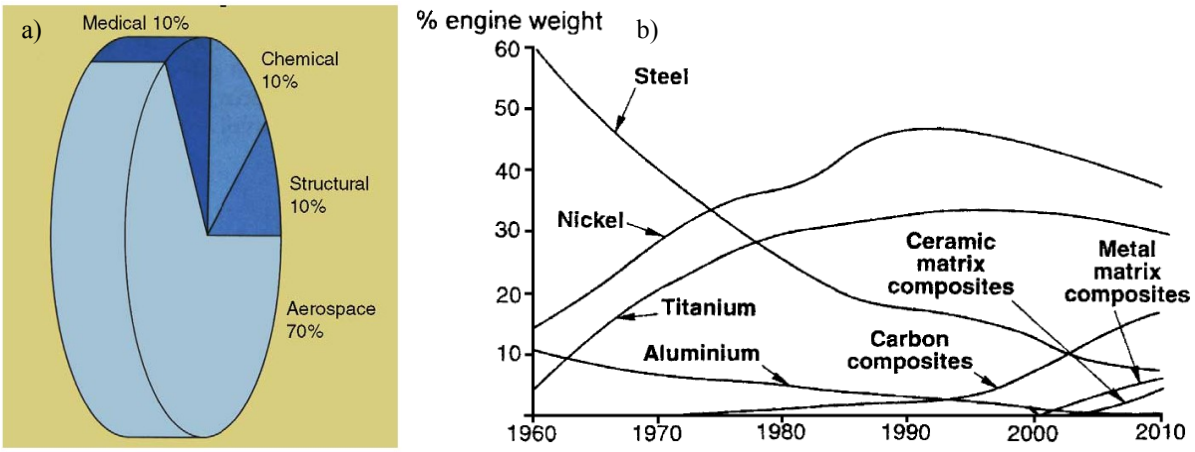

Figure 8: (a) Consumption of superalloys [3] and (b) materials utilisation in aircraft engines [2]

Other uses of nickel based superalloys include heat treatment and marine equipment, nuclear reactors, petro-chemical plant and food processing equipment, see Table 2.

Table 2: List of some nickel based superalloys and their use in different applications [17]

Types of alloys	**Applications**
Inconel 600, Inconel 601, RA333	Heat treatment equipment, high temperature chemical processing equipment
Hastelloy X, Inconel 601, Inconel 617, Inconel 625	Aero-engine turbine combustors, heat shields, aircraft duct and exhaust system, turbine shroud rings
RR1000, Inconel 718, Waspaloy	Aero-engine turbine discs, shaft and turbine cases
Inconel 713, Inconel 100, B-1900	Turbine blades

2.2 Tool wear

2.2.1 Types/patterns of wear

The loss of material from a tool is termed tool wear. High shear and normal stresses during machining on the rake and flank faces of the tool can generate high localised cutting temperature. These induce tool wear, which in turn compromises tool life and diminishes machined surface quality and dimensional accuracy [25]. The cost of any machining operation can be minimised by selecting the appropriate combination of workpiece material and cutting tool. This also helps in the prediction of a tool life [5].

Tool damage can be categorised as either progressive wear or fracture [5]. Progressive wear may take many forms, such as flank wear, crater wear, thermal cracks, notch wear and built-up-edge (BUE) [26] whereas tool fracture can be on a small scale such as chipping or on a larger scale such as fracture or catastrophic failure [5].

i) Flank wear

Flank wear mainly occurs on/adjacent to the cutting edge i.e. the tool nose, the main flank face and the minor flank face as shown in Figure 9 (a) [27]. Non uniformity in this type of wear is observed which generally becomes more severe at the tool nose. Hard particles and inclusions in the workpiece material generate flank wear [25]. Flank wear is generally used to measure the tool life [26]. According to the ISO 3685 standard, the tool wear/life criteria most commonly used for ceramic tools are:

a) The maximum width of flank wear land VB_Bmax. =300µm, if the flank wear is considered to be regularly worn and if notch wear is also observed at the depth of cut line then the maximum width of notch wear VB_Nmax.=600µm,

ii) Crater wear

At a short distance from the cutting edge, on the rake face of the cutting tool crater wear is observed, see Figure 9 (b). This causes a reduction in the tool strength and a rise in temperature and friction between the chip and the rake face. Wear index (q) is used to determine the tool life, which is obtained by dividing the crater depth Kt by the cutting edge distance from the centreline of the crater Km as given in Equation (1) [26];

$$q = K_t / K_m \qquad (1)$$

In the case of high speed steel and carbide tools, the ‘q’ value should be less than 0.6 and 0.4 respectively. However, crater wear is difficult to measure, therefore this tool life criteria is not generally employed [28].

iii) Thermal cracks

Figure 9 (c) shows the small thermal cracks that appear perpendicular to the cutting edge. These cracks develop as a result of repeated heating and cooling cycles (thermo-mechanical fatigue) associated with interrupted cutting, or as a result of varying coolant supply. These thermal gradients cause cracks and breakage of small fragments of the tool material [5].

iv) Notch wear

Notch wear (depth-of-cut notching) is shown in Figure 9 (d). This type of wear is seen both on the major and minor cutting edges. Many reasons are reported in the literature for its occurrence involving oxidation of the tool material, severe work hardening of work piece material [29] and the saw-tooth edge of the chips [5]. This type of wear is more severe for high temperature alloys including superalloys and austenitic stainless steel which rapidly work harden during machining. Notch wear appears at the depth of cut line which is in contact with the machined surface from the previous cut [25]. Sometimes notch wear causes fracture, however it can be avoided to some extent by using chamfered edge cutting tools, round inserts and employing a depth of cut greater than the work hardened layer [5].

v) Built-up-edge (BUE)

Built-up-edge (BUE) as shown in Figure 9 (e) refers to pressure welding of the chip to the cutting tool tip. BUE formation normally forms at low cutting speeds [5] due to low temperature and high pressure [30] particularly with non-ferrous materials such as aluminium, nickel, cobalt and titanium alloys, soft low carbon steel and ductile stainless steels. Small fragments of the tool material are carried away with the breakage of BUE which typically results in severe attrition wear [5]. However, high tool temperatures/stresses produced at higher cutting speeds can diminish the BUE due to the generation of a flow zone and recrystallisation of the material [31].

vi) Chipping/Fracture

When small pieces of the cutting edge detach from the tool, then this phenomenon is termed as chipping and if it occurs at a larger scale, then it is called fracture, see Figure 9 (f). In contrast to the flank wear which is a gradual process, this occurs rapidly and degrades the surface finish, surface integrity and dimensional accuracy of the workpiece. In addition, progress of crater wear toward the tool tip can produce chipping [25].

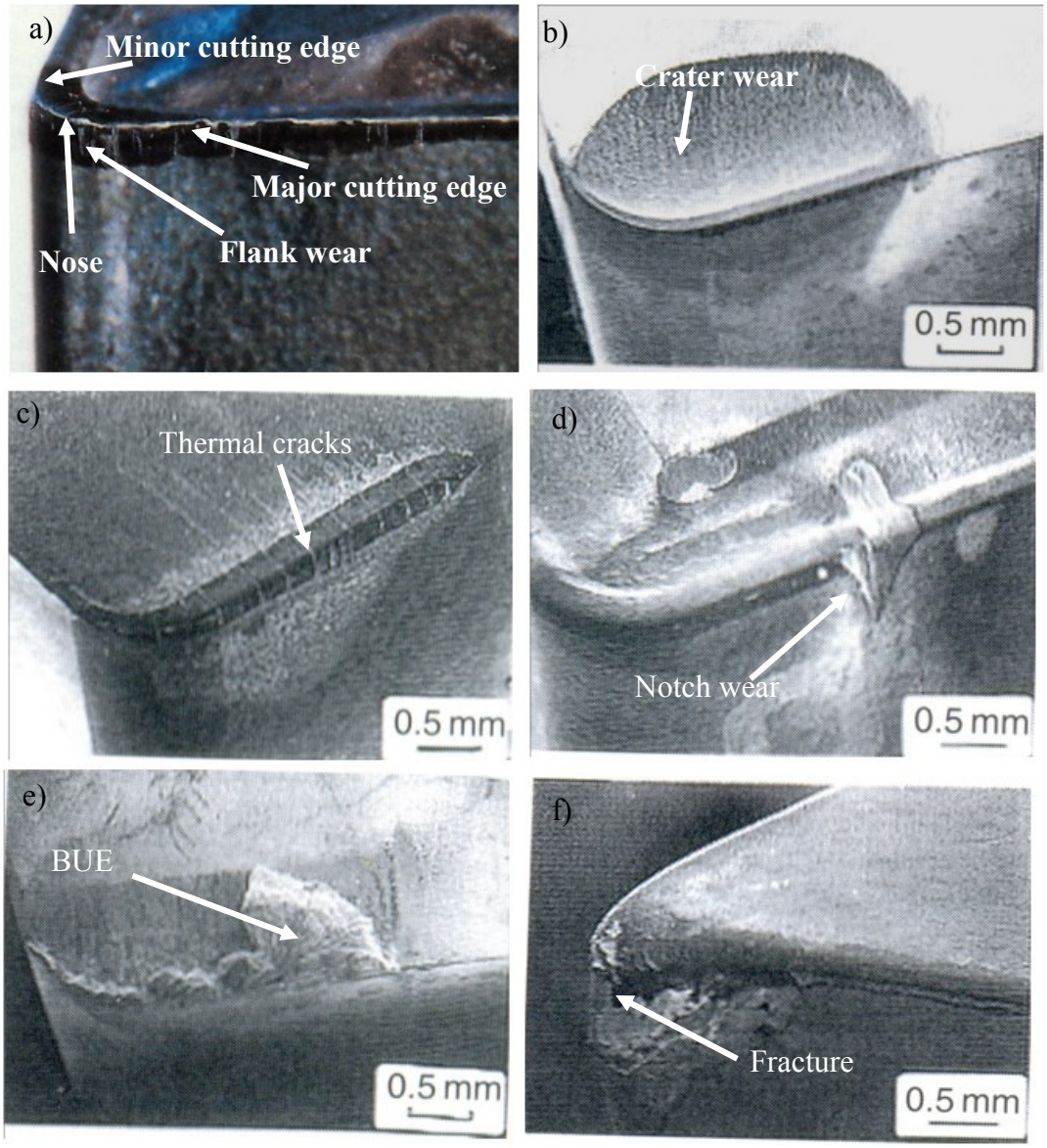

Figure 9: Types/patterns of wear (a) flank wear [27]; (b) crater wear; (c) thermal cracks; (d) notch wear; (d) BUE and (f) fracture [5]

2.2.2 Tool wear mechanisms

The mechanisms associated with the tool wear are complex. Different factors involving tool material & workpiece properties, geometry of the cutting tool and operating parameters affect tool wear mechanisms. Analysis of different types of wear mechanism are described below [5];

i) Abrasive wear

The sliding action between hard particles of workpiece material and the cutting tool results in abrasive wear. Possible sources of hard particles are either the workpiece or broken parts of the cutting edge [27]. The types of hard particle depend on the alloy e.g carbides of titanium and niobium in nickel based superalloys, cementite in steels and silicon carbide in silicon-aluminium alloys [5]. Figure 10 (a) shows a schematic illustration of abrasive wear. Abrasion is a type of mechanical wear, therefore it strongly depends on the tool hardness [27] and is independent of cutting speed and temperature rise [5].

ii) Diffusion wear

Diffusion is a chemical type of wear and depends on the chemical affinity between the tool and workpiece as well as their chemical properties [27]. Some tool materials exhibit strong affinity with the workpiece e.g polycrystalline diamond (PCD) reacts with hardened steels while polycrystalline boron nitride tool (PCBN) is relatively inert. This type of wear is independent of tool hardness but strongly depends on temperature and accelerates with an increase in the cutting speed and temperature. The amount of diffusion wear can be determined by knowledge of the metallurgical relationship between the workpiece and cutting tool material [27]. Illustration of diffusion wear is shown in Figure 10 (b) which highlights diffusion of iron (Fe) atoms of the workpiece into the tool and carbon (C) & cobalt (Co) atoms of the tool into the workpiece. In comparison to 'Fe' and 'Co', carbon atoms diffuse at much faster rate due to their high mobility (70×10^3 higher than Iron atoms) [5].

iii) Adhesive/Attritional wear

Close contact between the tool and workpiece can cause formation of a bond between them with material transfer from one surface to another subjected to the condition that this bond exceeds the local strength of the material [32]. The workpiece material attachment may take the form of particles or a layer and is called BUE. Sometime successive welding and hardening of these layers can take place and become part of cutting edge [27]. Dislodging of

individual particles or layer particles from the cutting edge result in attrition wear. This type of wear occurs at low cutting temperature [5].

iv) Oxidation and corrosion wear

Chemical reaction of tool material constituents with the atmospheric oxygen causes oxidation wear. This wear often occurs around 800ºC with direct exposure of the atmosphere to the free surface of a tool/chip contact region. Reaction of cobalt and tungsten produces porous oxides while some oxides are harder like aluminium oxide (Al_2O_3) [5]. Notch wear on the major and minor cutting edges particularly at the depth of cut position is the result of oxidation as air enters and reacts as shown in Figure 10 (c) [27]. If additives are present in the cutting fluid such as sulphur or chlorine, these can also react with the tool material to produce chemical products which cause abrasion on the tool surface termed corrosive wear [5].

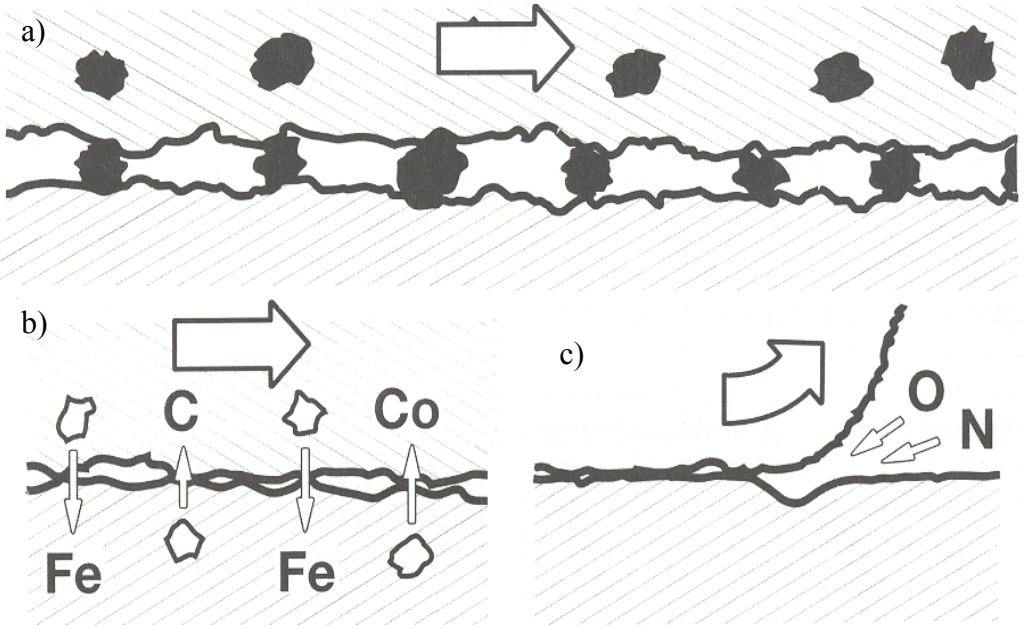

Figure 10: A schematic illustration of different tool wear mechanisms during machining (a) abrasive wear; (b) diffusion wear and (c) oxidation [27]

2.3 Workpiece surface integrity

Workpiece surface integrity (SI) is assessed by a combination of different superficial and in-depth properties that affect the performance of an engineering surface [33]. The concept of surface integrity was first introduced by Field and Kahles [34-36]. They defined surface integrity as 'the inherent or enhanced condition of a surface produced in machining or other surface generating operation' [34]. They presented comprehensive reviews on SI emphasizing the nature of metallurgical alterations produced as a result of non-conventional and conventional machining processes [35] and proposed different SI data sets for assessment, see Table 3 [36]. Typically, machining processes induce different types of defects and the most commonly found in practise are described below; [33];

- Cracks: These are external or internal separations with sharp outlines. A microcrack is one which can only be seen with 10x or higher magnification.
- Metallurgical transformations: Due to high temperature and pressure during machining, changes in the microstructure involving phase transformation, re-cast layers, re-solidified and re-deposited materials occur.
- Residual stresses: Cutting forces, cutting temperature and deformation cause residual stresses in the machined surface and sub-surface. These are either tensile or compressive.
- Pits and craters: Shallow depressions produced on the machined surface are termed as pits and craters; the former is generally the result of chemical or physical attack.
- Intergranular attack: This involves grain boundary weakening due to corrosion or liquid metal embitterment.
- Inclusions: These are small, non metallic elements in the metal.
- Plastic deformation: High stresses produced as a result of friction generate severe surface or sub-surface plastic deformation.

Table 3: Data sets for the evaluation of surface integrity [36]

Minimum SI data set	**Standard SI data set**	**Extended SI data set**
Surface finish Microstructure (10x or less) Microcracks Macrocracks indications Microstructure • Microcracks • Plastic deformation • Phase transformation • Intergranular attack • Tears, pits, laps, protrusions • Built-up-edge • Re-deposited and melted layers • Selective etching Microhardness	Minimum SI data set Fatigue test • Flat specimens with tapered area at room temperature employing full reverse bending Residual stress profile Stress corrosion test	Standard SI data set Fatigue test (extended to get design data) Additional mechanical tests • Tensile • Stress rapture • Creep Specialised: friction, wear, sealing, bearing performance • Fracture toughness • Low cycle fatigue • Elevated or cryogenic temperature • Crack propagation • Surface chemistry

Assessments for the minimum SI data set are the least expensive to perform; therefore it should be considered in the first instance. The standard SI data set is used for further in-depth analysis of more crucial applications and involves the minimum SI data set together with basic fatigue, residual stress and stress corrosion testing. The standard SI data set together with some additional mechanical tests and fatigue programmes which are statistically designed, is termed the extended SI data set which is used for the detailed analysis of component design [35]. Some of the important aspects of surface integrity are discussed below;

2.3.1 Surface roughness and surface damage

Surface roughness is the most commonly employed parameter used to describe the geometric features of a workpiece surface. In the absence of vibrations & BUE, it mainly depends on feed rate (f) and tool nose radius (r). The different arithmetic parameters which are used to determine the surface roughness are included in ISO 13565-2:1997 standards [37]

i) Ra (Centre line average): This is called the arithmetic average roughness and is a measure of deviations about the centre line within the evaluation length. This parameter is most frequently used and can be measured easily even with the least sophisticated profilometer, however in-length characteristics, difference between peaks and valleys and small variations in the machined profile cannot be determined using this parameter [33]. The formula used to calculate 'Ra' for turning operation is given below [38];

$$Ra\ (\mu m) = f^2.50/r \qquad (2)$$

where 'f' is the feed rate (mm/rev) and 'r' is the nose radius (mm).

ii) Rt: This parameter is used to indicate maximum peak to valley height of the filtered profile over the evaluation length. Large deviations about the mean line can be determined using this parameter. Rt is employed with Ra as a general indicator [33] and can be calculated for turning operation with the equation given below [38];

$$Rt\ (\mu m) = k.f^2.1000/8r \qquad (3)$$

Where 'k' is a constant whose values is different for different materials e.g 1.00 for steel and 1.4 for cast iron [38].

iii) Other parameters used include Rz (average peak to valley height), Rq (root mean square roughness), Rp (the value of highest single peak above the centre line) and Rv (the deepest valley below the centre line) [33].

All the above mentioned parameters are used in two-dimensional (2D) roughness measurement, however surface texture parameters which are measured over an area are called three-dimensional (3D) and denoted by 'S' instead of 'R' to indicate that they are calculated over an area [5]. Several different techniques are used to measure surface roughness which can involve electronic, optical, visual type measurements and scanning probe microscopy methods [33].

Surface waviness occurs due to lack of machine rigidity and is superimposed on the surface roughness [5].

Surface damage analysis requires close examination of a specimen under a scanning electron microscope (SEM). Typical defects include side flow, chip debris, BUE, ridges and grooves, micro-cracking, surface tearing, cavity formation, breakage of carbides and plastic flow. Figure 11 illustrates typical surface damage produced in turning operations [21].

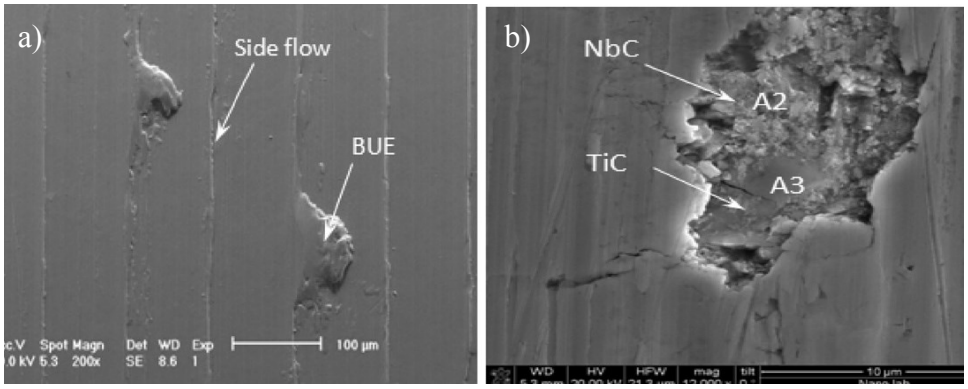

Figure 11: Typical surface damage produced in turning of Inconel 718 using whisker reinforced ceramics tools (a) side flow & BUE and (b) carbide cracking [21]

2.3.2 Microhardness

Thermal, mechanical or chemical changes induce variations in the hardness of the surface and sub-surface of a machined specimen and its analysis is important in order to examine the possible effects produced as a result of machining operations [39]. Successive machining operations involving roughing, semi-roughing and finishing are used to generate the final machined surface. Subsequent machining passes are significantly influenced by the preceding machining passes. Such effects are more prominent for nickel alloys which show a rapid work hardening tendency [40]. With such materials the hardness of machined specimens is generally found to be greater at the surface and near surface compared to the bulk of the material where heat and strain effects diminish. This work-hardening behaviour in turn has a significant effect on the yield strength of the material. Additionally, sequential cuts are extremely difficult to take for nickel alloys due to their work-hardening behaviour under high strain loads and in order to overcome this problem, depth of cut should be greater than the depth of the work hardened layer [40]. The use of a continuously varying depth of cut is another solution to this problem [41].

Microhardness testers equipped either with Knoop or Vickers indenters are used to measure microhardness. Mechanical properties such as tensile strength, elastic modulus etc. can be predicted on the basis of microhardness tests [42]. Considerable variations within a short distance are expected, therefore loads below 1kg are commonly used. When comparing Vickers and Knoop indenters, it has been observed that the former is less influenced by form errors on the machined surface and is cheaper to use, however misreading is greatly reduced with the Knoop indenter due to the longer diagonal and smaller indentation depth [43].

2.3.3 Microstructure

Strain aging and recrystallisation of the material is the result of mechanical (stress and strain effects) and thermal (high temperature and rapid quenching) loads on the workpiece surface during the machining operation. An increase in workpiece hardness and reduction in ductility is the result of strain aging while the opposite is true for recrystallisation which can cause greater ductility and reduced hardness. White layer formation at the machined surface is observed when strain aging is prevalent whereas when recrystallisation is present then a dark layer also appears just beneath the white layer which has a hardness value in-between the hardness of bulk material and white layer, see Figure 12. Extensive literature has been published when investigating the white layer formation and there is a general consensus that compared to the bulk material, it contains a fine grain size and sometimes a nano-crystalline structure. Although its hardness is greater than the bulk material, due to its brittleness it can easily initiate crack propagation and ultimately influence the fatigue strength [40]. It is reported that the thickness of the white layer can vary from a few hundred nano-meters [41] to around 10-20 μm [40].

Plastic deformation is another important concern relative to microstructure alterations. Elongation of the grain structure in the cutting direction and slip at the grain boundaries are common examples of plastic deformation quoted in the literature [5]. Typically, it is mainly confined in a very narrow zone beneath the machined surface [40]. Plastic flow is generally the result of plastic deformation which in turn can initiate cracks, laps, built-up-edge and burrs [5]. Carbide cracking is the most common defect observed in machining of nickel alloys particularly in finishing applications where feed rate and depth of cut are very small and their range is often comparable to the size of carbide particles, which further facilitates the cracking. Plastic deformation is dependent on different factors involving tool macro-geometry (tool angles, nose radius etc.), micro-geometry (edge preparation), cutting speed, feed rate, depth of cut and the type of workpiece material (grain size, microstructure) [40]. Furthermore, increasing tool wear produces an increase in plastic deformation due to rubbing as a result of greater tool workpiece contact, see Figure 13 [44]. Sometimes, plastic deformation also contributes to the creation of white layers [45-46].

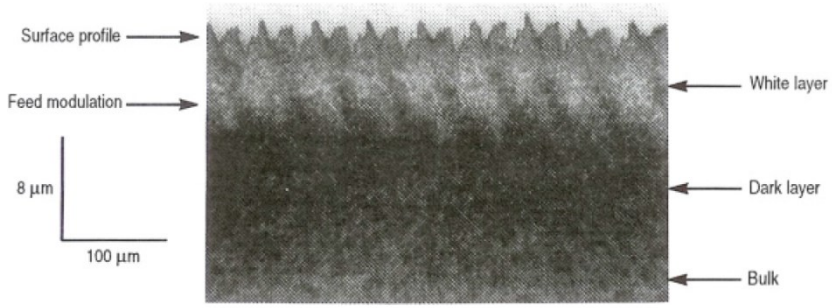

Figure 12: Micrograph of hard turned machined surface of 52100 steel showing white and dark layers [33]

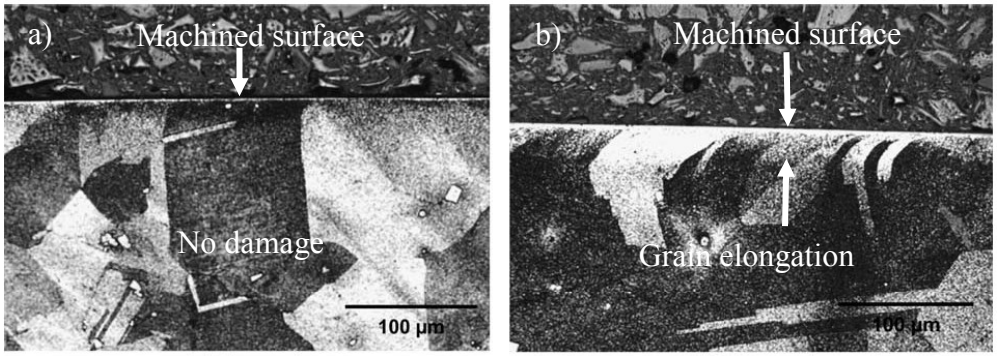

Figure 13: Microstructural deformation of Inconel 718 (a) new tool and (b) worn tool [44]

2.3.4 Residual stresses

Stresses which are produced in a material due to thermal effects and plastic deformation during machining and are present even after the removal of loads, are termed residual stresses [40]. Three separate models can be used to represent residual stress generating mechanisms [5].

i) Thermal phase transformation model: This model is also called the thermal or hot model in which heat produces phase change. A decrease in specific volume due to the phase change produces tension in the surface layer which in turn promotes tensile residual stresses; see Figure 14 (a), alternatively, an increase in specific volume results in a compressive zone.

ii) Thermal/plastic deformation model: This is the mixed model in which the surface first expands due to heat and then plastic flow relieved this expansion which is confined to the surface. Contraction of the surface after cooling generates tensile residual stresses [Figure 14 (b)].

iii) Mechanical plastic deformation model: Figure 14 (c) illustrates that when workpiece surface layers are compacted by mechanical action, compressive residual stresses are induced. This model is also called the mechanical or cold model [5].

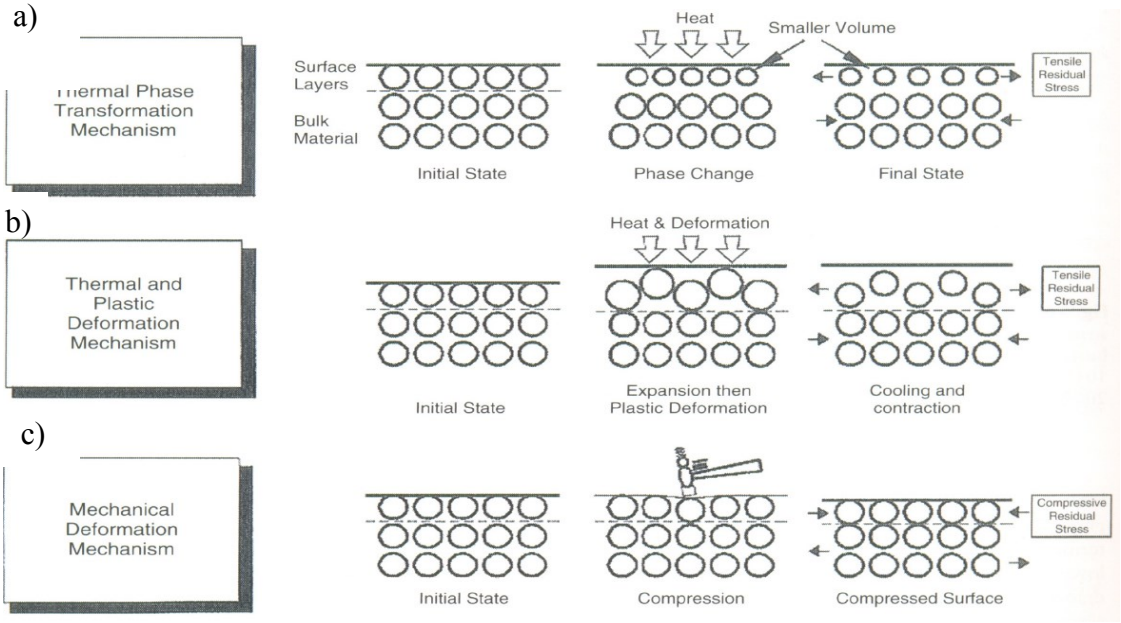

Figure 14: Three models of residual stress generation [5]

Both thermal and mechanical effects are responsible for the generation of residual stresses in a machined component, the dominance of thermal effects producing tensile stresses, and mechanical effects producing compressive stresses [43]. Crack initiation is the result of tensile residual stresses which in turn affect the fatigue life of the product. Removal of tensile residual stresses after machining operations or the use of preventive measures in order to avoid them during cutting, is necessary particularly for aerospace/safety critical components [40]. In order to induce compressive residual stresses and to improve the fatigue life of a machined component, special finishing treatments such as shot peening and rolling processes are used. The magnitude and penetration depth of induced stresses depend on the shot peening and rolling conditions [47].

Residual stresses can be determined by using different methods, however X-ray diffraction (XRD) and hole drilling (employing a strain gauge rosette) are preferred techniques [48]. In the X-ray diffraction method, the distance is measured between the crystallographic planes to determine the stress. According to Bragg's law shown in the equation below, polycrystalline materials diffract the X-rays at a known angle 2θ. An angular shift in the diffraction peaks is produced due to the change in the value of stress which in turn affects the change in the spacing between the crystallographic planes [49].

$$n\lambda = 2dSin\theta \qquad (4)$$

In the hole drilling method, three strain gauges are attached to the machined part at 3 different angles (0, 90º, 135º) around a central point where a blind hole is drilled. Stresses at that blind hole point are relaxed causing a corresponding change in the values of stresses in

the surrounding region which produce local strains which in turn are measured with the strain gauge rosette [50].

2.3.5 Fatigue

Safety of aero engine parts is of prime concern because they are subjected to cyclic stresses which may lead to fatigue failure [51]. There are two main types of fatigue, low cycle fatigue (LCF) and high cycle fatigue (HCF) [36]. The former is associated with aircraft take-off, landing and manoeuvring where stresses occur at high amplitude and low frequency. Chatter and airflow between the different aeroengine stages is associated with high cycle fatigue [18] and is judged most important [36] because half of aero engine parts are damaged due to fatigue and ~50% of failures are the result of HCF [52].

In general, S-N curves are plotted to determine material performance in terms of fatigue where 'S' stands for the magnitude of cyclic stress and 'N' the number of cycles to failure. This plot is used to calculate the endurance limit of any material which is defined as 'the amplitude of cyclic stress which can be applied without failure up to the run-out value of 10^7 cycles'. Fatigue testing for low and high cyclic stresses is conducted both at room and elevated temperatures [36].

Nucleation of cracks can initiate from flaws present in the turbine disc which in turn can reduce fatigue life. The dimensions of these flaws can be determined using different non-destructive (NDE) methods and involve eddy current, X-ray radiography and ultrasonic methods etc. The ultrasonic method is the most widely employed technique for turbine disc applications in which inclusions, tears, seams and laps etc. can be detected using high frequency sound waves [18].

2.4 Machining of nickel based superalloys

2.4.1 Machining of nickel based superalloys using carbide cutting tools

Cemented carbides are the most widely employed tool material for the machining of nickel alloys. Normally, K10/K20 (ISO-classification) grades are recommended [5] having 94% Tungsten carbide (WC) and ~6% Cobalt, with a sub-micron grain size [38]. Extensive research on the use of WC tooling was done in the late seventies [53]. Over the past few years, research on novel coatings and the use of different cooling techniques has been undertaken.

2.4.1.1 Recent trends in the development of coatings

Uncoated carbide cutting tools are recommended at low cutting speeds (35m/min) [5]. Notching at the depth of cut line was observed be to the dominant failure mode while diffusion and abrasion are the main wear mechanisms reported in the literature [1-2]. Uncoated WC tools cannot be employed in the machining of nickel alloys at elevated cutting speed because extreme temperatures/stresses generated in the cutting zone make them unsuitable for this application, however with the introduction of hard PVD and CVD coatings, a two fold improvement in the value of cutting speed is possible. The family of TiAlN PVD coatings developed in late 1990's [43] is extensively used [54] for the machining of nickel alloys [55] having improved tool life over other TiN and TiCN coatings, due to a favourable combination of hardness and oxidation resistance at elevated temperatures [56]. Coatings based on TiAlN are commonly employed with either TiN [54] or in a multilayered structure [57] due to the mechanical advantage associated with this approach.

Over the last 5-7 years, novel nanostructure and superlattice PVD single & multi-layer coatings has been widely investigated both for roughing and finishing applications by different researchers [9, 58-64], see Table 4. Nano-structure coatings typically have a grain size less than 100nm which are more stable at high temperature and have high wear resistance compared to micro-crystalline structures [58]. In the superlattice concept, two materials with the same crystalline structure are layered so that an energy barrier to the motion of dislocations can be provided at the interface between the layers. As a result, good mechanical and tribological properties are induced [59].

Table 4: Effect of various types of state of the art PVD coating in turning of nickel alloys

Authors	**Coating details**	**Workpiece/ operating parameters**	**Key results**
Ducros and Sanchette [59]	Superlattice multilayer and nanolayer coatings 1. CrN-TiN 2. TiN-AlTiN 3. CrN-AlTiN *Note: For multilayer, coating period >100nm while for nanolayer, it was < 100nm.*	Inconel 718 Vc=20-50 m/min F=0.1-0.3 mm/rev DoC=0.5-2.5mm coolant	For both roughing and finishing, nano-layer TiN-AlTiN coating was the best in terms of tool wear and cutting forces due to its higher hardness, better abrasive wear resistance and good tribological properties. *Wear mode*: Notch wear at the depth of cut line.
Devillez et al. [58]	1. TiAlN nano-structure (2-4 µm) 2. AlTiN nano-structure (3µm) 3. TiAlN+WC/C multilayer (2-6 µm) 4. TiAlN+MoS2+Ti multi-layered (3 1µm)	Inconel 718 Vc=100m/min F=0.1-0.2 mm/rev, DoC=1.5mm dry	AlTiN was the best coating due to its better chipping and abrasion resistance. *Wear mode*: Abrasion and coating delamination.
Settineri et al. [9]	Nano-structure multilayer coatings 1. TiN+AlTiN 2. TiN+AlTiN+MoS_2 3. CrN+CrN:C+C	Inconel 718 Vc=35-140 m/min F=0.25mm/rev DoC=0.5mm wet, dry and MQL	TiN+AlTiN+MoS_2 showed better performance due to optimal Al/Ti ratio with good abrasion resistance and better adhesion to the substrate and outermost layer of MoS_2 limits the adhesion of the chip. *Wear mode:* Abrasion, BUE, thermal cracks and coating delamination.

Table 4: Effect of various types of state of the art PVD coating in turning of nickel alloys (contd.)

Authors	**Coating details**	**Workpiece /operating parameters**	**Key results**
Fox-Rabinovich et al. [60]	1. AlTiN monolayer 2. AlTiN/Cu nano-structure multilayer	Inconel 718 Vc=40m/min F=0.125 mm/rev DoC=0.25mm coolant	Tool life of AlTiN/Cu coating was significantly higher (2.3 times) compared to mono-layer AlTiN due to higher hardness, reduced thermal conductivity and improved lubricity at elevated temperatures. *Wear mode*: BUE formation
Biksa et al. [61]	Nano-structure multilayer coatings (~3µm) 1. AlTiN 2. AlTiN/CrN 3. AlTiN/VN 4. AlTiN/MoN 5. AlTiN/WN 6. AlTiN/NbN	Inconel 718 Vc=40-60m/min F=0.125mm/rev DoC=0.25mm coolant	Better performance of AlTiN coating was observed with MoN and NbN due to the formation of lubricious oxide tribo-films on the surface that had reduced friction and BUE formation. *Wear mode*: BUE formation and chipping.
Dosbaeva et. al. [62]	Nano-structure multilayer coatings 1. TiAlCrN 2. TiAl55CrSiYN 3. TiAl60CrSiYN	Inconel 718 Vc=40 m/min F=0.1225mm/rev DoC=0.5mm	TiAl60CrSiYN coating outperformed others in terms of tool life due to its enhanced ability to form protective oxide tribo-films that had reduced adhesive interaction with the workpiece material.

Table 4: Effect of various types of state of the art PVD coating in turning of nickel alloys (contd.)

Authors	**Coating details**	**Workpiece/ operating parameters**	**Key results**
Fox-Rabinovich et al. [63]	Nanostructure coatings 1. AlTiN 2. TiAl55CrSiYN 3. TiAl60CrSiYN 4. TiAl60CrSiYN/TiAlCrN 5.TiAl55CrSiYN/TiAlCrN	1. Direct aged (DA) Inconel 718 Vc=40m/min 2. Powder metallurgical (PM) ME-16 nickel alloy Vc=50m/min F=0.125mm/rev and DoC=0.25mm were the same for both materials	For DA Inconel 718, TiAl60CrSiYN/TiAlCrN and TiAl55CrSiYN/TiAlCrN multilayered coatings showed better tool life due to their reduced intensity in BUE formation while for powder metallurgical ME-16, multilayer coating of TiAl55CrSiYN/TiAlCrN performed better. *Wear mode*: BUE formation.
Uhlmann et al. [64]	Nanostructure coatings 1.TiAlN-monolayer (2.5µm) 2.TiAlN+cBN (1µm) 3.TiAlN+cBN (1.4µm) 4. TiAlN+cBN (2µm) 5.TiAlN+cBN(0.4µm) +cBN(1µm) 6.TiAlN+cBN(0.4µm) +cBN(1.4µm)	Inconel 718 Vc=50m/min, F=0.1mm/rev DoC=0.5mm dry	cBN coatings outperformed the TiAlN coatings in terms of tool life, cutting forces and surface roughness with no breakage and fracture was seen with the former.

It is suggested that AlTiN coatings outperform conventional TiAlN coated products due to the higher aluminium (Al) content which provides increased thermal resistance [58]. Additionally, improved tool life of ~50% and 150% has been seen when AlTiN is combined with MoS_2 [9] or Cu [60] respectively in turning of Inconel 718 because of its lubricating properties and hence reduced tendency to weld to workpiece material. However, the addition of Cr, Si and Y in TiAlN based PVD coatings (TiAlCrSiYN) has shown benefits (~50%) in terms of tool life over state of the art commercial AlTiN coated inserts. This has been due to the improved oxidation, wear resistance and grain size refinement caused by Cr, Si and Y elements respectively [62]. Furthermore as can be seen in Figure 15, improvements in tool life using TiAlCrSiYN/TiAlCrN multilayer coating of up to 15% and 65% compared to monolayer TiAlCrSiYN and AlTiN respectively are reported when turning Direct Aged (DA) Inconel 718 and Powder metallurgy (PM) ME-16. This improvement was attributed primarily to a reduction in the intensity of BUE formation, higher hardness and good resistance to plastic deformation [63]. Built-up-edge formation and coating delamination were observed to be the main wear modes in the Ti,Al based coating products.

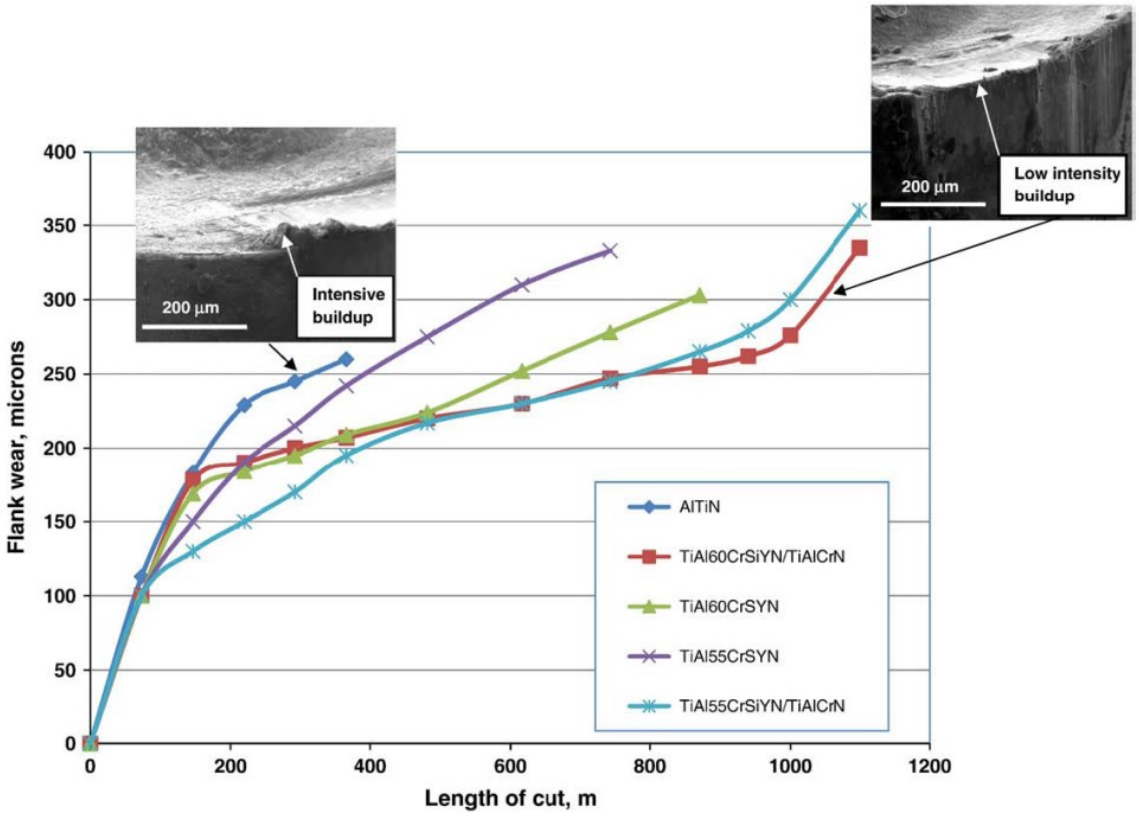

Figure 15: Flank wear vs machining length of different nano-structured coatings with SEM images when turning Inconel 718 [63]

Nanocrystalline cBN coatings have also shown potential when dry turning of Inconel 718 [64]. The coating was deposited on a WC substrate in a multilayer system. To increase the binding and adhesion of the cBN layer, TiAlN was the first layer in contact with the substrate and cBN deposited as the outermost layer while boron carbide was used as an intermediate layer, as shown in Figure 16 . Up to a 2-fold improvement in tool life was observed with the cBN coating compared to a TiAlN coated insert with no fracture or breakage. Additionally, an ~8% reduction in cutting force and ~40% reduction in surface roughness was recorded with the cBN system compared with the TiAlN coating. The better performance was reported to be due to its higher hardness and good temperature stability.

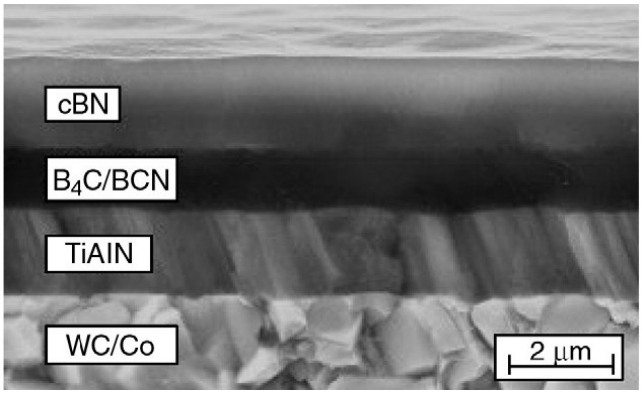

Figure 16: SEM image of cBN layer system [64]

From a CVD coating point of view, better performance has been observed with multilayer CVD coating TiCN/Al_2O_3/TiN than with PVD TiAlN and TiN/AlN coatings, particularly in finishing applications [7, 65]. With this CVD coating, a ~3-6 times improvement in tool life was observed by Kamata et al. [7] at Vc=60m/min, F=0.1mm/rev and DoC=0.1mm under wet cutting conditions when compared with TiN/AlN and TiAlN coated inserts respectively. For the same CVD coating, Bhatt et al. [65] recorded a 200% improvement in tool life compared with a TiAlN PVD coating at a cutting speed of 100m/min, feed rate of 0.125mm/rev and 0.25mm depth of cut when dry cutting. The better performance was due to its ability to act as a barrier against the propagation of cracks and fatigue stresses generated on the rake face as a result of chip removal. Furthermore, the coating was ~5 times thicker than the PVD coatings [65].

Workpiece surface integrity is of prime concern for nickel based alloys because they are used in critical parts of the engine. Surface tearing, cavities, carbide cracking, plastic deformation, metallurgical transformations, increased microhardness, work hardened layers, high levels of tensile residual stress levels, tensile layers and white layer formation are the common surface integrity problems reported in the literature when machining nickel alloys

with carbide tools [4, 40, 44]. Although some improvement in tool life and wear have been seen with coated tools, in terms of surface integrity, coatings do not appear to provide any significant advantage over uncoated tools [40]. Moreover, Sharman et al. [44], Outeiro et al. [66], Arunachalam et al. [67] and Ozel and Ulutan [68] observed higher workpiece tensile residual stresses with coated tools in comparison to their uncoated counterparts when turning Inconel 718. This was due to the fact that the coating prevented heat dissipation into the tool bulk, thus promoting greater heat localisation and hence higher tensile residual stresses. However, Arunachalam et al. [67] suggested that compressive residual stresses could be generated in turning of Inconel 718 with coated carbide tools using round shaped negative rake inserts (12mm diameter) with honed cutting edges, in the presence of a cutting fluid. In contrast, Li et al. [69] observed higher tensile residual stresses with uncoated tools when compared to coated inserts in finish turning of RR 1000, which seems to conflict with the results reported when turning Inconel 718. The discrepancies in the results were attributed to the different thermo-mechanical properties of both alloys (RR 1000 and Inconel 718) and/or due to the difference in the machining conditions used in the trials. Comprehensive reviews on machinability of nickel alloys have been presented by Choudhury and El-Baradie [70], Rachid et al. [4] and Ulutan and Ozel [40]. They recommended uncoated carbide tooling at relatively low cutting speed when finishing due to concerns over higher tensile residual stresses generated with coated inserts.

2.4.1.2 Effect of cutting environment: state of the art

The use of cutting fluid is generally recommended in the machining of nickel alloys with carbide tooling [38], due to improvements in tool life and the surface quality of the workpiece. Additionally, coolant lowers tensile residual stresses compared to dry cutting because it reduces the bulk temperature/heat [67]. In recent years, alternative cutting environments have been assessed with carbide tools in order to improve the tool life and surface integrity of the machined component. These techniques involve high pressure (HP) cooling [8, 71-72], air jet assisted machining (AJA) [73], minimum quantity lubrication (MQL) also called near dry cutting [74-76], micro-litre lubrication (μLL) [77], cryogenic machining [75, 78] and a combination of cryogenic and MQL [75]. In addition, dry cutting [54, 79] has also been evaluated as an alternative to wet cutting as the cost of cutting fluids is up to 4 times the cost of cutting tools [54] and accounts for ~17% of the total manufacturing cost [74]. It also has negative effects on the environment and human health [77], therefore greater attention has been paid by researchers to dry or near dry machining [80].

Some conflicting results were reported in terms of tool life when turning Inconel 718 at higher cutting fluid pressure. Ezugwu and Bonney [72] recorded up to a 7-fold improvement in the tool life in rough turning (DoC=2.5-3 mm) Inconel 718 at a cutting fluid pressure of 203bar compared to conventional cutting fluid supply. In contrast, no significant improvement in the tool life was recorded by Sharman et al. [71] when finishing. Here depth of cut and feed rate were fixed at 0.25mm and 0.35mm/rev respectively while cutting speed was varied between 40, 60 and 80 m/min with cutting fluid pressure up to 450bar. The authors argued that under finishing conditions, temperature generation was not sufficient to obtain the benefits of increased cooling produced by a high pressure jet [71]. The use of high pressure cutting fluid was unable to provide any significant benefit in terms of surface roughness [71-72] and surface integrity, however a reduction in the level of tensile stresses (~45%) was obtained at 450bar compared to conventional 5bar cutting fluid pressure due to the increased cooling ability of high pressure jet [71]. With pressures of up to 150bar, long continuous tubular chips were obtained but beyond this pressure, short and fragmented chips were recorded [71-72]. Courbon et al. [8] noticed a reduction in the value of cutting force by ~200N at a cutting fluid pressure of 130bar as opposed to 50bar. This effect was prominent only at low cutting speeds (46-53 m/min) due to a reduction in the tool chip contact length, while the pressure effect was negligible at higher cutting speeds (60-74 m/min) with no change in the value of cutting force.

Air jet assisted (AJA) turning is a relatively new approach reported by Obikawa et al. [73] in finish turning of Inconel 718. A full schematic illustration of this method is shown in Figure 17. Similar to MQL, compressed air is channelled through the tool holder to a nozzle at the flank face but in this case an oil mist is not used. An external nozzle is also employed to supply an emulsion type cutting fluid through different application angles to the tool tip. If instead of air, compressed nitrogen is supplied via the internal nozzle, it is called nitrogen jet assisted turning (NJA). Improvement in tool life up to 30% was observed in AJA machining compared to conventional wet machining for application angles of 10-30º at cutting speeds of 78m/min and 90 m/min, feed rate of 0.1mm/rev and DoC=0.2mm using CVD coated ($TiCN/Al_2O_3$) carbide tools. This was attributed to greater penetration of cutting fluid in the cutting zone due to the compressed air jet hence increasing the heat transfer from the cutting tool to the environment. No difference in the value of tool life was observed between AJA and NJA machining. The authors concluded that the tool wear caused by oxidation due to the air jet was negligible in the presence of sufficient cutting fluid to the tool face.

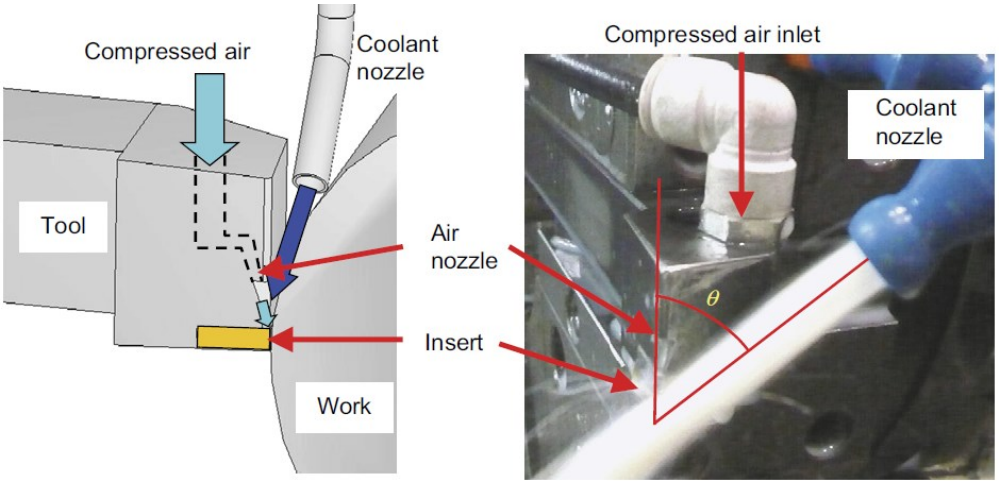

Figure 17: A schematic illustration of AJA machining method [73]

Better workpiece surface roughness and smaller depth of deformation of grain boundaries beneath the machined surface was observed by Yazid et al. [74] in MQL (50ml/h) compared to dry cutting, due to better lubrication effects with the former. PVD coated TiAlN carbide tools were used in turning of Inconel 718 with feed rates of 0.10mm/rev and 0.15mm/rev and depths of cut of 0.30mm & 0.50mm at cutting speeds of 90m/min, 120m/min and 150m/min. Samples were found to be work hardened to a greater depth (~500µm) when machined in a dry environment compared to the MQL (~250µm) environment. Thakur et al. [76] optimised the lubrication parameters in finish turning of Inconel 718 with uncoated carbide (K20) tools in an MQL environment. They found that an inclined nozzle supplying lubricant at a pressure of 13 MPa and flow rate of 10ml/min with a cutting speed of 40m/min proved to be the effective operating parameters in reducing the cutting force (145%), cutting temperature (180%) and flank wear (155%). Obikawa et al. [77] evaluated the cutting performance of CVD coated carbide ($TiCN/Al_2O_3/TiN$) inserts when turning Inconel 718 in micro-litre lubrication machining in which oil consumption was <1.00ml/h, much smaller (~10-100 times) than MQL [77]. In terms of tool life, ~113 % improvement was observed compared to dry cutting using a special nozzle, designed for oblique spraying at an angle of 45º, see Figure 18. Additionally, comparable results in terms of tool life were recorded with wet cutting at constant cutting speed, feed rate and depth of cut of 78m/min, 0.1mm/rev and 0.1mm respectively.

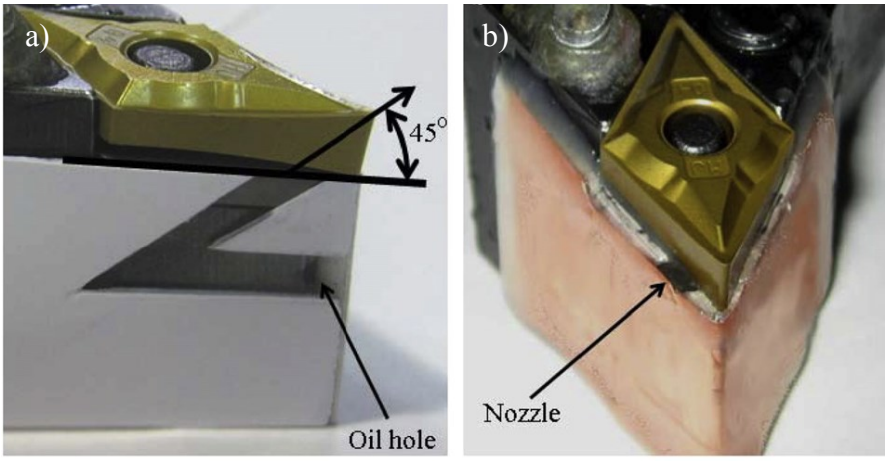

Figure 18: Special nozzle for oblique spraying (a) tool without a cover of copper sheet and (b) complete tool [77]

Cryogenic machining involves the application of liquid nitrogen to the rake face of the cutting tool in the direction of cutting [75, 78], however an additional nozzle can also be placed onto the workpiece to cool it prior to the cutting operation [75]. Pusavec et al. [75] compared surface integrity aspects of cryogenic machining with dry and MQL in turning of Inconel 718 under constant cutting conditions, where cutting speed, feed rate and depth of cut were 60m/min, 0.05mm/rev and 0.63mm respectively. Liquid nitrogen was applied both onto the rake face of the insert and the workpiece. Compared to dry and MQL cutting environments, lower surface roughness was obtained by up to ~22% and ~13% respectively. Although no significant differences in the value of surface residual stress were recorded, higher compressive stresses and a thicker compressive zone (70µm) beneath the machined surface was achieved with cryogenic operation when compared to dry cutting (40µm). Slight deformation of the grain boundaries up to 1-2 µm beneath the machined surface in the direction of cutting speed was observed for cryogenic machining but this increased to 5-10 µm with the dry and MQL environment. In another study, Thakur et al. [78] showed steady and progressive flank wear with reduced cutting forces (10-15 %) when the tool was treated cryogenically compared to an untreated tool. A Taguchi fractional factorial design (L8) was used to evaluate the effect of the cryogenic environment (tool with and without cryogenic treatment) at cutting speeds of 40m/min and 60m/min, feed rates of 0.08 and 0.20 mm/rev and depths of cut of 0.5 and 1 mm. The authors attributed the reduction in cutting force to higher wear resistance of the tool as a result of densification of the cobalt binder, which in turn increased the binding strength between carbide particles, present in the WC-Co (K20) tool. The cryogenic treatment did not provide any significant benefit in terms of workpiece surface integrity relating to work hardening or surface residual stresses.

Cost of production can be reduced by eliminating cutting fluids. Devillez et al. [79] and Cantero et al. [54] proved the feasibility of dry cutting over wet cutting by using CVD (TiCN-Al_2O_3-TiN) and PVD (TiAlN+TiN) coated inserts respectively in semi-finish turning of Inconel 718. A constant feed rate of 0.1mm/rev and depth of cut of 0.5mm were used in both cases. For the CVD coating, a cutting speed of 60m/min was considered to be the optimum which limited residual stress and provided an acceptable surface finish (Ra~1.3µm). Additionally, for the selected cutting speed condition the lubricant did not appear to influence the microstructural deformation and microhardness gradient in the machined surface layer in comparison to wet machining [79]. In the case of the PVD coated insert, a cutting speed of 50m/min was recommended in order to avoid chipping and notch wear.

2.4.2 Machinability of nickel based superalloys using conventional ceramics

Publications concerned with the machining of nickel alloys using conventional ceramics involving aluminium oxide (alumina), mixed alumina, silicon carbide whisker reinforced alumina and silicon nitride based ceramics are limited when compared with carbides. Ceramics are reported to produce adverse surface integrity, therefore their use is restricted to roughing applications [38]. To date, whisker reinforced compacts are the most widely employed material, however increasing applications have been found with Sialon tool materials. Mixed alumina tools have also been evaluated and in some cases they have outperformed silicon nitride based ceramics [81-82]. Use of pure oxides are not recommended in the machining of nickel alloys due to poor thermal shock resistance [83] and extensive notching at the depth of cut line. Ezugwu and Tang [84] evaluated alumina when turning Inconel 718 at a constant cutting speed of 152m/min, feed rate of 0.125mm/rev & depth of cut of 2.00mm and reported 769µm notch wear after only 1min of machining [84]. Notching at the depth of cut line is the major problem associated with ceramics; however this can be minimised using round inserts due to the small approach angle which in turn thins out the chips. Problems associated with round tool geometry relate to the fact that sharp corners cannot be generated, and when this is required, diamond and square shaped inserts should be used as alternatives [83].

2.4.2.1 Mixed alumina and Sialon ceramic tools: current trends

In the case of mixed alumina ceramic tools, round tool geometry has been evaluated at higher cutting speeds of 450-500 m/min, feed rates of 0.10-0.15 mm/rev and depth of cuts of 0.35-0.5 mm [85-87]. Poor performance in terms of tool life was observed with flank wear

of 300µm after machining only 185mm. Flank and notch wear were the dominant wear modes as shown in Figure 19 [86]. Higher workpiece tensile residual stresses (~1200 MPa) were recorded in dry cutting [85], while the use of coolant generated compressive residual stresses (-800 MPa) [86]. Additionally, up to a 2-fold increase in cutting temperature and ~40N higher cutting forces were observed with dry cutting in comparison to employing MQL [87]. Lower values of surface roughness (<0.5µm) were attributed to the larger nose radius associated with the round insert which reduced the cusp height of the machined surface [86-87].

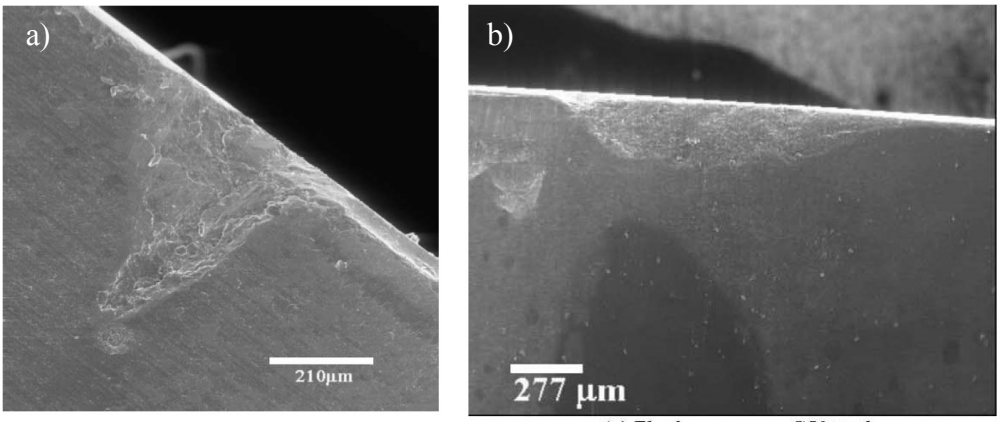

Figure 19: Typical wear pattern of mixed alumina ceramic tool (a) notch wear and (b) flank wear [86]

Axinte et al. [41] evaluated Sandvik manufactured Sialon grade 6080 at cutting speeds of 175-250 m/min, feed rates of 0.15-0.25 mm/rev and depth of cuts of 1-2 mm when turning RR_X (powder manufactured nickel based alloy) however, exact details of the workpiece material were not mentioned by the authors. Rapid failure of the insert was observed after a spiral length of ~50m due to large chipping. Similarly, a tool life of less than 130sec was recorded by Vagnorius and Sorby [88] with the above mentioned Sialon grade at V=300m/min, F=0.2mm/rev and depth of cut of 1.0mm when turning Inconel 718. Kennametal grades of Sialon tools KY2000 and KY2100 are generally recommended both for semi-finishing and roughing applications [89-91]. For semi-finishing applications, cutting speeds between 125-133 m/min are suggested with feed rate and depth of cut of 0.2mm/rev and 0.4mm respectively [91]. In case of roughing, a cutting speed of 250m/min, feed rate of 0.2mm/rev and depth of cut of 1.5mm were the preferred operating parameters [90]. Both round and square tool geometries have been evaluated and higher values of cutting force (~200N) were recorded with the former due to the larger contact radius [89].

Recently, Sialon-Si_3N_4 functionally graded nano-composite ceramics were evaluated in finish turning of Inconel 718 without coolant at constant feed rate and depth of cut of

0.1mm/rev and 0.1mm respectively with cutting speed varied from 80-270 m/min [92-93]. The tools were manufactured by adding nano-sized particles of Si_3N_4 and Al_2O_3 with micro powder of the same composition. The composition of different composites is given in Table 5 [92]. Graded structures were produced with five layers and coded GSS1 and GSS2. The corresponding composition of each layer is given in Table 6 while Figure 20 highlights the cube shaped model of the graded material [92].

Table 5: Composition of different composites [92]

Composites	Si_3N_4 (0.5 μm)	Si_3N_4 (0.02 μm)	Al_2O_3 (0.5 μm)	Al_2O_3 (0.1 μm)	AlN (0.5 μm)	$TiC_{0.7}N_{0.3}$ (0.5 μm)	Y_2O_3
SAAT10	53.25	17.75	0	10	5	10	4.0
ST10	61.50	20.50	3.2	0	0	10	4.8
ST15	57.75	19.25	3.2	0	0	15	4.8
ST20	54.00	18.00	3.2	0	0	20	4.8

Table 6: Composition of the graded structure [92]

Specimen code	1st (5th) layer	2nd (4th) layer	3rd layer
GSS1	ST10	ST15	ST20
GSS2	SAAT10	ST15	ST20

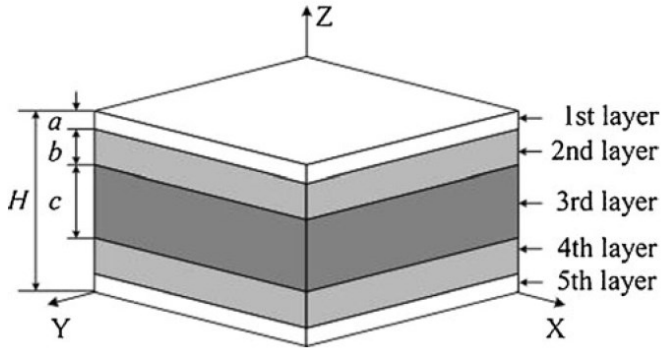

Figure 20: Cube shaped model of five layered graded material with symmetrical structure [92]

For comparison, homogeneous reference materials (SAAT10 and ST10) and Kennametal grade KY1540 were tested against the graded materials. Relevant properties of all evaluated materials are presented in Table 7 [92].

Table 7: Mechanical properties of the tool materials [92]

Tools	Flexural strength (σ_f, MPa)	Fracture toughness (K_{IC}, MPa $m^{1/2}$)	Vicker's hardness (HV, GPa)
GSS1	980±60	9.54±0.52[a]	16.91±0.30[a]
GSS2	810±30	9.33±0.46[a]	16.98±0.24[a]
ST10	860±90	8.19±0.91	16.29±0.23
SAAT10	645±95	7.80±0.55	16.59±0.31
KY1540		7.45±0.61	18.24±0.25

With a tool life criterion of 300µm flank wear, an ~8min tool life was recorded with the GSS1 tool at a cutting speed of 200m/min which was ~77% higher than for GSS2 & SAAT10 and 34% higher than for KY1540 & ST10. The longer tool life with GSS1 was attributed to its higher flexure strength and fracture toughness [92]. When the cutting speed was increased to 200m/min [92] and 270m/min [93], less than 3.5min tool life was recorded with no significant difference among the evaluated materials [92-93]. Surface roughness ranged between 1-2 µm for all the tool materials but a decreasing trend was noticed with increase in the cutting speed [92].

Ezugwu et al. [81] observed ~50% improvement in tool life using mixed alumina ceramic tools over Sialon when machining Inconel 718 at a cutting speed of 270m/min, feed rate of 0.125mm/rev and depth of cut of 1.5mm in the presence of coolant. They evaluated nano-ceramic tools in their study in which the major phase (Si_3N_4 or Al_2O_3) had a nanometer grain size. The authors attributed the poor performance of Sialon ceramic tools to high cutting temperature generated at elevated cutting speed which in turn softened the constituent materials (Si_3N_4, TiCN or SiC) and subsequently weakened the bond strength.

2.4.2.2 Performance of Whisker reinforced ceramic inserts

To date, Sandvik CC670 whisker reinforced alumina ceramic has been widely investigated in turning of nickel based alloys particularly Inconel 718 and Nimonic C-263. Sandvik recommend operating parameters for this grade of Vc=200-300 m/min, F=0.15-0.2 mm/rev and DoC=1-3 mm [30]. In an earlier publication, Gatto and Iuliano [94] evaluated CC670 in its coated (TiAlN and CrN) and uncoated state at constant depth of cut of 1.5mm under dry operating condition. Cutting speed and feed rate were at 3 levels i-e 300, 400, 530 m/min and 0.08, 0.12, 0.22 mm/rev respectively. The better performance of the TiAlN coated insert was attributed to its higher maximum working temperature capability compared to CrN and the uncoated inserts. For a fixed machining volume of $40cm^3$, the TiAlN coated insert produced lower flank (57-68 %) and notch wear (33-38 %) in comparison to the uncoated and CrN coated inserts at a higher cutting speed of 530m/min and feed rate of 0.12mm/rev. Recrystallisation in the immediate subsurface of the workpiece with a grain size of 200-300nm was observed by Zhou et al. [95] when using a CC670 whisker reinforced ceramic insert in high speed turning of Inconel 718 under constant operating parameters at: Vc=300m/min, F=0.2mm/rev, DoC=0.3mm. New, semi-worn (VB_Bmax.=150µm) and worn tools (VB_Bmax.=300µm) were employed in the presence of coolant. Electron backscatter diffraction (EBSD) was used to characterise the deformation depth and thickness of the

deformed layer which was of the order of 50µm with the new tool. This was further increased to ~100µm and 250µm when semi-worn and worn tools were employed [95], a white layer (WL) occurring only with worn tools. In dry machining, the WL was not present with new tools, while semi-worn and worn tools did produce WL's. In related work the WL was found to consist of nano-crystalline grains (50-150 nm) which included the phases of the parent bulk material [96]. Ezilarasan et al. [97] optimised machining conditions in turning Nimonic C-263 superalloy using CC670 inserts for minimum cutting force, flank wear and surface roughness. A cutting speed of 250m/min, feed rate of 0.05mm/rev and depth of cut of 0.50mm were the preferred cutting parameters with a measured cutting force of 461N, flank wear of 270µm and surface roughness Ra of 2.36µm. Feed rate and depth of cut were found to influence flank wear more significantly than cutting speed which suggests that higher productivity could be achieved by employing higher cutting speeds without significantly affecting tool wear. In general, an increase in the microhardness value of the machined surface up to twice that of the bulk hardness was observed with the hardened layer extending to a depth of ~600µm. Workpiece residual stresses were tensile; 725-850 MPa and were observed when using worn inserts (after 9 min of machining) [98].

Ezugwu et al. [99] studied the performance of SiC whisker ceramic inserts under conventional and high pressure cooling at 11, 15 & 20.3 MPa. Cutting speed was evaluated at 200m/min, 270m/min and 300m/min while feed rate was 0.1mm/rev and 0.2mm/rev. Depth of cut was held constant at 0.5mm. Tool life was seen to increase up to a cutting fluid pressure of 15MPa but further increase in the pressure to 20MPa caused a reduction due to accelerated notching produced by high pressure water jet impingement erosion. In addition, work hardening up to a depth of 200µm beneath the machined surface was observed irrespective of the cutting fluid pressure. Additionally, plastic deformation of the surface layer extended to between 30-50 µm below the machined surface under high pressure cooling.

Whisker ceramic insert WG-300 from Greenleaf Company was evaluated in hybrid machining of Inconel 718 [100] involving liquid nitrogen cooling of the tool and plasma assisted heating of the workpiece. Testing has also been undertaken on laser assisted turning of Waspaloy [101]. In the former case, the approach provided 170% higher tool life, 250% improvement in surface roughness and 30-50 % reduction of cutting forces compared to conventional machining. In laser assisted turning of Waspaloy, a 50-60 % improvement in tool life and 20% reduction in the value of cutting forces were observed compared to conventional machining. In addition, laser assisted machining avoided the strong work

hardening effect due to a reduction in the resultant dislocation density as a result of higher temperature (~400ºC) [101].

In an investigation carried out by Zhou et al. [21] on the surface damage in finish turning of Inconel 718 under the operating parameters listed in the Table 8, cracking and breakage of niobium (NbC) and titanium carbide (TiC) were the most common types of damage observed on the machined surface. According to the authors, cutting environment (dry, wet) and tool wear (new, semi-worn VB_Bmax.=200µm, VB_Bmax.=300µm) produced more pronounced effects on the surface damage than the overall effect of operating parameters. Under dry cutting conditions, chip debris, BUE and side flow were considerably higher in the presence of tool wear.

Table 8: Variable factors and levels when turning Inconel 718 using silicon carbide whisker ceramic inserts [21]

Variable factors	**Levels**
Cutting speed (m/min)	100, 200, 300, 400
Feed rate (mm/rev)	0.1, 0.15, 0.2
Depth of cut (mm)	0.3

2.4.3 Machining of nickel based superalloys using polycrystalline cubic boron nitride (PCBN) tooling

Figure 21 highlights the different costs for finish turning of Inconel 718 relative to material removal rate. Despite the low cost of carbide tools, they are generally employed at relatively low cutting speeds (~50-80 m/min), therefore cost per kg associated with these tools is quite high. Coated whisker ceramic tools can be used at much higher cutting speeds (up to 600m/min). These tools cannot be used for finish machining of critical parts due their unfavourable cutting edge geometries, but their application on large turbine discs produced from advanced Ni alloys has proven to be cost efficient, as shown in Figure 21 by the lowest cost/kg rating. Higher capital cost PCBN tools can improve the stock removal rate by employing higher cutting speeds (~300m/min) and significantly reduce finish machining times and provide a competitive alternative to coated carbide tools. Moreover, they showed more uniform and predictable tool wear patterns for long spiral cutting lengths and enabled a full face of the component can be machined without tool change [10]. Due to all these stated benefits, the use of PCBN tools has increased in the machining of nickel alloys and the following section summarises research carried out in this area.

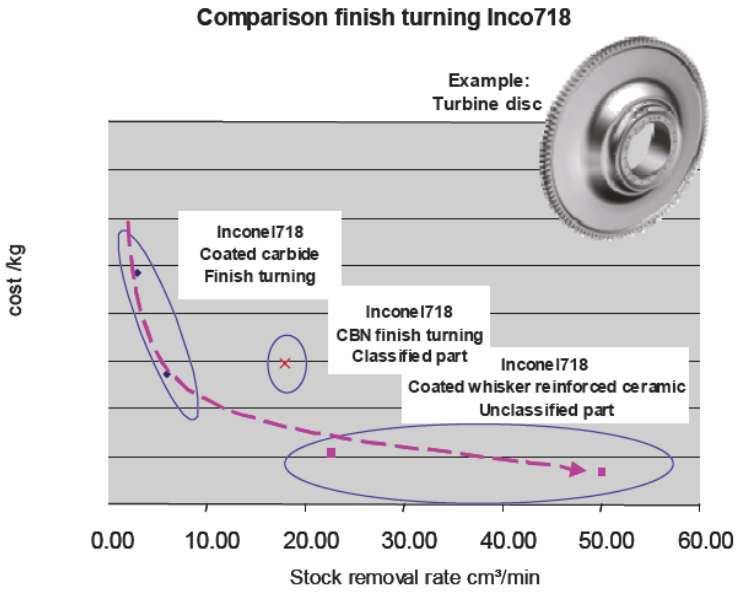

Figure 21: Cost modelling in terms of cost/Kg for finish turning of Inconel 718 material using coated carbides, PCBN and coated whisker ceramic tools [10]

2.4.3.1 Effect of tool edge preparation

It is well known that edge preparation plays a vital role in the machining performance of PCBN cutting tools and is necessary in order to maintain the integrity of the cutting edge. Different types of edge preparation have been evaluated in high speed turning of Inconel 718. In work undertaken by Uhlmann and Ederer [102], an unchamfered & honed tool cutting edge was preferred over a chamfered and honed edge. In the latter arrangement ~11% higher tool wear and 21% higher cutting forces were recorded due to higher mechanical loading as a result of larger tool chip contact length. All edges were honed to give a 20µm radius while with chamfered inserts, chamfer width was varied from 0.10mm to 0.25mm at a constant chamfer angle of 20º. Figure 22 clearly demonstrates that chamfered edges generated higher cutting forces in comparison to their unchamfered counterparts [102].

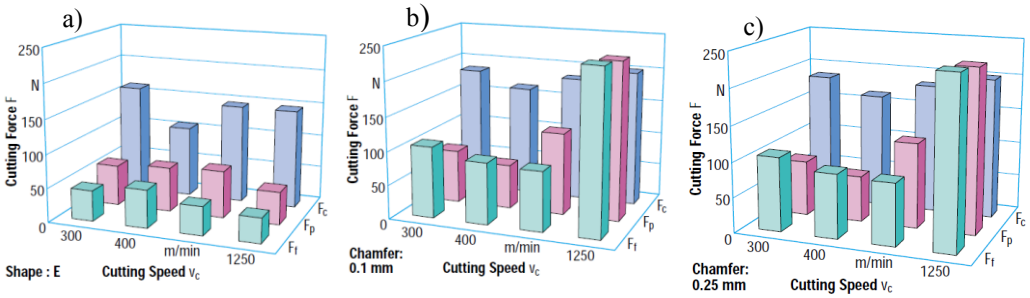

Figure 22: Cutting force components of different tool geometries (a) unchamfered & honed edge; (b) chamfered & honed edge with chamfer width of 0.10mm and (c) chamfered & honed edge with chamfer width of 0.25mm [102]

In another study [42], a chamfered (0.1mm×30) and honed edge generated compressive residual stresses and a higher degree of work hardening in the machined sub-surface up to a depth of 50µm compared to a tool employing only a chamfered. This was due to the larger contact area associated with the chamfered and honed edge which in turn increased the ploughing effect, thereby inducing higher mechanical deformation and increasing compressive material deformation beneath the machined surface (see Figure 23) [42].

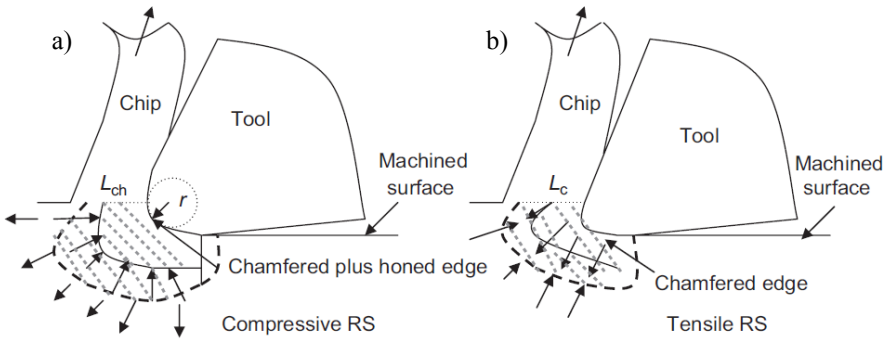

Figure 23: Schematic illustration of generation of residual stresses with (a) chamfered plus honed edge and (b) chamfered edge [42]

It has been reported that cutting forces are influenced by the thermal softening of accumulated material ahead of the cutting edge. Cutting speed, feed rate, depth of cut and tool edge geometry significantly influence the accumulation of material. Pawade et al. [103] observed that using a chamfered and honed cutting edge proved to be effective in reducing machining forces at 125m/min by directly influencing thermal softening of the accumulated material ahead of the tool, as shown in Figure 24. Its effectiveness however was not as significant at higher cutting speeds (300m/min, 450m/min), where thermal softening was dominated by the cutting speed. The authors conclude that in the case of a sharp edge, surface roughness is only affected by feed rate and nose radius while with modified edge geometries, their effect is suppressed due to the extension of material accumulated ahead of the cutting tool beyond the tool point [103].

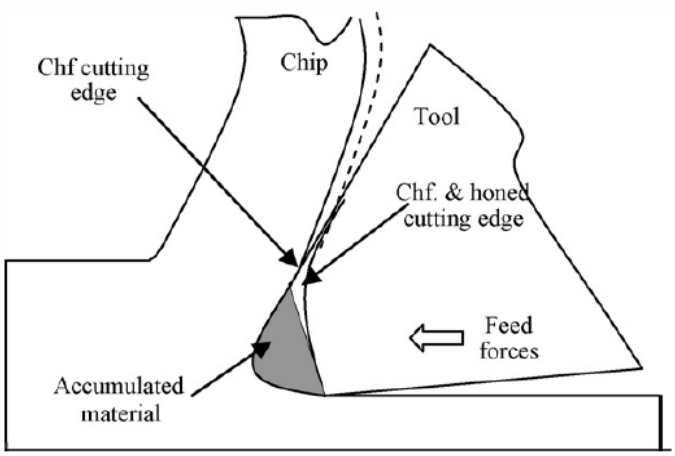

Figure 24: Schematic illustration of chamfered cutting edge with material blockage [103]

Kato et al. [104] preferred 30µm edge radius tools over 10µm in end milling of Inconel 718 where ~50% higher tool life was observed with the former at a cutting speed of 150m/min, feed rate of 0.05mm/tooth and 0.1mm depth of cut.

2.4.3.2 Effect of tool geometry

In general, round tool geometry is preferred however this has limitations in relation to workpiece geometrical requirements, therefore rhomboid (C-type) and square inserts have also been evaluated in the machining of Inconel 718. Round and C-type tool geometries were compared in terms of tool life [105], residual stresses and surface roughness [85] when facing Inconel 718 at a cutting speed of 225m/min, feed rate of 0.15mm/rev and depth of cut of 0.5mm in the presence of coolant. Breakage of the cutting edge at the notch region caused by rapid crater wear was observed with both tool geometries, however, up to a 2-fold improvement in tool life was observed with the round insert due to reduction of pressure in the notch region facilitated by the smaller approach angle [105]. Figure 25 shows the effect of insert geometry on surface roughness, measured at 3 points from the periphery in a facing operation, a schematic of which is illustrated is depicted in Figure 26. Here the C-type insert generated higher surface roughness values (Ra=3.8µm) compared with the round inserts (Ra=0.4µm) [85].

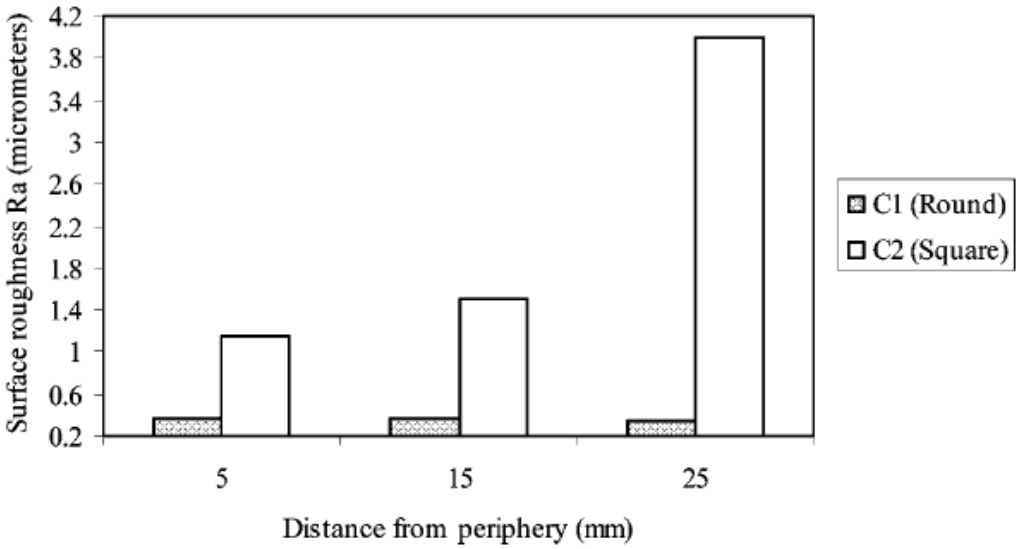

Figure 25: Effect of tool geometry on surface roughness [85]

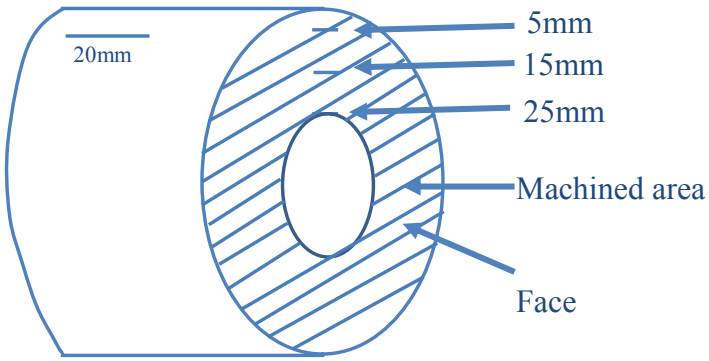

Figure 26: Schematic illustration of a machined specimen showing the measurement points

The higher value of surface roughness with the C-type geometry was attributed to its smaller nose radius and deposition of broken BUE onto the machined surface. Compressive residual stresses were produced with the round insert up to 15mm from the periphery which then changed to tensile stresses, whereas C-type tools produced only tensile stresses employing 6mm radius , see Figure 27 [85]. In other work, round inserts also outperformed square and triangular inserts employing 6mm radius in high speed turning of Inconel 718 where a ~63% lower surface roughness value was recorded with the former due to its larger radius [86-87].

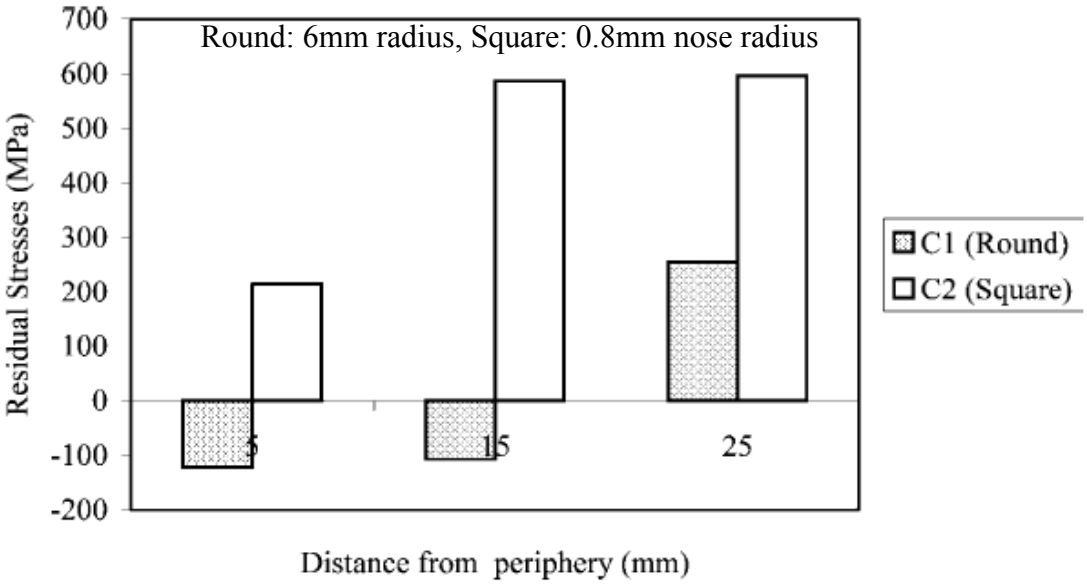

Figure 27: Residual stresses as a function of tool geometry [85]

In the machining of Inconel 718, forged and powder processed Rene 95, Lee et al. [106] identified seizure and pullout of material by the chip as the main cause of notching at the depth of cut line. They further concluded that notch formation in PCBN tools could be avoided by using less than 90º side cutting edge angle and employing negative rake geometry which reduces the lateral flow of the material at the side. More precisely, Klocke et al. [107], Koing and Gerschwiler [108] recommended a value of 30-45º for side cutting edge angle. Figure 28 shows the difference between approach and side cutting angles in single point turning.

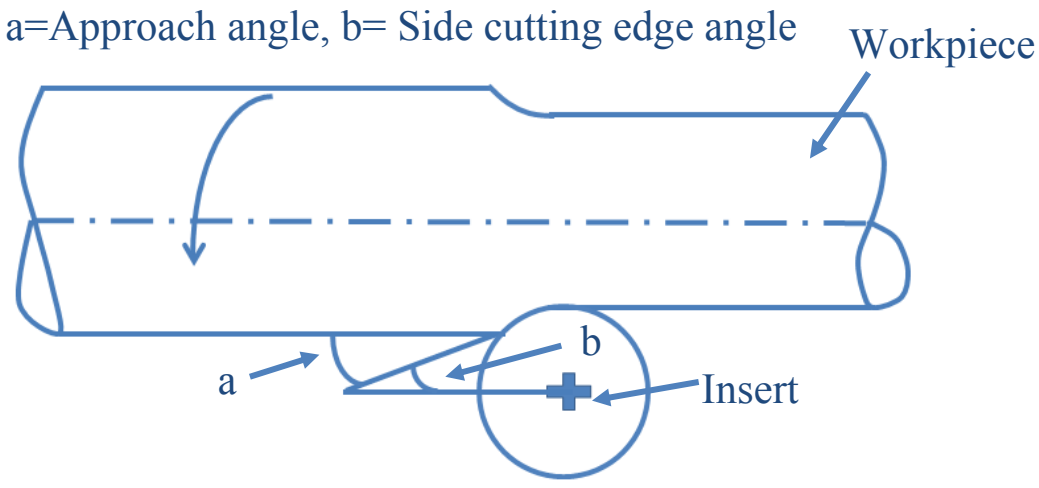

Figure 28: Approach and side cutting edge angles in single point turning

2.4.3.2 Effect of tool surface condition

Recently, Bushlya et al. [109] investigated the effect of TiN coating on the performance of PCBN cutting tools in high speed turning of Inconel 718. Three levels of feed rate (0.10, 0.15 and 0.2 mm/rev) and cutting speed (250, 300, 350 m/min) were employed. Constant depth of cut was used at 0.3mm and tests were carried out in the presence of coolant. Lower values of cutting forces with the coated tools were expected due to their low coefficient of friction but surprisingly, ~10-20% higher values of cutting force were recorded compared with the uncoated cutting tools due to a ~34% larger edge radius, see Figure 29 [109-111].

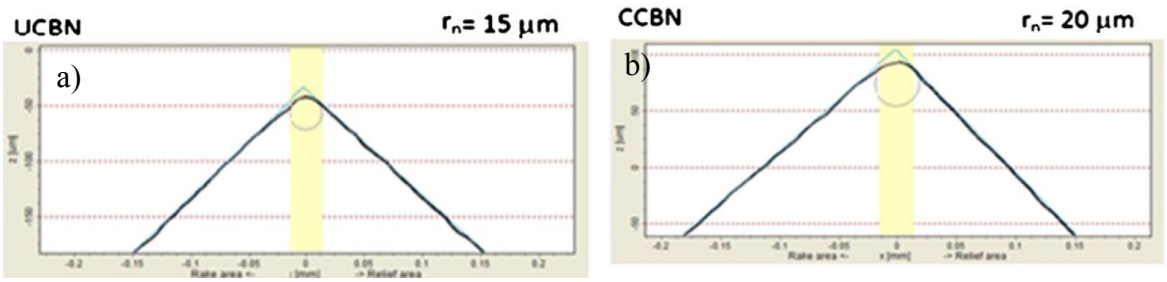

Figure 29: Cutting edge profile of a) uncoated and b) coated tools [110]

Figure 30 shows that the benefit of the coating was limited only to a cutting speed of 250m/min where ~20% higher tool life was recorded. When cutting speed was increased to 300m/min and 350m/min, no significant difference in tool life was observed due to rapid oxidation of the TiN coating. Additionally, at the highest cutting speed of 350m/min, tool fracture occurred with both uncoated and coated tools [110].

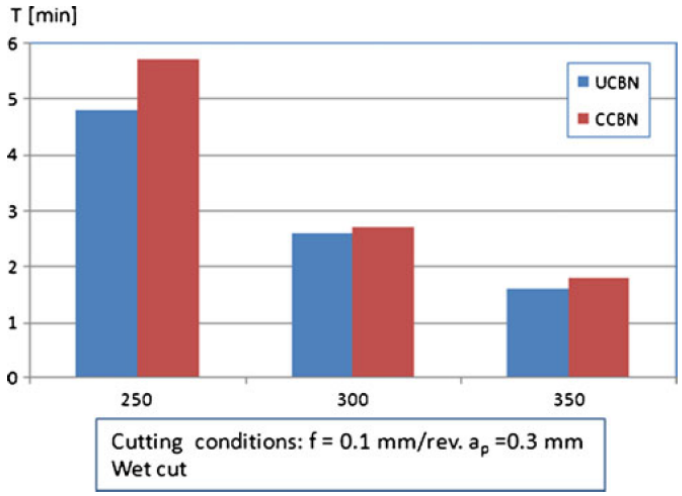

Figure 30: Tool life at a cutting speed of 250, 300 and 350 m/min with 300µm tool life criterion [110]

Additionally, thermal cracks and coating delamination were also seen on SEM wear scar micrographs of the worn tools as shown in Figure 31 but their influence on tool life was limited. Furthermore, Focused Ion Beam (FIB) milling revealed deep propagation of the cracks into the body of the tool (Figure 32) [111].

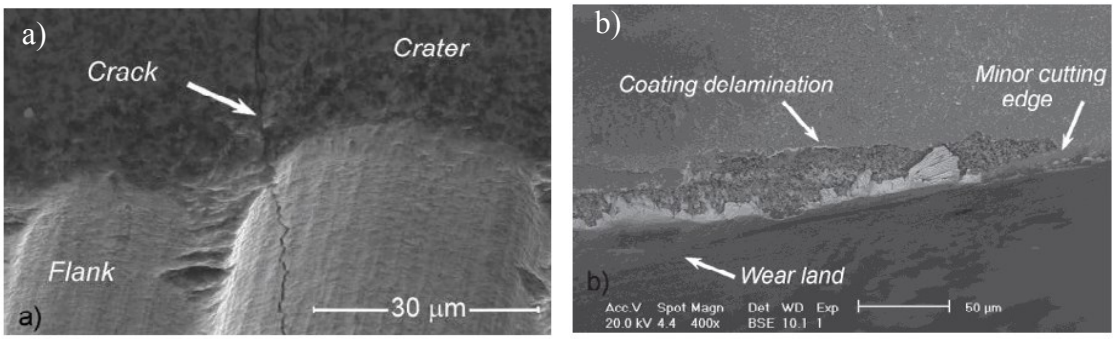

Figure 31: (a) Thermal cracks and (b) coating delamination [111]

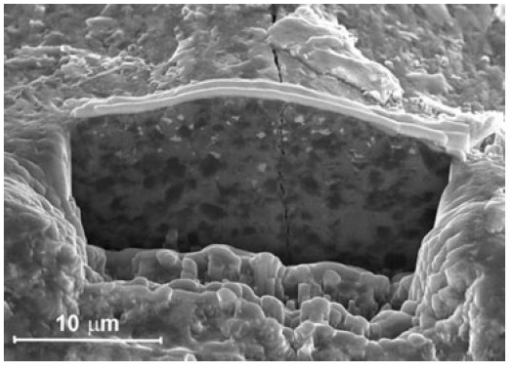

Figure 32: Crater of uncoated PCBN tools showing FIB milling [109]

When machining with the coated tools, a dramatic increase in the value of surface roughness (~100%) was recorded over the uncoated inserts due to severe material side flow. It was suggested that the larger edge radius on the coated tools caused greater plastic deformation between the tool and workpiece and subsequently increased material side flow at the trailing edge. In addition, the TiN coated insert generated higher temperatures due to its low thermal conductivity (28 W/mK). This had further intensified the side flow of the material from the trailing edge of the tool due to workpiece material softening [110].

The effect of TiN coatings has been analysed in terms of workpiece microstructure [111], nanohardness [110] and residual stresses [111]. Significant bending and elongation of the grain boundaries were observed in the direction of cutting speed up to a depth of 10-15 µm both with coated and uncoated PCBN tools but which was more severe with the coated insert. This was due to the higher temperature generated with the coating which increased the plasticity of the material, hence allowing more intensive deformation [111]. Moreover, all samples were strain hardened to a depth of ~60µm with a maximum hardness of ~680HV

before dropping to a bulk hardness of 550HV. Nano-hardness values were slightly higher for the specimen machined with the coated tools due to the higher ploughing effect associated with the larger edge radius [110]. Figure 33 shows that both types of PCBN tool generated compressive residual stresses, however lower values of sub-surface compressive residual stresses were seen with the coated tools due to low thermal conductivity of the coating which increased cutting temperatures. Furthermore, the depth of the stress profile was smaller (~100 µm) with the uncoated tools in comparison to their coated counterparts (~120 µm) [111].

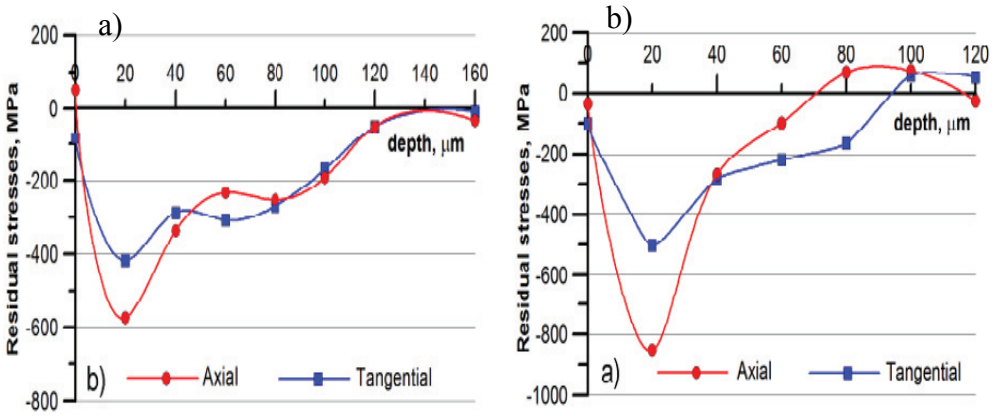

Figure 33: Residual stresses profile (a) coated and (b) uncoated PCBN tools [111]

2.4.3.3 Effect of cutting environment

Sadao [112] compared the performance of PCBN tools in dry and MQL (droplet volume 5cc/min) cutting environments when finish turning of Inconel 713 at a constant feed rate (0.1mm/rev) and depth of cut (0.1mm) with cutting speed varied between 90-200 m/min. At 90m/min, a significant improvement (5-times) in tool life was recorded with MQL compared to dry cutting, however at the higher cutting speed of 200m/min, no significant difference in tool life was seen. A marked reduction in the value of cutting temperature (45%) and improvement in surface finish (22%) was also observed by Silva and Soares [87] with MQL over dry cutting in high speed turning of Inconel 718 using constant operating parameters at Vc=500m/min, F=0.10mm/rev and DoC=0.35mm.

In another investigation, the effect of cutting fluid pressure was studied by Kato et al. [104] when machining Inconel 718 using PCBN endmills. An external nozzle supply was used for low and high pressure (5MPa) evaluation, while an internal (through spindle) supply was also tested using high pressure. This latter arrangement produced ~50% higher tool life compared with the use of an external nozzle. Additionally significant adhesion of the workpiece on the tool was observed with an external coolant supply irrespective of the

pressure. It was believed that the fluid was unable to reach the cutting edge with the external nozzles.

Arunachalam et al. [85] evaluated the effect of dry and wet cutting on residual stresses and surface roughness when facing age hardened Inconel 718 at 2 levels of cutting speed (150m/min & 225m/min) at a feed rate and depth of cut of 0.15mm/rev and 0.5mm respectively when employing round insert (12mm ø). At both cutting speeds, tensile residual stresses were generated when dry cutting whereas use of cutting fluid produced compressive residual stresses up to 15mm from the periphery which then changed to tensile residual stresses (see Figure 34). The dominance of mechanical effects/compressive stresses with the cutting fluid was attributed to its higher capacity of heat removal from the machined surface.

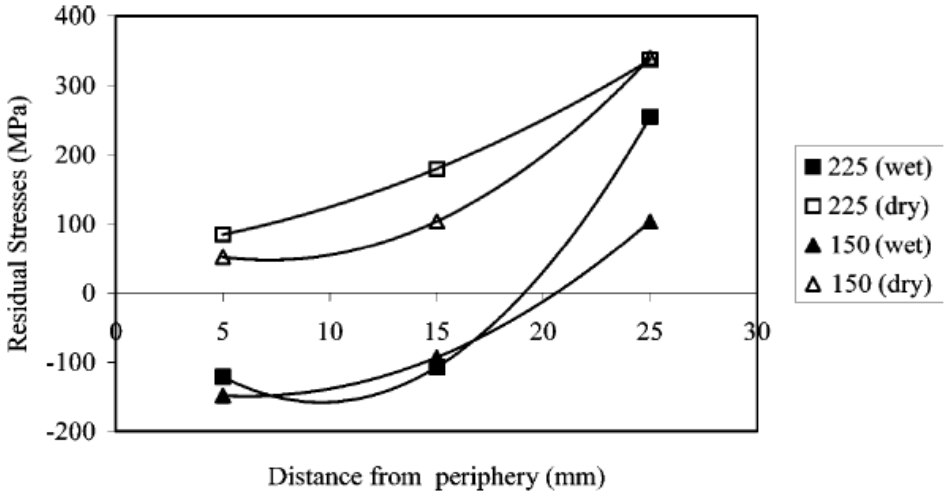

Figure 34: Effect of cutting fluid on workpiece residual stress at two different cutting speeds of 150m/min and 225m/min [85]

Figure 35 highlights the effect of cutting fluid on the value of surface roughness and it is quite evident that higher values of surface roughness were recorded in dry cutting due to the deposition of BUE on the machined surface as shown in Figure 36. A ~50% improvement in surface finish was observed in the presence of cutting fluid [85].

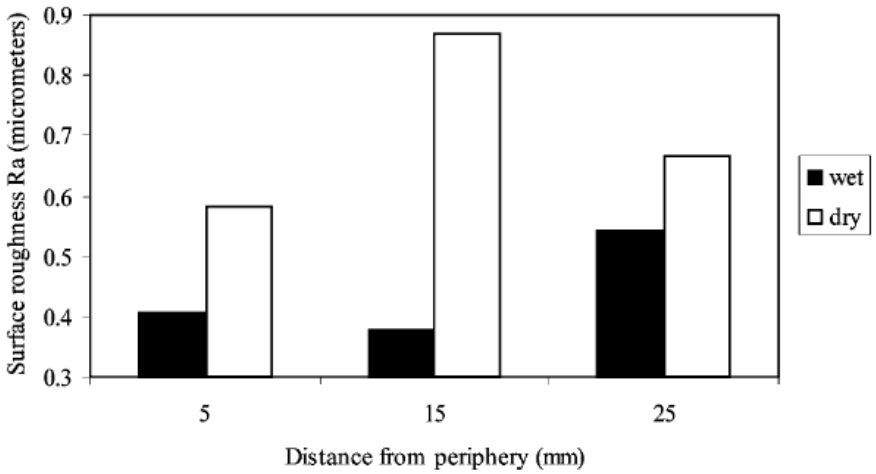

Figure 35: Effect of cutting fluid on surface roughness [85]

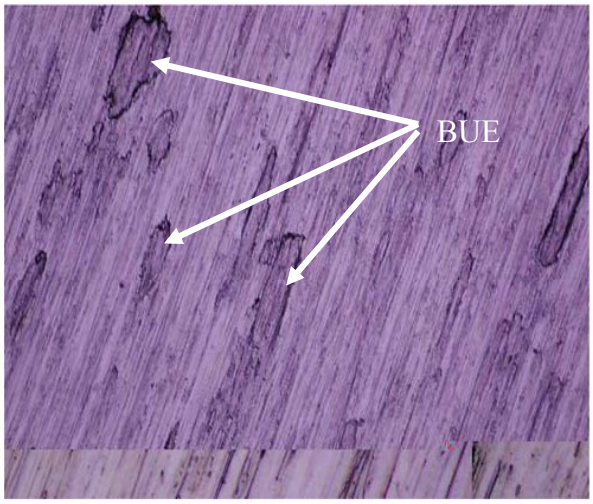

Figure 36: Optical micrograph showing the deposition of BUE's on the machined surface in dry cutting [85]

2.4.3.4 Effect of CBN content, grain size and binder phase

In general, low content (30-50%) PCBN tools with a ceramic binder (TiC or TiN) and fine grain size (1-2 µm), are generally preferred in high speed machining of nickel based superalloys [5, 107-108]. However over the past few years, investigations have been carried out in order to find out the optimum combination of CBN content, grain size and type of binder. Table 9 details the level of CBN content and binder types assessed by Takatsu et al. [113], in all cases the grain size was 1µm except BZN tooling with 3µm grain size . Cutting speed, feed rate and depth of cut were kept constant at 90m/min, 0.1mm/rev and 0.5mm respectively and tests were conducted in the presence of coolant.

Table 9: CBN contents and type of binder [113]

CBN content (% by volume)	Binder
50	TiC
60	TiC
70	TiC
90 (BZN by GE)	Ni/Co metallic binder

Welding of the workpiece material was prevalent in all the tests while chipping was observed to be the decisive factor for tool life determination. After 3min of cutting, the BZN tool exhibited 100µm less flank wear compared to all other tools in the study due to its better chipping resistance and higher hardness [113]. It is important to note that hardness of PCBN tools increases linearly with the increase in CBN content, provided that grain size and binder remain fixed [114]. Similar findings were observed by Kono et al. [115], where ~40% higher tool life was observed with PCBN inserts having 85% CBN content (BN100) compared to 65% CBN (BN200). Both inserts had a TiN ceramic binder and were evaluated at Vc=100m/min, F=0.2mm/rev and DoC=0.2mm. Additionally, Wick [116] also preferred BN100 over BN200 when turning superalloys due to the high hardness of the former.

Shintani et al. [117] studied 3 different types of PCBN tool in turning of Inconel 718 and Table 10 shows the percentage of CBN content, grain size and binder type for the tools evaluated in the study.

Table 10: Details of CBN contents, binder type and grain size [117]

CBN content (% by volume)	Binder	Grain size (µm)
60	TiC	3
60	TiN	3
80-85	Co-binder	6

Cutting speed ranging from 60m/min to 240m/min was tested at a fixed feed rate (0.1mm/rev) and depth of cut (0.1mm). The maximum tool life for all three tools was obtained between 120m/min to 180m/min with mutual diffusion between the binder phase and workpiece material identified as the main cause of tool wear. The PCBN tool with the TiN binder showed the longest tool life due to its better diffusion resistance. Interestingly, low CBN content tools performed better than higher ones, which conflicts with the results reported by Takatsu [113] and Kono [115]. It is important to note however that hardness is not only a function of CBN content alone. Harris et al. [114] showed that an insert with 80% CBN had lower hardness (9.5 GPa) than one with 50% CBN (10.5 GPa) at a temperature of

1250ºC, as shown in Figure 37. PCBN insert with 50% CBN content had smaller grains (1-2µm) compared to the 80% CBN content tool (8µm). Thus the grain size is another important parameter contributing the hardness in PCBN tools. Although the hardness details of PCBN tools were not mentioned by Shintani et al. [117], it could be expected that 60% CBN content tools might have higher hardness due to the smaller grain size (3µm) in comparison to products with larger grains (6µm).

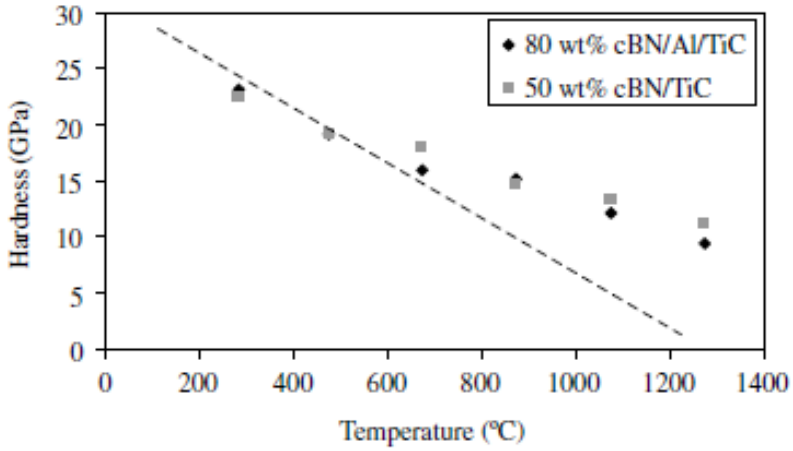

Figure 37: Hardness comparison between 80 and 50 wt. % CBN content PCBN tools [114]

Recently, Costes et al. [118] evaluated the effect of grain size, binder and CBN content on tool life at a cutting speed of 200m/min, feed rate of 0.2mm/rev and 0.3mm depth of cut using round tool geometry, see results in Figure 38. It was observed that high CBN content (above 80%) gave an average tool life of 2.8min which could be increased by a factor of four with the PCBN tools having a CBN content below 65%. Additionally, the combination of a ceramic binder with high CBN content gave low values of tool life whereas longer tool lives were recorded when a ceramic binder was employed with low CBN content tools. Grain size was also varied from 2µm to 8µm but variation in the grain size with low CBN content was not significant.

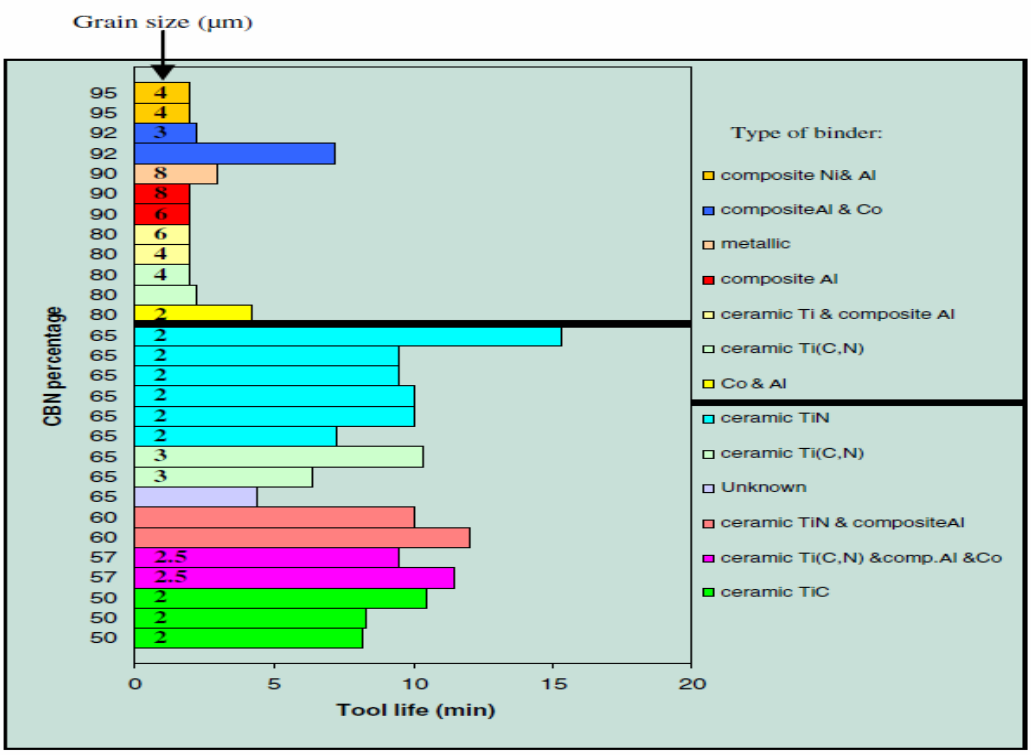

Figure 38: Tool life of different CBN content PCBN tools [118]

Further investigation was carried out to study the effect of CBN content, i-e 30%, 45% and 60% at 3 different cutting speeds of 250m/min, 350m/min and 450m/min with TiC binder and a 1µm grain size. Results are summarised in Figure 39 which shows that a cutting speed of 450m/min was not suitable due to catastrophic fracture and chipping of all PCBN tools after 5min of machining [118].

		CBN content					
		30 %		45 %		60 %	
Vc (m/min)	250	45 s	300 s	45 s	300 s	45 s	300 s
	350	45 s	300 s	45 s	300 s	45 s	300 s
	450	45 s	300 s	45 s	300 s	45 s	300s
Progressive wear (1)	Catastrophic wear (2)	Chipping (3)	(1) + (3)	(2) + (3)			

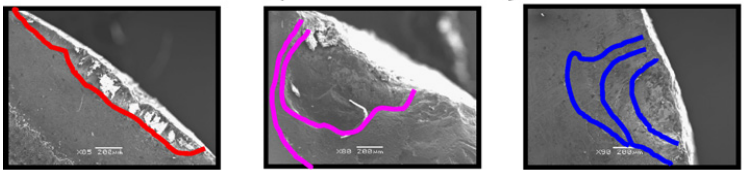

Figure 39: Effect of CBN content and cutting speed on tool wear [118]

In terms of tool wear, poor results were obtained with the 30% CBN insert as chipping and catastrophic failure were observed after 45sec at a cutting speed of 350m/min. Tool wear progression was relatively uniform with 45% and 60% CBN content. No reason was reported by the authors for the poor performance of the 30% CBN insert. Figure 40 shows that variation in CBN content did not produce any significant difference in cutting forces at a cutting speed of 250m/min after 5min of machining. As cutting speed was increased to 350m/min however, thrust force increased by ~1100N with the 30% CBN tool in comparison to the 45% and 60% CBN inserts due to the catastrophic fracture observed with the former [118]. Additionally, in end milling and turning of Inconel 718, low CBN content (50-55%) PCBN tools with ceramic binder outperformed high concentration (80-90% vol. CBN) products having a metallic binder where a ~ 3 and 5 times improvement in tool life was reported respectively [104, 119].

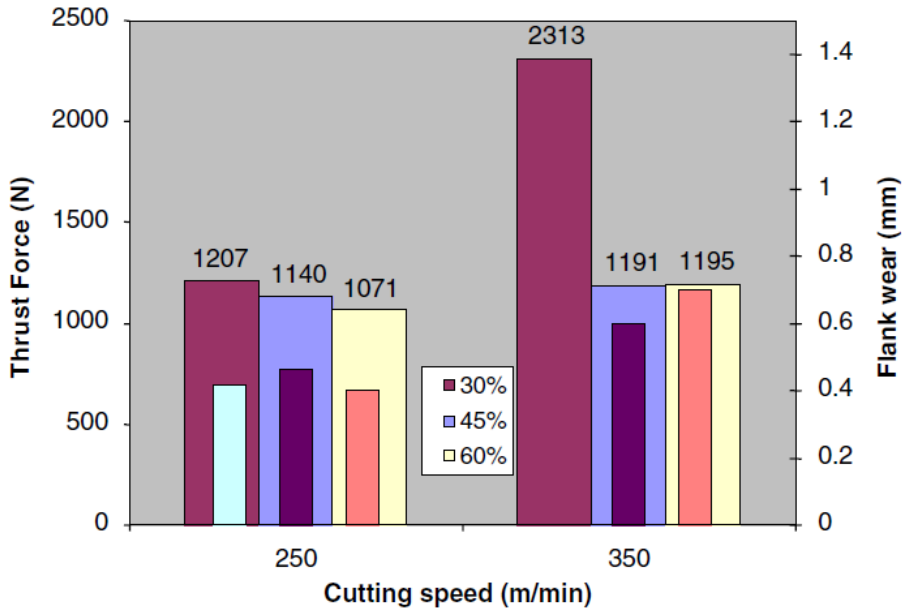

Figure 40: Effect of cutting speed on flank wear and thrust force: Forces wide columns, flank wear narrow columns [118]

2.4.3.4 Effect of operating parameters

The performance of several high concentration (90% by volume) PCBN products with a metallic binder (Ni/Co or Co) involving BZN 6000 from General Electric (GE), CB50 from Sandvik and BX950 from Toshiba Tungaloy Co Ltd. has been assessed on a range of nickel alloys using recommended operating regimes [104, 112, 120-123]. Full details of the operating parameters, tool geometry and workpiece material are presented in Table 11.

Cutting fluid was used with the BZN 6000 and BX950 tooling while CB50 was evaluated dry.

Table 11: Tool geometry, workpiece material and operating parameters of high concentration PCBN tools from different suppliers

Authors	**Tool details**	**Tool geometry**	**Workpiece material and operating parameters**
Richards et al. [121]	BZN 6000 (GE: 90% by vol. CBN and 10% Ni/Co binder)	Round negative insert with chamfered plus honed edge	Inconel 718 (Vc=120m/min-250m/min) Incoloy 800 (Vc=170m/min-230m/min) Nimonic 263 (Vc=120m/min-200m/min) Constants: F =0.3mm/rev, DoC=2mm
Focke et al. [120]	Borazon	Square negative insert	Inconel 718 (Vc=52m/min-182m/min) Constants: F=0.2mm/rev, DoC=2.54mm
Kato et al. [104]	BZN 6000	Square negative insert	Inconel 718 Constants: Vc=90m/min, F=0.1mm/rev, DoC=0.5mm
Darwish [122-123]	CB50 (Sandvik: 90% by vol. CBN and WC 4.6, Co 4.6, Ni 0.8 binder)	Not detailed Nose radius (0.5mm)	Inconel 718 (Vc=32m/min, 125m/min) F=0.075mm/rev-0.6mm/rev, DoC=0.5mm-2mm
Sadao [112]	BX 950 (Toshiba Tungaloy Co Ltd. :90% by vol. CBN and Co binder)	Square insert	Inconel 713 (Vc=90m/min-200m/min) Constant: F=0.1mm/rev, DoC=0.1mm

On Inconel 718, the BZN 6000 gave ~11min tool life at a cutting speed of 120m/min which was reduced to just 1 min as cutting speed was increased to 250m/min. In addition, poor tool life was also observed when machining Incoloy 800 and Nimonic 263 where tool life did not exceed 2min over the range of parameters tested. Flank wear was quite uniform but notch wear at the depth of cut line determined the tool life which penetrated deep into the PCBN layer [121]. BZN 6000 showed the same wear behaviour in the Kato et al. [104] work where after 3 min, notch wear dictated tool life and was ~20µm higher than the flank wear. When turning Inconel 713 using BX950, tool life was 2.5min at 200m/min but increased 3-fold when cutting speed was decreased to 90m/min [112]. In the research by Focke et al. [120] using Borazon tooling, supplier details and CBN concentration are not mentioned but it

is believed that this product was from GE and equivalent to BZN 6000. After 4 min of machining, Borazon exhibited 304μm flank wear at a cutting speed of 52m/min which was reduced to 254μm at 182m/min as the increased temperature caused the yield strength of the workpiece material to drop. In dry turning of Inconel 718 with CB50, surface roughness (Ra) in the range of 0.69-1.5 μm was observed. Not surprisingly, feed rate was found to have a dominant effect on surface roughness while cutting speed produced no effect, however a marginal increase in the value of surface roughness was observed with increase in the depth of cut. In addition, a ~240% and ~100% rise in the value of resultant force was observed with an increase in feed rate and depth of cut respectively. Based on product composition details in Sandvik literature [30] it is possible that CB50 is analogous with BZN 6000 but coded to reflect a Sandvik product [122-123].

Low concentration PCBN grades with ~50% CBN content and ceramic binders (TiC, TiCN or TiN etc.) are generally recommended by the tool manufacturer's for finish turning of Inconel 718 under wet cutting conditions [38]. The effect of cutting speed on tool wear, cutting forces and surface roughness has been investigated when using C-type inserts tipped with Amborite DBC50 (50% CBN and TiC binder) [102]. Here feed rate (0.1mm/rev) and depth of cut (0.5mm) were held constant while cutting speed was varied in the range of 300-1500 m/min. Tool life data was not presented however tool wear was assessed at feed distances of 31, 63, 94.5 and 126 mm. Notch wear was the main wear mode which was observed both on the major and minor cutting edges. Tool wear was less than 200μm up to a cutting speed of 600m/min after a feed of 31mm but when cutting speed was increased to above this value, catastrophic fracture and chipping leading to tool failure was observed. A reduction in the value of cutting force (~30-60 N) was observed at a cutting speed of 400m/min due to softening of the workpiece material, however no significant effect of cutting speed on surface roughness was found and values were within the range of 2.4-4.3 μm after 20mm feed distance. In another investigation, Costes et al. [118] recorded a tool life of 6min when turning Inconel 718 with PCBN tools employing 60% CBN content and TiC binder. Operating parameters were held constant at Vc=250m/min, F=0.2mm/rev and DoC=0.5mm using round inserts. Energy dispersive X-ray (EDX) measurements were conducted on the broken inserts and it was observed that elements from the workpiece including Ni, Cr, Fe and Nb were diffused in the tool crater up to a few microns deep. Similarly Shintani et al. [117] and Arunachalam and Mannan [105] also observed diffusion wear with PCBN tools in turning of Inconel 718. Round PCBN inserts (RNGN120300E25) were also evaluated by Bushlya et al. [109, 111] at constant depth of cut of 0.3mm while cutting speed and feed rate

were tested at 3 levels (see Table 12) in a full factorial design. A PCBN grade with 50% by volume CBN content and ceramic TiC-based binder was employed [109, 111].

Table 12: Levels of cutting speed and feed rate [109, 111]

Factors	**Levels**		
	1	**2**	**3**
Cutting speed (m/min)	250	300	350
Feed rate (mm/rev)	0.10	0.15	0.20

It was observed that tool life was slightly reduced with an increase in feed rate from 0.1mm/rev to 0.20mm/rev, while an increase in cutting speed from 250m/min to 350m/min produced a drastic reduction in the value of tool life from 5min to ~1.7min. Additionally, surface roughness was 0.5µm Ra at the low feed rate of 0.1mm/rev due to the ploughing action caused by the smaller uncut chip thickness, whereas at 0.20mm/rev roughness measured ~0.25µm Ra [109, 111]. Abrasion was identified as the dominant tool wear mechanism due to the abrading action of highly abrasive carbides of Ti and Nb from the Inconel 718 matrix, which tended to remove the binder phase at a higher rate than the CBN. This was due to the fact that the hardness of the TiC-binder (520HV) was significantly lower than the hot hardness of CBN (~2400HK) at 850-950ºC. Furthermore, adhesion of workpiece material and cracks were also present on the tool surface [109].

In contrast to work reported by other authors [105, 117-118], elements from the workpiece did not appear to propagate into the tool and therefore the absence of diffusion wear was claimed [109]. The differences in the results were attributed to the difference in the analytical techniques used to conclude the diffusion wear of PCBN tools. Costes et al. [118] carried out EDX on the broken inserts while Shintani et al. [117], Arunachalam and Mannan [105] performed energy dispersive X-ray analysis on the tool crater and concluded that of diffusion wear had occurred. In the work by Bushlya et al. [109], FIB milling was used on a chip lamella followed by EDX mapping. This was considered to be more reliable than the other afore-mentioned techniques. It was also reported by Angseryd et al. [124] that careful sample preparation is necessary to accurately determine the chemical wear of PCBN tools otherwise considerable scatter in the results can occur.

Emerson [125] tested both high CBN concentration (GE BZN 6000) and low concentration PCBN inserts (Amoborite DBC50 by E6) in turning of Inconel 718 at constant feed rate and depth of cut of 0.13mm/rev and 1.27mm respectively. Cutting speed was varied from 46m/min to 457m/min. For both types of insert, 92m/min was found to be the optimum cutting speed in terms of tool wear. Contrary to other authors [105, 117-118], this study

reported that wear rates of both inserts at 304m/min were very high due to rapid diffusion of boron and nitrogen atoms.

Recently, Seco has introduced a new PCBN grade: CBN 170 which contains 65% volume CBN and a TiCN ceramic binder reinforced with SiC whiskers embedded in the matrix to increase its fracture toughness. The performance of this grade has been studied by M'Saoubi et al. [126] when finish turning of Inconel 718 at constant feed rate (0.15mm/rev) and depth of cut (0.25mm) in the presence of coolant. Two levels of cutting speed of 200m/min and 300m/min were used together with triangular tool geometry (TNGN110308E25) and a tool wear criteria of $VB_B max.$=400µm. A tool life of ~6min was recorded at Vc of 300m/min which increased to 16min as cutting speed was reduced to 200m/min. The surface roughness values were within the range 0.90µm to 1.17µm Ra, irrespective of the tool condition and operating parameters employed. All workpiece samples were found to be strain hardened to a depth of ~100µm from the machined surface both with new and worn tools. Tool wear had a significant effect on maximum principal stresses which were up to ~800MPa with new tools and increased by ~125% when employing worn PCBN tools. Additionally, electron back scattered diffraction (EBSD) mapping was conducted see Figure 41, which shows evidence of recrystallised areas near the machined surface.

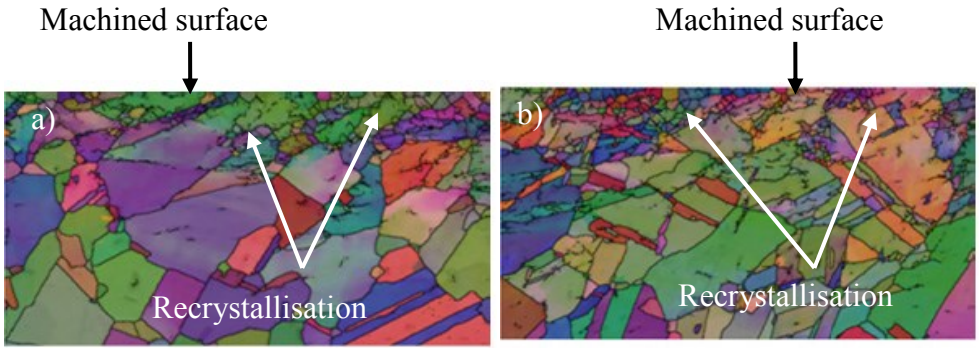

Figure 41: Evidence of recrystallisation near the machined surface (EBSD maps) (a) New tool and (b) Worn tool [126]

Arunachalam and Mannan [105] optimised operating parameters in terms of tool life and surface roughness (Ra) when facing age hardened Inconel 718 using round shaped tool geometry with sharp edges. Testing involved cutting speed at 4 levels, feed rate at 3 levels and depth of cut at 2 levels with coolant, see Table 13.

Table 13: Levels of cutting speed, feed rate and depth of cut when facing Inconel 718 with PCBN tools [105]

Factors	**Levels**			
	1	**2**	**3**	**4**
Cutting speed (m/min)	150	225	300	375
Feed rate (mm/rev)	0.10	0.15	0.20	
Depth of cut (mm)	0.5		1.00	

A maximum tool life of ~6min was obtained at a cutting speed of 150m/min which was reduced to ~1min at 300m/min and 375m/min. In terms of material removal rate, best results were obtained at 225m/min with a feed rate of 0.15mm/rev and depth of cut of 0.50mm, here the tool life was 3.5min. Surface roughness (Ra) was less than 0.80µm in all trials at the end of tool life due to uniform tool wear progression. Although PCBN grade details were not mentioned in the paper, diffusion of Co binder was the main reason given as being responsible for tool wear, therefore binderless tools were suggested as alternatives [105]. In other work [85], they further investigated the effect of cutting speed on residual stresses, cutting forces and surface roughness at constant feed rate of 0.15mm/rev and 0.5mm depth of cut. Figure 42 (a) shows a change in the value of surface residual stress from compressive to tensile with an increase in cutting speed from 150m/min to 375m/min. It was suggested that at higher cutting speeds, the metal spent a very short time in the shear zone and generated heat was not conducted away, which in turn raised the temperature. Due to this temperature rise, residual stresses were tensile and cutting forces reduced, see Figure 42 (b). Lower values of surface roughness (~20%) were recorded at the higher cutting speed of 375m/min rather than at 150m/min. This was expected as in high speed machining (HSM), workpiece surfaces soften and many surface flaws are wiped out, thereby reducing the surface roughness [103].

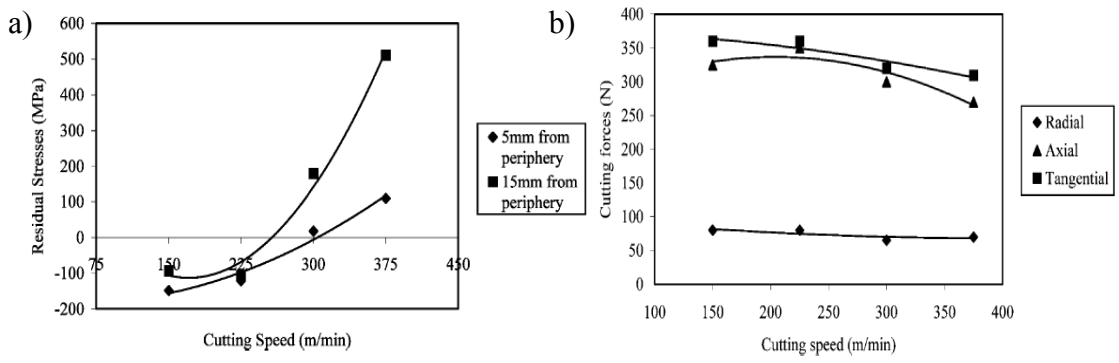

Figure 42: Effect of cutting speed on a) residual stresses and b) cutting forces [85]

Figure 43 highlights the effect of depth of cut (0.05mm and 0.5mm) on surface residual stresses at a constant speed of 225m/min and feed rate of 0.15mm/rev, values which were suggested as optimal by the authors in their previous work. Up to 15mm from the tool entry, compressive residual stresses were recorded because plastic deformation was dominated by mechanical effects, however as machining progressed, thermal effects prevailed producing tensile residual stresses at a distance of 25mm from the periphery. Increasing operating temperatures and consequent softening of the workpiece material produced better surface finish i-e reduction in the Rt value from 0.35µm to 0.2µm as shown in Figure 44 [85]. In facing of Rene 77, Wick [116] recommended PCBN tools at a cutting speed of 125m/min, feed rate of 0.10mm/rev and 1.40mm depth of cut. Using these parameters, he obtained 6-8 times higher tool life compared to carbides.

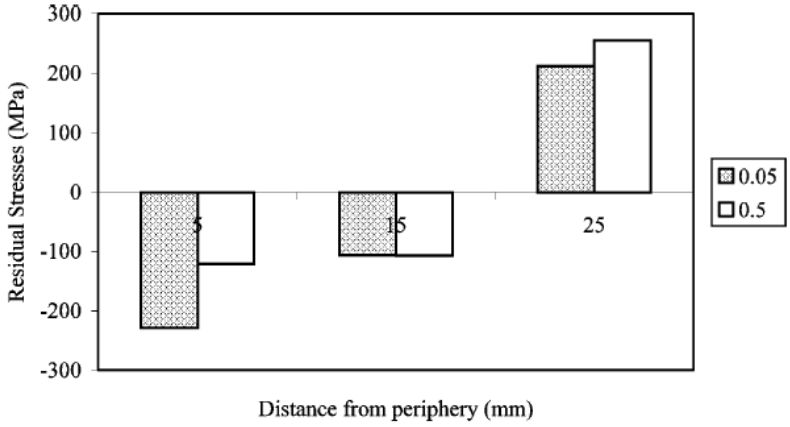

Figure 43: Effect of depth of cut on residual stresses [85]

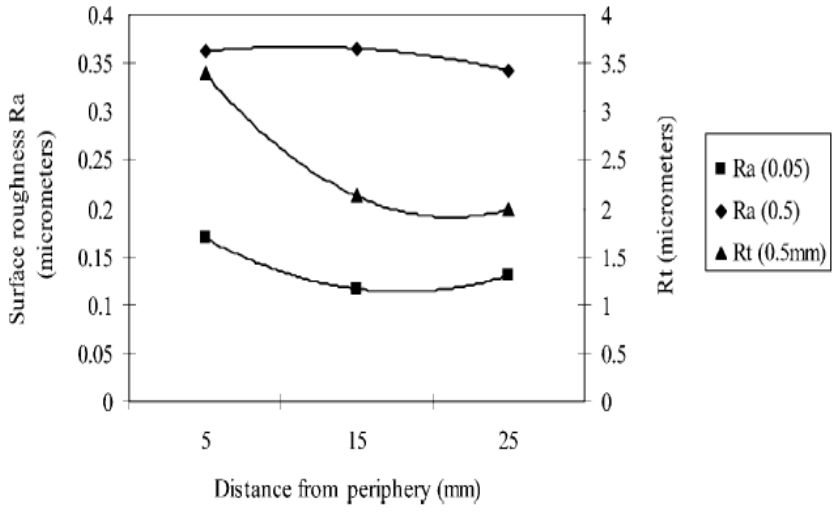

Figure 44: Effect of depth of cut on surface roughness [85]

Pawade et al. [42, 103, 127], studied the effect of operating parameters on cutting forces, surface roughness, surface damage, residual stresses and the degree of work hardening (DWH) in longitudinal turning of Inconel 718 without coolant. A Taguchi fractional factorial design (L27 orthogonal array) with 3 levels of cutting speed (125, 300, 475 m/min), feed rate (0.05, 0.1, 0.15 mm/rev) and depth of cut (0.50, 0.75, 1.00 mm) was employed. As with observations made by Arunachalam et al. [85] when facing, lower values of cutting force were recorded at the higher cutting speed of 475m/min, due to softening of the workpiece at elevated temperatures. Cutting, feed and radial forces were lowered by the factor of 1.5, 2 and 6 respectively. Analysis of variance calculations (ANOVA), showed that depth of cut and feed rate were statistically significant at the 5% level on cutting and feed forces, however, none of the factors/interactions were statistically significant relative to radial force. The authors attributed this behaviour to the edge preparation (chamfer, chamfer plus hone) employed. They argued that direction of the radial force was more or less parallel to the chamfered cross section on the cutting edge as described schematically in Figure 45 [103].

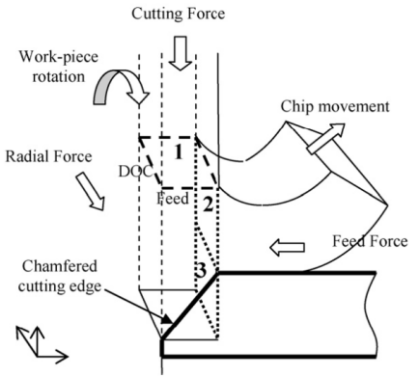

Figure 45: Schematic illustration of chamfered edge showing the effect of cutting, thrust and feed forces on undeformed chip cross sectional area [103]

In terms of ANOVA, cutting speed was significant in terms of surface roughness with better surface finish and less surface damage observed at the highest cutting speed of 475m/min in comparison to the cutting speed of 125m/min [103]. This agrees well with the previous observations made in facing of Inconel 718 [85]. Additionally, machined surfaces generated at 300m/min showed fewer flaws compared to the surfaces produced at 125m/min [103]. None of the operating factors were statistically significant on residual stresses at the 5% level. Furthermore, at the lowest cutting speed of 125m/min, residual stresses were tensile while at the highest cutting speed of 475m/min, they were compressive [42]. These results appear to contradict the results reported earlier by Arunachalam et al. [85], however,

differences in the findings were due possibly to either tool geometry (rhomboid by Pawade et al. [42] and round by Arunachalam et al. [85]), cutting environment (dry by Pawade et al.[42]. and wet cutting by Arunachalam et al. [85]) or the type of machining operation (longitudinal turning by Pawade et al. [42] and facing by Arunachalam et al. [85]). Pawade et al. [42] explained the generation of residual stresses from quantum theory of heat dissipation, according to which, at low cutting speed, chip stayed in the machining zone for a longer time. Consequently, thermal dominant machining/tensile residual stress prevailed due to the high rate of heat dissipation into the machined surface. Although it is a fact that the highest cutting speed of 475m/min produced lots of heat due to high material removal rate, at the same time the chips had the greater ability to dissipate heat, thus plastic deformation was dominated by the mechanical effects, resulting in compressive residual stresses; see Figure 46. Additionally, burnt chips at Vc of 125m/min showed the poor rate of heat dissipation while silver coloured chips at 475m/min indicated effective heat removal from the machined surface [42].

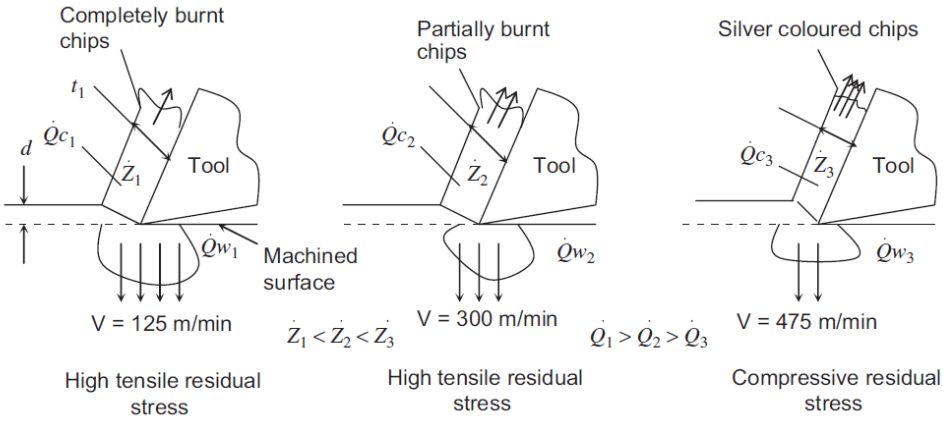

Figure 46: Generation of residual stresses at cutting speeds of 125m/min, 300m/min and 475m/min [42]

All machined samples were strain hardened to a depth of ~300µm with a maximum value of 490Hv, compared to the bulk hardness value of 270Hv. Microhardness measurements for all the machined specimens were within the range 370-490Hv for the first 30µm depth from the machined surface as shown in Figure 47 (a). As a result of the severe work hardening, the yield strength of all samples was increased to a similar depth in the machining affected zone (MAZ) as observed with the microhardness measurements. Thus, a clear demarcation between the unaffected and MAZ zones is shown in Figure 47. Based on ANOVA calculations, operating parameters affected the degree of work hardening up to a

depth of 100µm from the machined surface. None of the factors and interactions were statistically significant at the 5% level after 100µm depth [42].

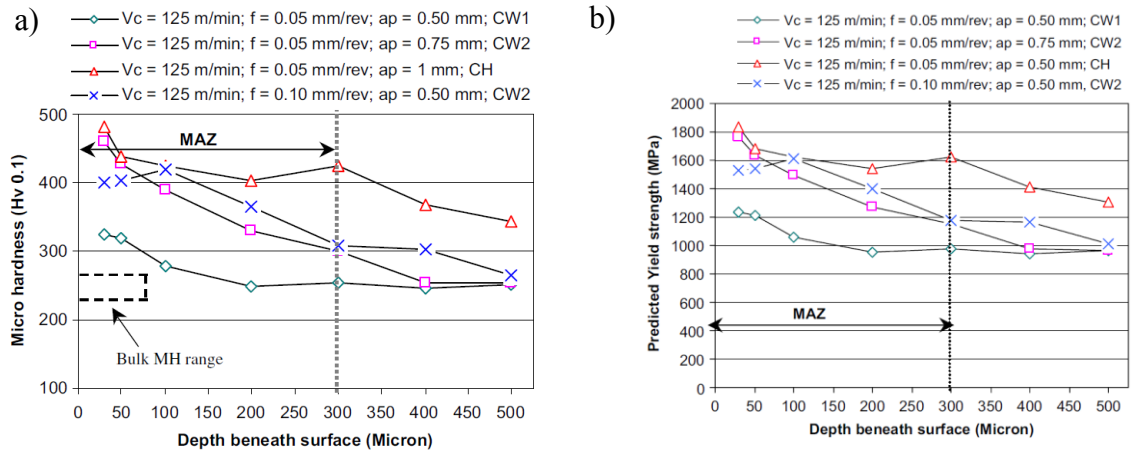

Figure 47: Variations with depth below the machined surface in (a) microhardness and (b) yield strength [42]

It is well documented that the sum of specific shear energy and specific friction energy is equal to the total specific cutting energy, where the former accounts for ~75% of the total [26]. Pawade et al.[128] used an analytical model to determine the specific shear energy in high speed turning of Inconel 718 and compared results with experimentally calculated values. Shear band spacing is commonly observed during chip formation in the machining of Inconel 718 and the model predicted an increase in the shear band spacing with an increase in the feed rate due to a corresponding increase in the cross sectional area of the material under plastic deformation; see Figure 48 (a). Furthermore, feed rate had a strong effect on specific shear energy followed by cutting speed such that an increase in its magnitude occurred with a reduction in the feed rate and cutting speed as shown in Figure 48 (b). The authors claimed that this was possibly due to the size-effect where an increase in the ploughing forces could be expected with a reduction in the chip cross sectional area, therefore higher specific energy is required in machining. It was also observed that ~50% lower specific energy was required at the highest cutting speed of 475m/min than at 125m/min. In addition, results indicated that percentage error between theoretical and experimental specific energies was within 0.5-7% [128].

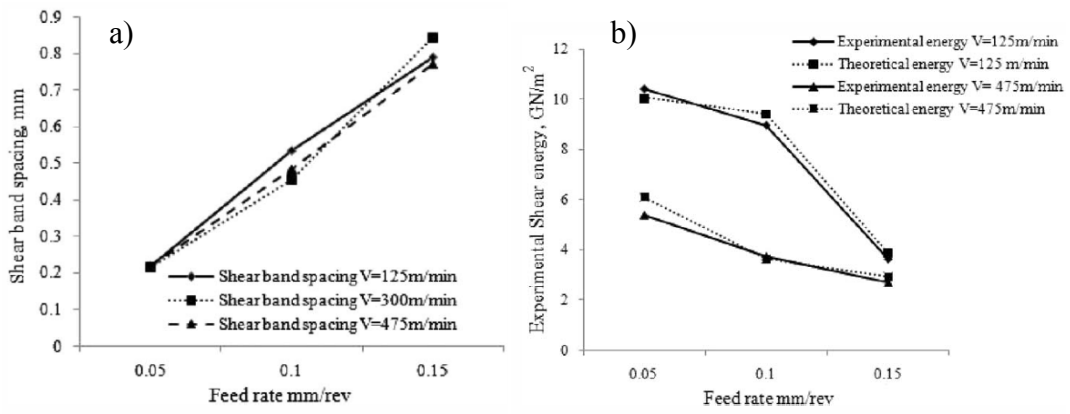

Figure 48: (a) Predicted shear band spacing with different feed rates and (b) Theoretical and experimentally calculated specific shear energies [128]

Jemielniak [129] recorded a tool life of ~6.6min when employing triangular inserts at a cutting speed of 250m/min, feed rate of 0.08mm/rev and depth of cut of 0.20mm when cutting with coolant. In another work, Klocke et al. [107] recommended PCBN tools for a grooving operation on a Waspaloy turbine disc operating at 200-300 m/min. A ~90% reduction in production time was recorded in comparison to carbide cutting tools.

2.5 Brief survey on the current status of coated PCBN tooling

Although coated PCBN tools came onto the market approximately 10-12 years ago relevant publications are limited. Ota et al. [130] patented the PVD coating procedure for PCBN inserts using an Ion platting method. In their work, workpiece surface roughness (Rz=3.00µm) was the criteria for judging tool performance when turning of SCM415 steel (~61HRC) at Vc of 160m/min, F=0.08mm/rev and DoC=0.1mm under dry cutting conditions. A tool life of 75 min was recorded with the coated PCBN (TiN~3µm) tool which decreased to 45min when an uncoated insert was employed. Additionally, 3µm was found to be the optimum coating thickness as lower or higher values produced deterioration in tool performance. Thick coatings (>3µm) showed greater susceptibility to peeling due to high stresses as a result of the greater thickness while thin coatings (<3µm) quickly diminished, causing no improvement over their uncoated counterparts. For better adhesion, a substrate surface roughness of less than 0.20µm was suggested as necessary. Therefore polishing and surface preparation of the substrate was identified as critical in the coating procedure. For the same coating thickness (3µm), no significant benefit in terms of tool life was seen when a single layer TiN coating was compared against multilayered structures (TiN/TiAlN, TiN/TiC/TiN, TiN/TiC and TiN/TiAlN/TiCN etc.). Coated inserts with a CBN content of 40-75 % outperformed low (<30%) and high (90%) content PCBN tools due to a good

combination of wear resistance and toughness. Severe edge chipping was noticed with high concentration products producing poor workpiece surface roughness shortly after the start of cutting. In other work, a CVD coating method was patented by Ban et al. [131] employing high concentration PCBN inserts (85% CBN content) with a ~22μm thick TiN+TiCN+TiOCN+alumina+TiCN+TiN coating. In dry turning of cast Iron, ~3 times longer tool life was recorded with this coated insert compared to an uncoated tool (lasted 4min) at a cutting speed of 610m/min, feed rate of 0.23mm/rev and depth of cut 0.64mm, based on maximum flank wear criteria of VB_Bmax.=510μm. In addition, tool life was further increased to 16min when post coating wet blasting was employed, due to a change in the residual stresses of the coating from tensile to compressive. The approach involved a slurry of water and alumina particles.

Harada et al. [11] also reported ~33% lower values of surface roughness with a TiN coated insert due to a uniform tool wear pattern in comparison to uncoated tools in continuous and interrupted turning of SCM415H steel (~58-62HRC) at Vc of 200m/min, feed rate of 0.1mm/rev and DoC=0.1mm when operating without coolant. This was attributed to the uniform tool wear pattern observed in the presence of the coating. Coelho et al. [15] recorded ~38% higher tool life with TiAlN-nano coated PCBN inserts compared with uncoated tools when turning AISI 4340 at Vc of 150m/min, feed rate of 0.07mm/rev and 0.2mm depth of cut. Additionally, the uncoated tools generated ~40N higher cutting force compared to the former due to rapid tool wear. In turning of DIN100Cr6 (~62HRC) steel, ~119% and 74% longer tool lives were reported by Galoppi et al. [14] with TiAlN and TiN coated inserts respectively compared with uncoated tools at constant depth of cut of 0.20mm. A cutting speed of 91m/min and feed rate of 0.152mm/rev was found to be the optimum. When evaluating a TiN coated PCBN, Diniz et al. [13] reported improved performance when dry cutting over wet cutting when turning AISI 52100 steel at Vc=100m/min, F=0.08mm/rev and DoC=0.30mm, with lower flank wear (~33%) and reduced surface roughness (~41%) with the former. When turning W320 steel, Sales et al. [16] optimised cutting speed and feed rate values at 200m/min and 0.1mm/rev respectively for a TiN coated PCBN insert while depth of cut was constant at 0.10mm.Compared to uncoated tooling, Poulachon et al. [12] recorded ~45% longer tool life with TiN coated (45min) PCBN inserts when turning hardened 100Cr6 steel at a cutting speed of 150m/min, feed rate (0.10mm/rev) and depth of cut (0.20mm). When cutting speed was increased to 250m/min, no significant difference in terms of tool life was observed for either coated or uncoated tooling. Here the tool life was reduced to 8min. Recently, a range of PVD coated PCBN tools involving TiN, TiSiN, TiAlN

and AlCrN have been tested by Saoubi et al. [132] in turning of 16MnCr5 steel. Cutting parameters were kept constant at Vc=200m/min, F=0.15mm/rev and DoC=0.20mm. All the coating products failed to provide any benefit in terms of tool life compared to uncoated PCBN inserts which appears to contradict results reported in the earlier investigations where significant benefits were observed with coated tooling. This was most likely due to the difference in the workpiece material employed in the current work. In addition, better performance of the TiSiN coating was observed compared to all the other coated tools which were attributed to its high thermal stability and hardness.

2.6 Statistical experimental design techniques

2.6.1 Introduction

In an experiment, a test or series of tests are carried out for simultaneous evaluation of two or more input variables so that variation in the output response can be observed and analysed. In statistical experimental design, experiments are initially planned, then experimentation is conducted for appropriate data collection and finally meaningful conclusions are drawn from statistical analysis [133]. For a particular set of experimental conditions, different methods are employed to analyse the influence of different factors on the output response and to obtain 'best/preferred' combination of factors. Statistical methods are considered to be very 'objective' particularly for experimentation in which errors are expected**.** Full and fractional factorial designs are the two main broad categories of experimental design. In the former case, levels of one factor are evaluated against each level of all other factors**.** Although all main effects and their interactions can be analysed when using this methodology an extensive number of tests are required and the cost of tooling, workpiece material can be quite high. If this is the case then fractional factorial designs should be adopted at least for initial screening purpose as they require fewer tests. For example, 256 tests are required for 4 factors each at 4 levels in case of full factorial design, however main effects with acceptable confidence can be analysed by accommodating a fractional factorial L16 orthogonal array involving only 16 tests. In Taguchi methodology [134], main effects and interaction plots are generated and the relative influence of individual test factors with their corresponding sensitivity associated with each level relative to selected output responses (tool life, cutting forces, surface roughness etc.), is analysed by conducting analysis of variance (ANOVA).

2.6.2 Taguchi experimental design procedure

In Taguchi experimental design, a suitable orthogonal array (OA) is selected from the standard available designs. For example L4, L8, L16, L32 and L36 are examples of 2 and 4 level combinations, while for 3 level factors L9 and L27 are available and 2 and 3 level factors can be accommodated in L12 and L18 OA arrays. Factors and their corresponding levels can be assigned in the orthogonal array using linear graphs and assignment tables. Finally, analysis of the experimental data is carried out [135]. Comprehensive details of the useful sets of orthogonal arrays and linear graphs can be found in [134, 136]. The main disadvantage linked with this methodology is that it is intended only for main effects and the importance of interactions is underestimated. However, Taguchi stated that careful selection of specific factors and their corresponding levels can eliminate the interaction effects [135].

2.6.3 Overview of the analysis of variance (ANOVA) technique

In the 1930's, Sir Ronald Fisher developed this method for the interpretation of experimental data so that necessary decisions could be made [134]. In the analysis of variance (ANOVA) approach, differences in the average performance of a group of examined factors on the output response can be detected statistically by distributing the total variability into its individual components. Essentially, variation in the mean of an individual factor is compared with the experimental errors. In the case of fractional factorial designs, a confirmation run is performed in order to validate the conclusions drawn from the analysis. Further details can be found in Ross [134].

2.6.4 Regression, stepwise backward elimination (SBE) and stepwise forward entry (SFE) linear regression procedures

Regression is a statistical process in which the relationship among different variables affecting the selected response is predicted. In case of linear regression, the response is a linear function of the variable. It is well known that the 'fit' of the regression equation can be improved by increasing the number of variables [137]. However, step wise regression procedures can be adopted to choose important variables which significantly affect the response by conducting an F-test and identifying corresponding P-values. Two methods are commonly employed for this purpose i-e 'stepwise backward elimination' and the 'stepwise forward entry procedure'[138-139]. The stepwise approach is used with the fractional factorial modified Taguchi L36 orthogonal array employed in the Phase 1C experimental work reported in section 4.3. In the stepwise backward elimination (SBE) procedure, an

initial model is generated which involves the main effects together with all possible interactions between factors that can be accommodated. This will depend on the available degrees of freedom (DoF) in the design at the expense of partial confounding and the introduction of non-orthogonality. To construct the final 'hierarchical' model, non-significant interactions are removed one-by-one (the interaction which is non-significant and has the highest P-value compared to the other interactions) while maintaining the main effects in the model, unless all interactions present in the model appear to be significant. Hierarchical models are those in which interactions must be supported by the main effects whether they are significant or not. Hence the final model involves main effects and interactions which are statistically significant. The corresponding adjusted value of R-squared [R^2(Adj)] and the residual error are calculated to determine the fit of the model [138-139].

In contrast to backward elimination, the significance of each individual interaction is checked in a stepwise forward entry (SFE) procedure one at a time by adding it to the main effects and calculating the corresponding R-Sq(Adj) value. In certain cases, both methods can be employed alternately, then it is called 'bidirectional elimination'. The SBE procedure can be used in the first instance to determine the statistically significant interactions affecting the response and then applying the SFE procedure to investigate the contribution of each interaction (that has already been identified from backward elimination) separately with the main effects by calculating the R^2(Adj) value again. Essentially, the importance of each interaction can be determined e.g the least important interaction is the one with the smallest increase in R^2(Adj) value when added with the main effects [138-139].

3. EXPERIMENTAL WORK

Experimental work comprised three main phases. Phases 1 and 2 involved optimisation of tool geometry, edge preparation, cutting environment and operating parameters, while in Phase 3 a newly developed PCBN grade and various coating products were evaluated when high speed turning Inconel 718. Appropriate sub-phases under each main phase were planned as described below;

- Phase 1A: Preliminary experimental trials when turning Inconel 718
- Phase 1B: Benchmarking of Mitsubishi Inconel 718 workpiece using production approved carbide/PCBN inserts and operating parameters
- Phase1C: Influence of tool geometry, edge preparation, cutting environment, surface condition and operating parameters on tool wear/life, surface roughness and cutting forces
- Phase1D: Evaluation of edge preparation and cutting speed on workpiece surface integrity
- Phase 2A: Effect of cutting environment, cutting speed and feed rate on tool wear/life, surface roughness and cutting forces
- Phase 2B: Assessment of cutting environment, cutting speed and feed rate effects on workpiece surface integrity
- Phase 3A: Evaluation of alternative PCBN grade and tool coatings on tool wear/life, surface roughness and cutting forces
- Phase 3B: Effect of alternative PCBN grade and tool coatings on workpiece surface integrity
- Phase 3C: Effect of PCBN grades and cutting environment on residual stresses

From mainstream Phase 1C testing, variation in tool geometry was reduced from 2 to 1 level while levels of cutting speed and feed rate were reduced from 3 to 2 levels. Preferred edge configuration was selected from Phase 1D. Following on from Phase 1D, in Phases 2A and 2B, cutting environment, cutting speed and feed rate were further optimised in terms of tool life and workpiece surface integrity in order to narrow down the operating variables to the final set. In Phase 3, a new PCBN grade and various coating products were evaluated according to the parameter combination optimised in the previous phases.

A comprehensive description of experimental work and corresponding test arrays together with details of workpiece materials, equipment and tooling are described in the following sections.

3.1 Workpiece materials

The workpiece material used in all the experimental trials was nickel based superalloy Inconel 718 however bars obtained from different suppliers had varying microstructures. For preliminary experimental trials (Phase 1A), a bar measuring 99mm diameter × 87mm long having a grain size of ~75µm, as shown in Figure 49 was used. The material was supplied by Rolls-Royce (RR) ~13 years ago for an alternative PhD project involving 3D modelling of high speed ball nose end milling of Inconel 718 using carbide tooling [140]. The material was solution treated at 950-980ºC for 1 hour in vacuum at 1bar followed by precipitation treatment at 720ºC for 8 hours then cooled to 620ºC and held for a further 8 hours followed by air cooling. The bulk hardness was ~44HRC.

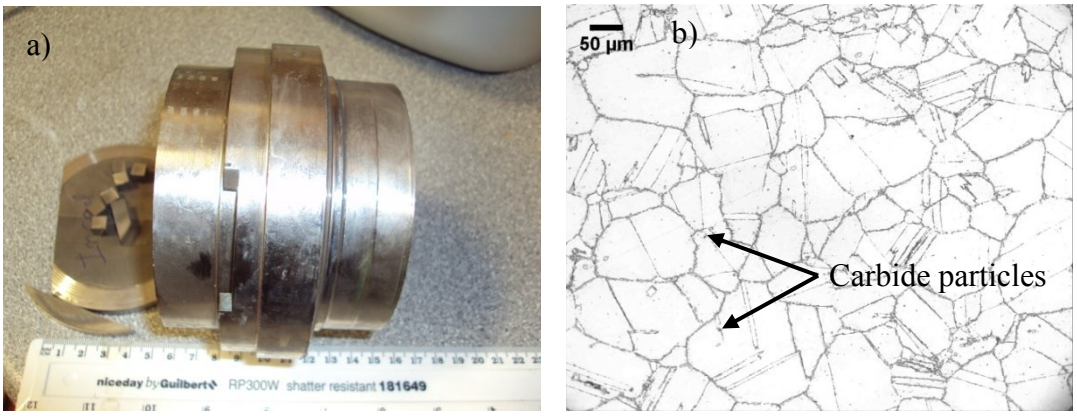

Figure 49: RR Inconel 718 (a) bar and (b) microstructure

Due to the lack of suitable Inconel 718 bar material for mainstream machinability testing, trials for Phases 1B, 1C and 1D experimental work were performed using four small bars, each with a length of 122mm and a diameter (Ø) of 90mm, see Figure 50 (a). These were supplied by Mitsubishi Heavy Industries (MHI), which were supplied from another previous project within the Machining Research Group (MRG). The bars were sent to Wallwork Heat Treatment Birmingham Ltd. for solution treatment and age hardening to ~46HRC using the heat treatment procedure detailed above employed for the RR material. Figure 50 (b) shows the microstructure of the MHI material with a grain size of 7-8 µm in which γ″ and δ precipitates resides along with carbide particles. The micrograph was sent to RR; Mark Hardy-Corporate Specialist for nickel based superalloys RR and Colin Sage-

Machining Specialist RR, in order to assure its conformity with standard RR disc material. In addition, the MHI material conformed to MSRR-7115 grade (RR internal material specification) whereas the Inconel 718 employed by RR for disc applications was according to MSRR-7256 grade. Unfortunately, the MHI workpiece appeared to be different from RR disc material, further details and discussion about the microstructure are presented in Section 3.4.2, however it was agreed that future trials would only be performed on specimens representative of RR material. Consequently, a bar 108mm diameter (Ø) × 375mm long was purchased from Superalloys International Ltd. (SI), USA, see Figure 51 (a), which was heat treated to a nominal hardness of ~44HRC. The heat treatment was again undertaken by Wallwork Heat Treatment Birmingham Ltd., using the previously detailed procedure. Figure 51 (b) shows the microstructure with a grain size of 10-12 µm. Gamma double prime (γ″) precipitates and carbide particles were observed however, delta (δ) precipitates which typically exhibit plate like structure were not seen in the micrograph. The SI material conformed to AMS 5662 (Aerospace Material Specifications) and according to Mark Hardy and Colin Sage, was similar to standard RR disc material, therefore trials in Phases 2 (2A, 2B) and 3 (3A, 3B, 3C) were conducted with this bar.

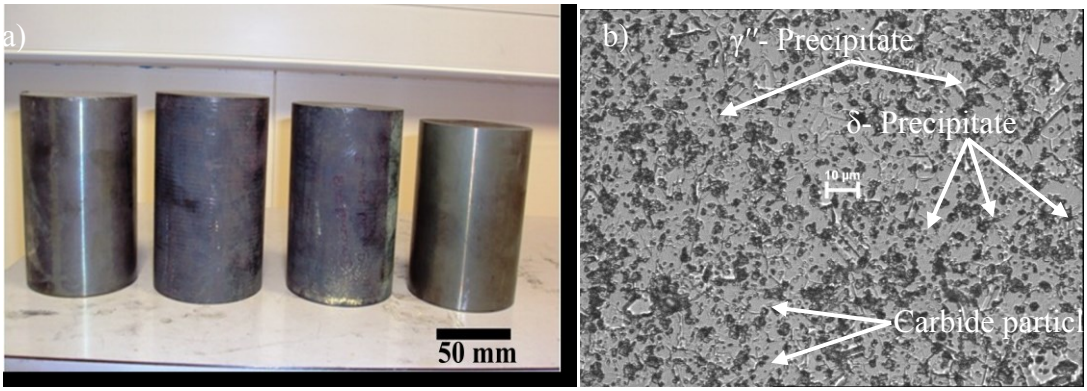

Figure 50: MHI Inconel 718 (a) bars and (b) microstructure

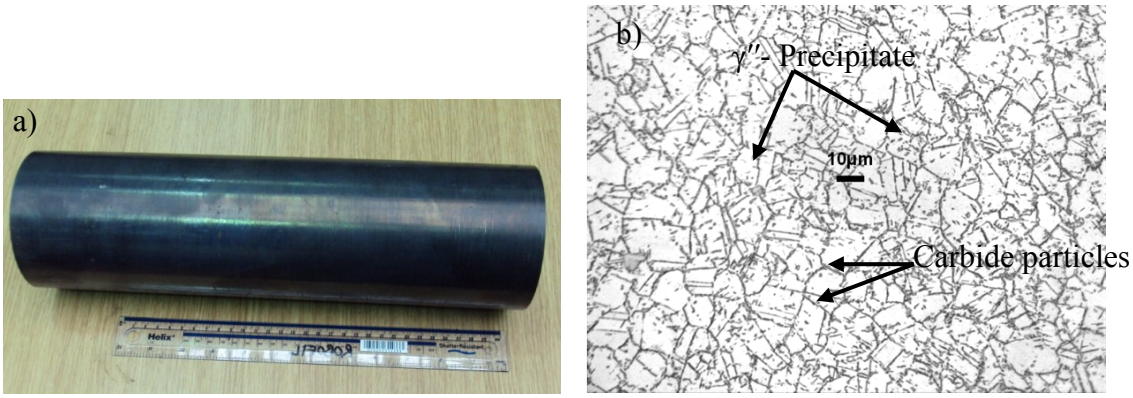

Figure 51: SI Inconel 718 (a) bar and (b) microstructure

Although the Inconel 718 bars were sourced from different suppliers (RR, Mitsubishi Heavy Industries and Superalloys International) the chemical composition in each bar was identical: Ni-19Cr-18.5Fe-5.1Nb-3Mo-0.9Ti-0.5Al-0.6C (wt. %).

3.2 Cutting tools

In machinability testing of Phases 1 and 2 (1A, 1C, 1D, 2A, 2B), low concentration (50% CBN) PCBN inserts with a ceramic binder (TiC) were evaluated. For Phase 3 trials (3A, 3B, 3C), medium content (65% CBN) PCBN tools having a TiCN binder phase reinforced with SiC whiskers were employed. In order to compare/benchmark the RR Inconel 718 with the MHI material, machining trials in Phase 1B were performed with uncoated/coated carbide and high concentration (90% CBN) PCBN cutting inserts on MHI material. Tests involved approved parameters used by RR in production in order to provide comparative results as a basis for mainstream testing.

3.2.1 Carbide and PCBN cutting inserts for benchmarking trials (Phase 1B)

Uncoated/coated carbide and high concentration (90% CBN-BZN 6000) PCBN tools were supplied by RR in order to benchmark Mitsubishi material. Full details of insert specification, manufacturer tool grade and edge preparation details are given in Table 14.

Table 14: Details of carbide and PCBN inserts supplied by RR

Type of tool	Insert specification	Manufacturer and tool grade	Edge preparation
PCBN	DNMA 150608-01020	Kennametal KD 120 (BZN 6000: 90% CBN plus Ni/Co metallic binder)	S-type (Chamfered and honed) (0.1mm× 20º and 20µm hone radius)
Uncoated carbide	DNMG150608	Sandvik H13A	-
Coated carbide	DNMG 150608 4µm thick CVD coating (TiCN-Al_2O_3-TiN)	Sandvik S05F	-

A tool holder product code PDJNR 2525M12 was supplied from Seco giving an inclination angle (λ) of -7º, normal rake angle (γ_n) of -6º, principal cutting edge angle (φ) of 93º and auxiliary cutting edge angle (φ_1) of 30º.

3.2.2 Low concentration PCBN inserts for preliminary trials and mainstream testing of Phases 1A, 1C, 1D, 2A and 2B.

Two different tool grades were used; Amborite DBC50 and DCC500 which were manufactured using 50% CBN and 50% TiC binder by E6 with a grain size of 2µm. The former was used in preliminary experimental trials (Phase 1A) while the latter was evaluated in the mainstream testing of Phases 1C, 1D, 2A and 2B experimental work. Both tool grades have the same chemical composition, however DCC500 was recommended by E6 due to its higher chipping resistance as a result of its more uniform structure compared to DBC50 [141]. Table 15 details the thermal properties of DCC 500 PCBN.

Table 15: Thermal properties of DCC 500 [142]

Thermal properties	**Temperature**		
	21ºC	**498ºC**	**999ºC**
Thermal diffusivity (mm^2/s)	13.98	8.72	7.92
Specific heat (J/Kg/K)	669.24	1177.11	1189.55
Thermal conductivity (W/mK)	38.21	41.63	37.96
Sample density (g/cc)	4.08	4.05	4.02

For Phase 1A trials, an off-the-shelf square insert (4 edges) ISO code SNMN 090316 with a chamfered (0.2mm×20º) and honed edge (coded as S-type) was used. The insert was clamped in a CSBNR 2525M09 toolholder which resulted in inclination and normal rake angles of -6º, a tool cutting edge angle of 75º and a clearance of 6º.

In Phase 1C experimental work, round and rhomboid (C-type) tool geometries shown in Figure 52 (a) were evaluated, the tools having codes of CNGA 120412 and RCMW 10T300 respectively. Both the C-type and round inserts were held in Jetstream toolholders; PCLNR 2525M12JET and SRSCR 2525M10JET respectively. Special fluid inducers were used in the toolholders as shown in Figure 52 (b) which delivered the coolant directly to the tool chip interface.

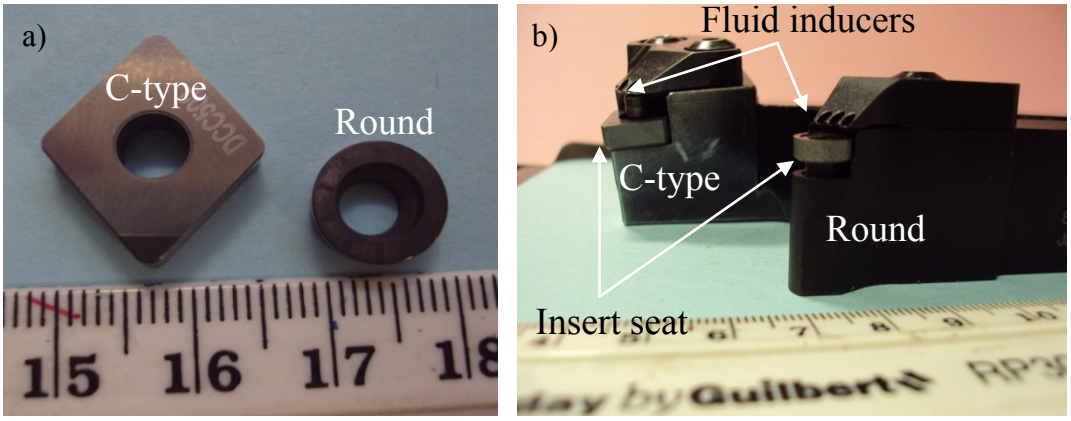

Figure 52: (a) C-type and round tool geometry and their respective (b) Jetstream toolholders

Details of the different tool geometries after the inserts were clamped in their tool holders are given in Table 16. There were Jetstream toolholders available to accommodate negative geometry C-type PCBN inserts but not the negative rake round inserts, however Seco offered Jetstream tool holders for positive 'c' lock 10mm diameter inserts or grooving inserts (MDT) with a ~ 3mm nose radius. After careful consideration, it was decided to opt for negative C-type inserts and positive/neutral 'c' lock round inserts with appropriate Jetstream tool holders.

Table 16: Tool geometry for round and C-type inserts in their respective tool holders

Tool insert	**Inclination angle (λ)**	**Normal rake angle (γ_n)**	**Principal cutting edge angle (φ)**	**Positive clearance**	**Nose radius (mm)**
Round	0º	0º	45º	7º	5
C-type	-6º	-6º	95º	6º	1.2

The effect of insert edge preparation involving an extra hone (25µm hone radius; coded as E25) and a chamfer (0.15mm×25º) plus hone (15µm); designated as S-type was also investigated, see Figure 53. In addition, the performance of a 1.5µm thick bi-layer physical vapour deposition (PVD) coating, comprising TiAlN (1µm-bottom layer) + TiN (0.5µm-top layer) was also evaluated.

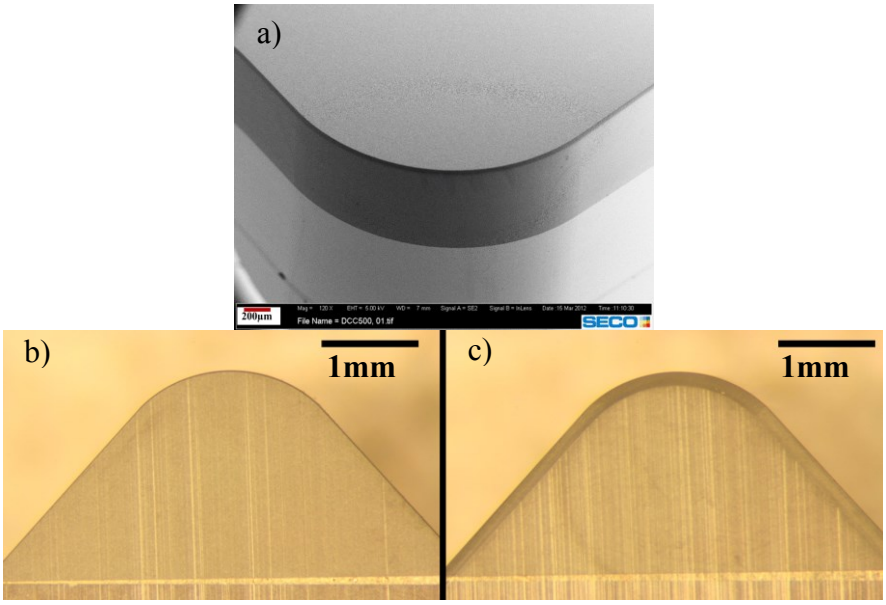

Figure 53**:** Edge preparation (a) SEM micrograph of E25, optical images of (b) E25 and (c) S-type

In Phase 1D tests C-type (CNGA 120412) fixed tool geometry was used but edge preparation was varied at 2 levels; E25 and S-type.

Phases 2A and 2B work involved fixed tool geometry in which uncoated C-type (CNGA 120412) inserts with an E25 edge preparation were used due to their better performance in Phase 1C testing compared to the round type tool geometry. All the finished uncoated/coated inserts for preliminary testing and Phase 1 and 2 work were supplied by Seco.

3.2.3 Medium concentration PCBN inserts and various coating products for Phase 3 test programme

Developed as a result of collaboration between E6 and Seco, PCBN grade; CBN170 having 65% by volume CBN content, 2µm grain size and TiCN binder phase with SiC whisker reinforcement was evaluated in Phase 3. Figure 54 details CBN 170 microstructure. According to the tool manufacturer [38], the inclusion of whisker ceramic fibres provides for increased tool life due to their high toughness and good wear resistance when machining nickel based superalloys without compromising surface integrity.

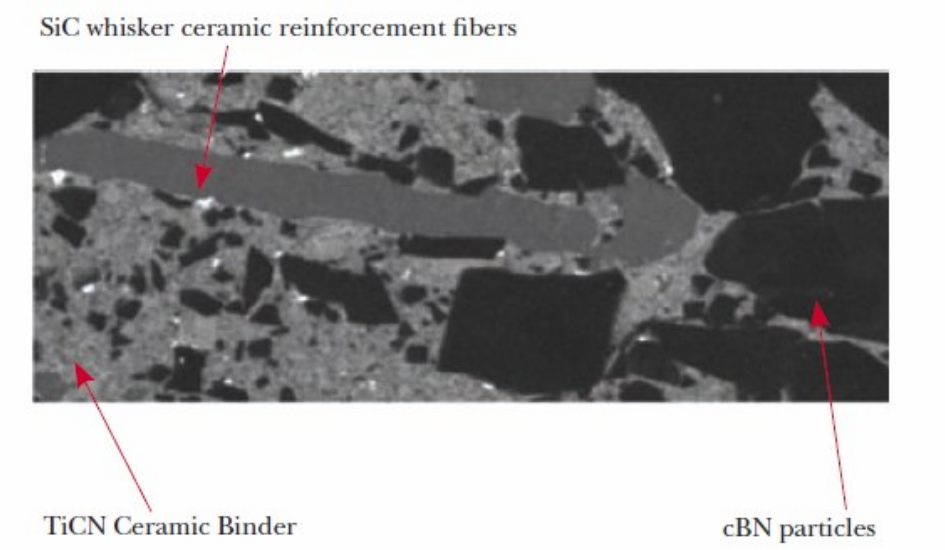

Figure 54: Micrograph of CBN 170 grade [38]

All Phase 3 (3A, 3B, 3C) testing used C-type fixed tool geometry CNGA 120408 with E25 edge preparation, see SEM micrograph shown in Figure 55**.** This geometry was quite similar to the C-type configuration evaluated in Phases 1C, 1D, 2A and 2B work except that the nose radius was 0.8mm for CBN 170 and 1.2mm for DCC 500.

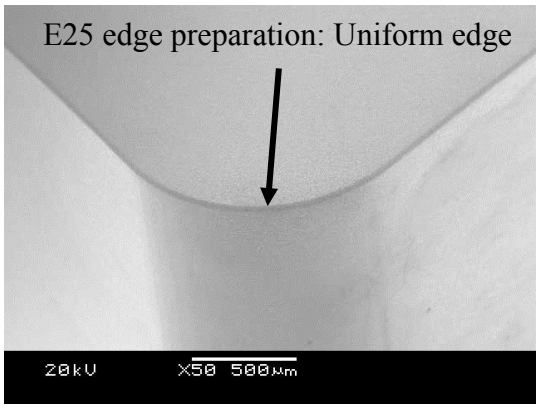

Figure 55: SEM micrograph of new CBN 170 PCBN insert

A variety of PVD coatings from different suppliers including Seco, Balzers and Teer coatings were investigated. All coatings were deposited on CBN 170 inserts and with one exception from Balzers, had non-uniform thickness on both the rake and flank faces. Figure 56 shows ball indenter photographs relating to the measurement of coating thickness on the Balzers coatings (ball dia 20mm) which was 1.62µm and 2.95µm on the rake (value B) and flank faces (value A) respectively.

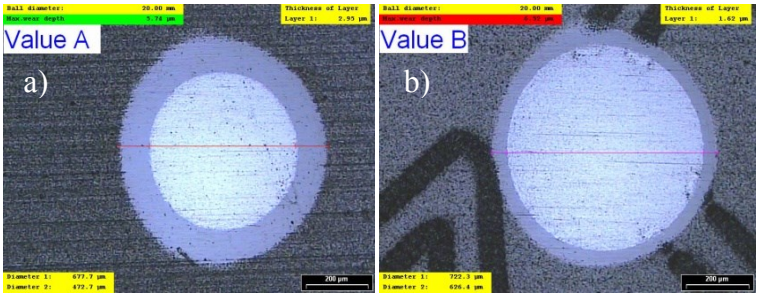

Figure 56: Pictures related to the measurement of coating thickness (a) flank face and (b) rake face

Table 17 provides comprehensive details of the coatings used, including suppliers, thickness, hardness, method of deposition, colour, residual stresses and in one case service temperature etc.

Table 17: Details of coatings

Coating	**Supplier**	**Thickness**	**Hardness**	**Method of deposition**	**Coating details**
TiSiN (Single layer)	Seco	1.5µm	35-40GPa. (3569-4079 HV)	PVD cathodic arc evaporation	Golden in colour, comprising Ti0.86, Si0.14
TiSiN/TiAlN (Multilayer laminated structure:9-10 layers)	Seco	2µm	30-35GPa. (3059-3569 HV)	PVD cathodic arc evaporation	TiAlN was the outermost layer, grey in colour
AlCrN: ALNOVA (Multilayer)	Balzers	2.95µm (F) and 1.62µm (R)	3200HV	PVD arc technology	Bright grey, Max. service temperature 1100ºC, RS: -3.00GPa
CrAlN (Multilayer)	Teer Coatings	3µm	3000HV	Reactive magnetron sputtering	Micro-crystalline, RS:-2GPa
CrAlN (Multilayer)	Teer Coatings	5.5µm	3000HV	Reactive magnetron sputtering	Micro-crystalline, RS:-2GPa

Notes: -RS: residual stresses.

- ALNOVA is the commercial name of the AlCrN coating supplied by Balzers.

-Surface preparation method (for Teer Coating products): 10min ultrasonic cleaning, then dried and placed in the coating chamber which was pumped down to a pressure 2×10^{-5} Torr prior to start of the coating process.

F: flank face and R: rake face

Cross sectional SEM micrographs of TiSiN and TiSiN/TiAlN were supplied from Seco and are shown in Figure 57. In addition to its higher hardness, the single layer TiSiN had a much denser structure compared to the columnar structure observed in the TiSiN/TiAlN coating. Furthermore, the single layer coating had a much smoother outer surface.

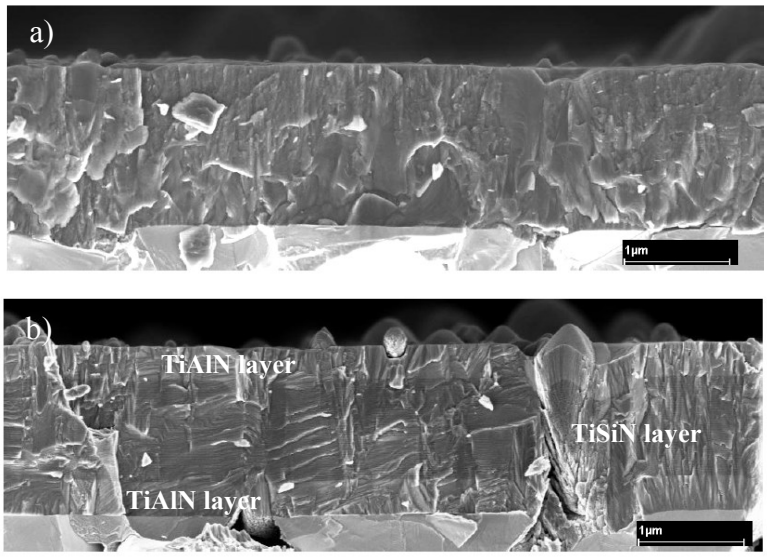

Figure 57: SEM cross sectional micrographs of (a) TiSiN single layer coating and (b) TiSiN/TiAlN multilayer coating

3.3 Equipment

3.3.1 Machine tool

All tests were carried out on a MHP MT-80 CNC turning centre, see Figure 58 which had a variable spindle speed of up to 3000 rpm with a 30kW motor. Further details in terms of its capacity, tool turrets etc. are given in the Table 18.

Table 18: Details of MHP MT-80 CNC turning centre

Maximum machine weight	7700kg
Maximum turning diameter between centres	500mm
Maximum component weight	385kg
Effective chuck to tailstock dimension	1000mm
Maximum tool positions on tool turret	12
Time of tool movement from one station to another in both directions	1.4s
Available power	30kW (40hp)

Figure 58: MHP MT-80 CNC turning centre

3.3.2 Cutting force measurement, experimental set up and cutting fluid application

A Kistler 9257A three component piezo-electric platform dynamometer was used for cutting forces measurement. Signals were processed via charge amplifiers (model 5011A) linked to a PC running Kistler Dynoware software for further analysis. The experimental set up is shown in Figure 59**.** In order to mount the cutting tool on the dynamometer, a bespoke fixture was employed to mount the dynamometer on the tool turret.

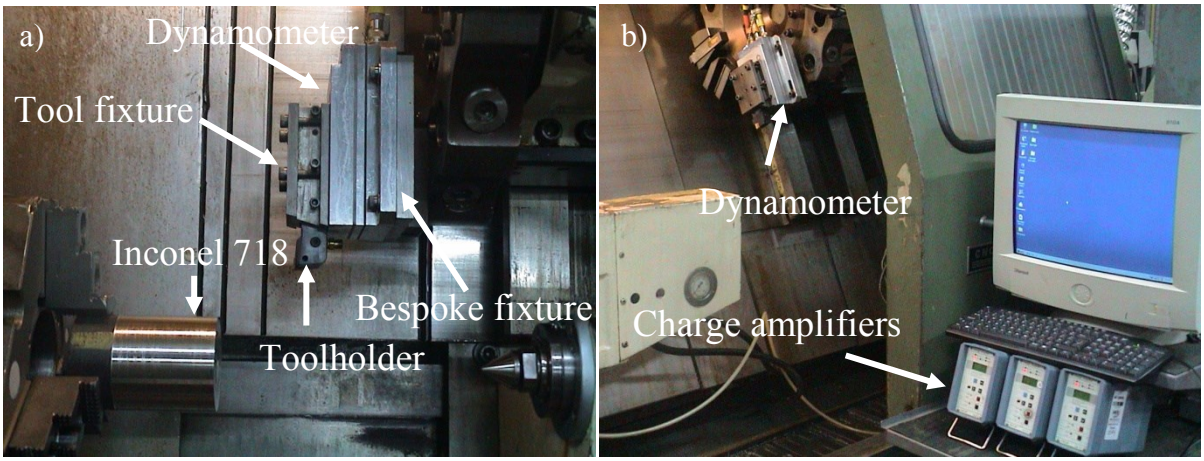

Figure 59: Dynamometer set up on lathe with (a) workpiece and (b) charge amplifiers

The preliminary trials (1A) were carried out dry, however all other tests were conducted wet using Houghton Hocut 3380 water based emulsion containing ~10% oil, which was checked using hand held refractometer (Model HR-099) shown in Figure 60. In order to benchmark the MHI Inconel 718 material against the RR material (Phase 1B), tests were performed under 10bar pressure at a flow rate of ~18litres/min with an external nozzle (3.5mm diameter and ~25mm from the cutting zone) positioned as shown in Figure 61 (a). Jetstream toolholders were used in all other phases of experimental work. For Phases 1C, 2A and 2B, the influence of cutting fluid pressure at 10bar and 100bar with corresponding flow rates of 6.5litres/min and 24litres/min, was investigated. However, Phase 1D and Phases 3A, 3B and 3C were undertaken at a constant cutting fluid pressure of 100bar and 10bar respectively. The cutting fluid was delivered using low pressure and high pressure pump units supplied by Pumps and Equipment Warwick Ltd.; see Figure 61 (b).

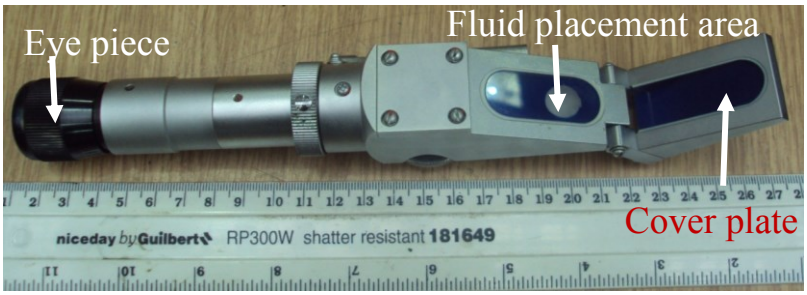

Figure 60: Hand held refractometer

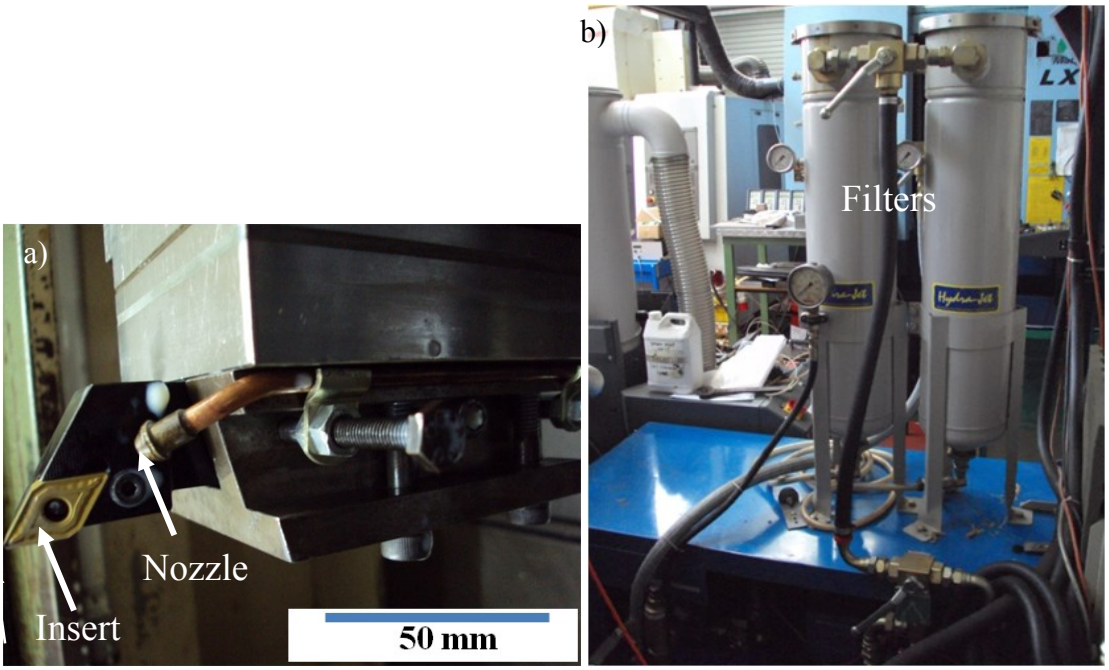

Figure 61: (a) Nozzle for 10bar -18litres/min and (b) low and high pressure units

3.3.3 Fixturing and tool wear measurement

Due to the small length of the bars used in Phases 1A, 1B, 1C and 1D trials, a fixture see Figure 62, was employed during surface roughness measurements.

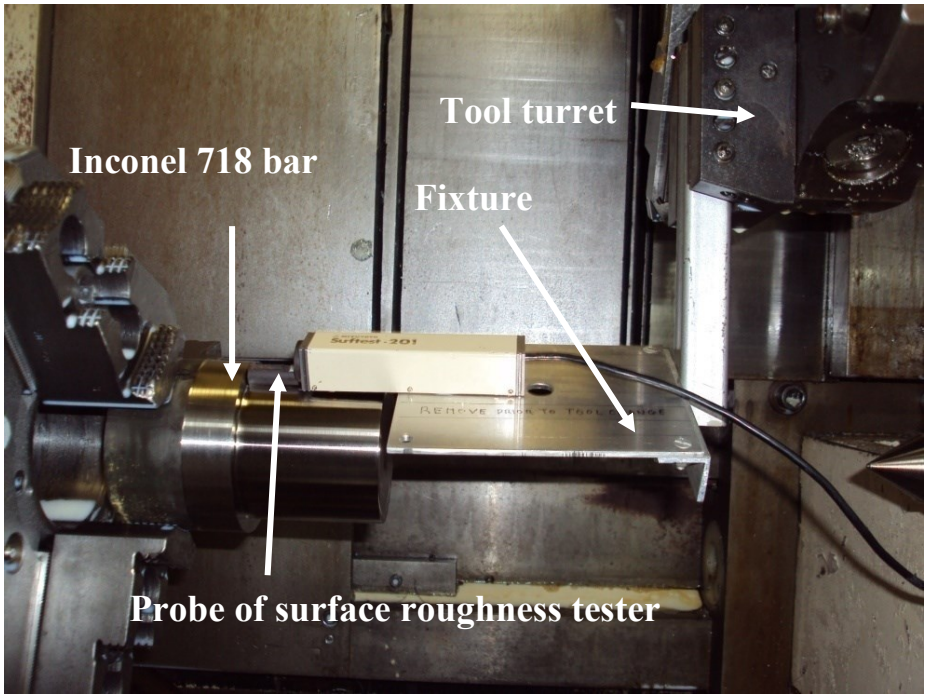

Figure 62: Fixture for surface roughness measurement

Tool wear was measured using a WILD M3Z microscope equipped with a X-Y digital micrometer platform (0.001mm resolution) connected to a Canon 400D DSLR digital camera

for image capture of new and worn inserts; see Figure 63 (a). Figure 63 (b) shows the tool wear measurement setup using a 'V' block for holding the cutting inserts. A round aluminium block with two inclined sides, each at an angle of 45º shown in Figure 64 (a), was produced to take isometric views of the worn inserts using a JEOL 6060 scanning electron microscope (SEM), see Figure 64 (b).

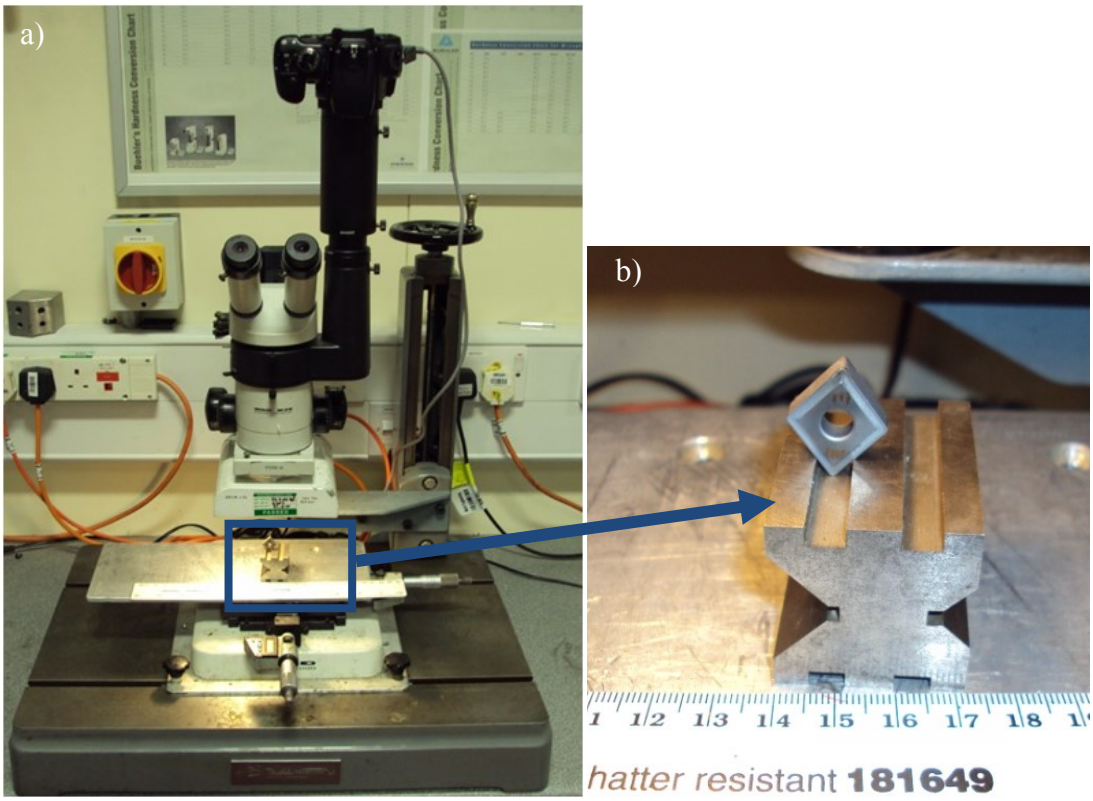

Figure 63: (a) Tool wear measurement set up and (b) fixture to hold the insert

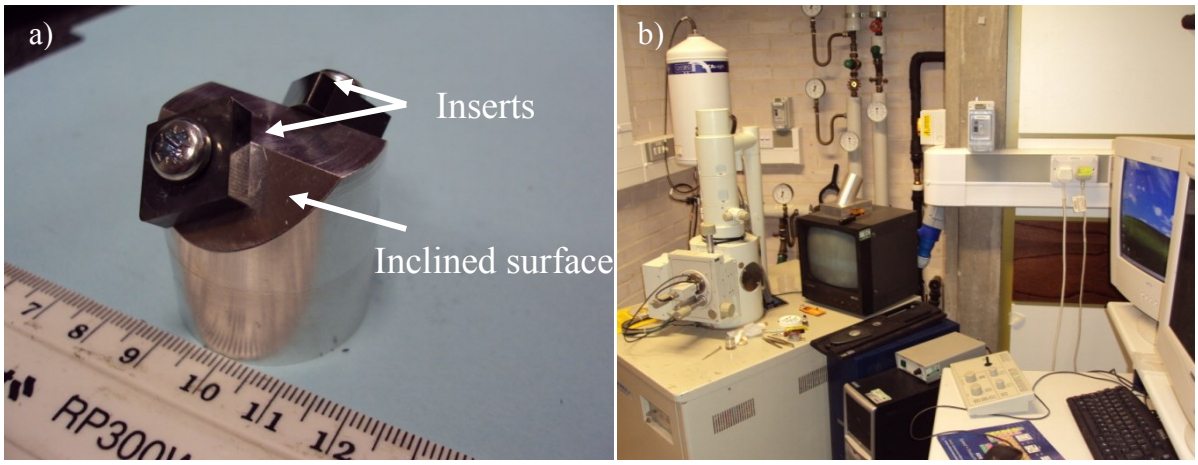

Figure 64: (a) Fixture for SEM micrographs and (b) SEM JEOL 6060

3.3.4 Workpiece surface roughness and integrity assessment

3.3.4.1 Surface roughness measurement

A Mitutoyo Surftest 301 portable surface roughness tester shown in Figure 65 (a) was used to measure workpiece surface roughness periodically over the course of a test. A cut off length of 0.8mm and evaluation length of 4.0mm were used. In Phase 1D and Phase 2B, assessment of surface roughness (2D) and topography was made from wire cut machined samples using a Taylor Hobson Talysurf series 120L laser transducer having a 2µm diamond tipped stylus with the same cut off and evaluation length used for periodic measurements, see Figure 65 (b). Surface roughness measurement (2D and 3D) on the Talysurf 120L is shown in Figure 66. Additionally, 3D maps were produced for selected samples.

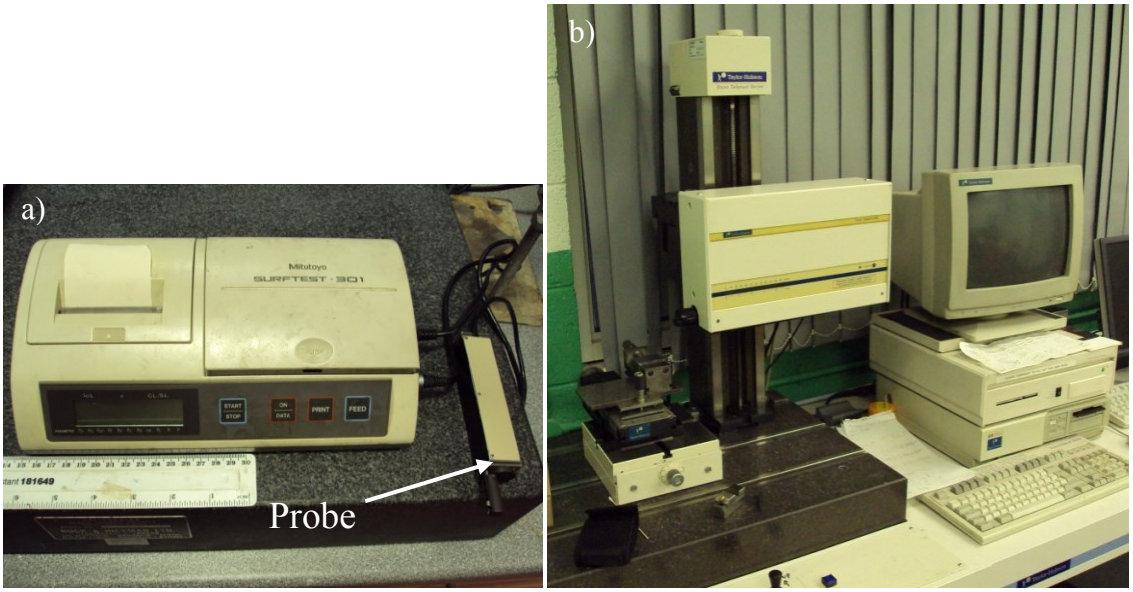

Figure 65: (a) Mitutoyo Surftest 301portable surface roughness tester and (b) Talysurf 120L

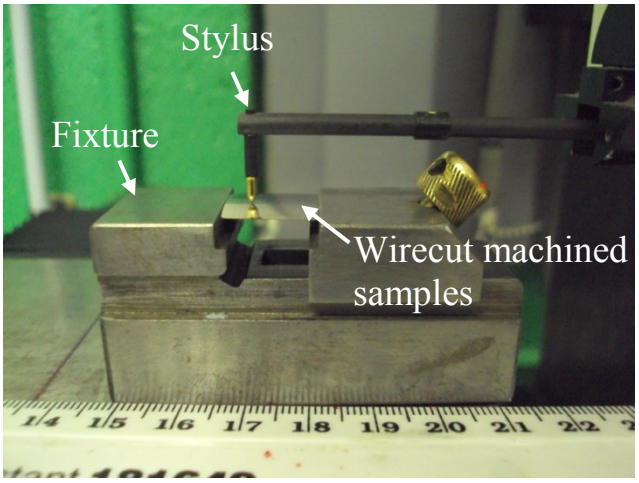

Figure 66: Setup for 2D and 3D surface roughness measurement on Talysurf 120L

3.3.4.2 Surface integrity assessment

Workpiece samples were cut using wire electrical discharge machining (WEDM) according to the direction shown in Figure 67**.** These were subsequently hot mounted in standard and edge retentive Bakelite powder using a Buehler-Simplimet 2 mounting press; see Figure 68 (a). This operated at a pressure of 29MPa and temperature of ~120ºC for 10min. Mounted samples were then ground and polished using the Buehler Alpha-2 speed grinder polisher shown in Figure 68 (b) according to standard Buehler procedure (see Table 19).

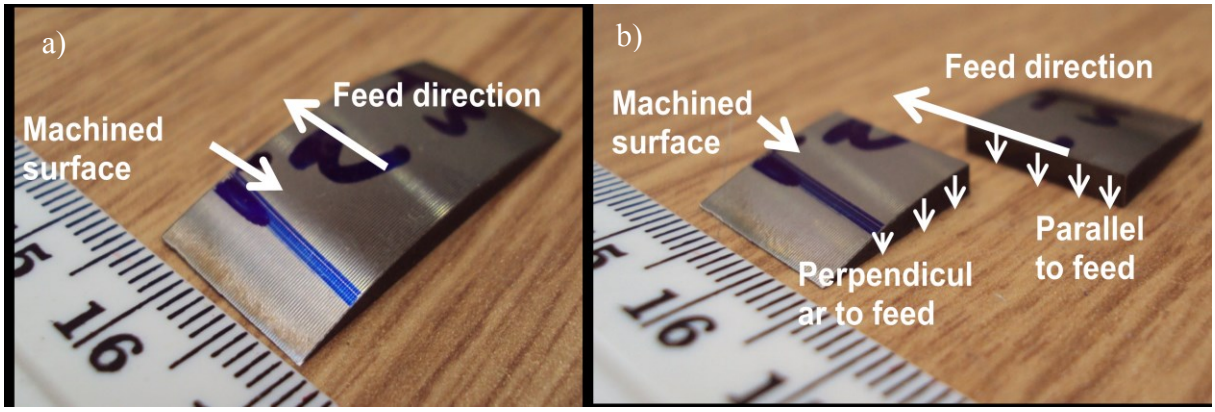

Figure 67: (a) Machined sample and (b) directions for surface integrity assessment

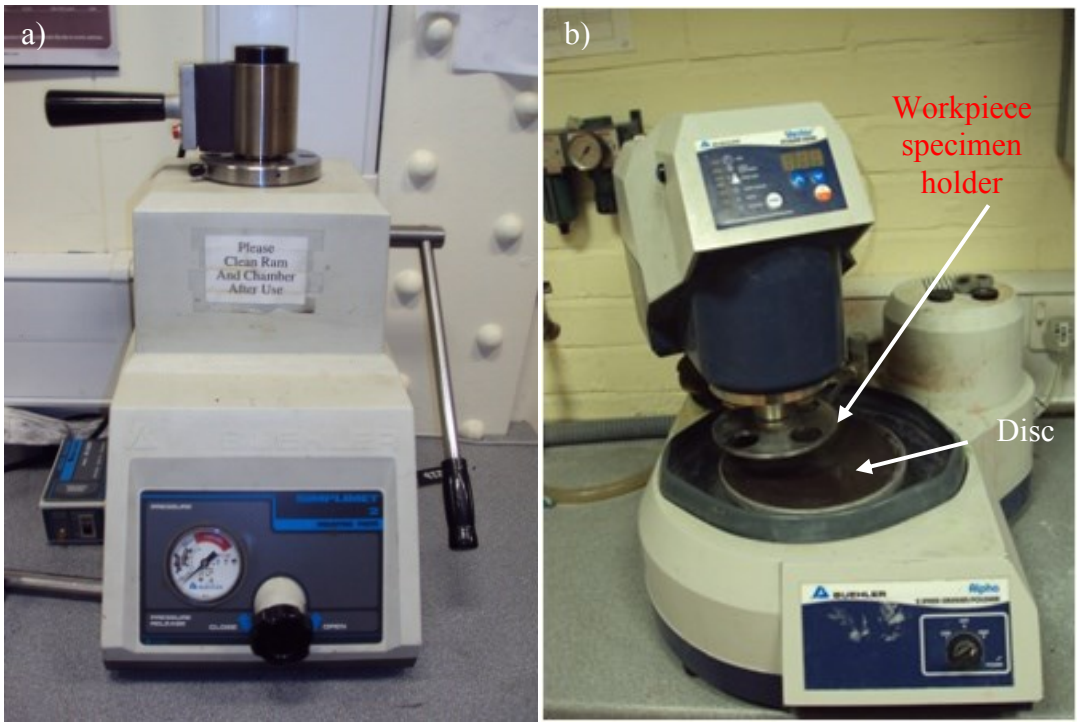

Figure 68: (a) Buehler mounting press and (b) Buehler grinder-polisher

Table 19: Procedure for grinding and polishing of Inconel 718 samples

Grinding				
SiC paper (Grit size-µm)	**Force (N)**	**Time (min)**	**Water ON/OFF**	**Speed (rpm)/rotating direction**
240	25N	5	ON	250/complementary*
1200	25N	5	ON	120/complementary
Polishing				
Polishing cloth	**Force (N)**	**Time (min)**	**Liquid suspension**	**Speed (rpm)/rotating direction**
Trident cloth	25N	5	9µm MetaDi supreme diamond suspension	120/complementary
Trident cloth	25N	5	3µm MetaDi supreme diamond suspension	120/complementary
Microcloth	25N	5	0.05µm Mastermet colloidal silica	120/contrary**

*Complementary: Workpiece specimen holder and grinder disc is rotating in the same direction

** Contrary: Workpiece specimen holder and grinder disc is rotating in the opposite direction

A Mitutoyo microhardness tester HM 124 with a Knoop diamond indenter was used to measure the microhardness of cross sectioned samples at a load of 25g for a dwell time of 15s. A Leica DM LM microscope fitted with a PixeLink camera was used for optical image analysis, which was linked to a computer running Omnimet 8.7 digital image software. Microhardness and optical microscopy equipment is shown in Figure 69**.**

All samples were etched immediately after the final polish using modified Kalling's No. 2 reagent with chemical composition; 10g CuCl2, 250ml HCl and 250ml ethanol. For RR and SI Inconel 718 workpieces, samples were etched for ~1min while for MHI material, a cotton bud soaked in fresh Kalling's was rubbed over the workpiece for ~5min to reveal the microstructure.

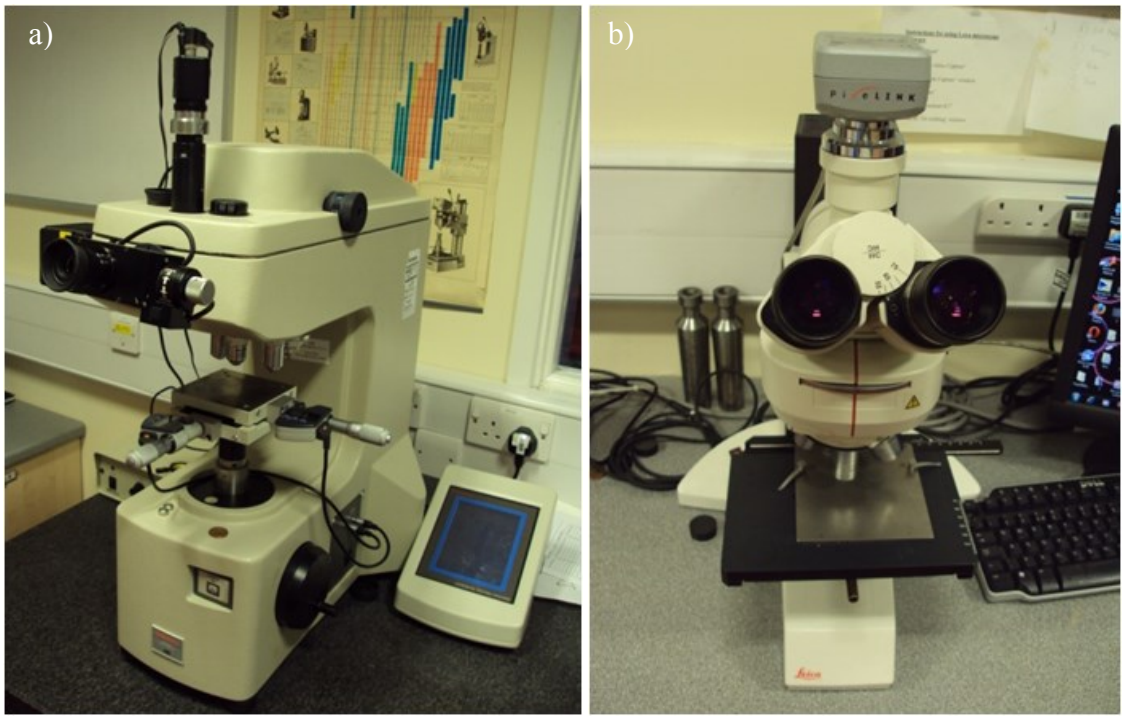

Figure 69: (a) Microhardness tester HM 124 and (b) Leica DMLM microscope

3.4 Experimental design and test arrays

Experimental procedures and the corresponding test arrays employed in the 3 experimental phases are detailed in the following sections.

3.4.1 Phase 1A: Preliminary experimental trials when turning Inconel 718

Phase 1A involved trials to determine the performance of an off-the-shelf PCBN tool (Amborite DBC50) in high speed turning of Inconel 718. The bar was already in stock and had been supplied by RR for a previous PhD project. Cutting speed and feed rate are the most important parameters affecting tool performance, therefore in order to assess their effects on tool wear, four tests were performed at constant depth of cut of 0.2mm under dry cutting conditions. Tests were stopped when either the maximum flank wear (VB_Bmax) reached 300µm or notch wear VB_N approached 600µm. Table 20 details the test array while Table 21 lists the fixed factors including tooling and workpiece material employed.

Table 20: Test array

Tests	Cutting speed (m/min)	Feed rate (mm/rev)
1	150	0.05
2	150	0.10
3	300	0.05
4	450	0.05

Table 21: Fixed factors and levels

Fixed factors	Levels
Depth of cut	0.2mm
Cutting environment	Dry
Tool geometry	SNMN 090316

3.4.2 Phase 1B: Benchmarking of Mitsubishi Inconel 718 workpiece using production approved carbide/PCBN inserts and operating parameters

MHI Inconel 718 material (4 bars) was proposed for Phase 1 trials however the microstructure shown previously in Figure 50 (b) appeared to be different from standard RR disc material due to the presence of delta phase precipitates. After further discussion with RR, it was agreed to perform a number of trials to benchmark the machinability of the MHI material. This involved approved operating parameters and cutting tools (PCBN/carbide inserts) used by RR in production for turning Inconel 718 for shaft applications in order to provide comparative results. New turning inserts (PCBN, uncoated and coated carbide) as well as worn tools (uncoated carbide inserts) were supplied by RR. Approved operating parameters and corresponding tool life details are shown in Table 22 while Table 23 details the test array. Replication tests (Tests 4 and 5) were performed with both the PCBN and uncoated carbide tooling. Full details of edge preparation, surface condition and tool geometry were previously presented in Section 3.2.1.

Table 22: RR approved cutting parameters and tool life

Insert type	Cutting speed (m/min)	Feed rate (mm/rev)	Depth of cut (mm)	Tool life (min)	Cutting environment
PCBN (KD-120) (BZN 6000)	220	0.15	0.25	5	Wet at 10bar, 55litres/min
Uncoated carbide	32	0.15	0.25	10	
Coated carbide	50	0.20	0.50	10	
Note: 10bar was the important factor while the flow rate of 55 litres/min depended on the individual pump ratings relative to the machine employed [143].					

Table 23: Test array for benchmarking trials

Test number	Types of tool	Cutting speed (m/min)	Feed rate (mm/rev)	Depth of cut (mm)
1	Coated carbide	50	0.2	0.50
2	PCBN	220	0.15	0.25
3	Uncoated carbide	32	0.15	0.25
4 (Rep of T2)	PCBN	220	0.15	0.25
5 (Rep of T3)	Uncoated carbide	32	0.15	0.25

Approved parameters relate to a tool life of 5min for PCBN and 10min for uncoated and coated carbide after which the inserts are discarded**.** Testing was performed until a maximum flank wear of 300µm was achieved, after which the worn inserts were compared to those supplied by RR after machining Inconel 718 used in production at RR Derby.

3.4.3 Phase 1C: Influence of tool geometry, edge preparation, cutting environment, surface condition and operating parameters on tool wear/life, surface roughness and cutting forces

Phase 1C aimed to perform a wide ranging preliminary investigation of key output measures including tool life, productivity, cutting forces and surface roughness to provide baseline data for future in-depth trials. In terms of experimental design, an L16 orthogonal array was initially identified/selected involving a total of 6 factors with 2 at 4 levels and the other 4 factors at 2 levels. Unfortunately, the L16 could not provide the necessary degrees of freedom to adequately evaluate interactions between variables. An L36 Taguchi design was deemed more realistic but this required the 2 factors at 4 levels to be limited to 3 levels while keeping the other 4 factors at 2 levels. With a modified L36 orthogonal array however, it was possible to accommodate a high proportion of interactions in addition to variation in 6 factors including tool geometry, edge preparation, cutting environment and surface condition; each at

two levels, with cutting speed and feed rate at three levels, see Table 24. In the event, this was the plan adopted with all trials performed at constant depth of cut of 0.2mm using DCC 500 PCBN tooling. Trials were conducted in a random order and confirmation tests were performed according to the results obtained from the statistical analysis and main effects plots.

Table **25** shows the modified Taguchi orthogonal array.

Table 24: Variable factors and levels

Factors	**Levels**		
Insert shape (A)	Round	C-type	
Edge preparation (B)	E25	S-type	
Cutting environment (C)	10bar	100bar	
Surface condition (D)	Uncoated	Coated [(Ti,Al)N+TiN]	
Cutting speed (m/min) (E)	150	300	450
Feed rate (mm/rev) (F)	0.05	0.10	0.20

Tool wear was measured in accordance with ISO-3682 with a tool life criterion of 300μm flank wear. A test was considered to be completed once the flank wear criterion was met. Optical photomicrographs were taken of tools both in the new and worn condition. ANOVA and main effects/interaction plots were generated using Minitab software (version 15.1.20.0). It was believed that a high error percentage was possibly due to the effect of interactions, which were not accounted for in the standard ANOVA model (based on main effects only). Therefore, the analysis was extended to a stepwise regression procedure to include most of the interactions at the cost of introducing non-orthogonality in the design. A total of 35 degrees of freedom (DOF) were available to accommodate main effects and interactions among the factors. An initial model was generated to accommodate main effects plus all 2-way interactions except one 2-way interaction between cutting speed and feed rate. This was not accommodated despite the available degrees of freedom due to complete confounding with other effects/interactions already in the model. However partial confounding still existed between the interactions added in the model. In order to simplify/reduce the non-orthogonality of the initial model, the stepwise backward removal method was employed to generate a final model by removing the interactions one by one (interaction which had the highest P-value among other interactions and appeared to be non-significant with a P value greater than 0.05) while keeping the main effects in the model. Thus the final model included the main effects and only those interactions which were

significant. To order the interactions according to their importance, a stepwise forward entry regression procedure was used to investigate the contribution of each interaction by adding them one-by-one to the main effects and calculating the R-Square adjusted (R^2Adj.) value again. Any corresponding increase in the R^2Adj value was compared with the one calculated based on main effects only.

Table 25: A modified OA L36 for process control variables (A-F) and their corresponding levels

Exp. No.	Tool geometry (A)	Edge Preparation (B)	Cutting environment (C)	Surface condition (D)	Cutting speed (E) (m/min)	Feed rate (F) (mm/rev)
1	Round	E25	10bar	Uncoated	150	0.05
2	Round	E25	10bar	Uncoated	300	0.1
3	Round	E25	10bar	Uncoated	450	0.2
4	Round	E25	10bar	Uncoated	150	0.05
5	Round	E25	10bar	Uncoated	300	0.1
6	Round	E25	10bar	Uncoated	450	0.2
7	Round	E25	100 bar	(Ti,Al)N+TiN	150	0.05
8	Round	E25	100 bar	(Ti,Al)N+TiN	300	0.1
9	Round	E25	100 bar	(Ti,Al)N+TiN	450	0.2
10	Round	S-type	10bar	(Ti,Al)N+TiN	150	0.05
11	Round	S-type	10bar	(Ti,Al)N+TiN	300	0.1
12	Round	S-type	10bar	(Ti,Al)N+TiN	450	0.2
13	Round	S-type	100 bar	Uncoated	150	0.1
14	Round	S-type	100 bar	Uncoated	300	0.2
15	Round	S-type	100 bar	Uncoated	450	0.05
16	Round	S-type	100 bar	(Ti,Al)N+TiN	150	0.1
17	Round	S-type	100 bar	(Ti,Al)N+TiN	300	0.2
18	Round	S-type	100 bar	(Ti,Al)N+TiN	450	0.05
19	C-type	E25	100 bar	(Ti,Al)N+TiN	150	0.1
20	C-type	E25	100 bar	(Ti,Al)N+TiN	300	0.2
21	C-type	E25	100 bar	(Ti,Al)N+TiN	450	0.05
22	C-type	E25	100 bar	Uncoated	150	0.1
23	C-type	E25	100 bar	Uncoated	300	0.2
24	C-type	E25	100 bar	Uncoated	450	0.05
25	C-type	E25	10bar	(Ti,Al)N+TiN	150	0.2
26	C-type	E25	10bar	(Ti,Al)N+TiN	300	0.05
27	C-type	E25	10bar	(Ti,Al)N+TiN	450	0.1
28	C-type	S-type	100 bar	Uncoated	150	0.2
29	C-type	S-type	100 bar	Uncoated	300	0.05
30	C-type	S-type	100 bar	Uncoated	450	0.1
31	C-type	S-type	10bar	(Ti,Al)N+TiN	150	0.2
32	C-type	S-type	10bar	(Ti,Al)N+TiN	300	0.05
33	C-type	S-type	10bar	(Ti,Al)N+TiN	450	0.1
34	C-type	S-type	10bar	Uncoated	150	0.2
35	C-type	S-type	10bar	Uncoated	300	0.05
36	C-type	S-type	10bar	Uncoated	450	0.1

A comparative test was also performed using PCBN inserts from Kennametal (supplied for Phase 1B by RR) and Seco (Test 36 of Phase 1C) at a cutting speed of 450m/min, feed rate of 0.1mm/rev and depth of cut of 0.20mm.

Table 26 gives relevant insert, toolholder and cutting fluid details.

Table 26: Details of grade, insert type, toolholder, cutting edge preparation and cutting fluid employed for Kennametal and Seco PCBN inserts

	PCBN-Kennametal	**PCBN-Seco**
Grade	KD-120 (BZN 6000: 90% CBN with Ni/Co binder)	DCC 500 (50% CBN, 2µm grain size with TiC binder)
Insert type	DNMA 150608	CNGA 120412
Tool holder	PDJNR 2525M15	PCLNR 2525M12JET
Cutting edge	S-type (0.10mm×20º)	S-type (0.15mm×25º)
Cutting fluid	10bar~18litres/min flow rate with an external nozzle, used in Phase 1B.	10bar~6.5litres/min with Jetstream toolholder

3.4.4 Phase 1D: Evaluation of edge preparation and cutting speed on workpiece surface integrity

Here the work investigated the performance of two types of edge preparation involving E25 and S-type at two different cutting speeds; 300m/min and 450m/min. A full factorial design in which two factors each at 2 levels was considered using both new and worn tools (VB_Bmax.=300µm). Published literature [42] suggested the importance of edge preparation and cutting speed on workpiece surface integrity. Tool geometry (C-type), surface condition (uncoated), feed rate (0.20mm/rev) and cutting environment (100bar) were fixed based on the results obtained in Phase 1C. Table 27 and

Table 28 detail the fixed factors and levels and the final test array respectively.

Table 27: Fixed factors and levels

Factors	**Level**
Tool geometry	C-type
Feed rate (mm/rev)	0.20
Cutting environment	100bar at 24litres/min

Insert surface condition	Uncoated

Table 28: Test array with corresponding levels

Test number	Edge preparation	Cutting speed (m/min)	Tool condition	
1	E25	300	New	Worn (VB_Bmax.=300µm)
2	S-type	300	New	Worn (VB_Bmax.=300µm)
3	E25	450	New	Worn (VB_Bmax.=300µm)
4	S-type	450	New	Worn (VB_Bmax.=300µm)

3.4.5 Phase 2A: Effect of cutting speed, feed rate and cutting environment on tool wear/life, surface roughness and cutting forces

A full factorial design was employed in Phase 2A involving variations in cutting speed, feed rate and environmental condition. In terms of productivity, a cutting speed of 300m/min and feed rate of 0.20mm/rev with C-type tool geometry was considered preferable. In addition, it had been reported that negative rake geometry generally induced compressive residual stresses in the machined surface [144], and therefore the C-type insert was selected for the present work. A feed rate of 0.15mm/rev was suggested to provide acceptable performance when machining Inconel 718 with PCBN, based on previous RR experience. As productivity was also a key consideration, the variable levels for cutting speed and feed rate specified for Phase 2 testing were 300 and 450 m/min and 0.15 and 0.20 mm/rev respectively. While greater levels of force and a reduction in tool life were recorded when employing high pressure (Jetstream 100 bar) due to thermal shock, swarf entanglement was more prominent when using lower cutting fluid pressure (Jetstream 10bar). The two levels of cutting fluid pressure were therefore maintained (10 and 100 bar) in the current trials. The variable factors and associated levels are detailed in Table 29**.**

Better performance in terms of edge preparation was observed with an E25 edge preparation both in Phases 1C and 1D, therefore it was selected for the current trials. Furthermore, an E25 edge preparation was recommended by Seco for finish turning of Inconel 718. From a surface condition viewpoint, previously published literature [66, 145] suggested that surfaces produced with coated tools showed higher tensile residual stresses in comparison to those machined with uncoated inserts. It was therefore decided that all tests in Phase 2 work would utilise uncoated inserts, with an investigation of suitable coatings to be undertaken in future Phase 3 trials. Fixed factors and their corresponding levels are detailed

in Table 30. Statistical analysis for workpiece surface roughness however, was not performed in the current phase because measurements were made against flank wear of cutting tool using the Mitutoyo Surftest 301 portable roughness tester. For further precision, samples were machined at these given parameters using both new and worn tools in Phase 2B and details along with statistical analysis is presented in Section 4.6.1.

Table 29: Details of variable factors and levels

Factors	**Levels**	
	1	**2**
Cutting speed (m/min)	300	450
Feed rate (mm/rev)	0.15	0.20
Cutting environment	10bar~6.5litres/min	100bar~24litres/min

Table 30: Details of fixed factors and levels

Factors	**Level**
Tool geometry	C-type
Edge preparation	E25
Depth of cut	0.20
Tool grade	DCC500

A tool life criterion of $VB_B max.$ = 200µm was employed based on RR practice. Full test array details are presented in Table 31. Due to limitations in workpiece material and tooling, only one replication test was performed for Test 1 while Test 7 of the current phase was compared with Test 23 of Phase 1C to assess the difference in machinability of MHI and SI Inconel 718 bars.

Table 31: Test array with corresponding levels

Test number	**Order number**	**Cutting speed (m/min)**	**Feed rate (mm/rev)**	**Cutting environment (bar)**
1	1	300	0.15	10
2	4	450	0.15	10
3	2	300	0.20	10
4	3	450	0.20	10
5	8	300	0.15	100
6	7	450	0.15	100
7	5	300	0.20	100
8	6	450	0.20	100

3.4.6 Phase 2B: Assessment of cutting environment, cutting speed and feed rate effects on workpiece surface integrity

Following on from tool life testing in Phase 2A, workpiece surface integrity aspects involving surface roughness, microhardness and microstructure were evaluated in Phase 2B employing both new and worn tools (VB_Bmax =200µm). The fixed and variable factors were the same as in Phase 2A. A bar length of 17mm was cut for each test as shown in Figure 70. Tests 1 & 3 from Phase 1D were compared against Tests 7 & 8 to investigate the difference in surface integrity between the MHI and SI materials however, exact comparisons could not be made due to the differences in the tool wear. (VB_Bmax =300µm for Phase 1D and VB_Bmax =200µm for Phase 2A). Additionally, 3D maps were produced only for Tests 3, 4 and 8.

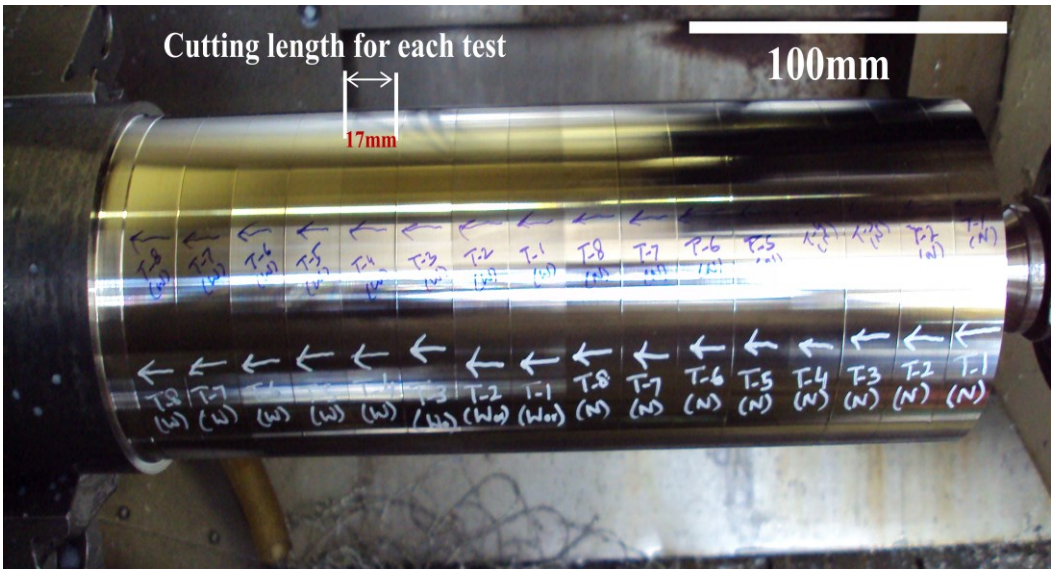

Figure 70: Inconel 718 bar for surface integrity trials using both new and worn tools

3.4.7 Phase 3A: Evaluation of alternative PCBN grade and coatings on tool wear/life, surface roughness and cutting forces

Phase 3A involved experimental trials to evaluate the performance of a recently developed PCBN grade (CBN 170) and various coatings on tool life. Testing used the RR tool life criteria adopted in Phase 2 trials. Full details of PCBN grade CBN 170 and the various coating products were presented in Section 3.2.3. Results from Phase 2 testing was used as a baseline for selection of Phase 3 test parameters. Initially it was decided to vary cutting speed at 2 levels (300m/min, 450m/min) while keeping the cutting environment (10bar) and feed rate (0.15mm/rev) fixed. However based on Seco recommendations, another level of cutting speed (200m/min) was incorporated in the test plan. A full factorial design

involving 2 factors (1 at 3 levels and other at 6 levels) was employed, which entailed 18 runs. A number of uncoated PCBN inserts product code CNGA 120408E25 each having 4 edges, were supplied to relevant companies for coating. The performance of the CBN 170 grade was compared against DCC 500 (Phase 2 trials), but there were minor variations in tool geometry, not least the use of a 0.8mm nose radius with CBN 170 grade inserts and 1.2mm nose radius with DCC 500 inserts. Fixed and variable factors with their corresponding levels are detailed in Table 32 and Table 33 respectively. Table 34 shows the test array for tool life evaluation. One replication test was performed with Tests 5 and 6.

Table 32: Fixed factors and levels

Factors	**Level**
Tool geometry	C-type
Feed rate	0.15mm/rev
Cutting environment	10bar at 6.5litres/min

Table 33: Variable factors and levels

Factors	**Levels**					
	1	**2**	**3**	**4**	**5**	**6**
Cutting speed (m/min)	200	300	450			
Surface condition	Uncoated	TiSiN	TiSiN/TiAlN	AlCrN	CrAlN (3µm)	CrAlN (5.5µm)

Table 34: Test array for tool life evaluation

Test number	Cutting speed (m/min)	Surface condition
1	200	Uncoated
2	200	TiSiN
3	200	TiSiN/TiAlN
4	200	AlCrN (ALNOVA)
5	200	CrAlN (3µm)
6	200	CrAlN (5.5µm)
7	300	Uncoated
8	300	TiSiN
9	300	TiSiN/TiAlN
10	300	AlCrN (ALNOVA)
11	300	CrAlN (3µm)
12	300	CrAlN (5.5µm)
13	450	Uncoated
14	450	TiSiN
15	450	TiSiN/TiAlN
16	450	AlCrN (ALNOVA)
17	450	CrAlN (3µm)
18	450	CrAlN (5.5µm)

The performance of the CBN 170 grade was compared against results reported by M'Saoubi et al. [126] in terms of tool life and surface integrity. Unfortunately variations in terms of tool geometry and cutting parameters, prevented an exact comparison, see Table 35.

Table 35: Details for the basis of comparison between Phase 3 and M'Saoubi et al.'s work [126]

Basis of comparison	Current work	M'Saoubi et al. [126]
Tool geometry	CNGA120408E25	TNGN110308E25
Depth of cut (mm)	0.20	0.25
PCBN grade, cutting speeds (200m/min and 300m/min), feed rate (0.15mm/rev) were same in both investigations.		

3.4.8 Phase 3B: Effect of alternative PCBN grade and tool coatings on workpiece surface integrity

Due to limitations in the number of coated insert edges available, it was decided to evaluate all coated inserts in the new condition at an optimum cutting speed of 300m/min (in terms of material removal rate and uniform wear progression). Worn edges were not evaluated as the coatings failed to provide any benefit in terms of tool life. Uncoated inserts were also used at a cutting speed of 300m/min and 450m/min, both in new and worn condition to benchmark the performance of CBN 170 against DCC 500. Additionally, despite the fracture/BUE observed at a cutting speed of 200m/min, longer tool life was recorded with the uncoated and TiSiN coated inserts in Tests 1 and 2, therefore it was decided to carry out workpiece surface integrity evaluation for these tests. The full test array is shown in Table 36. Cutting fluid pressure and feed rate was fixed at 10bar and 0.15mm/rev respectively.

Table 36: Test array for surface integrity evaluation with corresponding levels

Test	Surface condition	Cutting speed (m/min)	Tool condition
1	Uncoated	200	Worn (VB_Bmax =200µm)
2	TiSiN	200	Worn (VB_Bmax =200µm)
7	Uncoated	300	New
7	Uncoated	300	Worn (VB_Bmax =200µm)
8	TiSiN	300	New
9	TiSiN/TiAlN	300	New
10	AlCrN	300	New
11	CrAlN (3µm)	300	New
12	CrAlN (5.5µm)	300	New
13	Uncoated	450	New
13	Uncoated	450	Worn (VB_Bmax =200µm)

3.4.9 Phase 3C: Effect of PCBN grades and cutting environment on residual stresses

Phase 3C was designed to investigate the effect of tool condition (new and worn VB_Bmax =200µm), cutting environment (10bar, 100bar) and PCBN grade (DCC500, CBN 170) on workpiece residual stress. Tool geometry, feed rate and cutting speed were fixed (see Table 37). Four tests were planned and the full test matrix is shown in Table 38. The effect of tool condition and cutting environment was investigated using DCC500 PCBN. Except for good chip breakability, no significant benefit was found in terms of tool life and surface

integrity (microhardness, microstructure, surface roughness) when employing high cutting fluid pressure of 100bar. However, it was believed that the better cooling and lubricating effects would minimise heat transfer into the workpiece and hence benefit the residual stress state, therefore two levels of cutting fluid pressure were included in the test array. Sharman et al. [71] reported a ~700MPa reduction in the level of tensile residual stresses at a cutting fluid pressure of 450bar compared to flood cooling at 5bar which were ~1600MPa with the latter. Furthermore, Habak and Lebrun [146] also recorded a ~100-200 MPa decrease in the level of tensile residual stresses at 80MPa cutting fluid pressure compared to 20MPa when turning austenitic stainless steel (AISI 316L) using carbide inserts. Additionally, published literature [147] has highlighted the importance of high thermal conductivity of cutting tools on residual stresses when turning of Inconel 718 and it is well established that the percentage of CBN in PCBN tools has a direct bearing on thermal conductivity [141]. Since in the present work both PCBN grades employed had different CBN content and binder composition, it was decided to compare their performance in terms of residual stresses. However, it is worth mentioning that the tool nose radius was different for both PCBN inserts. Table 38 shows the test array with their corresponding levels.

Table 37: Fixed factors and levels

Factors	Level
Tool geometry	C-type
Feed rate	0.15mm/rev
Cutting speed	300m/min

Table 38: Test array with corresponding levels

Tests	Grade	Tool condition	Cutting environment
1	DCC 500	New	10bar
2	DCC 500	Worn ($VB_B max$ =200μm)	10bar
3	DCC 500	New	100bar
4	CBN 170	New	10bar
Note: Tool nose radius was 1.2mm and 0.8mm for DCC 500 & CBN 170 respectively.			

The hole drilling method was used for residual stress measurement. Two discs 27mm thick and 100mm diameter were wire cut from the bar of SI Inconel 718, see Figure 71 (a). Both sides of each disc were face machined down to 45mm diameter to accommodate the 4 tests, see Figure 71 (b). The discs were subsequently sent to Stresscraft Ltd. Leicestershire, UK for residual stress measurement. This entailed fixing strain gauge rosette type 'Vishay Precision Group EA-06-031RE-120' to each disc face prior to incremental drilling, which

was undertaken on a miniature 3 axis PC controlled drilling machine with a 0.60mm diameter drill, see Figure 72 (a) and (b).

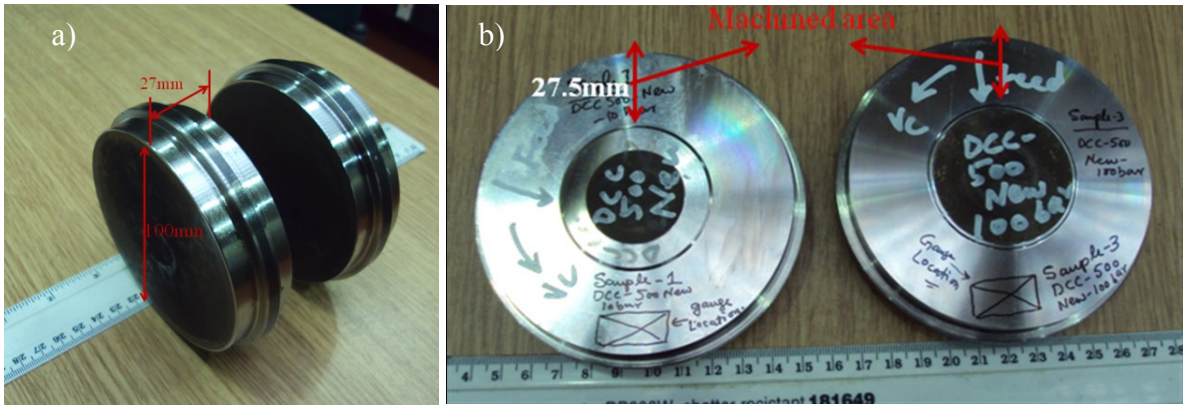

Figure 71: a) Discs specimens for deep hole drilling method and (b) sample showing the machined area

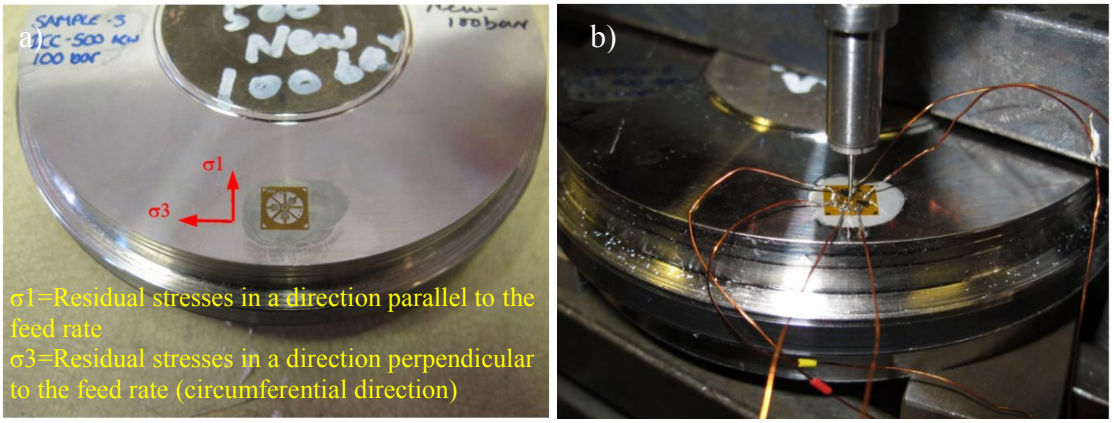

Figure 72: (a) Strain gauge installation and (b) incremental drilling set up

Four small discs each 50mm diameter and 20mm thickness were also produced from the same bar as shown in Figure 73 (a) in accordance with requirements for XRD analysis and facilities in Seco, Sweden were utilised for this purpose. The small diameter of the XRD samples meant that the cutting length was reduced to ~5mm, see Figure 73 (b) as machined speed limitations were exceeded beyond this length. Unfortunately, the XRD residual stress measurements were not reliable due to large standard deviation in the results. According to the Seco, this was likely due to certain problems in XRD machine, however it was decided that these measurements will be repeated after fixing the problem and hence have not been presented in the thesis.

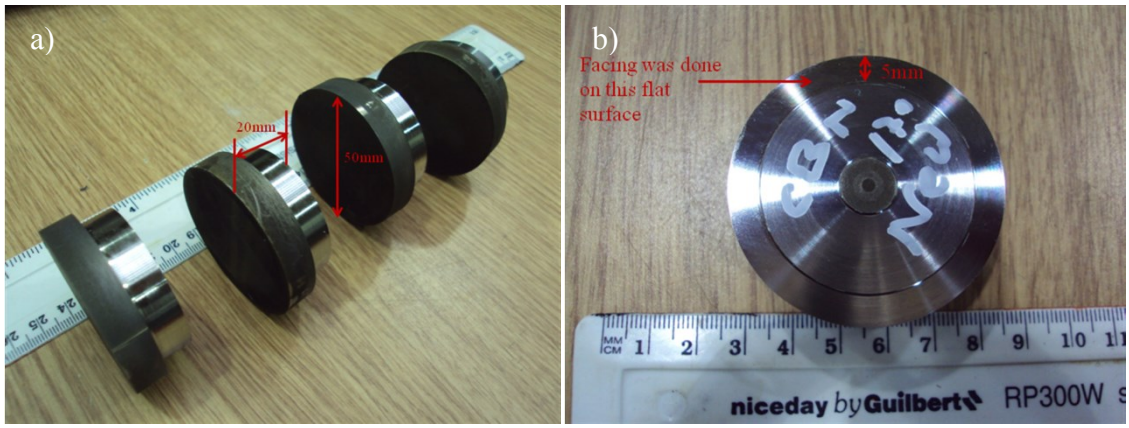

Figure 73: (a) Discs for XRD measurements and (b) sample showing the machined area

4. RESULTS AND DISCUSSION

4.1 Phase 1A: Preliminary experimental trials when turning Inconel 718

Tool life did not exceed 1.63min (Test 1) in any of the trials with a minimum of 0.43min recorded in Test 2. The highest volume of workpiece material removed however was seen in Test 4 (3.71cm^3) despite the marginally lower tool life of 0.92min, see Figure 74**.** Figures 75 and 76 detail SEM images of worn tools used in Tests 1, 2, 3 and 4 respectively. Substantial grooving at the tool nose and notching at the flank face was prevalent when machining at the lower cutting speed of 150m/min, irrespective of feed rate. In contrast, as cutting speed was increased to 300 and 450 m/min (Tests 3 and 4), rapid catastrophic fracture of the cutting edges were observed together with grooves/notches on the flank face. Notch wear was detrimental to tool life in Test 1 while flank wear determined the tool life for Tests 2, 3 and 4 as shown in Figure 77.

According to Shaw et al. [148], greater strain hardening of high temperature strength alloys can generally lead to a larger energy per unit volume at the edges of the chip. This is because the chip is free to expand due to greater strain at the edges compared to the central region, hence increasing the real contact area between the tool-chip interface for weld formation. As the welds at the tool-chip interface are severed, pieces of the tool material are detached which results in the formation of a groove at the tool nose. Further grooves are generated at the tool nose as machining progressed. The notch on the flank face was likely due to rubbing against uncut/re-deposited material on the workpiece or interactions with chip side flow. Different reasons of groove formation have been reported in the literature, which are dependent on factors such as tool and workpiece material combination, tool geometry, operating parameters and cutting environment [149-150].

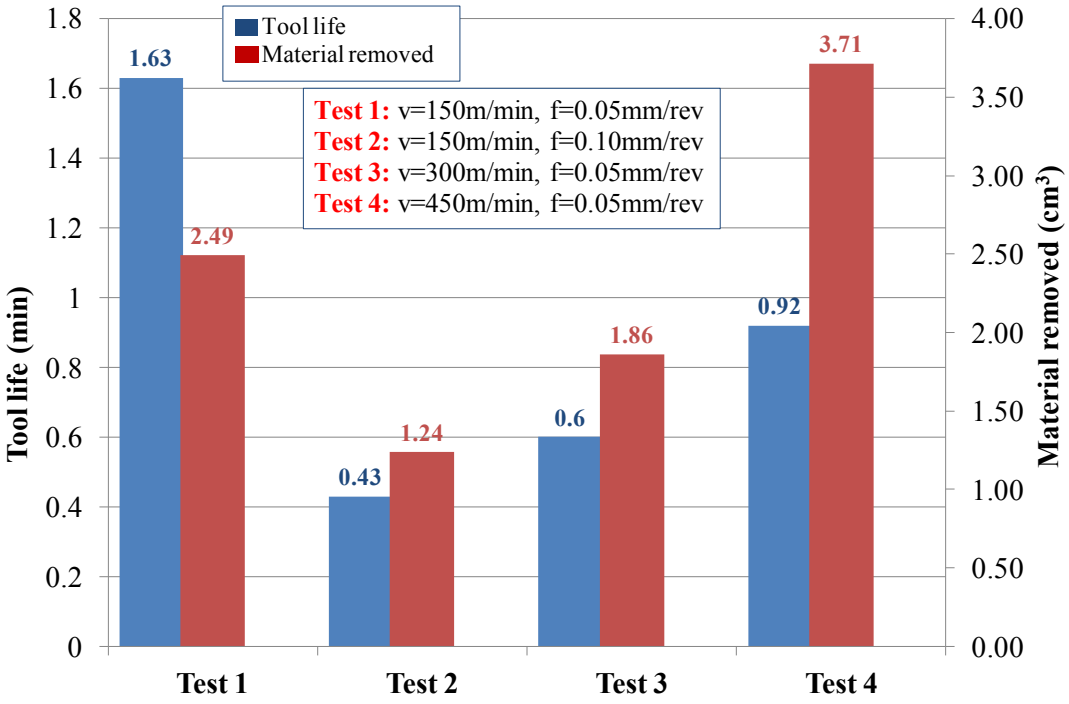

Figure 74: Tool life and volume of material removed in each test

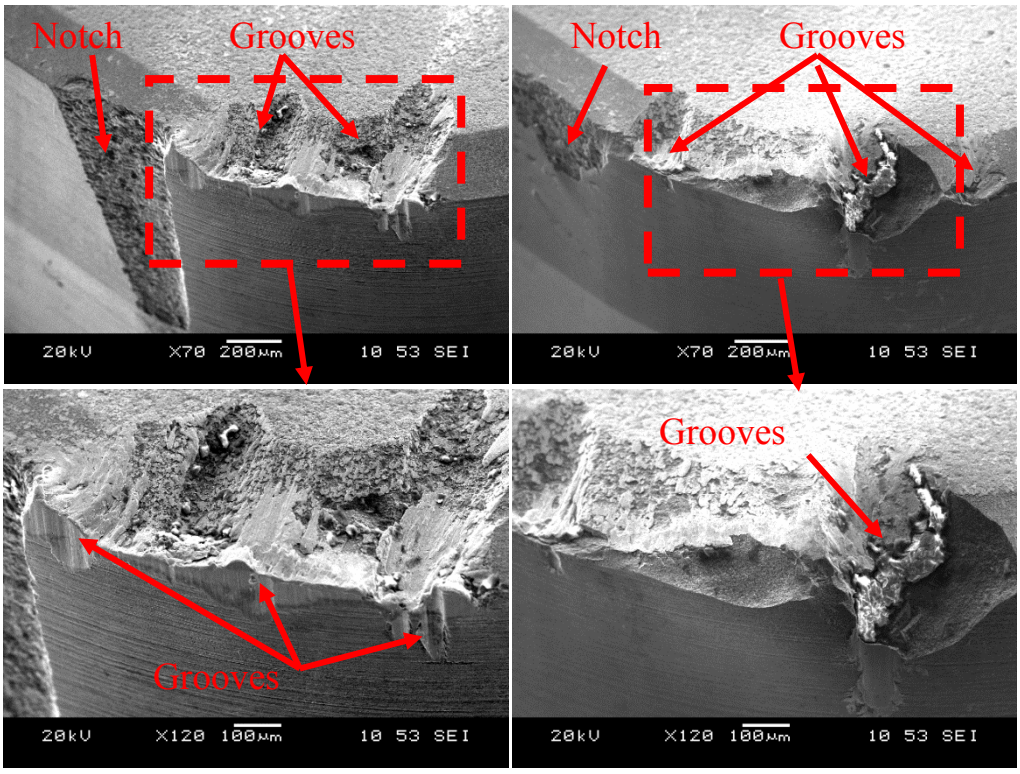

a) Test 1 b) Test 2

Figure 75: SEM images at the end of tool life of (a) Test 1 and (b) Test 2

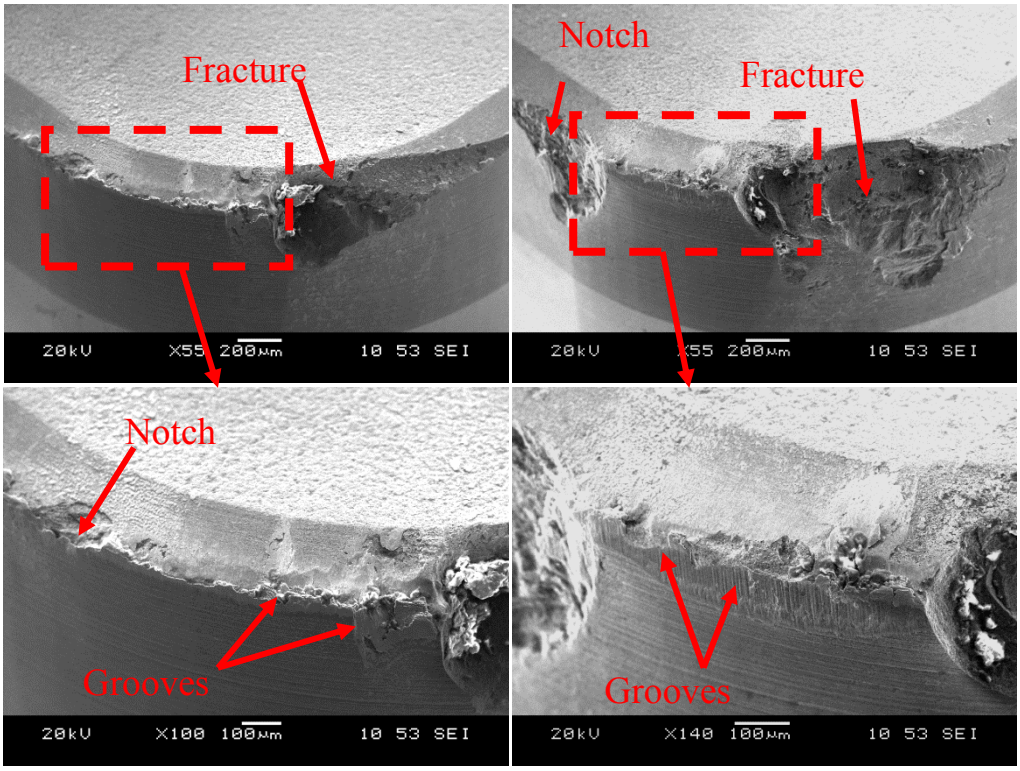

a) Test 3 b) Test 4

Figure 76: SEM images at the end of tool life of (a) Test 3 and (b) Test 4

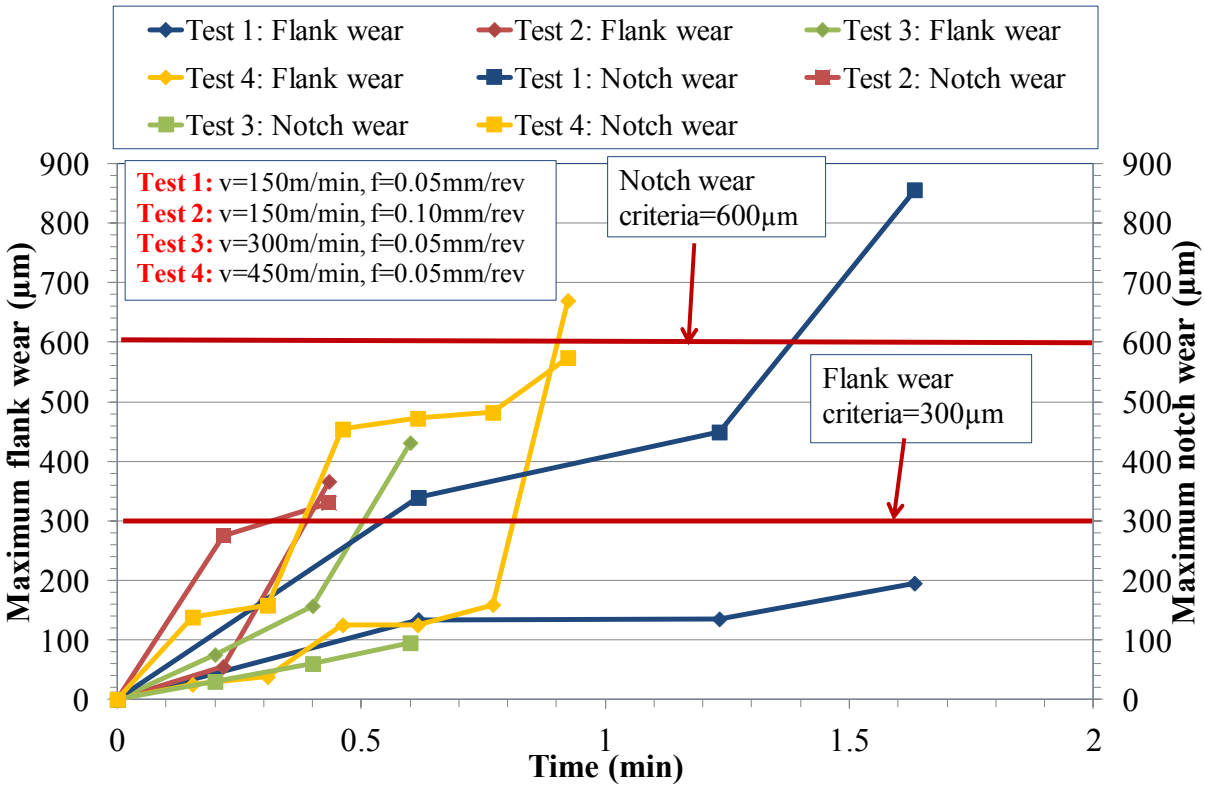

Figure 77: Maximum flank and notch wear against machining time

Figure 78 details workpiece surface roughness (Ra) measured at the end of tool life for each test. No significant difference in Ra values were observed in Tests 2, 3 and 4 irrespective of operating parameters, which were generally in the range of 1.28-1.38 µm. The surface roughness however was considerably higher in Test 1 (2.52µm Ra), most likely due to the large notch formed at test cessation.

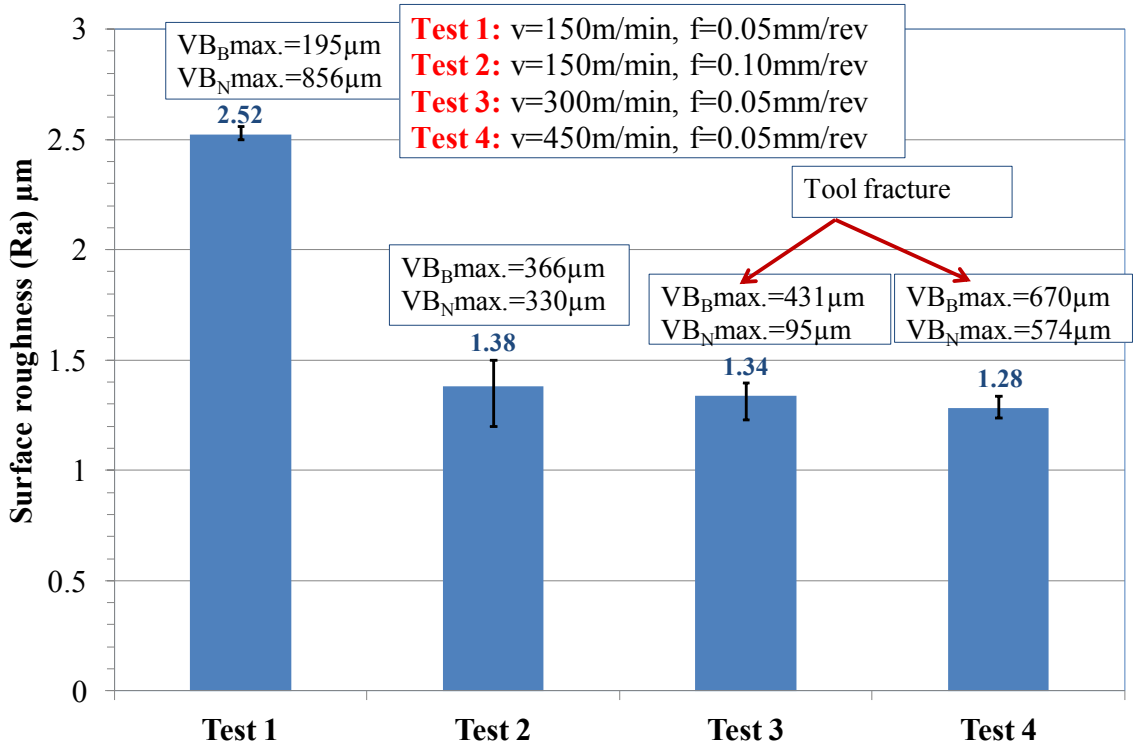

Figure 78: Surface roughness at the end of tool life in each test

4.2 Phase 1B: Benchmarking of Mitsubishi Inconel 718 workpiece using production approved carbide/PCBN inserts and operating parameters

4.2.1 Tool wear/life

Figure 79 shows flank wear evolution against machining time of RR supplied PCBN and carbide inserts when turning Inconel 718 sourced from Mitsubishi under production based operating parameters. In general, productivity term is referred to overall volume of material removed by the insert. However for finishing applications of critical parts, it is defined as the material removed by the insert to finish a full face of the component without tool change in a given time with acceptable surface finish. According to the information relayed from RR, ~5min machining is required to finish the whole face of the aeroengine disc using PCBN tooling at these given parameters with Ra values of <1.2µm. Despite the fact that a steeper wear rate was observed with the PCBN insert compared to the carbide variants (5 vs 28.6min using coated WC in Test 1), productivity of the former was superior (due to considerably

higher cutting speed employed), with ~65% and ~587% more material removed (after 5min of machining) compared to coated and uncoated WC tools respectively, see Figure 80. The extended tool life of the carbide inserts however led to greater overall volume of material removed as shown in Figure 81**,** with the results from replication involving the PCBN (Test 4) and uncoated WC (Test 5) inserts showing close agreement with Tests 2 and 3.

Flank wear was observed to be the principal wear mode in all trials with no sign of chipping or fracture of the inserts, which suggests that the parameters employed were appropriate; see Figures 82 and 83. Crater wear was seen only on the PCBN tool, which was most likely due to the longer tool chip contact length caused by the chamfer geometry. A defect resembling a notch was evident on the uncoated carbide inserts (both Tests 3 and 5) with an accumulation of burnt residue directly beneath the flank wear scar. Similar burnt marks were also recorded by Bermingham et al. [151] on uncoated WC tools when turning Ti-6Al-4V in the presence of cutting fluid however, no such residues was seen in cryogenic cutting operations. The presence of the residue was attributed to vaporisation of elements from the cutting fluid, which subsequently attached on the flank face. However, in the current work, such marks were not recorded when using PCBN and coated carbide inserts possibly due to their relatively smooth surfaces (0.12µm Ra for PCBN and 0.38µm Ra for coated carbide) in comparison to uncoated tools, which have higher surface roughness (0.61µm Ra) levels.

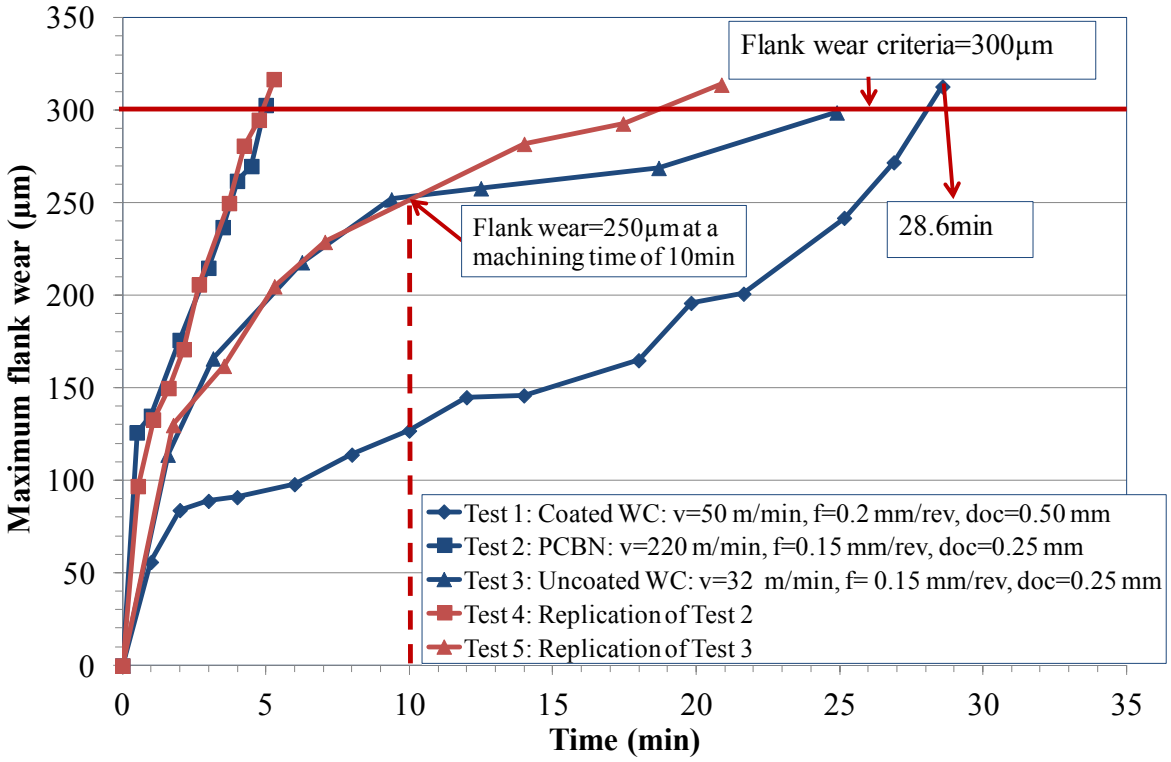

Figure 79: Maximum flank wear against machining time

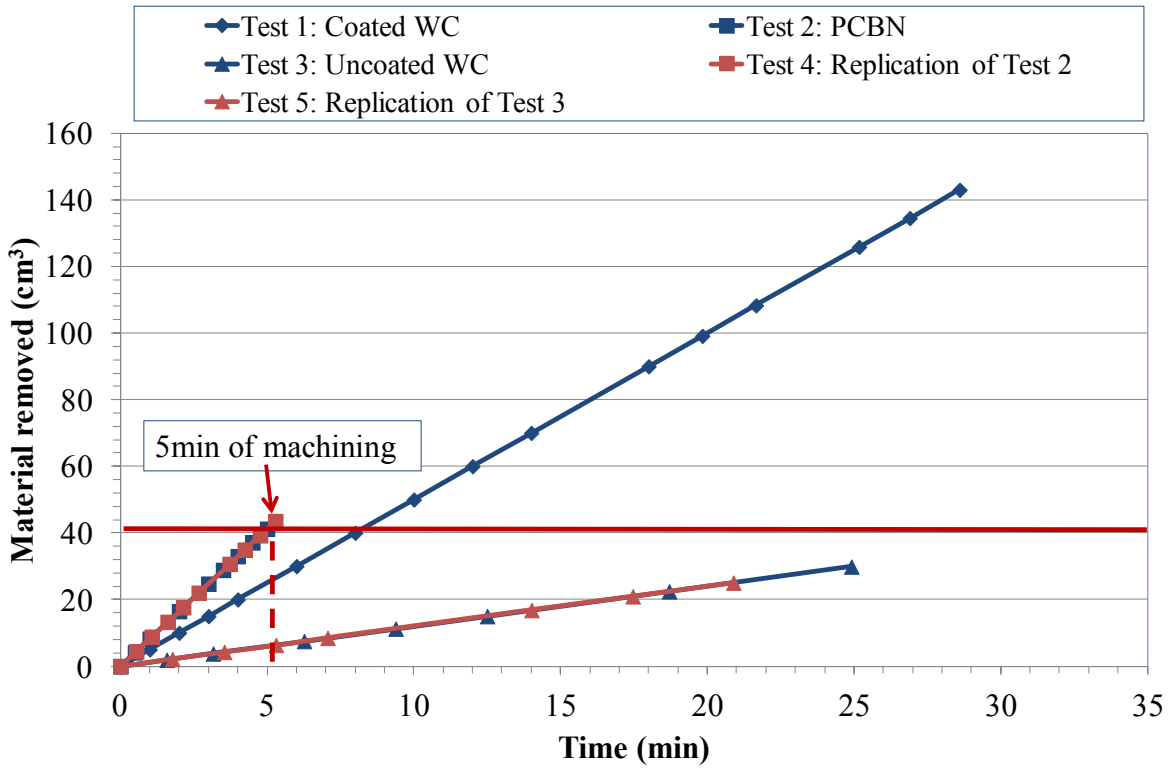

Figure 80: Rate of volume material removed

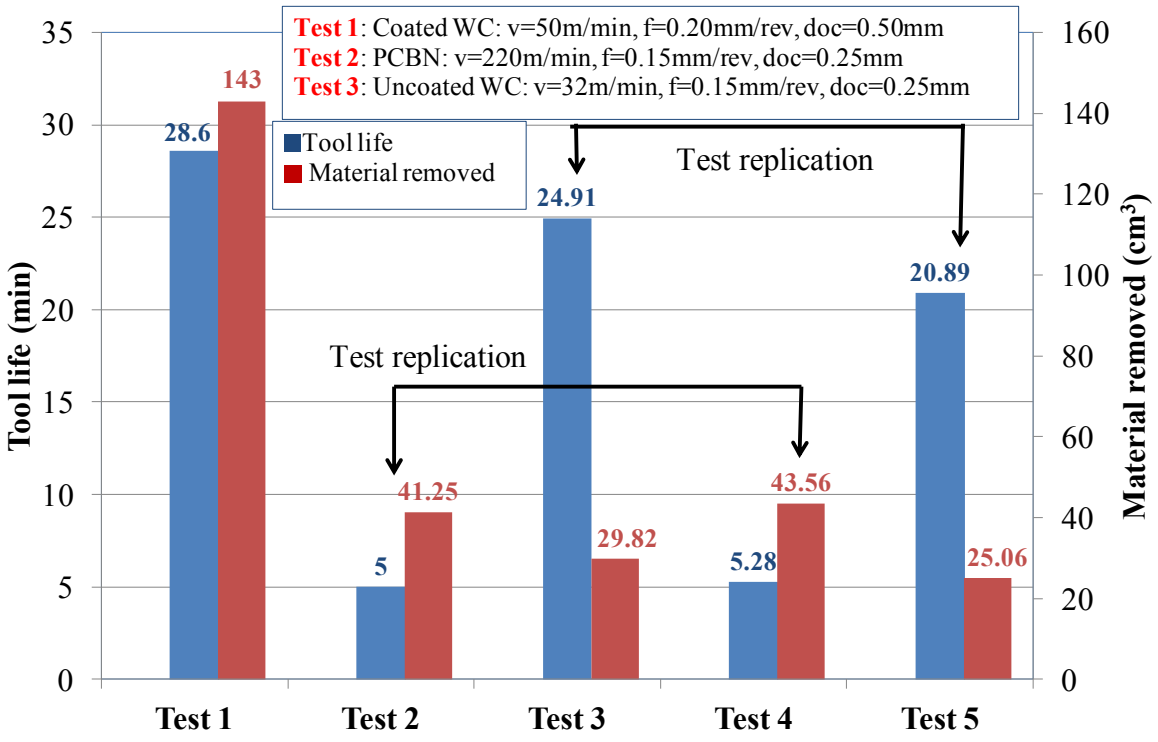

Figure 81: Tool life and overall volume of material removed in each test

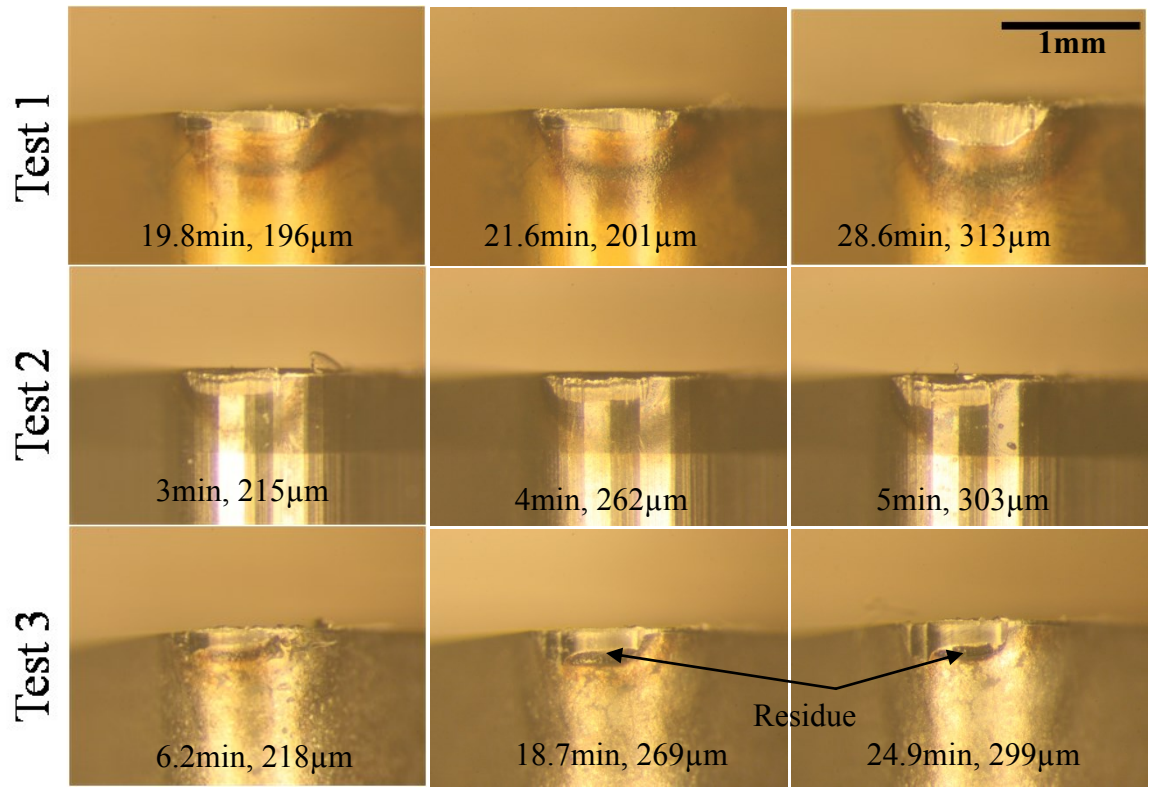

Figure 82: Micrographs of flank wear progression for Tests 1, 2 and 3

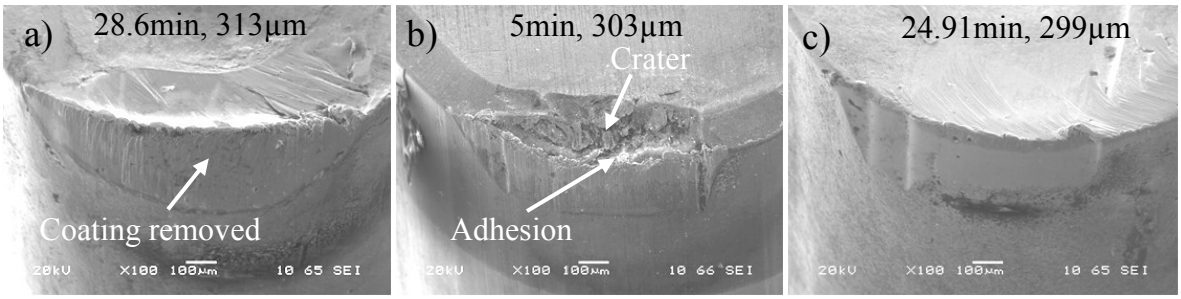

Figure 83: SEM micrographs at the end of tool life (a) Test 1, (b) Test 2 and (c) Test 3

The flanks wear of 2 equivalents (uncoated WC) which were previously used in finish turning of Inconel 718 components at Rolls Royce, Derby (each after 10min) were measured and analysed at the University of Birmingham. Figure 84 shows optical micrographs of the wear scar on both inserts at the nose and flank face locations, which were similar to that detailed in Figure 82 (uncoated WC insert). Flank wear measurement results were compared against data from Tests 3 and 5 when machining MHI Inconel 718 and are shown in Table 39**,** tool wear levels after 10min were approximately equal for both the RR and MHI alloy, the machinability of the latter was fairly representative of the Inconel 718 material used in RR in disc manufacturing. Therefore it was decided that the MHI workpiece material was suitable for mainstream Phase 1C experiments.

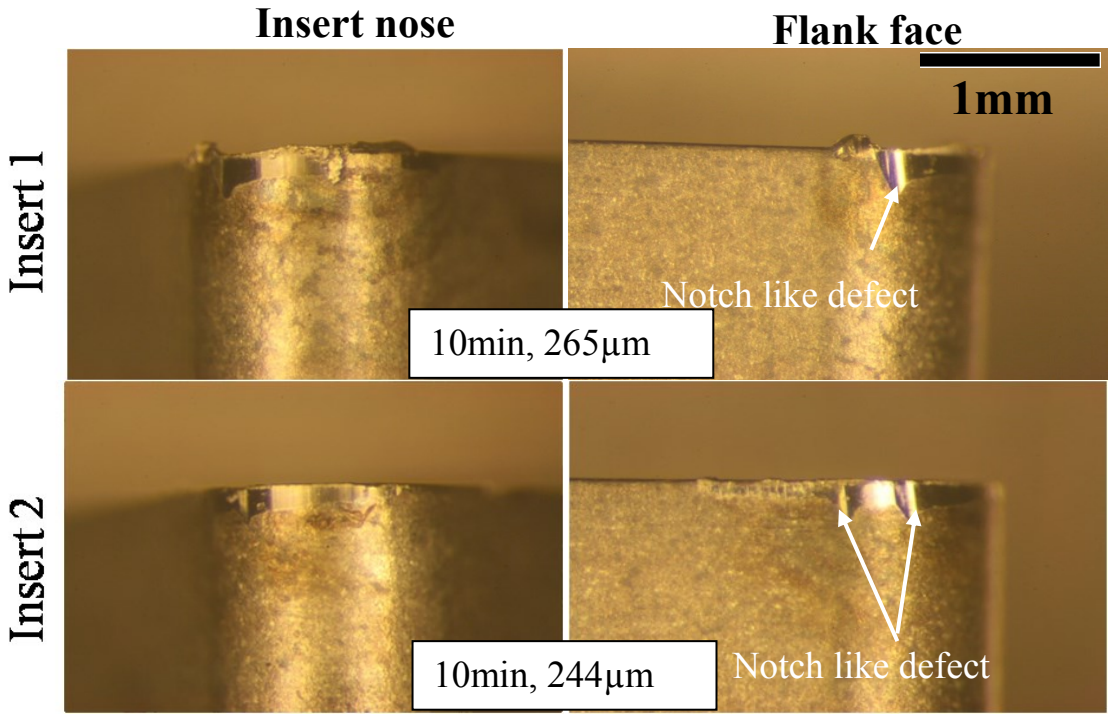

Figure 84: Micrographs of worn uncoated carbide inserts previously used for turning of Inconel 718 components at RR (10min machining time)

Table 39: Comparison of insert flank wear levels when turning RR and Mitsubishi supplied Inconel 718

Insert material	Machining time	Mitsubishi workpiece	RR workpiece
Uncoated carbide	10min	250µm	254µm*
Note: For Mitsubishi material, flank wear was extrapolated from Figure 79 * Average flank wear of 2 inserts			

4.2.2 Surface roughness

Due to the high feed rate employed in Test 1, workpiece surface roughness (Ra) was considerably higher (~2µm) at start of the test, compared to the other trials when utilising new inserts; see Figure 85. However, a steady decrease in surface roughness was observed as flank wear of the coated carbide insert increased. This was possibly due to the formation of a wiper flat at the nose radius as shown in Figure 86 with Ra of 0.82µm recorded at the end of tool life. In contrast, tests with the uncoated carbide inserts showed a continuous deterioration in surface roughness as cutting progressed with Ra measuring ~2.50µm at 300µm flank wear. This was most likely due to the notch-like wear scar seen on the secondary cutting edge as shown the micrographs in Figure 82. When employing PCBN inserts, surface roughness results was approximately constant (within a narrow range) over the test duration possibly due to uniform tool wear patterns except for Test 2, which showed an increasing trend after 250µm of flank wear.

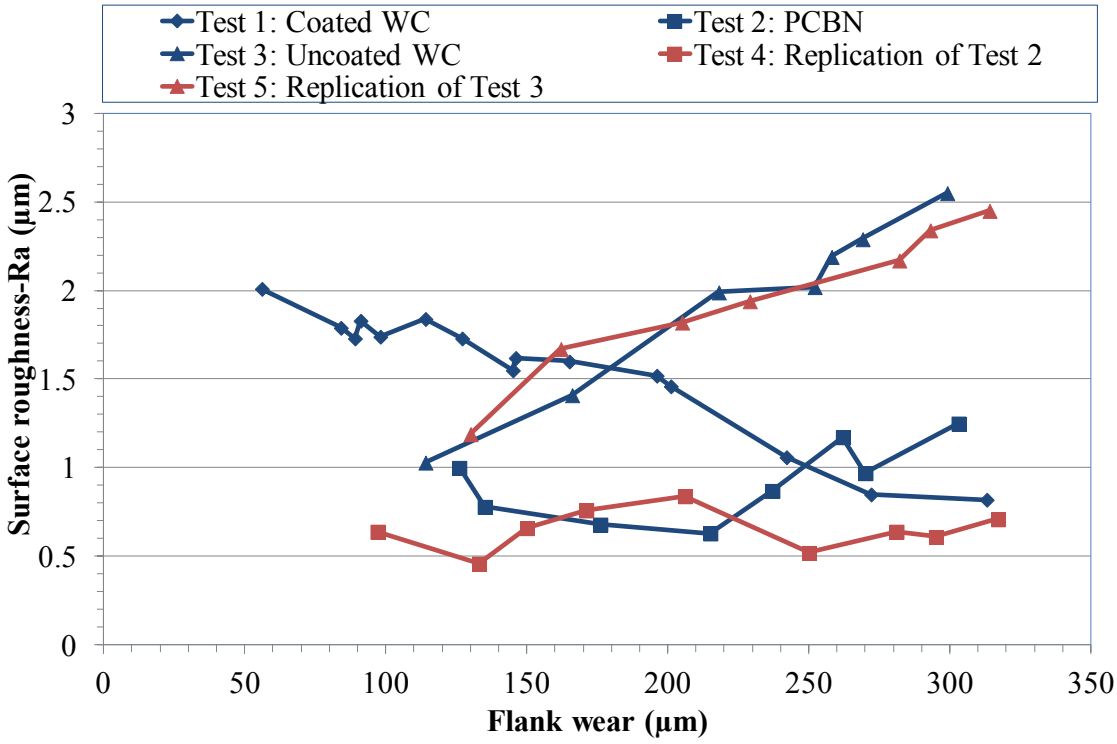

Figure 85: Variation in workpiece surface roughness against flank wear

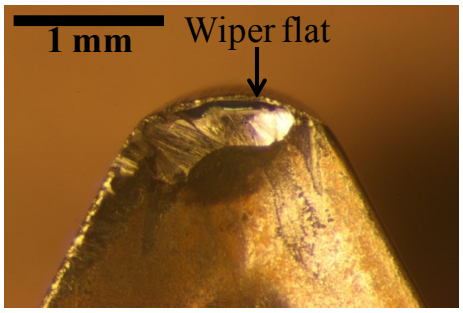

Figure 86: Optical micrograph of worn coated carbide insert

4.2.3 Cutting forces

Figure 87 shows the variation in cutting force components with respect to machining time for all tests. In general, the cutting forces when employing the coated WC (Test 1) was considerably higher (2 to 3 fold) compared to that obtained with the PCBN (Tests 2 and 4) and uncoated WC (Tests 3 and 5) due to the larger depth of cut and feed rate utilised in the former. The thrust force when using coated carbide increased up to ~1000N after 25min of machining while a steep rise was recorded with PCBN tools with a value of ~700N in 5min. Although utilising the same feed rate and depth of cut, the thrust force generated with the PCBN inserts was 3 times greater in comparison to uncoated carbide tools at test cessation. This was most likely due to the presence of the chamfer geometry on the PCBN insert, which increased the tool chip contact length. In addition, there was only a marginal increase (35-90 N) in cutting force components as machining progressed with the uncoated carbide inserts (Tests 3 and 5).

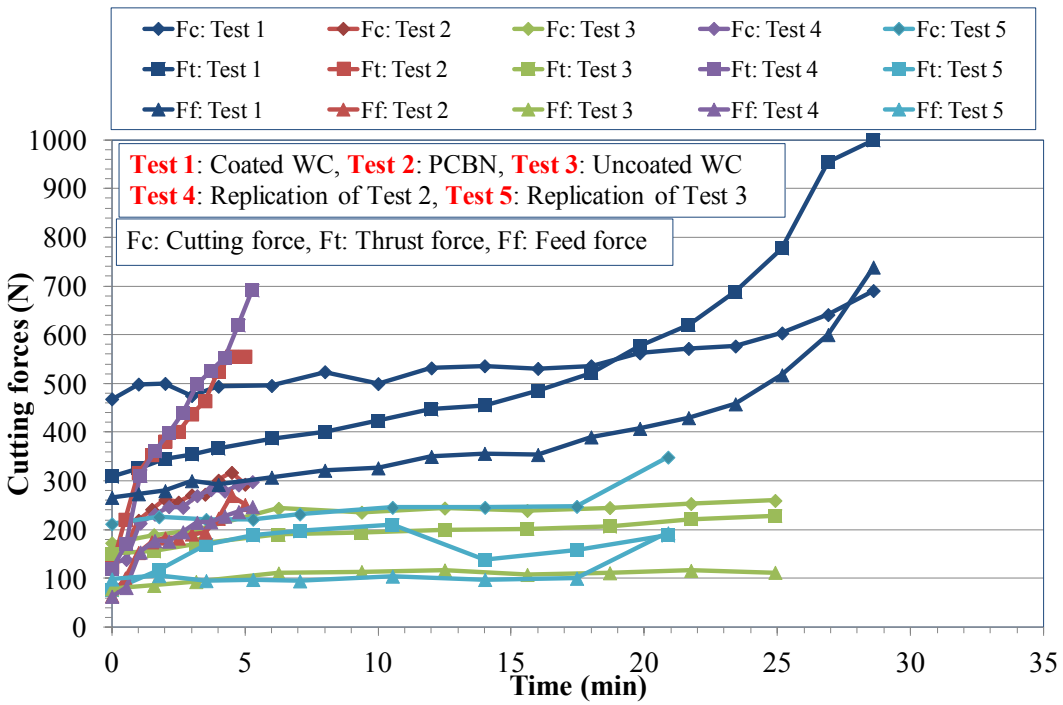

Figure 87: Cutting forces against machining time

4.3 Phase 1C: Influence of tool geometry, edge preparation, cutting environment, surface condition and operating parameters on tool wear/life, surface roughness and cutting forces

4.3.1 Tool wear/life

Figure 88 details the evolution of tool flank wear against machining time for round inserts at a cutting speed of 150m/min with corresponding SEM wear micrographs of Tests 1, 7 and 13 at the end of tool life presented in Figure 89. Maximum tool life of 44.8min was recorded in Test 4 with uniform wear progression. The trial was performed at the lowest feed rate level of 0.05mm/rev and at a cutting fluid pressure of 10bar employing an uncoated tool. Interestingly, when cutting fluid pressure was increased to 100bar while maintaining the same feed rate value (0.05mm/rev), tool life decreased to 18.7min with instances of severe chipping and notching observed; see SEM image from Test 7 in Figure 89 (b). Although a coated insert was utilised, the poorer performance with higher cutting fluid pressure was most likely due to thermal shocks (rapid heating and cooling cycles) and erosion caused by jet impingement, which appeared to be more prominent at low material removal rates (low cutting speed and feed rate). The results were in agreement with data reported by Ezugwu et al. [99] when turning of Inconel 718 with whisker ceramic inserts where accelerated notching wear was observed at a cutting fluid pressure of 20MPa compared to 15MPa. An increase in the notch wear was also recorded by Vagnorius and Sørby [152] when turning Inconel 718 using Sialon tools under a fluid pressure of 20MPa compared to flood cooling. As feed rate was increased from 0.05mm/rev to 0.10mm/rev at a cutting fluid pressure of 100bar (Tests 13 and 16), tool life improved to an average of 27.2min. Although slight chipping was observed in the wear scar micrograph of Test 13 but it was not detrimental to tool life. Additionally, material adhesion was evident in all trials. To analyse the effect of coating on tool life, Test 13 was compared against Test 16 where only the surface condition of the inserts was different. Coating did not appear to provide any benefit in terms of tool life with no significant difference in wear scar micrographs between coated and uncoated inserts. Optical micrographs of tool wear progression in Tests 4 and 13 and SEM images at the end of tool life from Tests 10 and 16 are shown in Figure B1-B3 in Appendix B.

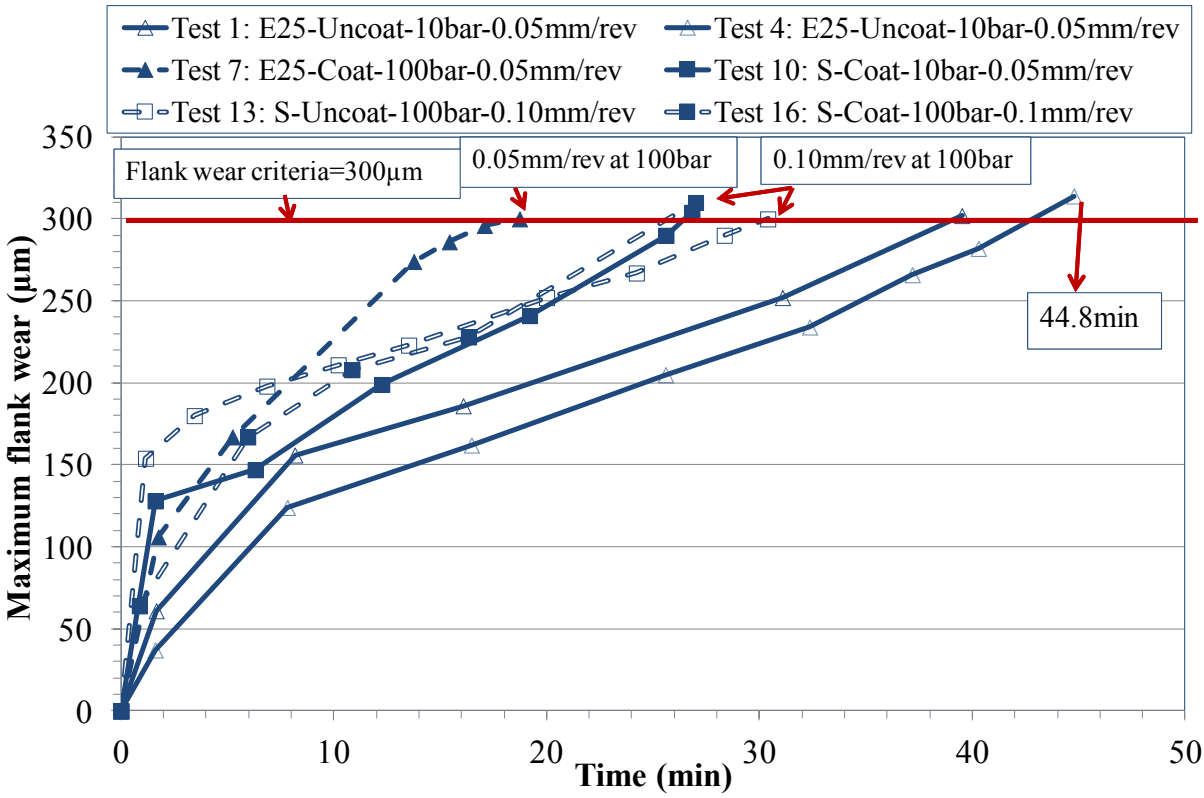

Figure 88: Maximum flank wear against machining time at a cutting speed of 150m/min

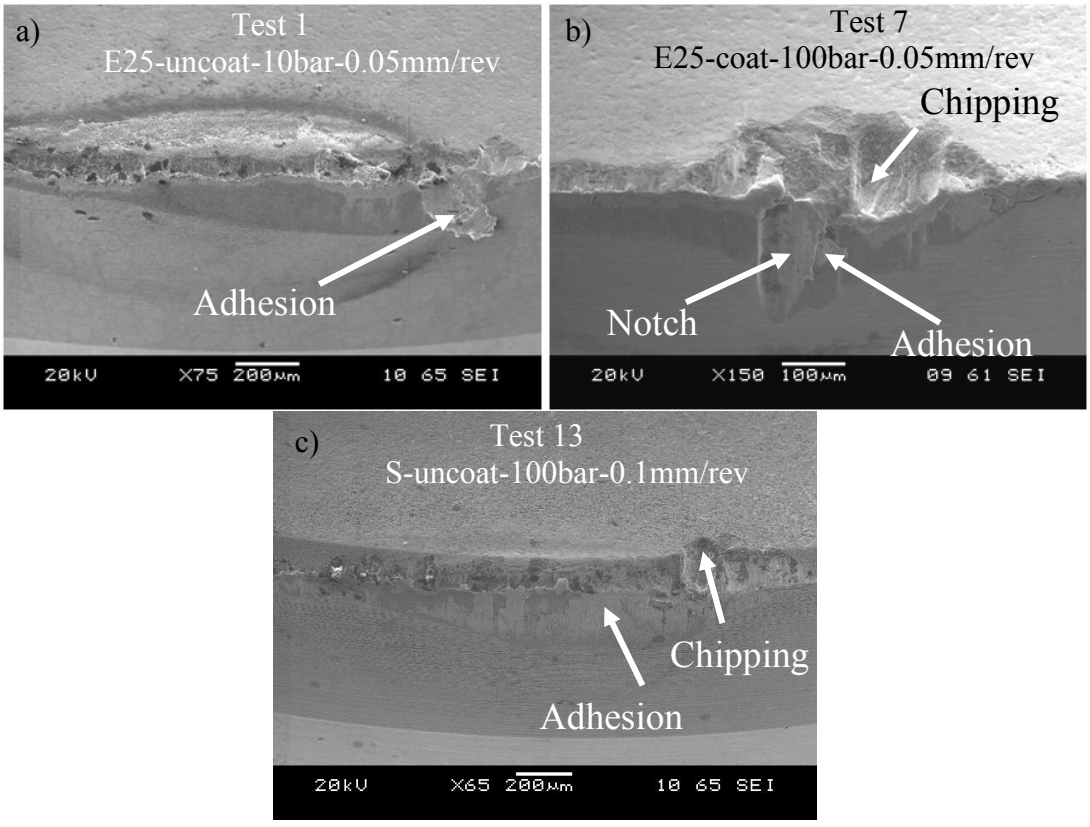

Figure 89: SEM micrographs of worn round insert at the end of tool life at a cutting speed of 150m/min (a) Test 1; (b) Test 7 and (c) Test 13

Figure 90 shows the evolution of tool flank wear against machining time for C-type inserts at Vc of 150m/min. Chip thickness significantly affect the value of tool life. At a feed rate of 0.10mm/rev (Tests 19 and 22), average value of tool life was 11.8min however this was reduced to just 2.7min when feed rate was increased to 0.20mm/rev (Tests 25, 28, 31 and 34). Effect of cutting environment, edge preparation and coating can be evaluated via direct comparison between Test 28 vs Test 34, Test 25 vs Test 31 and Test 19 vs Test 22 respectively. No significant difference in the value of tool life was observed due to the variations of edge configuration and tool surface condition, however ~62% higher tool life was observed when employing 10bar cutting fluid pressure compared to 100bar as observed for the round inserts.

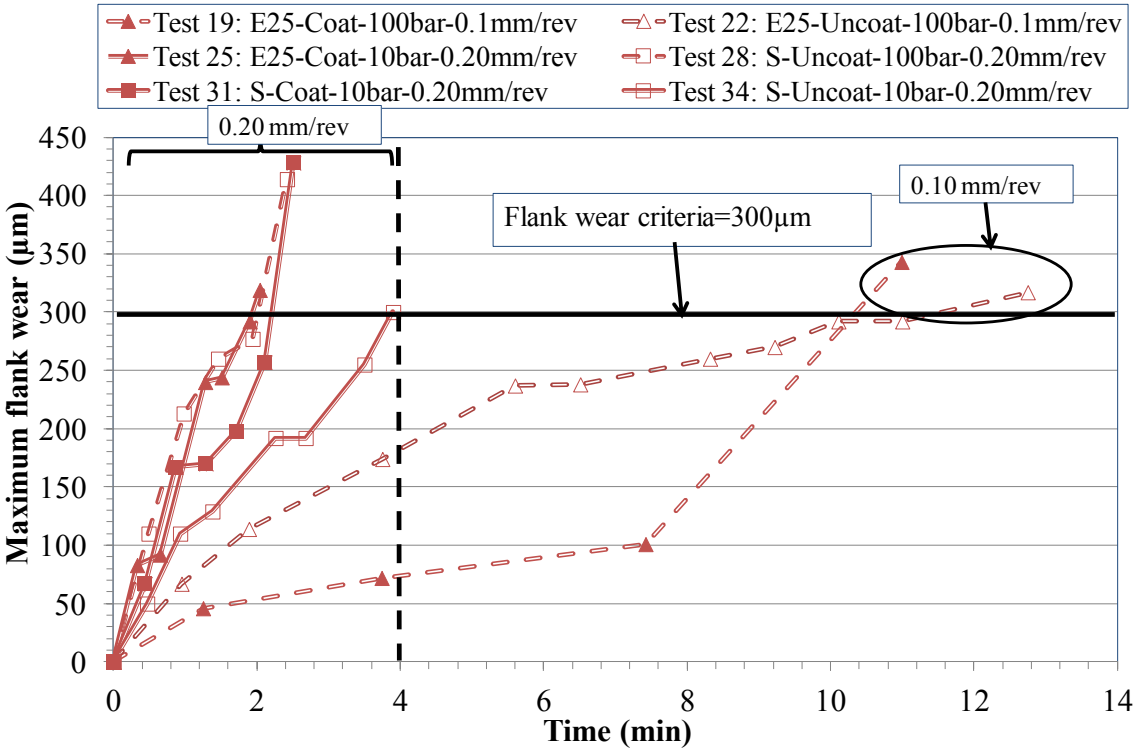

Figure 90: Maximum flank wear against machining time of C-type inserts at a cutting speed of 150m/min

SEM images of worn C-type inserts of Tests 22 and 28 at the end of tool life in Figure 91 show intensive grooving and BUE formation on the rake face. This type of wear was observed in all tests performed with C-type inserts. Optical micrographs of tool wear scar progression of Tests 19 and 25 are presented in Figure B4-B5 in Appendix B and Figure 91 shows the SEM images of the worn tools at the end of tool life of Tests 31 and 34. This BUE and grooving was possibly due to ploughing as a result of BUE accumulation (low temperature and high stresses) instead of shearing, which in turn increased the strain hardening of the workpiece material. Rubbing between the strain hardened layer and insert

contributed towards the formation of grooves on the tool surface and the fracture observed on the insert in Test 28 was due to BUE detaching from the tool surface.

Absence of grooving wear and BUE formation with the round inserts at 150m/min was attributed to the larger contact area, which reduced the stresses. Average value of tool life with the round inserts for the Tests 1, 4, 7, 10, 13 and 16 was ~5 times higher compared to C-type tools. Additionally round tools also exhibit smaller uncut chip thickness (h) compared to C-type geometry which is related to the feed rate (f) and tool approach angle (Ø) as detailed in Equations below [27];

$$h = f \times \sin Ø \quad (5)$$

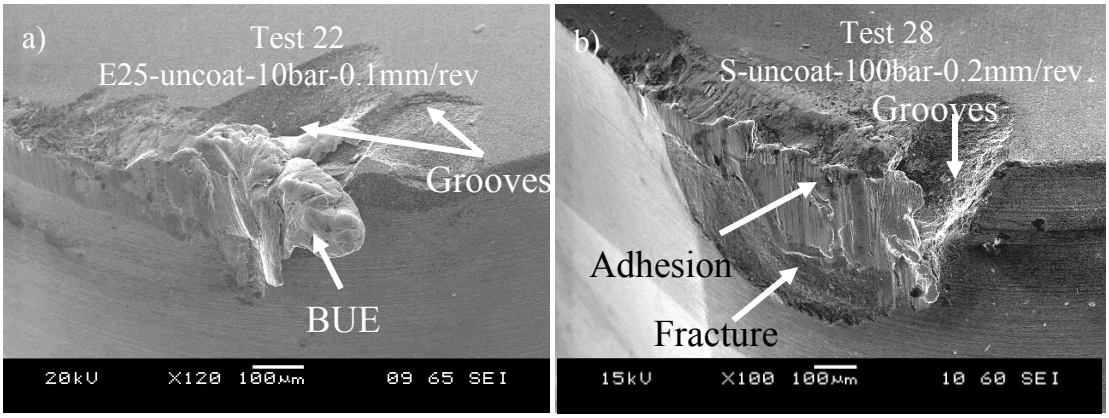

Figure 91: SEM images of worn C-type inserts at the end of tool life at a cutting speed of 150m/min of (a) Tests 22 and (b) Test 28

Graph of flank wear evolution at the intermediate cutting speed of 300m/min is shown in Figure 92. Contrary to the results from tests at lower cutting speed, average tool life with the C-type inserts (8.1min) was ~30% longer compared to the round inserts (6.2min) due to greater cutting edge strength as a result of the negative rake angle configuration associated with the former. With round inserts, ~35% reduction in the average value of tool life was recorded when feed rate was increased from 0.10mm/rev (Tests 2, 5, 8 and 11) to 0.20mm/rev (Tests 14 and 17). Average tool life was 8.6min for the trials performed with C-type inserts at a feed rate of 0.05mm/rev (Tests 26, 29, 32 and 35) which was reduced to 6.8min (Tests 20 and 23) with the increase in feed rate (0.20mm/rev). Certain tests can be compared directly to analyse the effect of coating (Test 20 vs Test 23, Test 32 vs Test 35, Test 14 vs Test 17), edge preparation (Test 26 vs Test 32) and cutting environment (Test 29 vs Test 35) where only the parameter under investigation was different. No disparity among the tool lives was recorded when changing the insert surface condition and edge periphery, however ~33% higher tool life was recorded at a cutting fluid pressure of 10bar in comparison to 100bar.

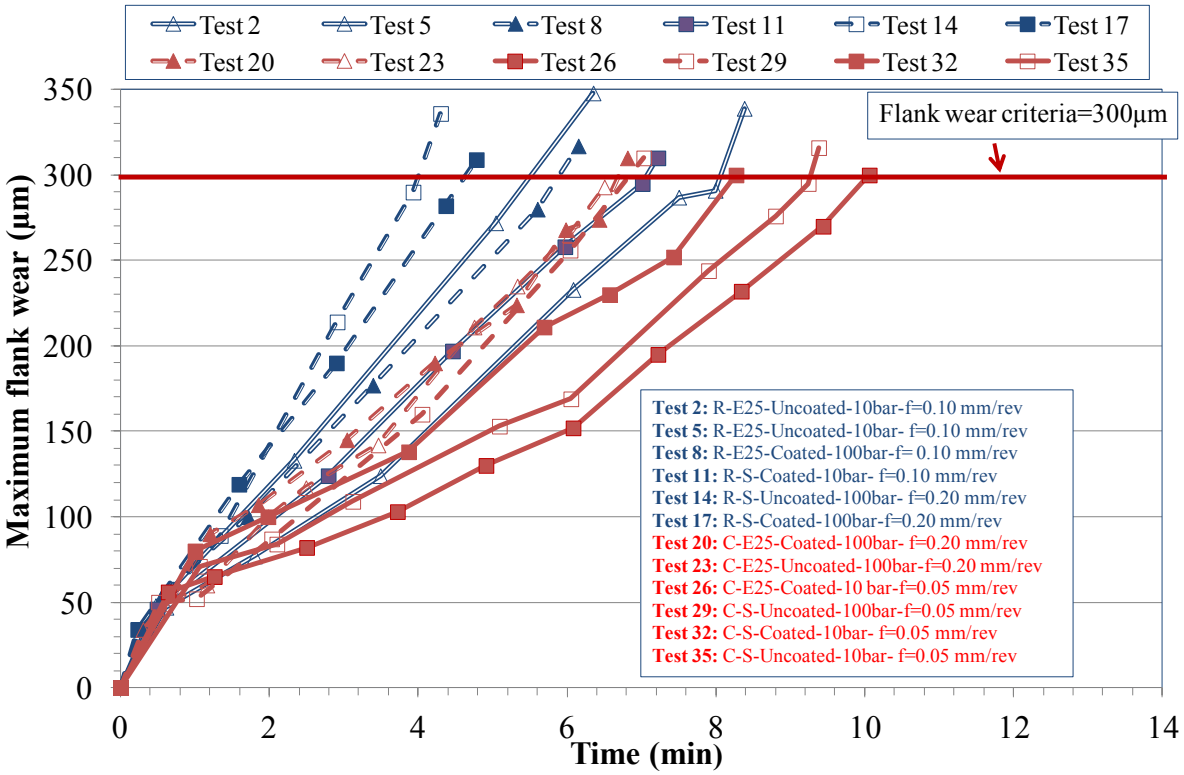

Figure 92: Maximum flank wear against machining time at a cutting speed of 300m/min

Figure 93 shows the SEM wear scar micrographs of Tests 20, 23 and 29 (C-type) and Tests 5, 8 and 17 (round) inserts at the end of tool life. Higher cutting speed diminished the presence of BUE and grooving observed with C-type inserts, therefore tool lives of both round and C-type inserts were comparable. When compared against experiments performed at 150m/min, material adhesion appeared to be more prominent together with severe abrasion marks seen on the flank face. High material adhesion was most likely due to the high cutting temperature and stresses as a result of elevated cutting speed. In addition, this high cutting speed can possibly initiate the workpiece softening which in turn increased the adhesion of workpiece material on the inserts. Strong abrasive marks were due to the action of hard carbide inclusions present in the Inconel 718 matrix, which rubbed the flank face of the inserts at much faster rate. Crater wear on the rake face however was predominantly seen in tests performed at the highest feed rate of 0.20mm/rev. This was attributed to the large uncut chip thickness, which increased the tool chip contact length. The crater wear pattern on the round inserts were similar to that reported by Arunachalam and Mannan [105] when turning Inconel 718. Optical micrographs of tool wear progression of Tests 2, 14, 23 and 26 along with SEM images of worn inserts at the end of tool life of Tests 11, 32 and 35 are shown in Figure B7-B11 in Appendix B.

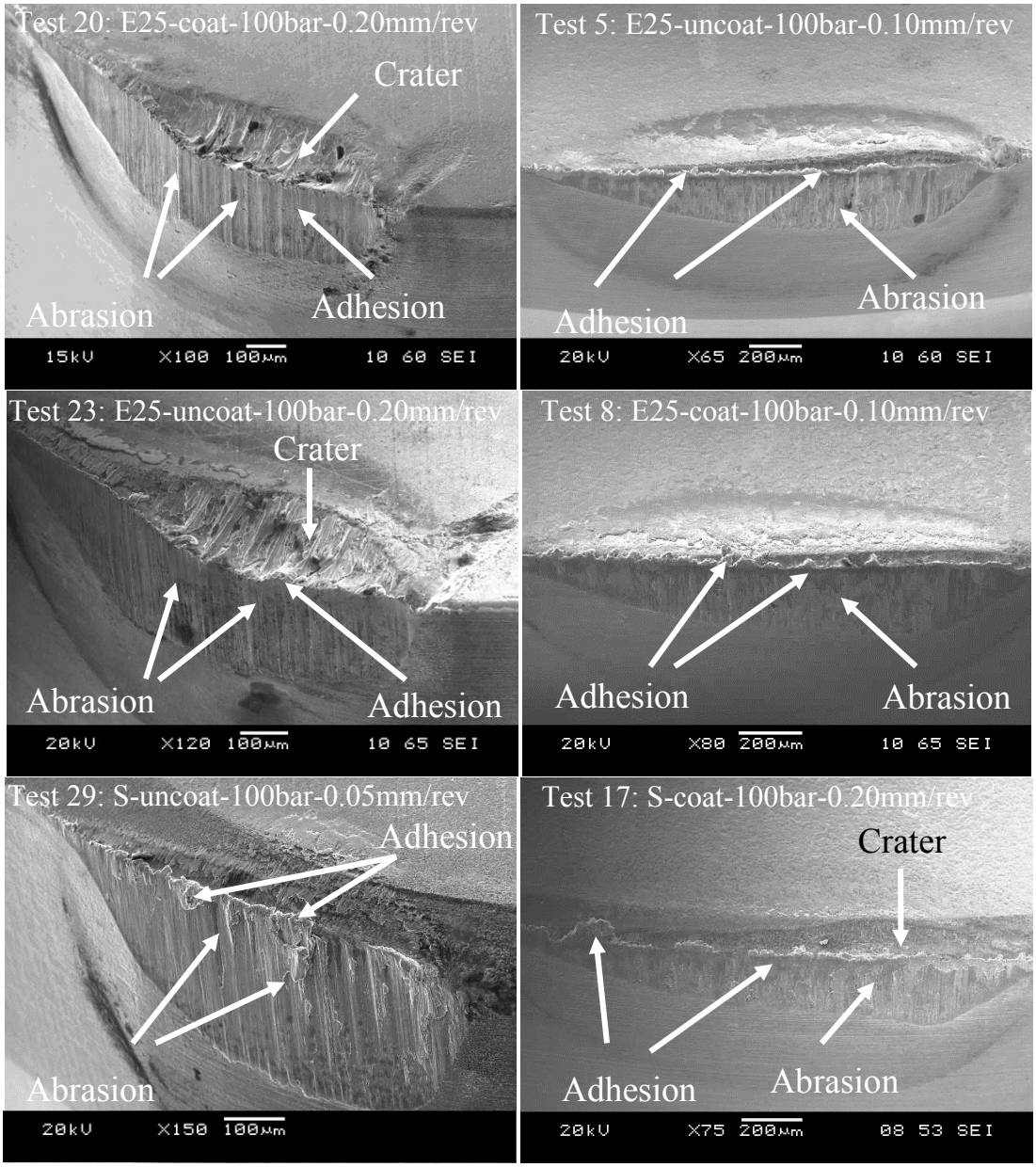

a) C-type b) Round

Figure 93: SEM micrographs of worn C-type and round inserts at the end of tool life at a cutting speed of 300m/min

Energy dispersive x-ray (EDX) analysis was performed for selected Tests and Figure 94 details the measurement location on the wear scar in Test 17 together with the corresponding element spectrum. The results confirm that the adhered material on the insert surface was Inconel 718 with high levels of Ni, Cr and Fe elements detected. This was in line with previously published data by Arunachalam and Mannan [105] and Costes et al. [118] who also recorded similar workpiece adhesion on PCBN tools when turning Inconel 718.

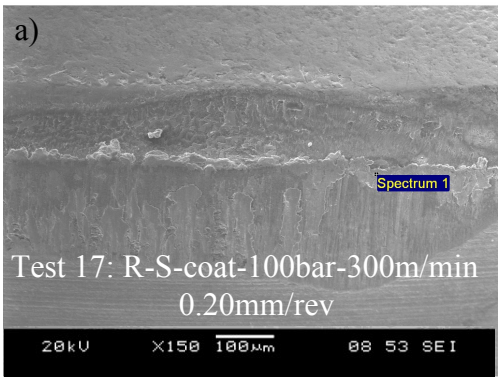

b)

Ni : 55.58% (wt.), 52.41% (atomic)
Fe: 19.15% (wt.), 18.99% (atomic)
Cr: 21.27% (wt.), 22.65% (atomic)
Ti: 2.39% (wt.), 2.75% (atomic)
Si: 1.63% (wt.), 3.21% (atomic)

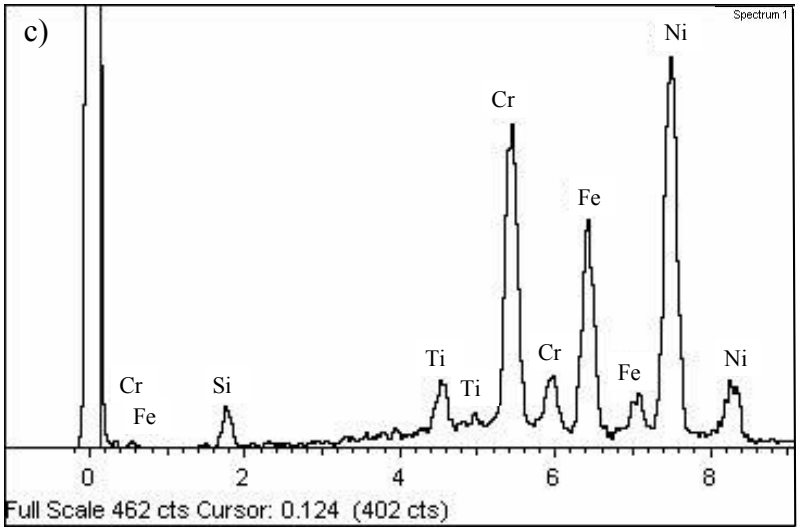

Figure 94: EDX analysis of Test 17 with (a) SEM image; (b) element details and (c) spectrum

Figure 95 details the flank wear curves for all tests performed at 450m/min. In all trials, tool life did not exceed 3.5min irrespective of the operating conditions with a minimum of 1.3min recorded in Test 9. No noticeable difference in the average value of tool life was observed both with round and C-type inserts. Additionally, due to the highest cutting speed, change in the feed rate from 0.05mm/rev (Tests 15, 18, 21 and 24) to 0.10mm/rev (Tests 27, 30, 33 and 36) and 0.20mm/rev (Tests 3, 6, 9 and 12) did not produce any significant effect on the tool life. Moreover, variations in the surface condition (Test 21 vs Test 24, Test 15 vs Test 18), edge configuration (Test 27 vs Test 33) and cutting environment (Test 30 vs Test 36) had no significant effect on tool life at the above mentioned cutting speed level.

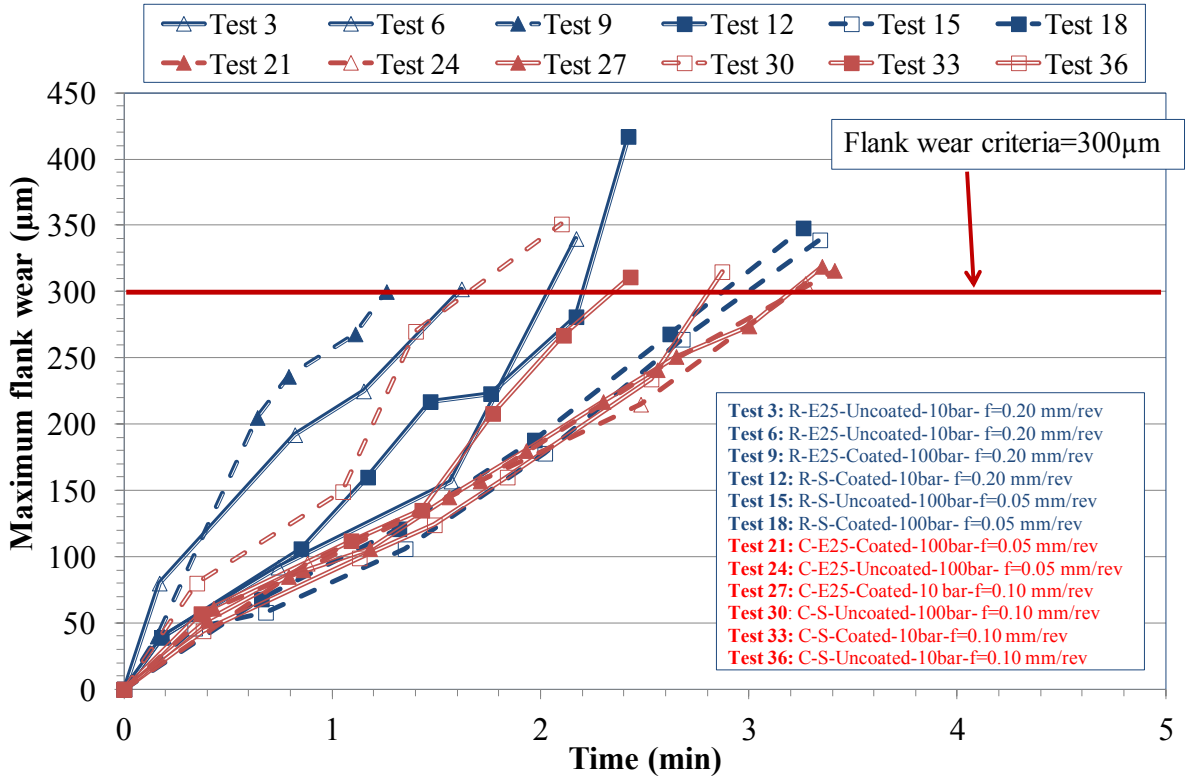

Figure 95: Maximum flank wear against machining time at a cutting speed of 450m/min

Figure 96 shows the SEM micrographs of Tests 21, 27 and 36 (C-type) and Tests 3, 12 and 18 (round) at the end of tool life at cutting speed of 450m/min. Abrasion and adhesion of workpiece material on the tool were still prevalent in addition to thermal cracks, fracture, chipping and crater wear, particularly for tests performed at higher feed rates of 0.10mm/rev and 0.20mm/rev. This broadly agreed with results previously published by Bushlya et al. [111], who reported that fracture was the primary failure mode of PCBN inserts when high speed turning Inconel 718 after 1.7min at a cutting speed of 350m/min, feed rate of 0.10mm/rev and depth of cut of 0.20mm. Additionally, no appreciable difference in tool life was apparent between the round and C-type geometries at this cutting speed level. In general, the use of coatings failed to provide any significant improvement in terms of tool life, which suggests that the selected composition may not have been appropriate for experimental conditions considered. Figure B12-B15 details tool wear progression of Tests 3, 18, 30 and 36 while SEM images at the end of tool life of Tests 15, 18 and 24 are presented in Figure B16.

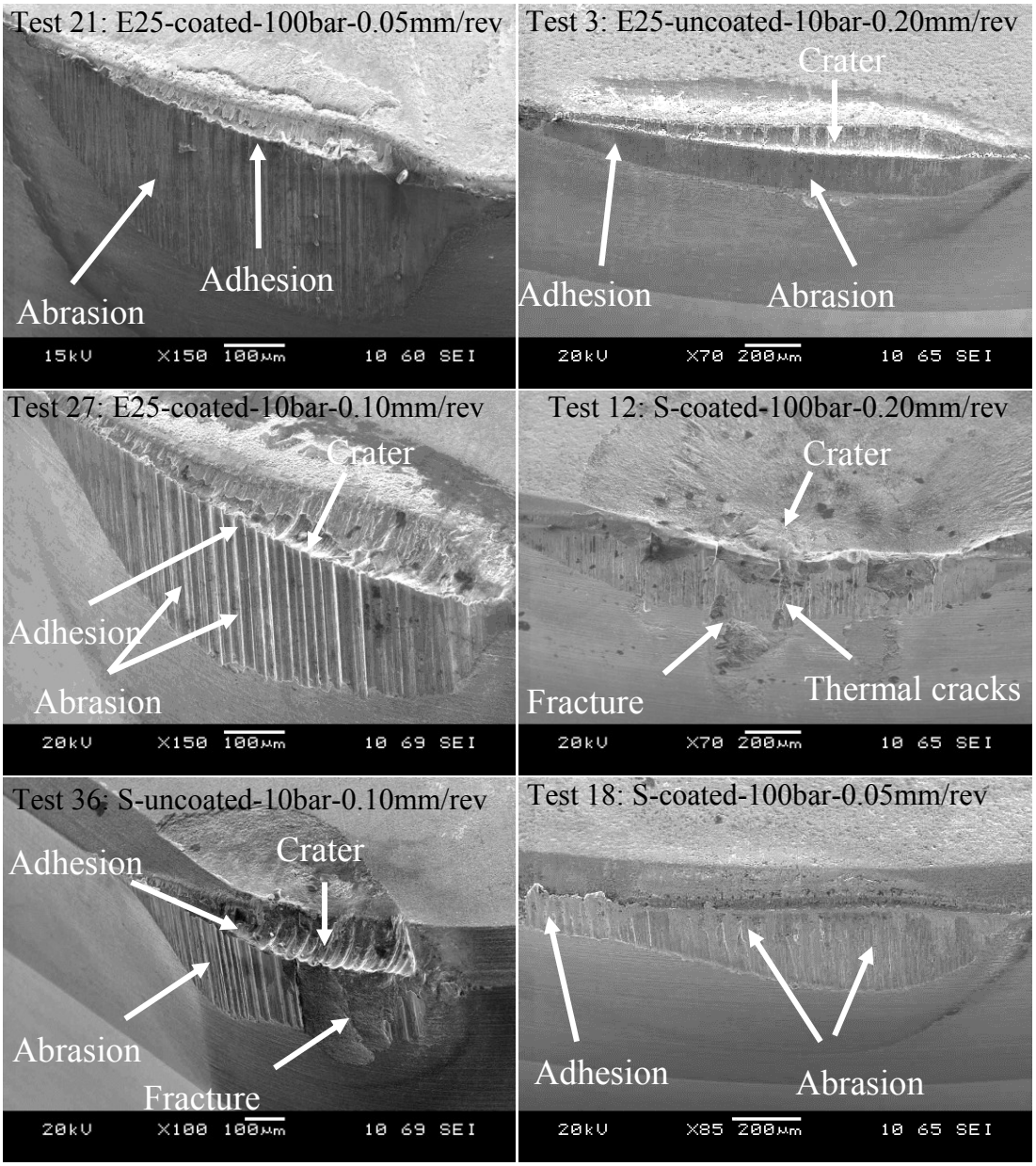

a) C-type b) Round

Figure 96: SEM micrographs of worn C-type and round inserts at the end of tool life at a cutting speed of 450m/min

In terms of productivity, a cutting speed of 300m/min and feed rate of 0.2mm/rev at 100bar fluid pressure was the preferred operating parameter combination. Figure 97 shows results of tool life and volumetric material removed from tests undertaken under these conditions (Tests 14, 17, 20 and 23) compared against Test 4, which recorded the longest tool life of ~45min. Despite a 6-fold shorter tool life, the C-type inserts used in Tests 20 and 23 removed ~22% more material compared to Test 4 and approximately 50% higher over corresponding round inserts. In addition, use of coatings did not appear to have any substantial influence on performance.

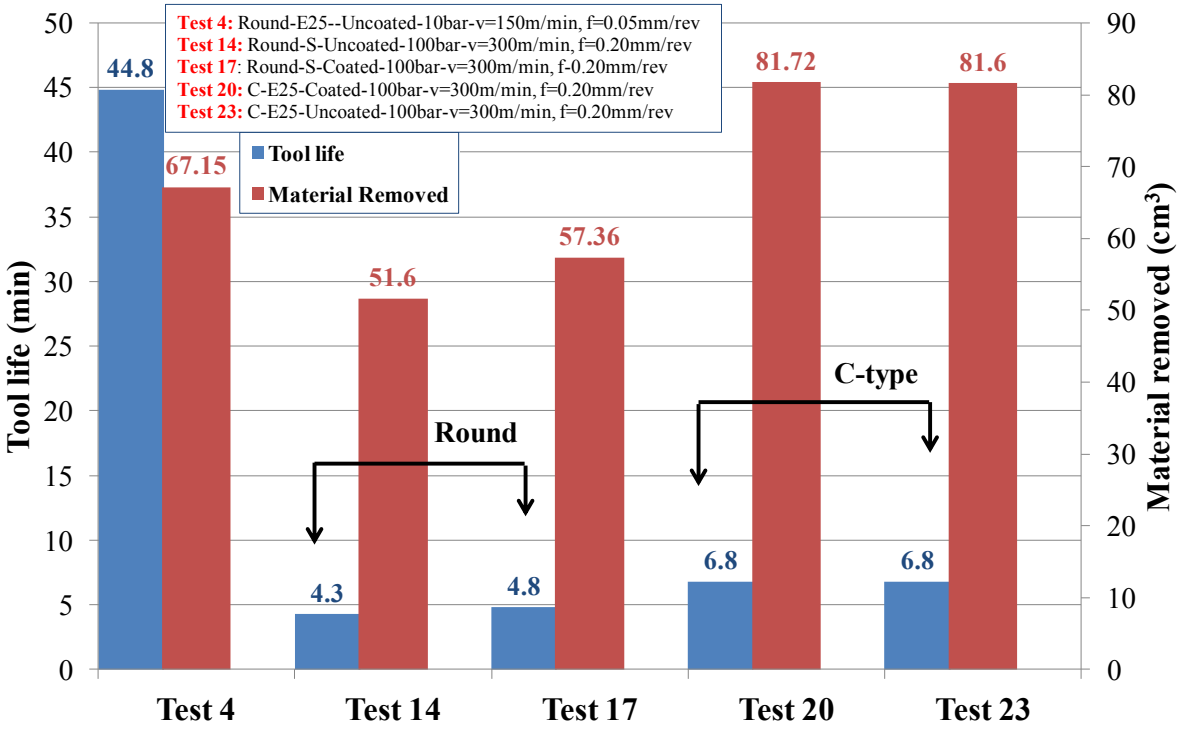

Figure 97: Tool life and material removed of Tests 4, 14, 17, 20 and 23

Main effects plot shown in Figure 98 suggests that tool life is maximised by employing uncoated, round inserts with an E25 edge preparation at a cutting speed of 150m/min and feed rate of 0.05mm/rev under 10bar cutting fluid pressure, which was confirmed by results in Test 4. Table 40 details the corresponding ANOVA and the results showed that cutting speed, tool geometry and feed rate were statistically significant factors affecting tool life with PCR's of 36.55%, 11.49% and 17.30% respectively while variations in edge preparation, cutting environment and surface condition had negligible effect on tool life. Essentially, main effects plot highlighted that round tools produced higher tool life compared to C-type geometry. This was due to the larger difference in tool life results between the 2 insert types when operating at 150m/min, contributing to the higher overall average. Not surprisingly, increasing cutting speed and feed rate led to a reduction in tool life due to higher cutting temperature/stresses and larger uncut chip thickness respectively. A relatively high error level of ~34% was however obtained which was considerably above the 15% generally acceptable with Taguchi experiments [134]. In the present work, this was most likely due to the variable interactions which are not accounted for in standard ANOVA calculations. This however will be addressed by an alternative stepwise analysis procedure to be discussed in the following section.

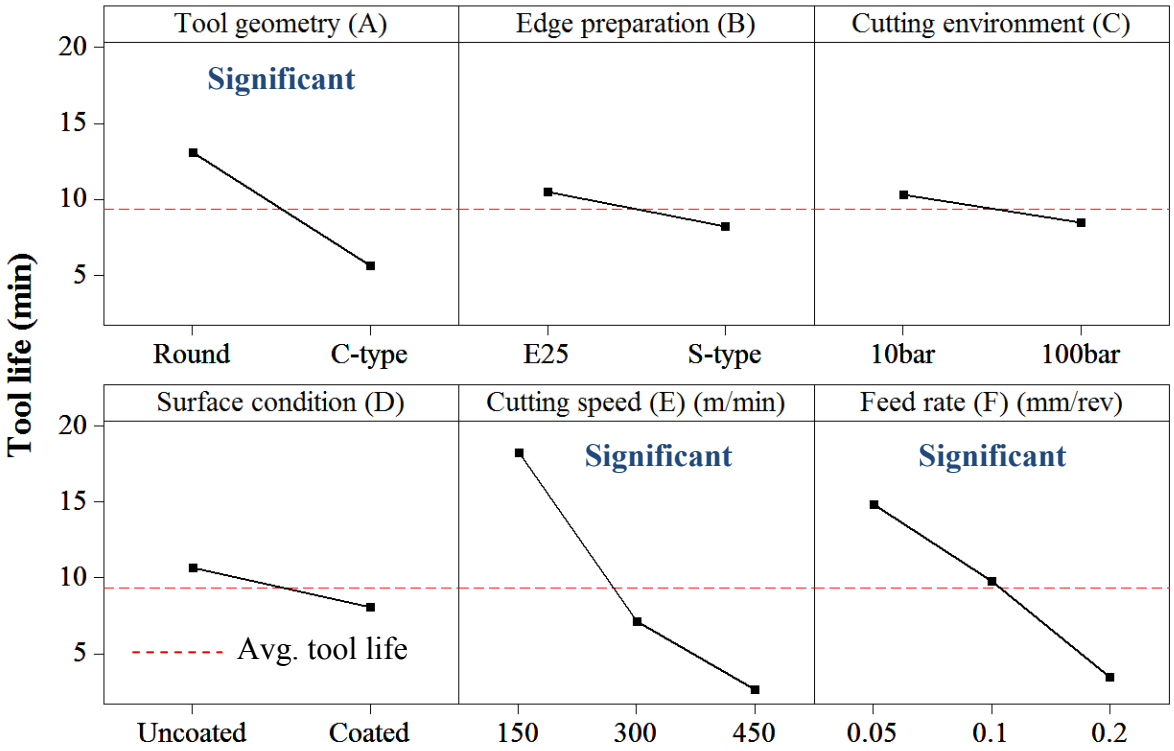

Figure 98: Main effects plots, means for tool life (Phase 1C)

Table 40: ANOVA table for tool life (Phase 1C)

Factors	DF	SS	MSS	F	P	PCR (%)
Tool geometry (A)	1	504	504	12.75	0.001*	11.49
Edge preparation (B)	1	45.74	45.74	1.16	0.292	0.1
Cutting environment (C)	1	29.67	29.67	0.75	0.394	0
Surface condition (D)	1	59.91	59.91	1.52	0.229	0.50
Cutting speed (E)	2	1556.60	778.30	19.69	0.000*	36.55
Feed rate (F)	2	778.65	389.33	9.85	0.001*	17.30
Error	27	1067.27	39.53		-	34.01
Total	35	4041.84	R-Sq(Adj)=65.99			

DF: Degrees of freedom, SS: Sequential sum of squares
MSS: Mean sum of squares, F: F- test value
F calculated for all factors=4.21
P: Probablility, PCR: Percentage contribution ratio
*Significant at the 5% level

Table 41 shows the interactions which have been found to be statistically significant following a step wise backward elimination and forward entry evaluation procedure with corresponding equations as presented in Equations B1-B5 in Appendix B. Full interaction plots for tool life are presented in Figure B17 of Appendix B. Interaction between tool geometry and cutting speed (A*E) had the greatest effect with a ~30% rise in the R-Sq (Adj) value. As mentioned earlier, this was most likely due to the large disparity in tool life results

between the round and C-type geometries for tests at 150m/min. The two interactions relating cutting environment to cutting speed (C*E) and feed rate (C*F) respectively were significant, especially when operating at the lowest cutting speed (150m/min) and feed rate (0.05mm/rev) levels under high cutting fluid pressure. The interaction between edge preparation and feed rate (B*F) was also significant as longer tool life was typically obtained when using inserts having an E25 edge preparation (instead of S-type) at a feed rate of 0.05mm/rev. It is well documented that accumulated material ahead of the cutting edge (a schematic illustration is shown in Figure 24 in literature review section) act as a cutting edge and subsequently enhance the tool edge strength [153]. At the lowest feed rate of 0.05mm/rev, chip formation is restricted only along the edge radius, which is 10μm higher with E25 compared to S-type edge periphery. It was thought that more material was trapped in front of the cutting edge with the former, hence increased its strength and the tool life.

Table 41: Interactions for tool life appeared to be statistically significant in a stepwise backward elimination and forward entry evaluation procedure (Phase 1C)

Stepwise backward elimination method	**Stepwise forward entry procedure**	
	R-Sq (Adj) after adding an interaction with main effect	**Increase in R-Sq (Adj) value**
A*E	85.87	30.12%
B*F	72.10	9.25%
C*E	69.23	4.90%
C*F	77.63	17.63%
R-Sq (Adj)= 92.74		
Error= 7.26%		

Figure 99 details the tool life benchmarking results between 2 different PCBN inserts manufactured by Kennametal (currently employed in production) and Seco respectively when turning Inconel 718. The latter was shown to outperform the former by a factor of ~2. This was most likely due to the higher chemical stability derived from the lower CBN content (50% of Seco vs 90% of Kennametal) in the Seco product, although differences in tool geometry, edge preparation and cutting fluid supply methods could have been contributing factors as shown in Table 26.

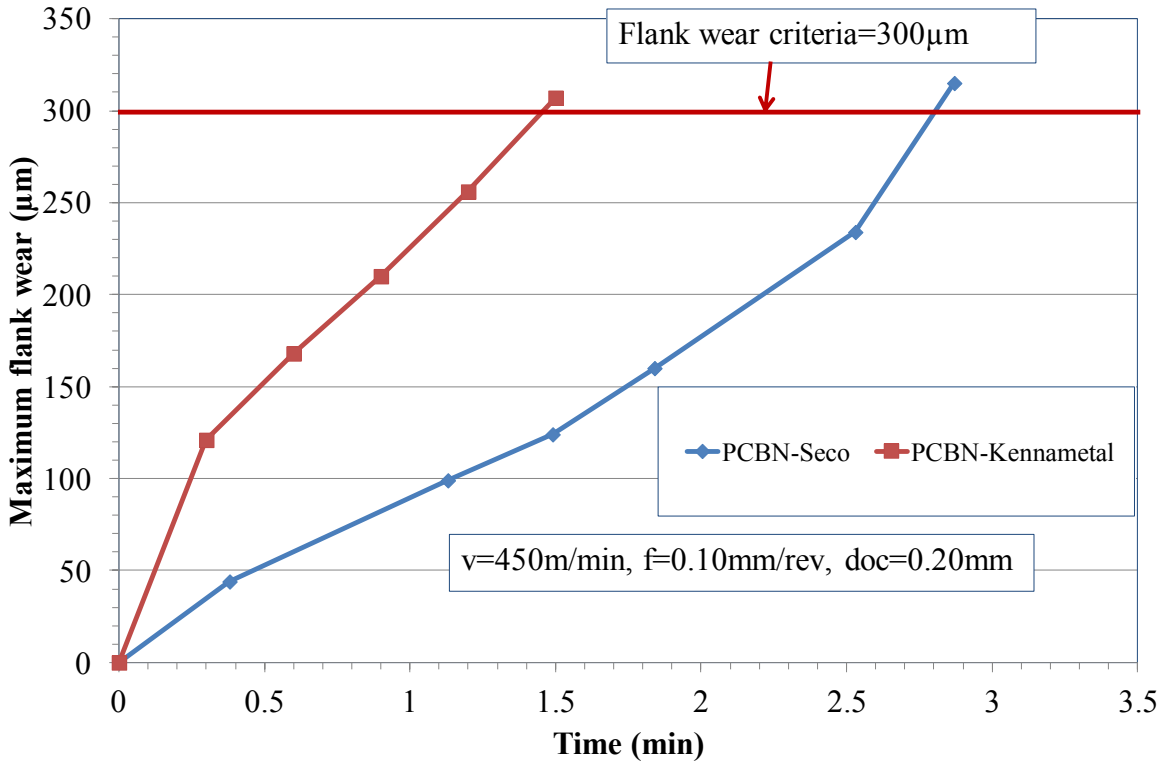

Figure 99: Comparison of tool life performance between PCBN inserts from Seco and Kennametal

4.3.2 Chip analysis

Figure 100 shows the typical difference in chips produced when cutting fluid pressure was varied from 100bar to 10bar. The use of high pressure delivery at 100bar enhanced chip breakability resulting in short and discontinuous swarf while the lower 10bar application generally produced long and continuous chips, which occasionally led to entanglement problems; see Figure 100 (a). Chip morphology was also influenced by tool geometry with long conical shaped chips obtained when utilising round inserts which contrasted with the continuous helical form chips generated with C-type tools as shown in Figure 101. Furthermore, chip width was substantially larger when using round inserts (~1.584mm) compared to C-type geometry (~0.726mm), probably due to the smaller approach angle and larger nose radius that simultaneously reduced the chip thickness [29]. In addition, tighter 'coiling' of the chips were prevalent when employing round inserts, while spiral pitch increased with C-type tools (~3.5 times). This was possibly due to the negative rake angle of the latter which increased chip compression hence the larger spiral pitch [29].

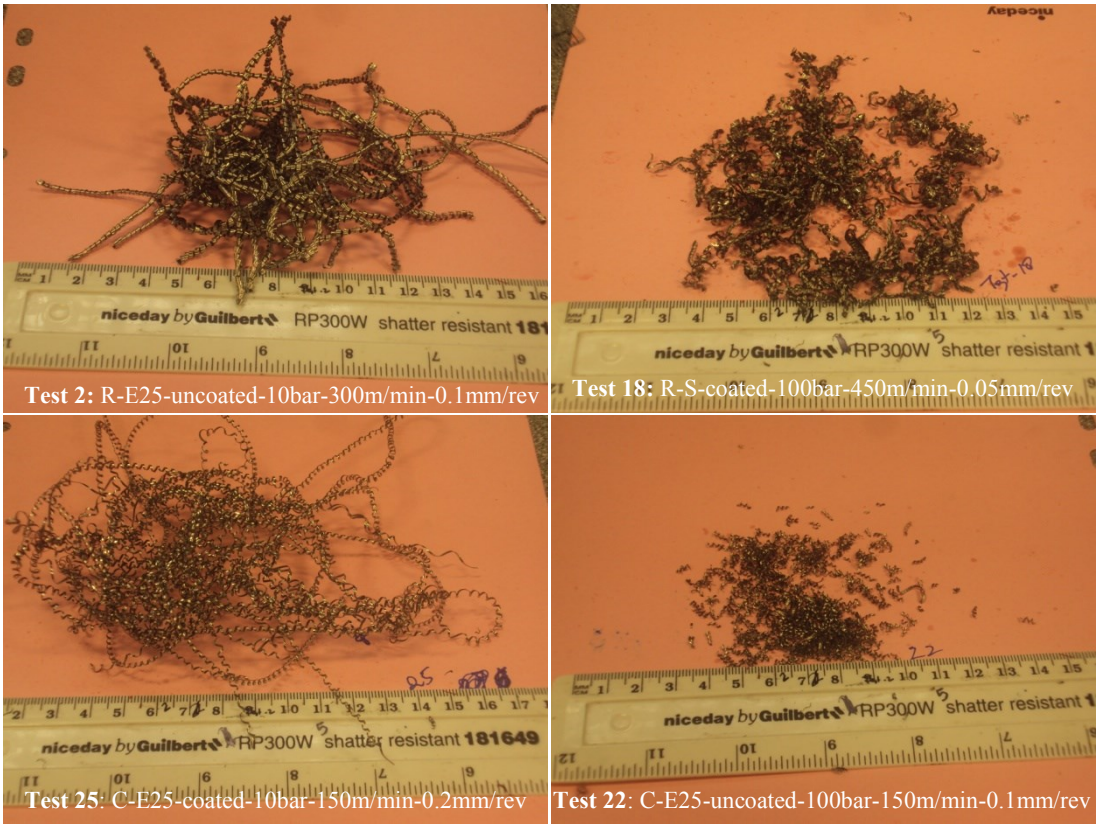

a) 10bar b) 100bar

Figure 100: Typical chips produced from tests at a) 10bar and b) 100bar fluid pressure

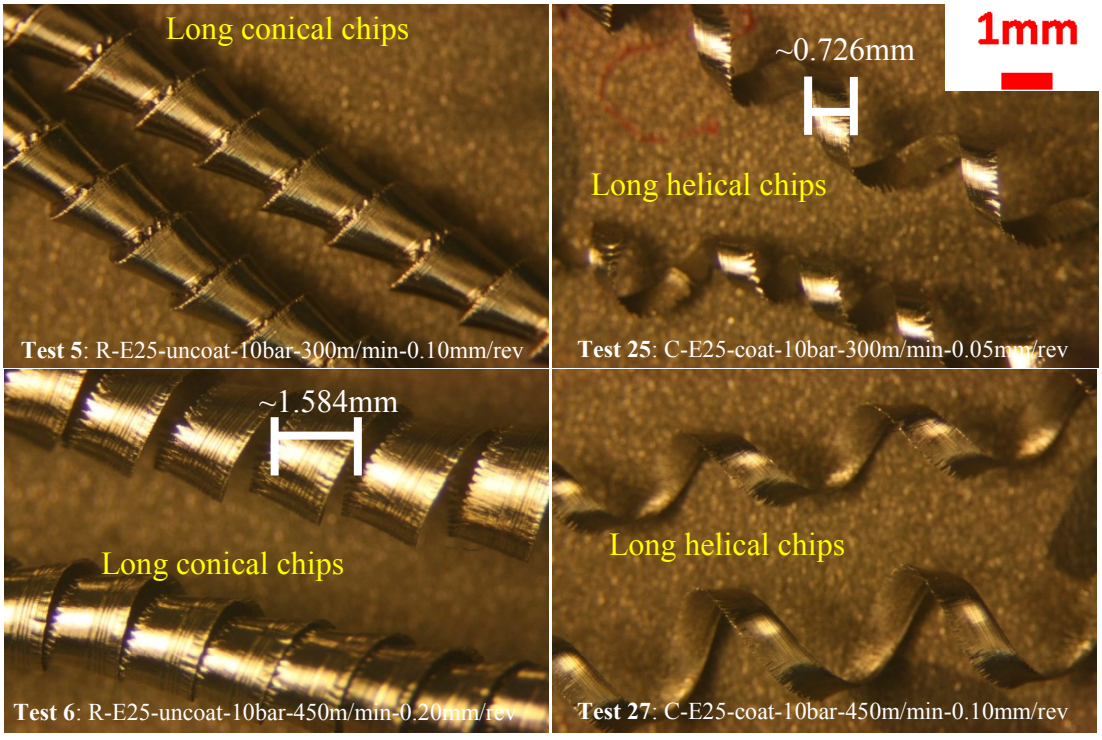

Figure 101: Difference in chip morphology when machining with round and C-type inserts

4.3.3 Surface roughness

Figure 102 details the evolution of workpiece surface roughness against flank wear of cutting tool at a cutting speed of 150m/min. Surface roughness did not exceed 0.50µm Ra over duration of the experiments for all tests performed with round inserts at a feed rate of 0.05mm/rev (Tests 1, 4 and 10) due to uniform wear progression with one exception in Test 7 where Ra value increased to ~1.00µm at the end of tool life. This was primarily due to notch wear and chipping seen in the wear scar micrograph (Figure 89). Workpiece surface roughness increased to 1.00-1.50µm Ra at ~200µm tool flank wear in Tests 13 and 16, performed with round inserts at a feed rate of 0.10mm/rev. This was likely due to unevenness generated at the tool nose due to workpiece material adhesion, see Figure 103. In contrast, surface roughness when utilising C-type inserts deteriorated particularly at a feed rate of 0.20mm/rev, with maximum Ra values of ~4.00µm recorded at the end of tool life. This was attributed to the greater grooving and BUE observed with the C-type insert geometry together with the large uncut chip thickness.

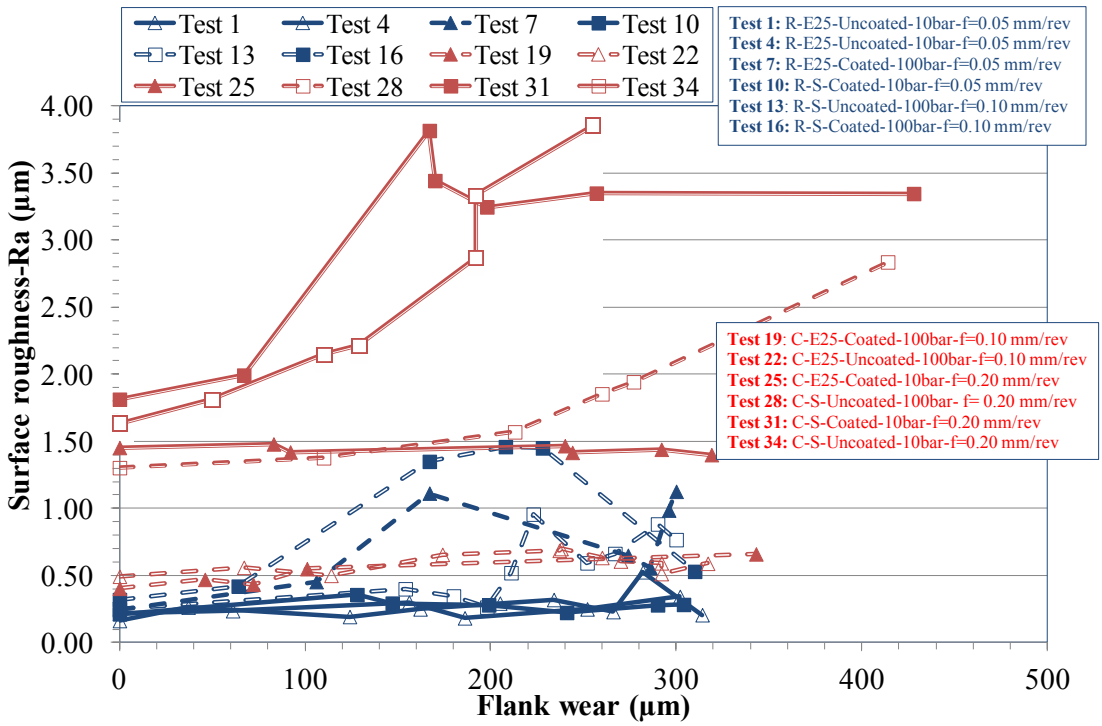

Figure 102: Workpiece surface roughness (Ra) against tool flank wear at a cutting speed of 150m/min

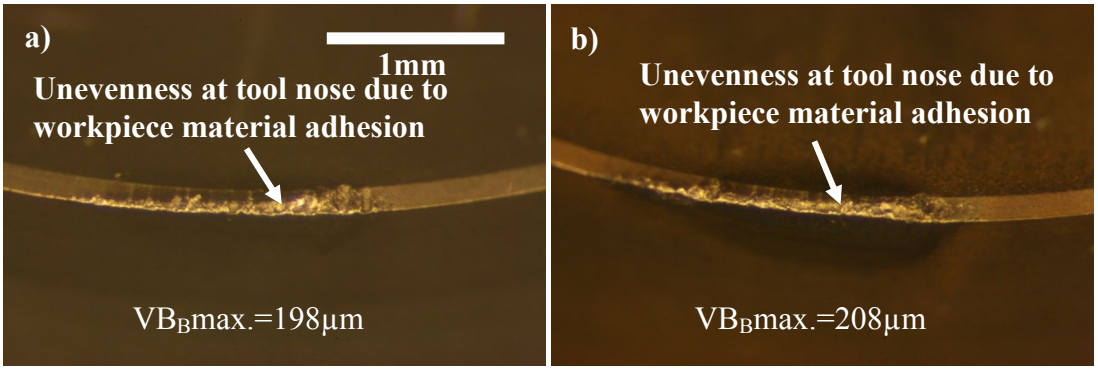

Figure 103: Optical micrographs of (a) Test 13 and (b) Test 16 at ~200µm flank wear

Measurements of workpiece surface roughness against tool flank wear at a cutting speed of 300m/min are shown in Figure 104. Roughness was < 0.60µm in all tests conducted at feed rates of 0.05mm/rev and 0.10mm/rev irrespective of other operating factors. For the trials performed at a feed rate of 0.20mm/rev (Tests 14, 17, 20 and 23), Ra was ~1.20µm at the start of cutting when employing C-type inserts compared to the round tool geometry where roughness was ~0.50µm. The lower surface roughness with the latter was attributed to the larger contact radius. In case of C-type inserts (Test 20 and 23), Ra was initially dropped to a value of 0.80µm for the first 150µm tool flank wear due to the formation of wiper flat radius (Figure 105) and then remained stable at the end of tool life. Formation of a wiper flat radius in Tests 20 and 23 was due to E25 edge configuration of these C-type inserts. In contrast, increase in surface roughness was observed in Tests 14 and 17 with increasing flank wear (~200µm). This was likely due to irregularly shaped wear scars produced on the chamfer location of round inserts as a result of initial wear, shown in Figure 106. However, at the end of tool life, Ra was dropped to 0.60µm in Test 14 while the opposite was true for Test 17 where an increase up to a value of 1.20µm was recorded. Figure 107 displays the optical micrographs from Tests 14 and 17 at the end of tool life, which shows that workpiece material adhesion was prevalent in Test 17 (performed with coated insert), likely due to the high cutting temperature generated as a result of the low thermal conductivity of this coating product.

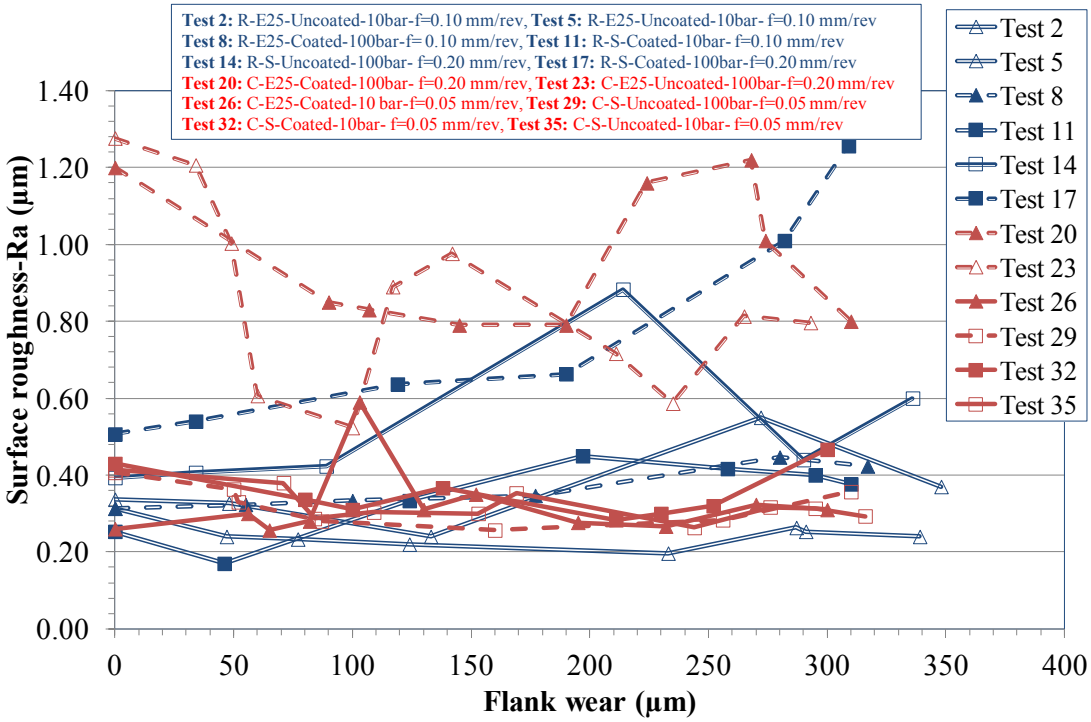

Figure 104: Workpiece surface roughness (Ra) against tool flank wear at a cutting speed of 300m/min

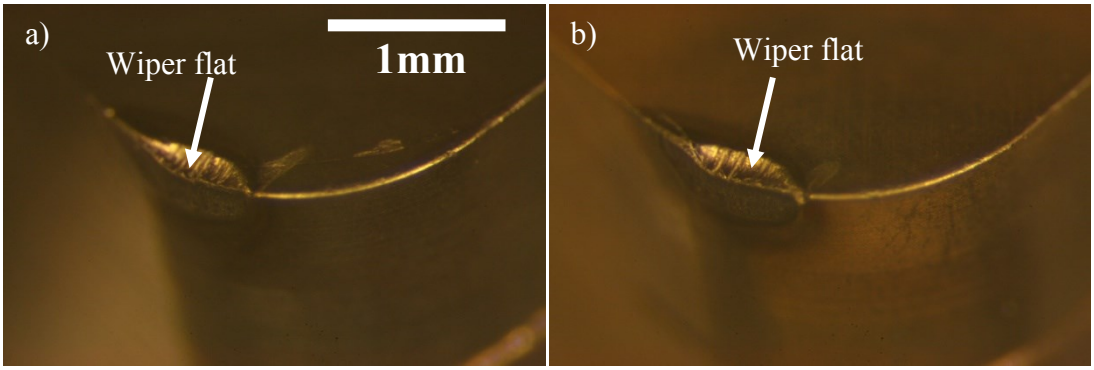

Figure 105: Optical micrographs of (a) Test 20 and (b) Test 23 at the end of tool life

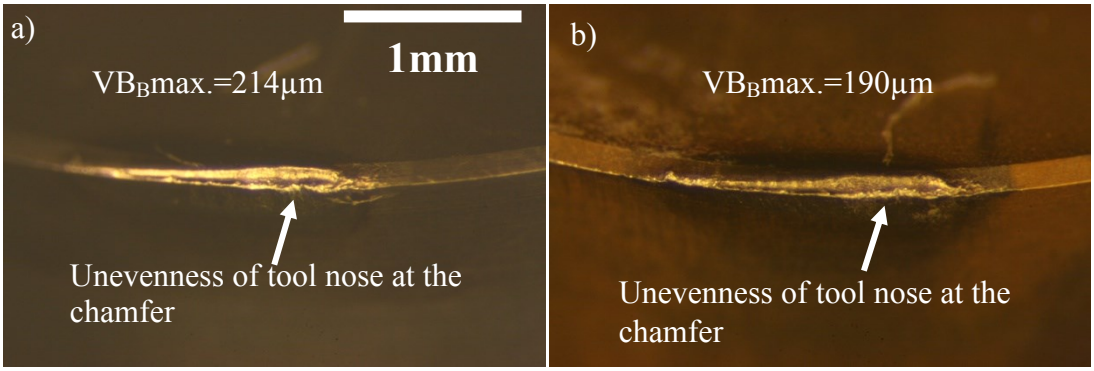

Figure 106: Optical micrographs of (a) Test 14 and (b) Test 17

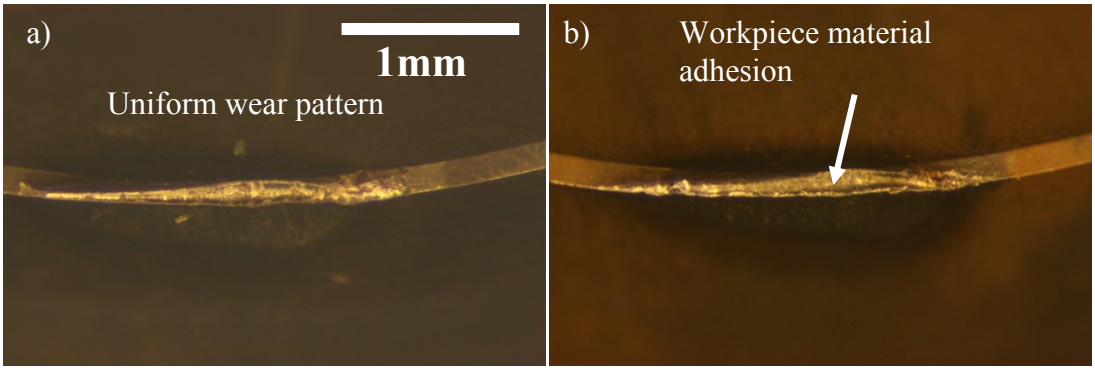

Figure 107: Optical micrographs of (a) Test 14 and (b) Test 17 at the end of tool life

Figure 108 displays the evolution of workpiece surface roughness versus tool flank wear at the highest cutting speed of 450m/min. The tests performed at a feed rate of 0.05mm/rev (Tests 15, 18, 21 and 24), Ra value did not exceed 0.60µm over the test duration with limited variability. In addition, a minimum surface roughness approaching 0.25µm Ra at the end of tool life was recorded for 2 tests performed with the round inserts (Test 15-0.26µm and Test 18-0.29µm). This was likely due to the uniform tool wear progression recorded in the trials together with low feed rate. Variation in workpiece surface roughness was observed against tool wear progression in all trials carried out at a feed rate of 0.10mm/rev and 0.20mm/rev. This was probably due to the change in the tool nose radius as a result of workpiece material adhesion, fracture and thermal cracks seen in the wear scar micrographs (Figure 96). At the highest feed rate of 0.20mm/rev (Tests 3, 6, 9 and 12), Ra increased to ~1.00µm while it was ~0.60µm at the end of tool life for the Tests 27, 30, 33 and 36 conducted at a feed rate of 0.10mm/rev.

Main effects plots for surface roughness measured at test cessation shown in Figure 109 while the corresponding ANOVA is detailed in Table 42. Tool geometry, edge preparation, cutting speed and feed rate were found to be statistically significant at the 5% level with respect to surface roughness, with the latter showing the highest PCR of 32.11%. Conversely, the PCR of cutting speed was moderate at 17.75% while both tool geometry and edge preparation had relatively low PCR's of 7.04% and 4.75% respectively. As expected, surface roughness increased with feed rate while superior surface finish was generally obtained when employing round tools due to the larger contact radius, which reduces the cusp height of the machined surface. Apart from the larger chip thickness, the higher mean surface roughness values seen at the lower cutting speed of 150m/min was due to the significant difference in wear behaviour of both inserts. The severe grooving and BUE prevalent in C-type inserts had a deteriorated effect on surface quality as previously highlighted in Figure 102.

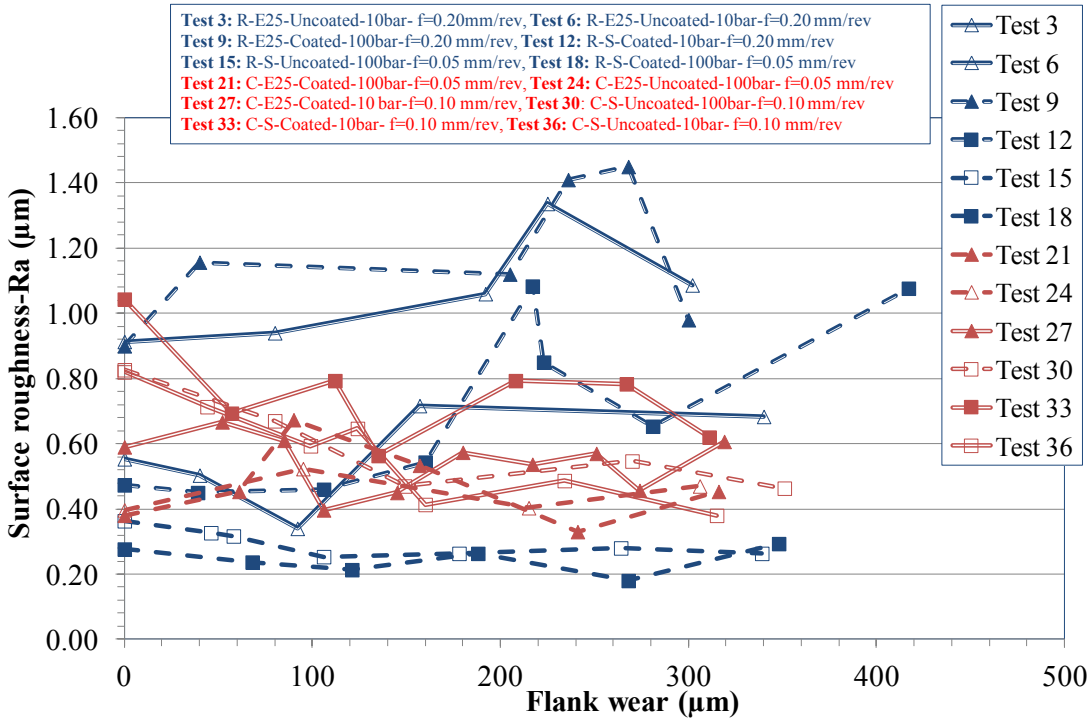

Figure 108: Surface roughness (Ra) against flank wear at a cutting speed of 450m/min

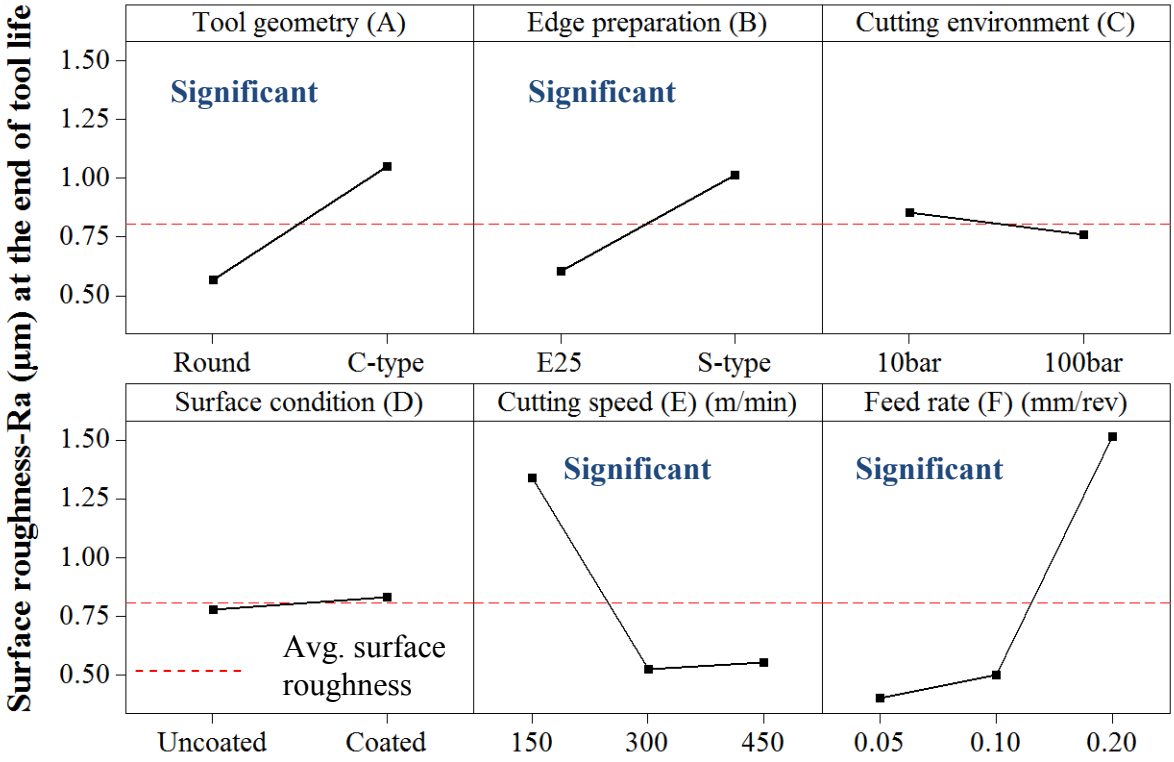

Figure 109: Main effects plots-means for surface roughness (Phase 1C)

Table 42: ANOVA table for surface roughness (Phase 1C)

Factors	DF	SS	MSS	F	P	PCR (%)
Tool geometry (A)	1	2.0977	2.0977	7.30	0.012*	7.04
Edge preparation (B)	1	1.5088	1.5088	5.25	0.030*	4.75
Cutting environment (C)	1	0.0793	0.0793	0.28	0.604	0
Surface condition (D)	1	0.0272	0.0272	0.09	0.761	0
Cutting speed (E)	2	5.1349	2.5675	8.94	0.001*	17.75
Feed rate (F)	2	9.0812	4.5406	15.81	0.000*	32.11
Error	27	7.7562	0.2873	-	-	***38.35***
Total	35	25.6854	$F_{table=}$4.2, R-Sq(Adj)=61.65			

The superior surface roughness when turning at the higher cutting speeds of 300m/min and 450m/min respectively was due to the reduction of BUE formation. Similar to the results concerning tool wear, the analysis of variance revealed an unacceptably high error level of 38.35% as interaction were not considered in the standard calculations.

Seven interactions were identified as statistically significant based on step wise backward elimination (SBE) and forward entry (SFE) linear regression procedure with 3 involving edge preparation*feed rate (B*F), cutting environment*feed rate (C*F) and tool geometry*edge preparation (A*B) resulting in an increase of >5% in the R-Sq (Adj) value, which underlined their influence over the other interactions present in the model, see Table 43. Full interactions plots for surface roughness are shown in Figure B18 in Appendix B and corresponding equations for surface roughness based on stepwise procedures are detailed in Equations B6-B13 in Appendix B. In general, inserts with S-type edge preparation produced higher surface roughness (compared to E25) which was attributed to the unevenness of tool nose along the chamfer. This effect was prevalent at the highest feed rate of 0.20mm/rev due to the large uncut chip thickness. The interaction between tool geometry and edge preparation (A*B) was characterised by the increase in Ra when employing C-type inserts with S-type edge condition. The pronounced effect of chamfer unevenness with C-type inserts was likely due to the smaller nose radius however this effect was suppressed with round insert due to its larger contact radius minimising this effect. Interactions plots suggest that workpiece surface roughness was marginally better when employing a cutting fluid pressure of 100bar compared to 10bar at a feed rate of 0.20mm/rev. Although no substantial benefit in terms of tool life and cutting forces was observed at a cutting fluid pressure of 100bar, a reduction in surface roughness was likely due to flattening of feed peaks as result of the greater mechanical impact associated with high cutting fluid pressure.

Table 43: Interactions for surface roughness appeared to be statistically significant in step wise backward elimination and forward entry evaluation procedure (Phase 1C)

Stepwise backward elimination procedure	**Stepwise forward entry procedure**	
	R-Sq (Adj) after adding an interaction with main effects	**Increase in R-Sq (Adj) value**
A*B	65.42	6.11%
A*C	61.66	0.01%
B*E	63.66	3.26%
B*F	69.97	13.49%
C*E	62.09	0.71%
C*F	66.84	8.41%
R-Sq (Adj)=92.7	65.42	6.11%
Error=7.3%		

4.3.4 Cutting forces

Figure 110 shows the typical trend of the respective force components recorded throughout the experiment. The thrust component was generally found to have the highest magnitude followed by the cutting and feed force, which contrasts with 'standard' turning operation where thrust force is 30-50% of the cutting force component. Similar trends however have been reported by several researchers when finish turning of hardened steels [154-156]. Since the depth of cut employed in the current tests was substantially smaller than the nose radius of the inserts (1.2mm for C-type and 5mm for round insert), chip formation was restricted to the curved region of the cutting edge which subsequently reduced the active approach angle (Kr). As a result of lower approach angle, the orientation of the resultant force rotates in a clock wise direction causing a corresponding decrease in feed force and rise in thrust force as shown in Figure 111. Additionally, this was further exacerbated when machining at elevated feed rates.

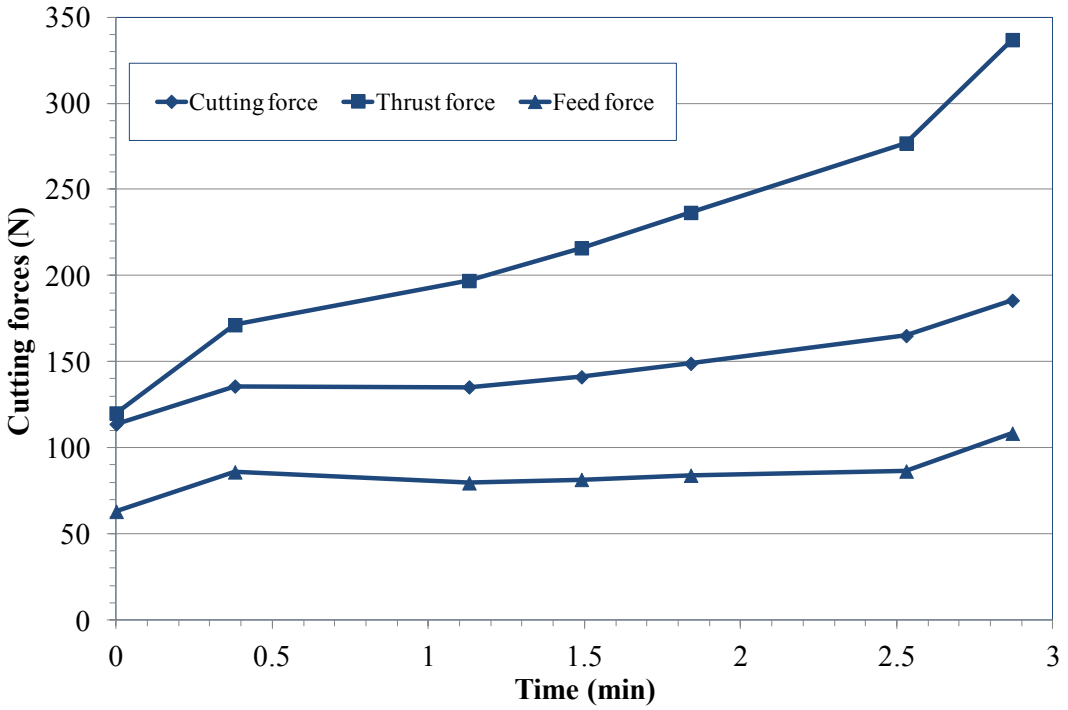

Figure 110: General trend of cutting force components against machining time (data from Test 36)

Kr=Approach angle, Fr=resultant force Ff=feed force, Ft=thrust force

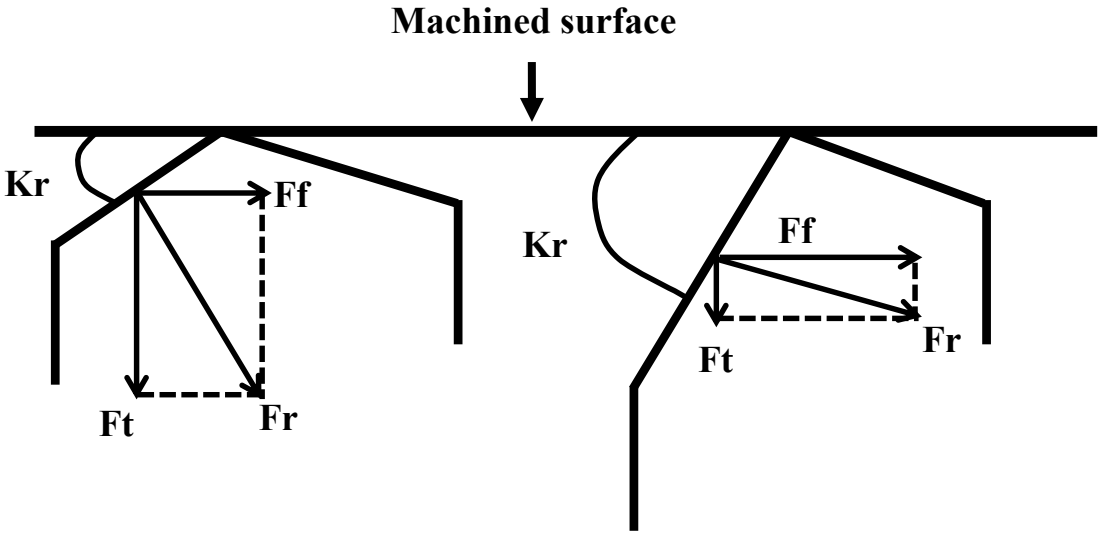

Figure 111: A schematic illustration showing the influence of change in the approach angle on resultant, feed and thrust force

4.3.4.1 Cutting force component

Figure 112 highlight the evolution of cutting force against machining time at a cutting speed of 150m/min. With round inserts, cutting force did not exceed 250N even at the end of tool life for the trials performed at a feed rate of 0.05mm/rev (Tests 1, 4, 7 and 10), irrespective of other operating variables. However when feed rate was increased to

0.10mm/rev (Test 13 and 16), a ~50-100N rise in cutting force was observed at test cessation. This was attributed to the increase in chip thickness, which is proportional to the feed rate. In case of C-type inserts, cutting force was < 200N at test cessation for the tests conducted at a feed rate of 0.10mm/rev (Tests 19 and 22), however it was increased to ~280N at a feed rate of 0.20mm/rev (Tests 28, 31 and 34) with an exception in Test 25 where cutting force was less than 185N. Higher cutting force with the former was likely due to S-type edge geometry with a chamfer feature, which increased the resistance to chip flow over the rake face due to the larger tool chip contact length.

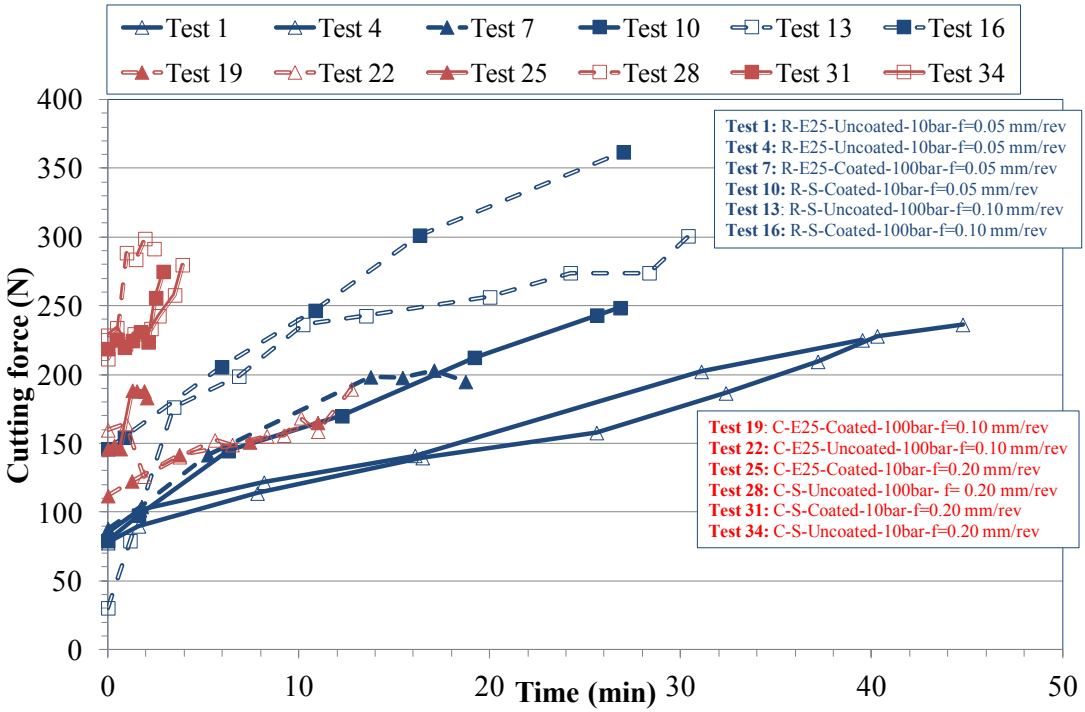

Figure 112: Cutting force against machining time at a cutting speed of 150m/min

Evolution of cutting force against machining time at a cutting speed of 300m/min is shown in Figure 113. With C-type inserts, cutting forces did not exceed 150N ever after 10min of cutting when operating at a feed rate of 0.05mm/rev (Tests 26, 29, 32 and 35). When feed rate was increased to 0.20mm/rev (Tests 20 and 23) however, cutting force doubled to ~300N after only ~6mins. Similarly, cutting force approached to a value of 350N at test cessation when employing round inserts at a feed rate of 0.20mm/rev (Tests 14 and 17) which was ~100N higher compared to the trials performed at a feed rate of 0.10mm/rev.

Figure 114 shows the evolution of cutting force against machining time at a cutting speed of 450m/min. Cutting force ranged between 250-300N was recorded at the end of tool life with round insert when operating at a feed rate of 0.20mm/rev however, Tests 15 and 18 conducted at a feed rate of 0.05mm/rev generated ~200N. With C-type insert, increase in the

feed rate from 0.05mm/rev to 0.20mm/rev caused a ~35% rise in the value of cutting force after 3min of cutting which was 135N with the former.

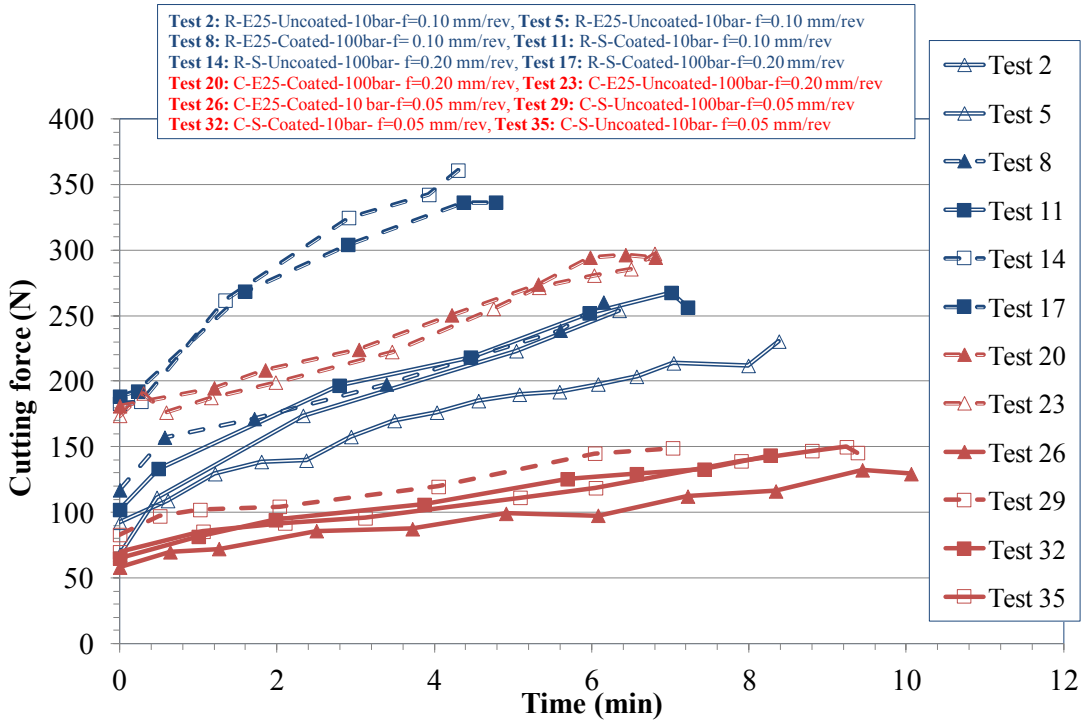

Figure 113: Cutting force against machining time at a cutting speed of 300m/min

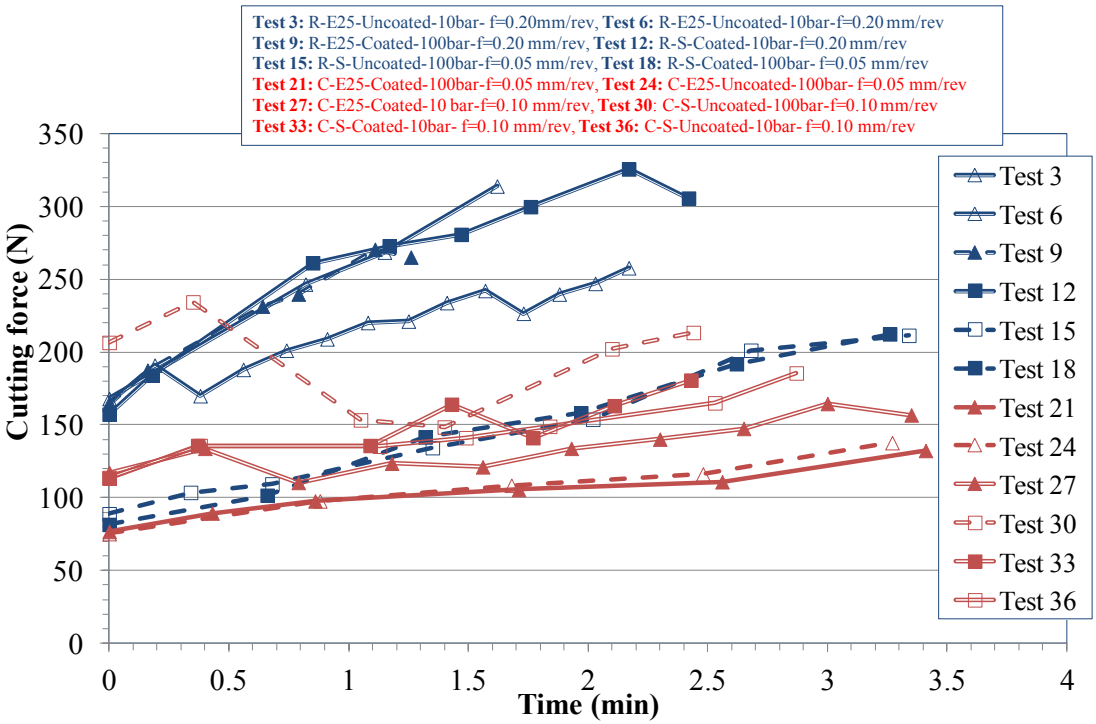

Figure 114: Cutting force against machining time at a cutting speed of 450m/min

The main effects plots and corresponding ANOVA table for cutting force at the end of tool life is shown in Figure 115 and Table 44 **r**espectively. Feed rate and tool geometry were found to have the greatest influence with PCR's of 45.19 and 29.94% respectively while both edge preparation and cutting speed although statistically significant had PCR's not exceeding 6%. Not surprisingly, the increase in cutting force with feed rate was the result of larger uncut chip thickness while the higher forces generated with round inserts was attributed to its larger tool contact radius. This agreed with data published by Nalbant et al. [89] when evaluating the performance of round and square inserts in turning Inconel 718. Similar trends were observed with the S-type edge geometry. The lower cutting forces obtained at higher cutting speeds was likely the result of increasing shear angle or workpiece softening. This was in line with studies detailed by Pawade et al. [103] and Arunachalam et al. [85] when high speed turning (375 and 475 m/min respectively) of Inconel 718 with PCBN tools.

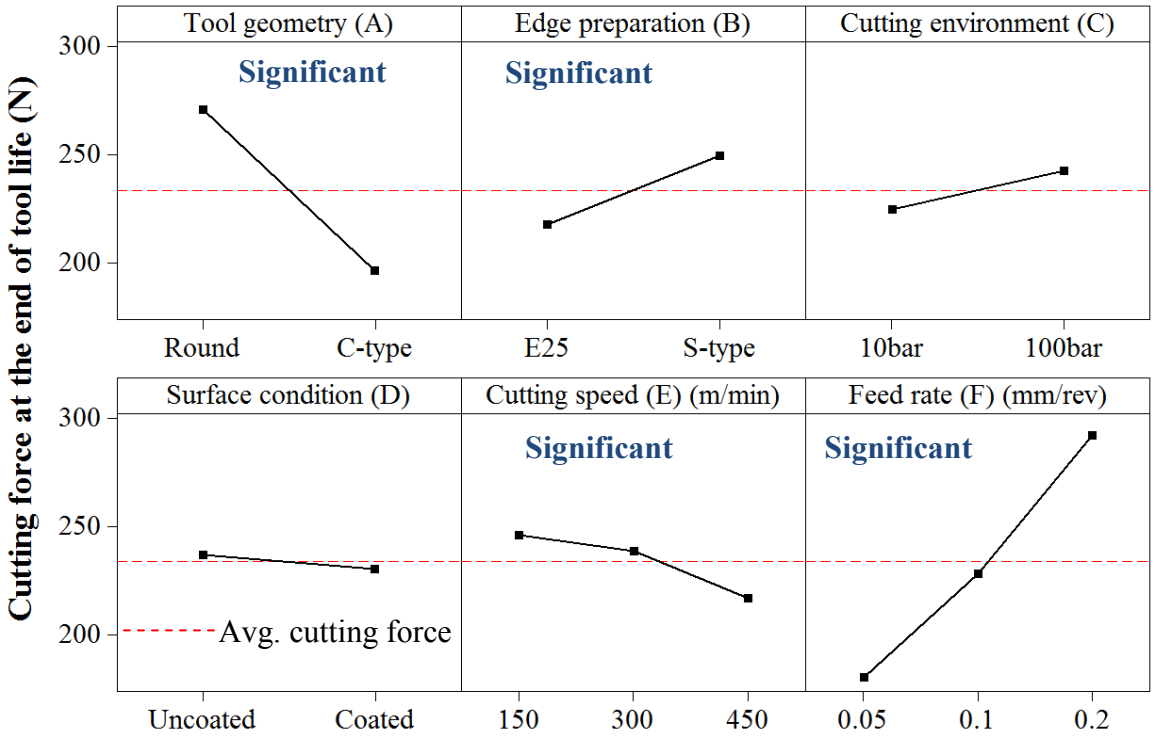

Figure 115: Main effects plots-means for cutting force (Phase 1C)

The level of error from the ANOVA was marginally above 15% probably due to the interactions between tool geometry*cutting speed (A*E) and edge preparation*surface condition (B*D) which were found to be significant following the stepwise forward removal and entry procedure, see Table 45. The former and latter caused a ~5% and 1.6% increase in the adjusted R^2 value respectively, according to the step wise forward entry routines. The complete interactions plots are detailed in Figure B19 of Appendix B with corresponding

Equations B14-B16 generated based on SBE and SFE procedures. The interaction between tool geometry and cutting speed (A*E) was characterised by the reduction of cutting force with the increase in cutting speed particularly with C-type geometry configuration, however no significant difference in cutting force was observed with the round insert which was in the range of 260-280N at the end of tool life. This was likely due to its larger radius minimising the effect of increase in shear angle or workpiece material softening.

Table 44: ANOVA table for cutting force (Phase 1C)

Factors	DF	SS	MSS	F	P	PCR (%)
Tool geometry (A)	1	49789	49789	65.65	0.000*	29.94
Edge preparation (B)	1	9157	9157	12.07	0.002*	5.12
Cutting environment (C)	1	2921	2921	3.85	0.060	1.32
Surface condition (D)	1	389	389	0.51	0.480	0
Cutting speed (E)	2	5482	2741	3.61	0.041*	2.42
Feed rate (F)	2	75526	37763	49.79	0.000*	45.19
Error	27	20478	758	-	-	***16.01***
Total	35	163742	$F_{table=}$4.2, R-Sq(Adj)=83.99%			

Table 45: Interactions for cutting force appeared to be statistically significant in step wise backward elimination and forward entry evaluation procedure (Phase 1C)

Stepwise backward elimination method	**Stepwise forward entry procedure**	
	R-Sq (Adj) after adding an interaction with main effect	**Increase in R-Sq (Adj) value**
A*E	87.95	4.71%
B*D	85.17	1.40%
R-Sq (Adj)= 89.62		
Error= 10.38%		

4.3.4.2 Thrust force component

In general, thrust forces were up to ~185% and ~450% higher than the corresponding cutting and feed forces respectively. Figure 116 shows the evolution of thrust force against machining time at a cutting speed of 150m/min. Thrust force did not exceed 600N at test cessation for the trials performed with round inserts at a feed rate of 0.05mm/rev however, when feed rate was increased to 0.10mm/rev, ~200N rise in thrust force was recorded. With C-type inserts, thrust force was less than 350N over a period of ~2-10 min irrespective of other operating variables except for Test 28 where it reached ~550N after 1.5min due to fracture of the insert; shown previously in Figure 91.

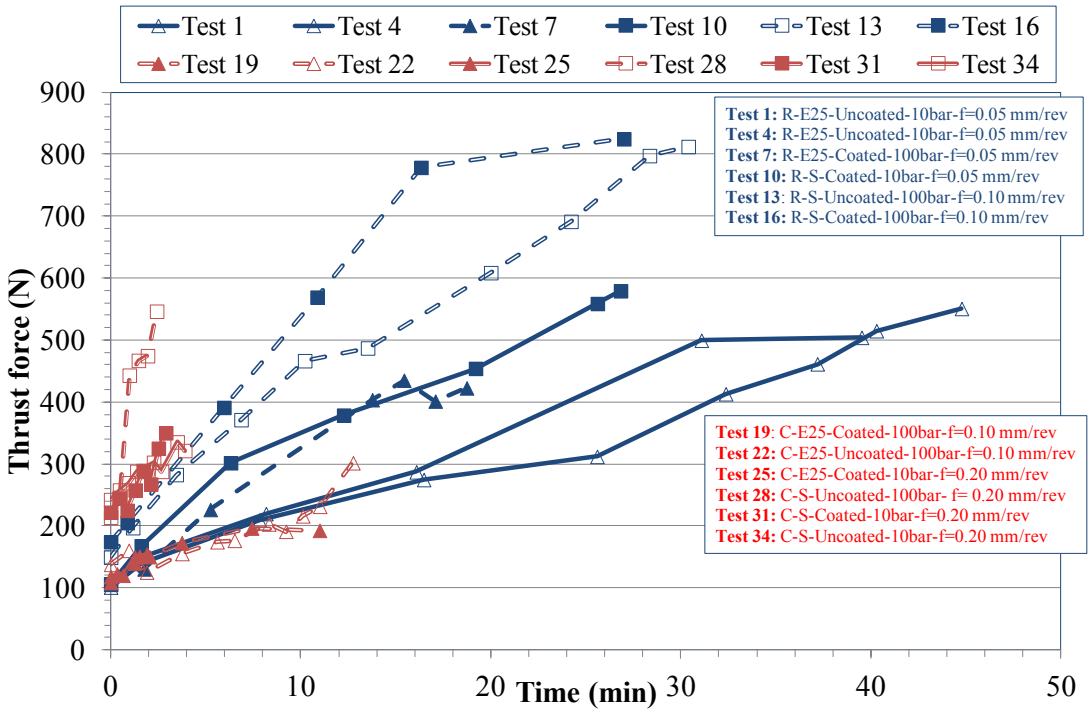

Figure 116: Thrust forces against machining time at a cutting speed of 150m/min

Evolution of thrust force against machining time at a cutting speed of 300m/min is shown in Figure 117. For the tests performed at a feed rate of 0.20mm/rev, thrust force increased to 700-900N with round inserts after 4.5min where it was less than 500N over a period of 6.8min using C-type geometry. Generally, the evolution of thrust forces at feed rates of 0.05mm/rev and 0.10mm/rev were gradual over 6-10min irrespective of tool geometry and operating variables. However, thrust force was ~100-200N higher with round insert compared to C-type configuration.

Figure 118 highlight the progression of thrust force against machining time at a cutting speed of 450m/min. At a feed rate of 0.05mm/rev, steep rise in thrust force (~700N) was observed with round inserts over a period of 3.5min, however for the same duration it was only 300N using C-type geometry. In all other tests, thrust force was < 600N irrespective of other operating condition with the exception for Test 12 where thrust force reached a maximum of 936N at test cessation due to the fracture and thermal cracks, shown previously in Figure 96.

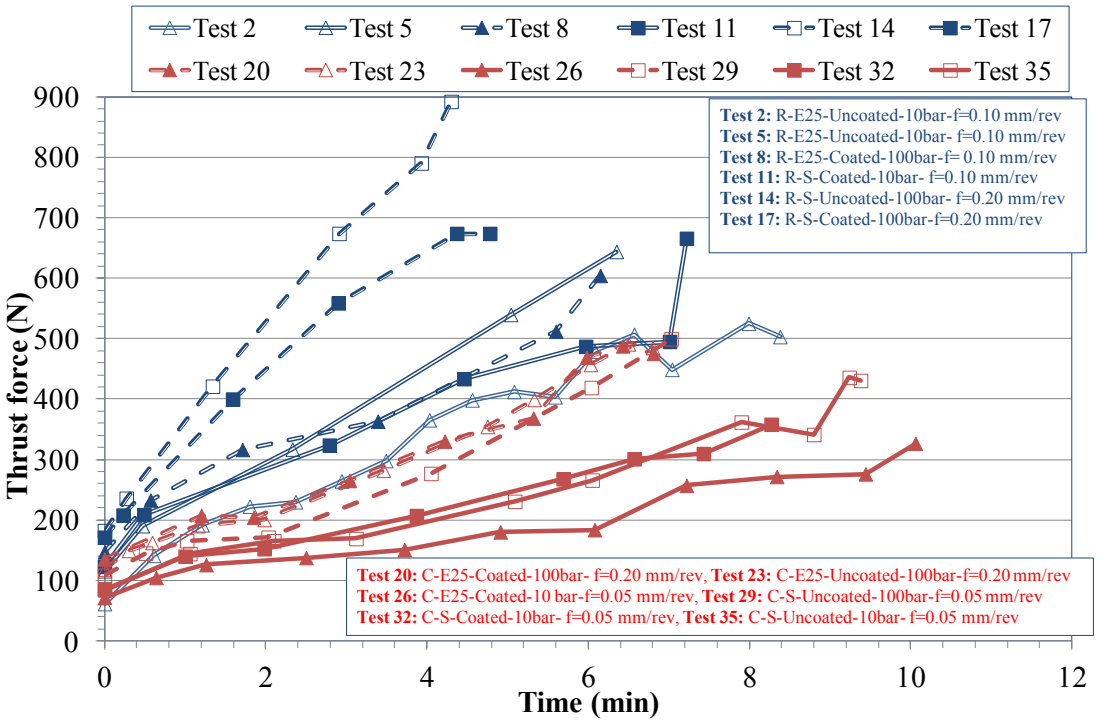

Figure 117: Thrust force against machining time at a cutting speed of 300m/min

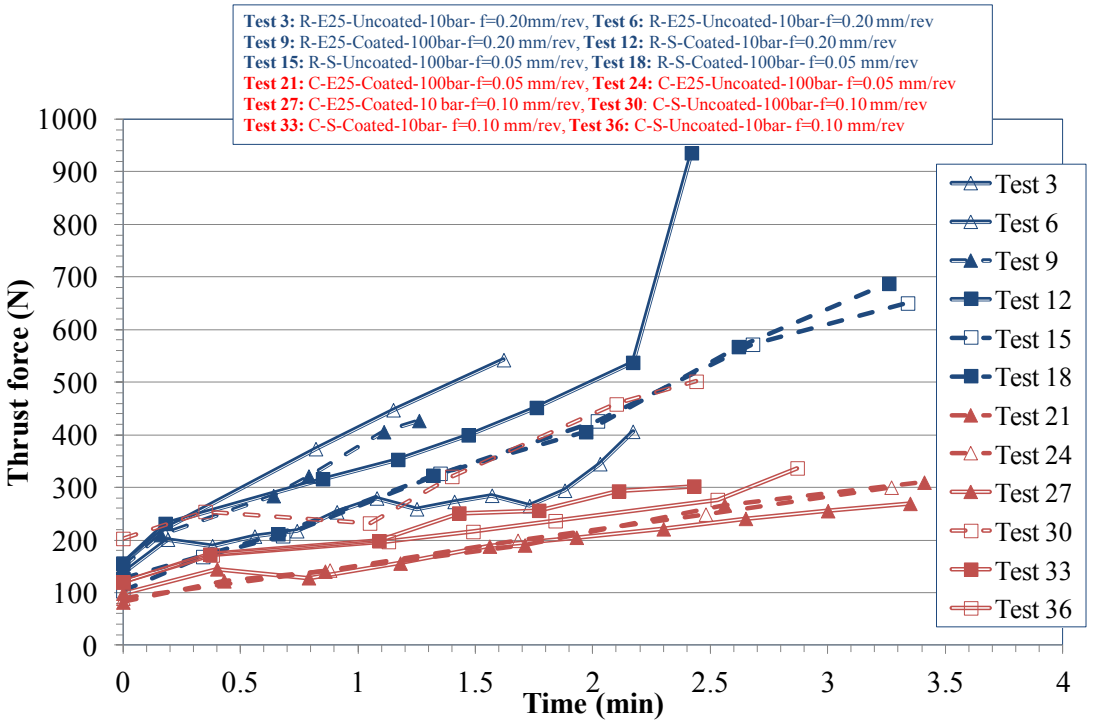

Figure 118: Thrust force against machining time at a cutting speed of 450m/min

Figure 119 displays the main effects plots for thrust force with the associated ANOVA detailed in Table 46. With the exception of feed rate, all of the variable factors were found to be statistically significant at the 5% level. Tool geometry showed the strongest influence with a PCR of 53.70% followed by edge preparation having a PCR of ~15%. The remaining 3 significant factors had PCR's of < 8%. As with the cutting force component, thrust force was

generally higher when employing round inserts and S-type edge finish condition. The greater mechanical impact at 100 bar fluid pressure similarly led to higher thrust forces. The results however contrasted with published data involving turning of Inconel 718 using round whisker ceramic [99] and square coated carbide [72] inserts where shorter tool chip contact lengths, uniform tool wear and lower cutting forces (30% and 16% for ceramic and carbide inserts respectively) were observed at high cutting fluid pressure of 203bar compared to conventional coolant supply. The decrease in thrust force obtained when utilising coated PCBN inserts was likely due to its lower coefficient of friction compared to the uncoated products which agreed with research on coated PCBN by Coelho et al. [15] in finish turning of AISI 4340. The higher thrust force obtained at Vc of 300m/min was likely due to uniform tool wear progression observed with the C-type geometry compared to its performance at 150 and 450 m/min, leading to greater volumetric material removed. Although edge preparation*cutting environment (B*C) was the sole interaction found to be statistically significant, see Table 47, the effect on the R-Sq (Adj) value based on step wise forward entry procedure was less than 2%. The ~15% error level detailed by the ANOVA however was within the acceptable limit of Taguchi experimental design suggesting that all important factors affecting thrust force had been considered.

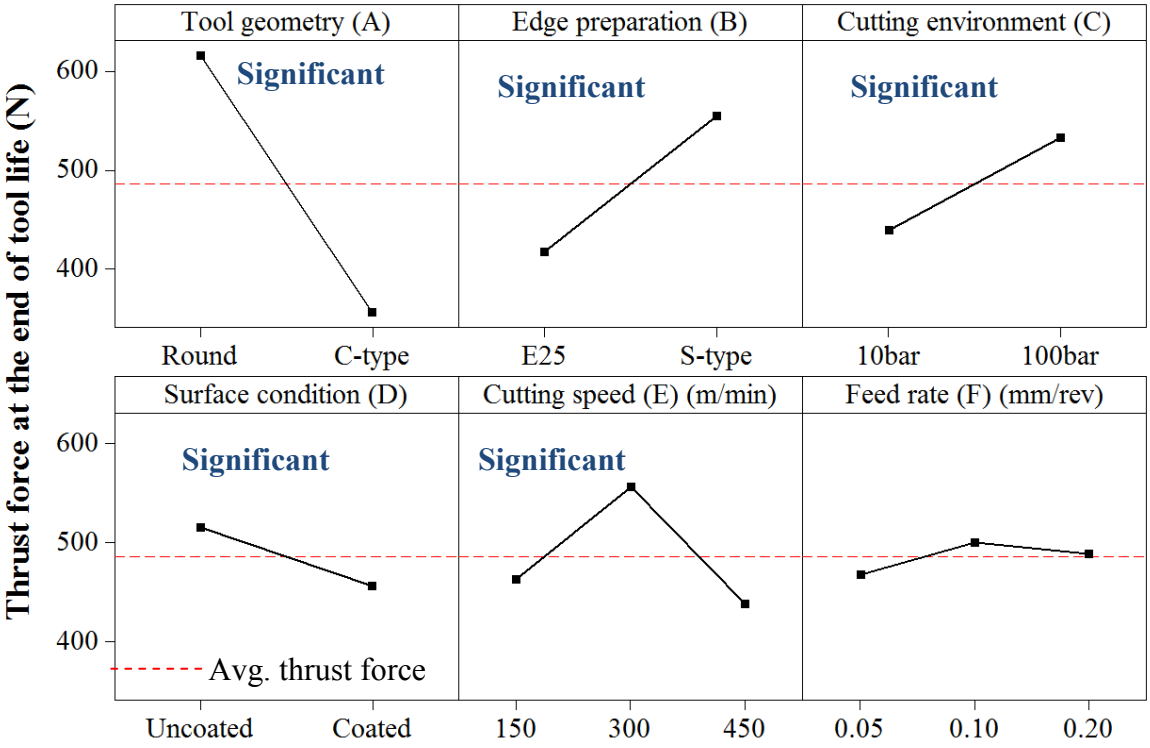

Figure 119: Main effects plots-means for thrust force (Phase 1C)

Table 46: ANOVA table for thrust force (Phase 1C)

Factors	DF	SS	MSS	F	P	PCR (%)
Tool geometry (A)	1	604550	604550	124.07	0.000*	53.70
Edge preparation (B)	1	170290	170290	34.95	0.000*	14.81
Cutting environment (C)	1	79001	79001	16.21	0.000*	6.63
Surface condition (D)	1	31480	31480	6046	0.017*	2.38
Cutting speed (E)	2	93361	46680	9.58	0.001*	7.48
Feed rate (F)	2	6467	3233	0.66	0.523	0
Error	27	131564	4873			***15***
Total	35	1116712	F_{table}=4.2, R-Sq (Adj)= 85			

Table 47: Interactions for thrust force appeared to be statistically significant in step wise backward elimination and forward entry evaluation procedure (Phase 1C)

Stepwise backward elimination method	**Stepwise forward entry procedure**	
	R-Sq (Adj) after adding an interaction with main effect	**Increase in R-Sq (Adj) value**
B*C	86.39	1.63%
R-Sq (Adj)= 86.39		
Error=13.61%		

4.3.4.3 Feed force component

Evolution of feed force against machining time at cutting speed of 150m/min is shown in Figure 120. Feed force did not exceed 100N ever over a test duration of ~20-40min for the tests performed with round inserts at a feed rate of 0.05mm/rev (Tests 1, 4, 7 and 10) however, when feed rate was increased to 0.10mm/rev (Tests 13 and 16) , ~50N rise was recorded at test cessation. With C-type geometry, feed force was less than 150N even after 10min of cutting for the trails performed at a feed rate of 0.10mm/rev (Tests 19 and 22). While a steep rise up to a value of ~200N was recorded after 3min of machining for the tests performed at a feed rate of 0.20mm/rev except in Test 25 where the feed force was <110N at the end of tool life, most likely due to E25 edge configuration.

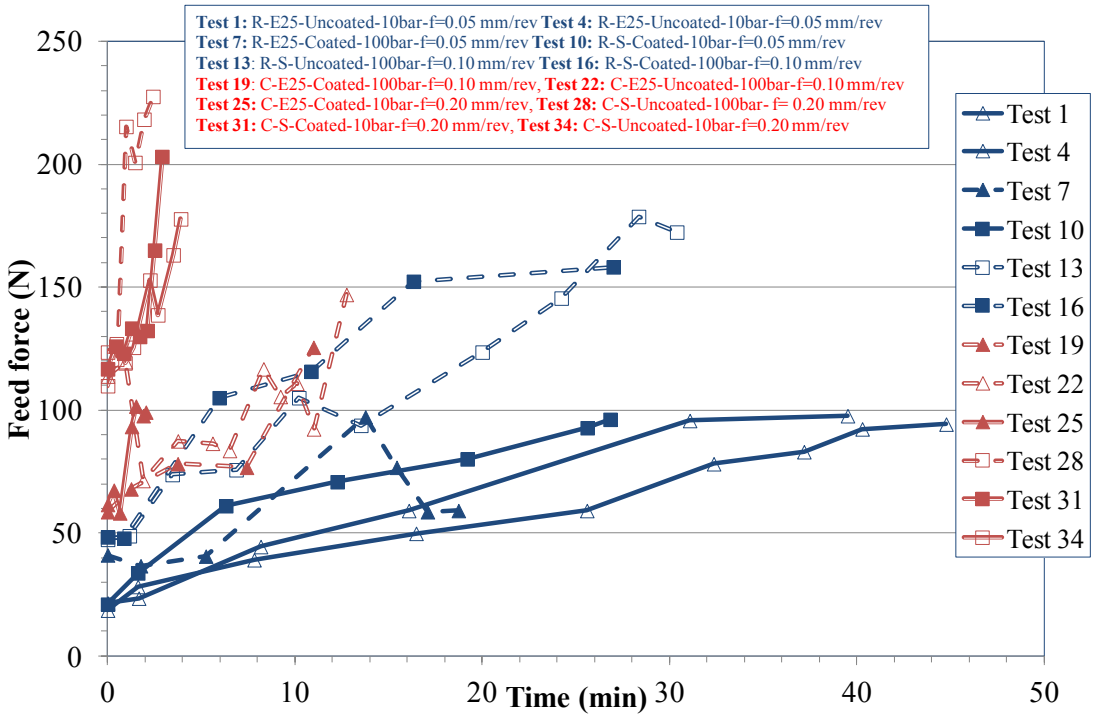

Figure 120: Feed force against machining time at a cutting speed of 150m/min

Feed force was less than 200N in all tests performed at cutting speeds of 300m/min and 450m/min, with a minimum value of ~52N in Test 3 at test cessation however, no clear trends were apparent linking feed force to the variable factors, see Figures 121 and 122.

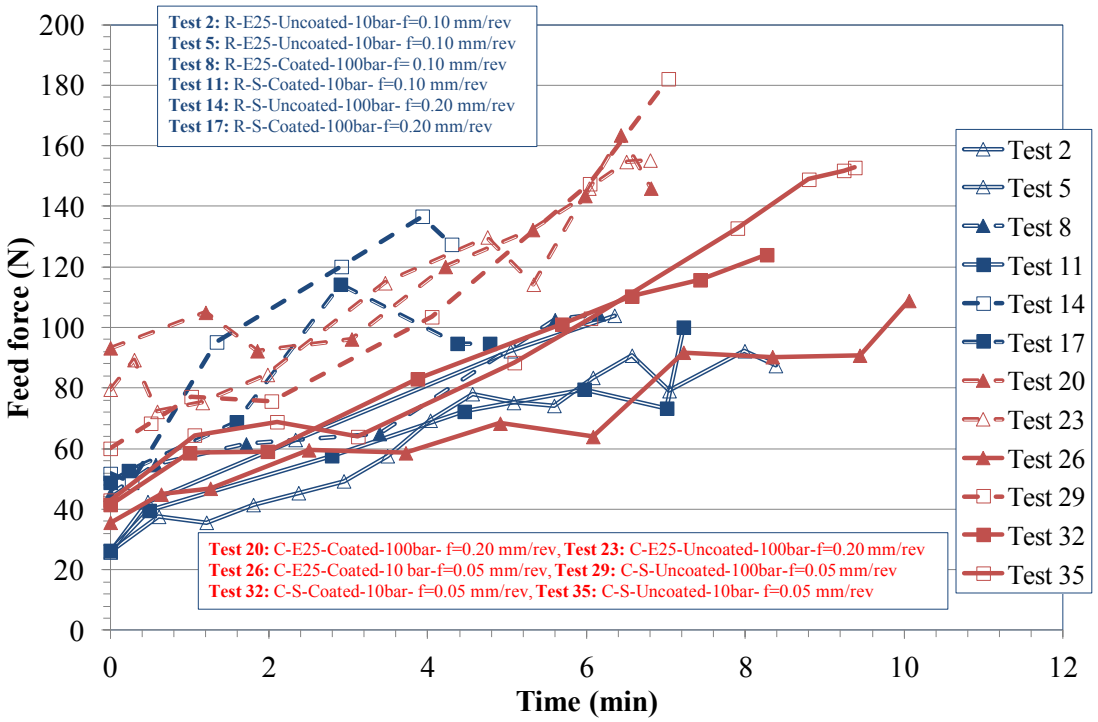

Figure 121: Feed force against machining time at a cutting speed of 300m/min

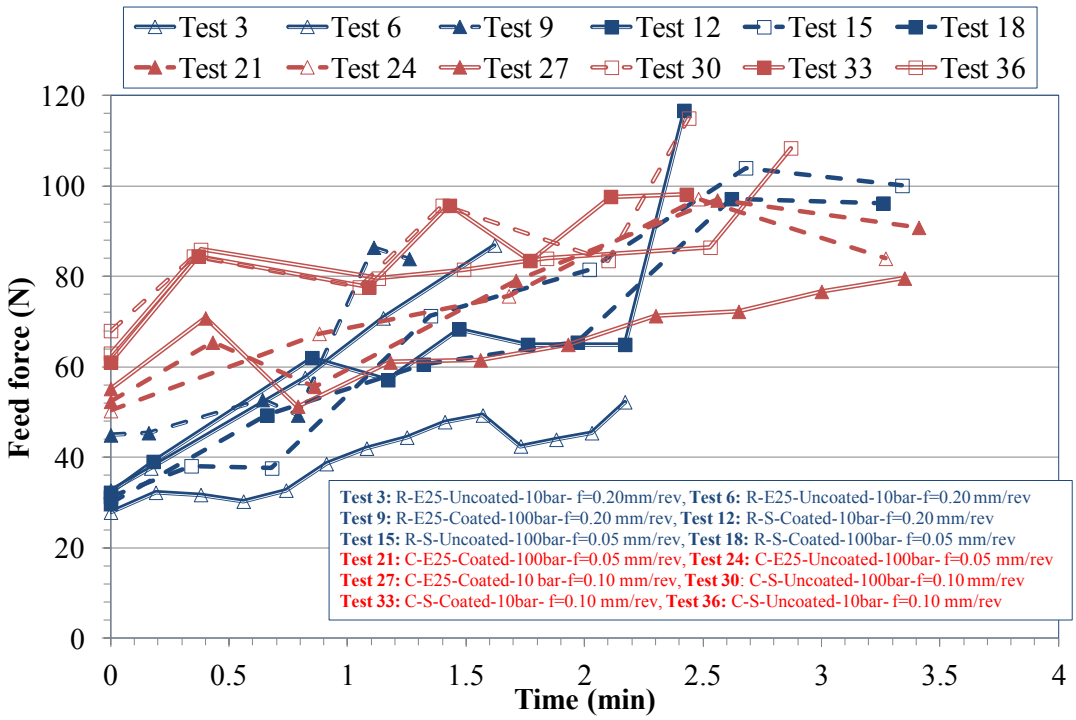

Figure 122: Feed force against machining time at a cutting speed of 450m/min

The main effect plots for feed force are detailed in Figure 123 with all factors being statistically significant at the 5% level according to the ANOVA shown in Table 48. Tool geometry, edge preparation and cutting speed had moderate PCR's of 19.65%, 22.34% and 20.57% respectively while the influence of cutting environment, surface condition and feed rate was limited, all with PCR's of < 6%. Contrary to cutting and thrust force components, C-

type inserts generated higher feed force compared to round tools. This was most likely due to the larger uncut chip thickness associated with the former tool geometry, which directly depends on the approach angle according to the Equation 5. The approach angles used for round and C-type inserts were 45º and 95º respectively. The effect of edge preparation, cutting environment and surface condition mirrored the trends seen with thrust force while the variations in feed force due to cutting speed was similar to observations made for cutting force. An analysis of the possible interactions revealed that none were statistically significant with regard to feed force despite the ANOVA showing a relatively high error level of 22.4%. This was likely due to either experimental error or the presence of interactions, which were not considered by chosen statistical experimental design.

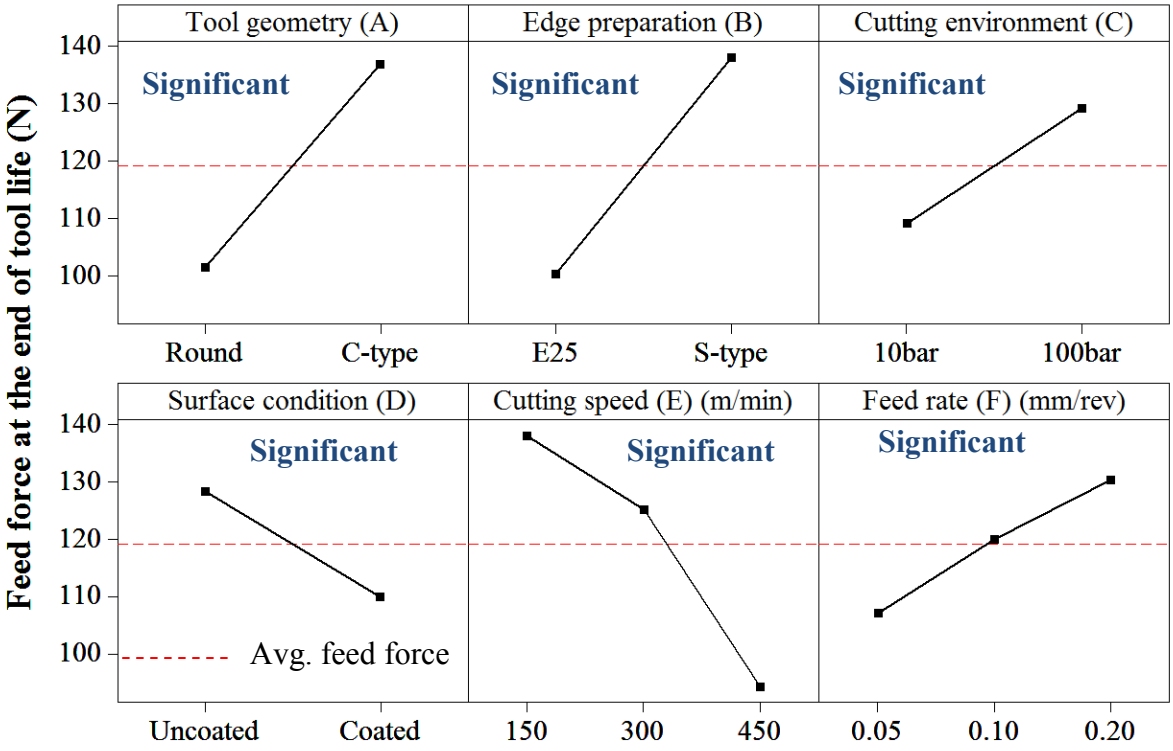

Figure 123: Main effects plots-means for feed force (Phase 1C)

Table 48: ANOVA table for feed force (Phase 1C)

Factors	DF	SS	MSS	F	P	PCR (%)
Tool geometry (A)	1	11365.7	11365.7	31.99	0.000*	19.65
Edge preparation (B)	1	12867.9	12867.9	36.22	0.000*	22.34
Cutting environment (C)	1	3606.4	3606.4	10.15	0.004*	5.80
Surface condition (D)	1	3080.30	3080.30	8.67	0.007*	4.86
Cutting speed (E)	2	12233.50	6116.8	17.22	0.000*	20.57
Feed rate (F)	2	3261.1	1630.5	4.59	0.019*	4.55
Error	27	9592.8	355.3			***22.23***
Total	35	56007.6	F_{table}=4.2, R-Sq(Adj)=77.77			

4.3.5 Confirmation experiment

Four confirmation experiments were conducted using preferred combination of factor levels in order to validate results for minimum surface roughness, cutting, thrust and feed forces respectively. A confirmation experiment for tool life however was not performed as the preferred variable levels for this response (A1 B1 C1 D1 E1 F1) already was present in L36 Taguchi orthogonal array (Test 4). The width of confidence interval (95%) for confirmation test results was calculated using the equation below [134];

Confidence Interval width (CIW)= $\sqrt{\mathrm{F}\alpha(1, ve)\mathrm{Ve}[(1/\mathrm{neff}) + (1/\mathrm{r})]}$ [6]

Where;

Fα=Tabulated F value for a 95% confidence interval

ve=Degrees of freedoms associated with error/residual

Ve=Mean sum of squares associated with error/residual

r=sample size for the confirmation experiment

$$\mathrm{neff} = \frac{\text{Total number of observations}}{1+[\text{Total degrees of freedoms associated with items used in estimating mean}]}$$

Table 49 details the measured values from the confirmation trials together with the associated confidence intervals/limits and estimated means for the respective response factors involving tool life, surface roughness, cutting, thrust and feed force components. Recorded values for tool life, cutting, thrust and feed force components and surface roughness were within the confidence interval/limits, which suggested that experiments were statistically acceptable with respect to the assessed responses.

Table 49: Comparison of calculated and recorded values from confirmation experiments

Responses	CIW	Estimated mean	Confidence interval /limits	Recorded value
Tool life	14.42min	30.79min (A1B1C1D1E1F1)	30.79± 14.42 =45.21min to 16.37min	44.8min (Test 4)
Surface roughness	1.22µm	[-0.16µm]=0 (A1B1C2D1E2F1)	0±1.22=1.22µm to [-1.22] 0µm	0.78µm
Cutting force	50.46N	96.66N (A2B1C1D2E3F1)	96.66±50.46 =147.12N to 46.20N	96.6N
Thrust force	159N	143.72N (A2B1C1D2E3F1)	143.72±159 =302.72N to [-15.28] 0N	281.2N
Feed force	43.18N	24.60N (A1B1C1D2E3F1)	24.60±43.18 =67.78N to [-18.58]0N	41.5N

4.4 Phase 1D: Evaluation of edge preparation and cutting speed on workpiece surface integrity

4.4.1 Surface roughness and topography

In general, surface roughness varies between 0.67 and 1.56µm Ra for the conditions tested, see Figure 124. When employing inserts with an E25 edge preparation, lower workpiece surface roughness was obtained with tools in the worn condition due to the formation of a wiper flat at the nose radius. Conversely, surface roughness increased (approximately 30 – 40%) with increasing wear of the S-type edge inserts, most likely due to the irregular shaped wear scar which developed on the chamfer location; see Figure 125. The corresponding 3D topography maps of machined surfaces produced with new and worn tools in Tests 1 and 3 (E25) are shown in Figures 126 and 127 respectively. In both cases, the reduction in Sa value was apparent with increasing tool wear.

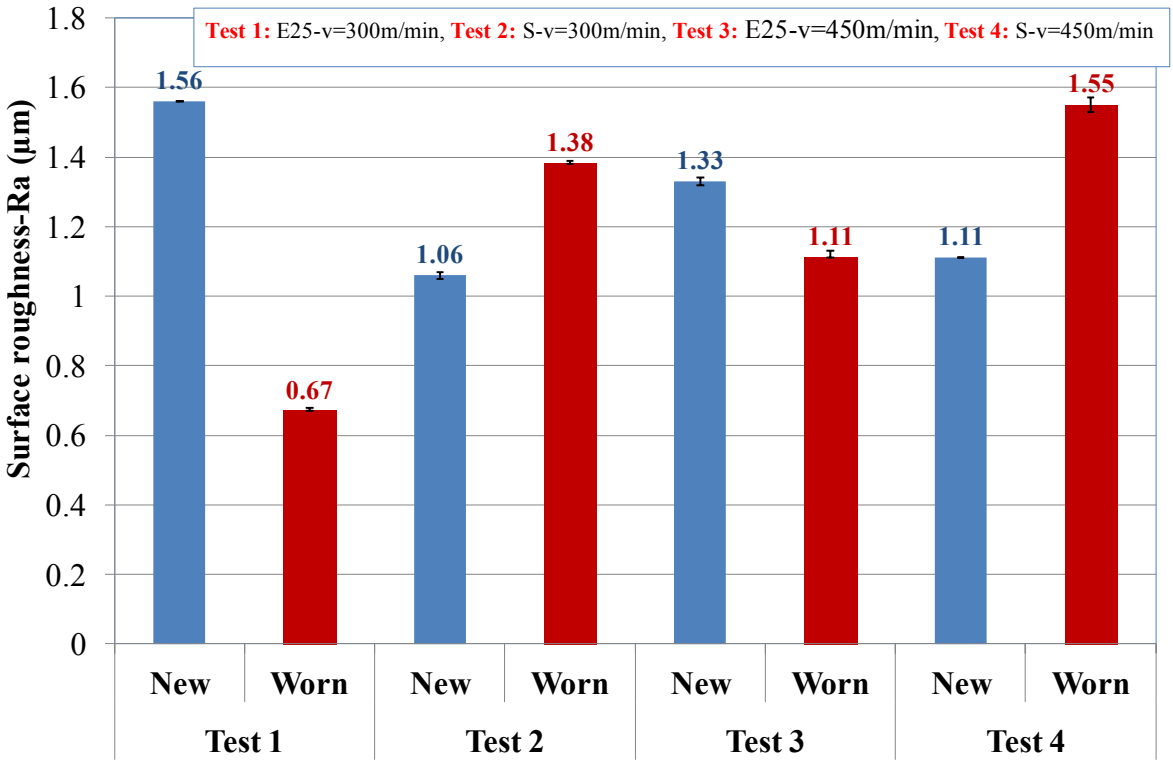

Figure 124: Surface roughness at each test with new and worn tools

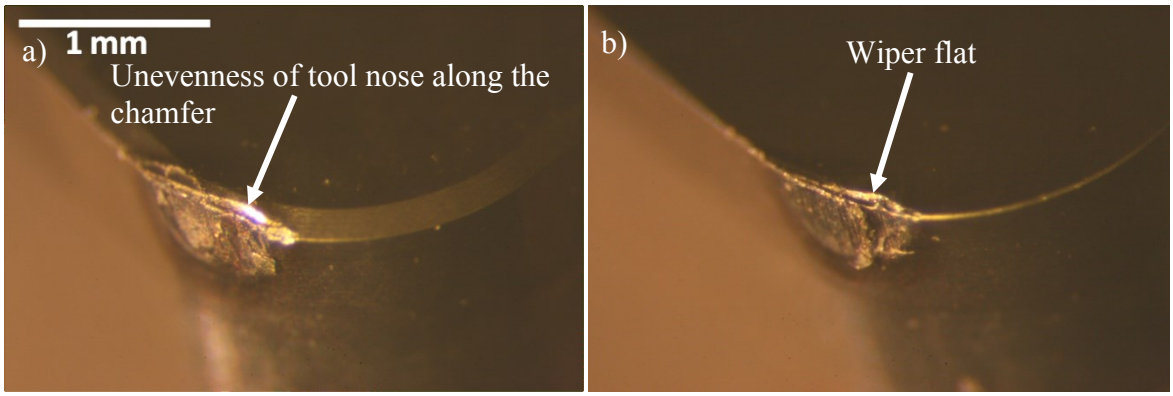

Figure 125: Wear scar micrographs of uncoated C-type inserts, (a) S-type and (b) E25

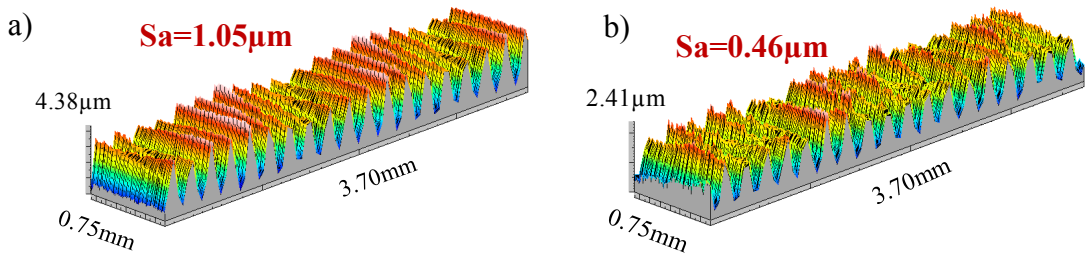

Figure 126: Workpiece surface topography in Test 1 following turning with a) new and b) worn inserts

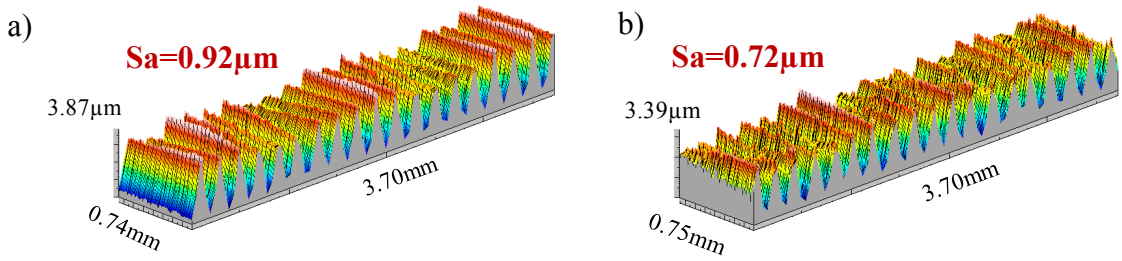

Figure 127: Workpiece surface topography in Test 3 following turning with (a) new and (b) worn inserts

Main effects plots both for both new and worn tools are shown in Figures 128 and 129 respectively. None of the variable factors were found to be statistically significant with regard to surface roughness over the range of parameters tested irrespective of tool condition, resulting in an error level of 100% based on the statistical analysis, see Table 50. This was probably due to the surface roughness being influenced by feed rate and tool nose radius, which were held constant in the current phase of the experiments. The full ANOVA tables/calculations are presented in Table C1 and C2 in Appendix C.

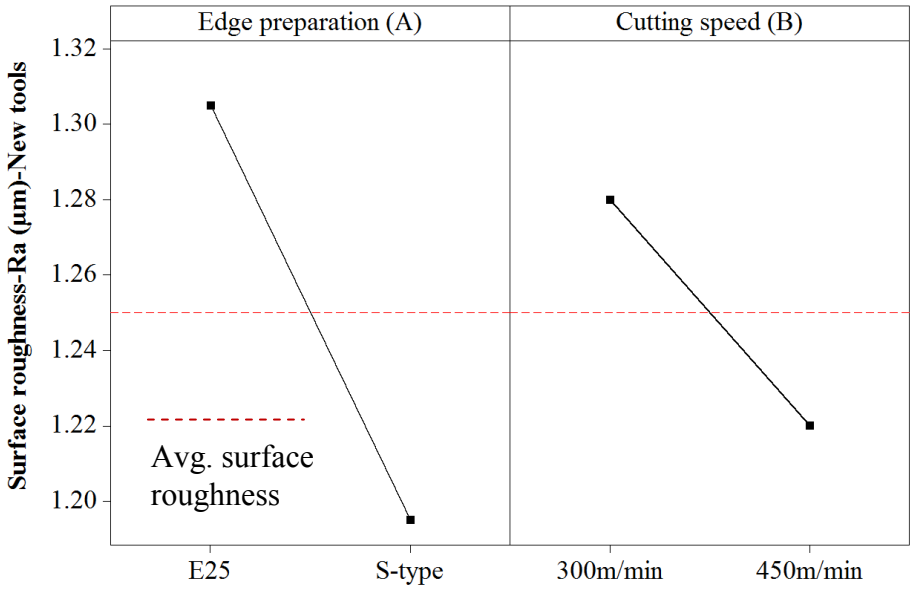

Figure 128: Main effects plots-means for surface roughness with new tools (Phase 1D)

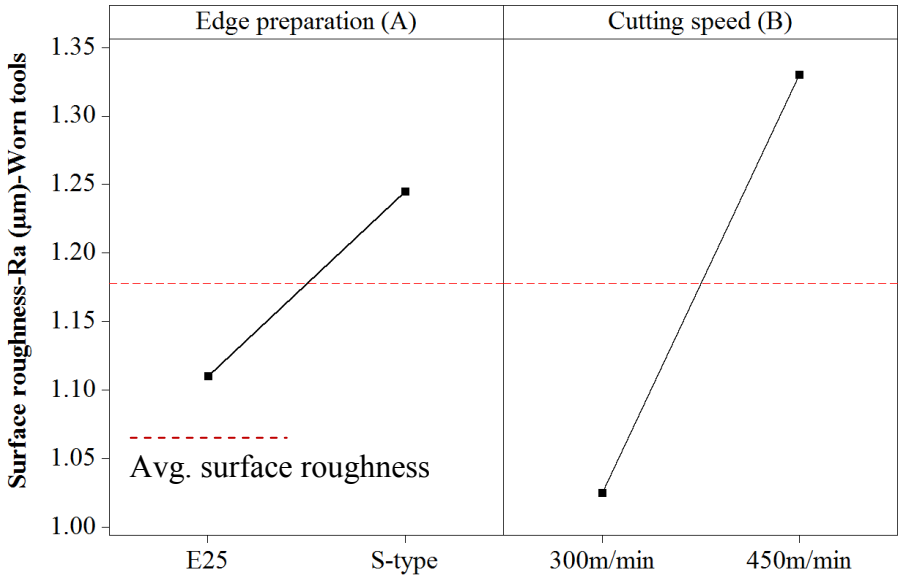

Figure 129: Main effects plots-means for surface roughness with worn tools (Phase 1D)

Table 50: P-values and PCR's for surface roughness with new and worn tools (Phase 1D)

Factors	DF	New		Worn	
		P	PCR (%)	P	PCR (%)
Edge preparation (A)	1	0.795	0	0.853	0
Cutting speed (B)	1	0.886	0	0.690	0
Error	1		***100***		***100***
Total	3	R-Sq (Adj)=0		R-Sq (Adj)=0	

4.4.2 Cutting forces

Cutting force was generally less than 200N irrespective of edge preparation, cutting speed and tool condition; see Figure 130 while there were no clear trends describing the influence of the variable factor levels, cutting force generally decreased with increasing cutting speed, with the exception of worn inserts at 450m/min. This was supported by the main effects plots detailed in Figure 131 for new inserts, with corresponding ANOVA calculations showing cutting speed to be a statistically significant factor having a PCR of 71.53%, see Table 51 (full ANOVA tables for all 3 force components are shown in Tables C3-C8 of Appendix C). In contrast, neither edge preparation nor cutting speed was found to have a significant effect on cutting force when using worn tools, see Figure 132 and Table 51, with relatively low PCR values of ~30% and 11% respectively. This was most likely due to the fact that the level of tool wear suppressed any edge preparation and cutting speed effects and showing corresponding high error level of 59.13%, based on statistical analysis.

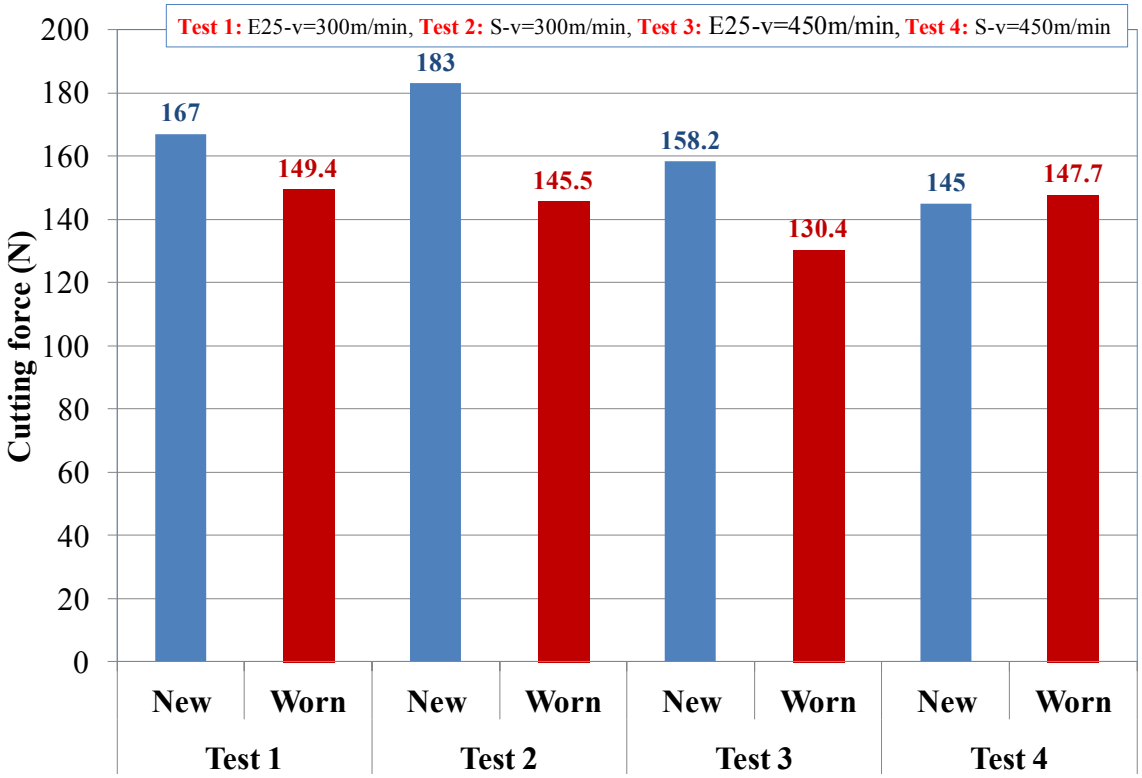

Figure 130: Cutting force at each test with new and worn tools

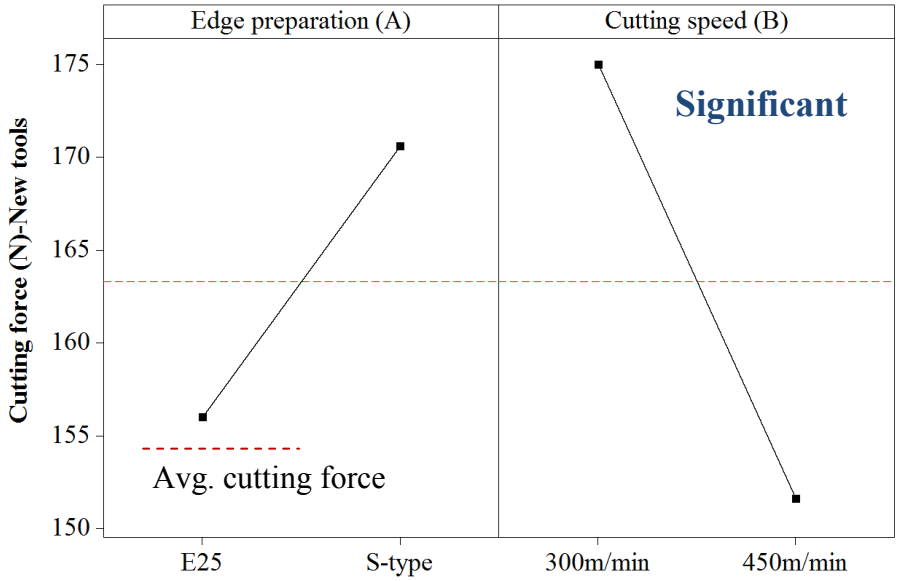

Figure 131: Main effects plots-means for cutting force with new tools (Phase 1D)

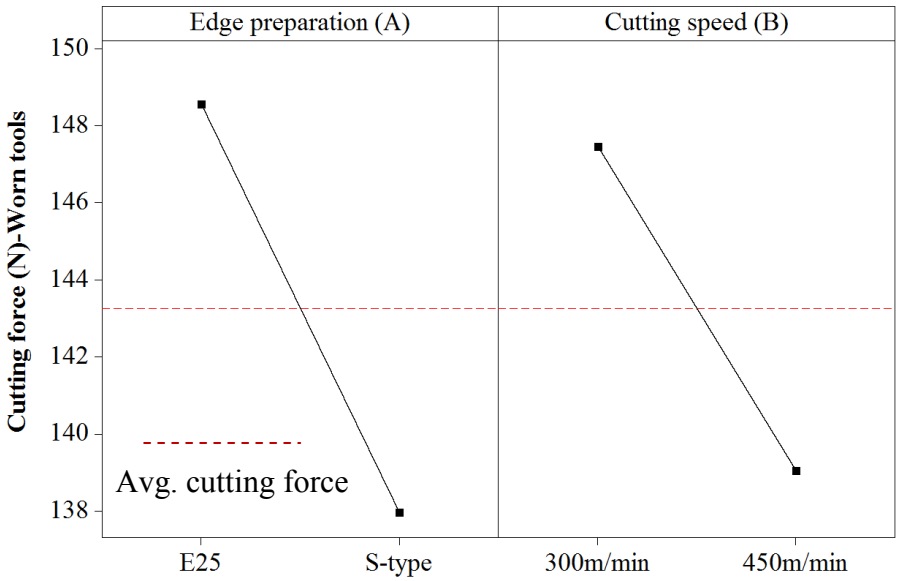

Figure 132: Main effects plots-means for cutting force with worn tools (Phase 1D)

Table 51: P-value and PCR's for cutting force with new and worn tools (Phase 1D)

Factors	DF	New		Worn	
		P	PCR (%)	P	PCR (%)
Edge preparation (A)	1	0.061	27.69	0.359	29.61
Cutting speed (B)	1	0.038*	71.53	0.429	11.26
Error	1		***0.78***		***59.13***
Total	3				

Figure 133 shows the thrust force recorded in each test using both with new and worn tools. In the case of new inserts, an increase in thrust force by 15-45 N was observed when employing S-type edge preparation (due to the T-land geometry which increased the resistance of chip flow over the rake face) compared to E25, however a marginal reduction (~5-30N) was recorded at higher cutting speeds (due to the increase in the shear angle and reduction in the tool-chip contact area). A significant rise (~3 to 4 times) in thrust force was obtained when utilising worn tools. This was attributed to reduction in the active approach angle due to the increase in tool nose radius (as a result of tool wear) and smaller depth of cut, explained previously in Section 4.3.4 and also due to the friction between tool and workpiece. The finding was in line with the results reported by Sharman et al. [44] who recorded ~10 times higher thrust force when turning Inconel 718 with worn carbide inserts compared to the new ones, at a cutting speed of 80m/min, feed rate of 0.15mm/rev and depth of cut of 0.25mm.

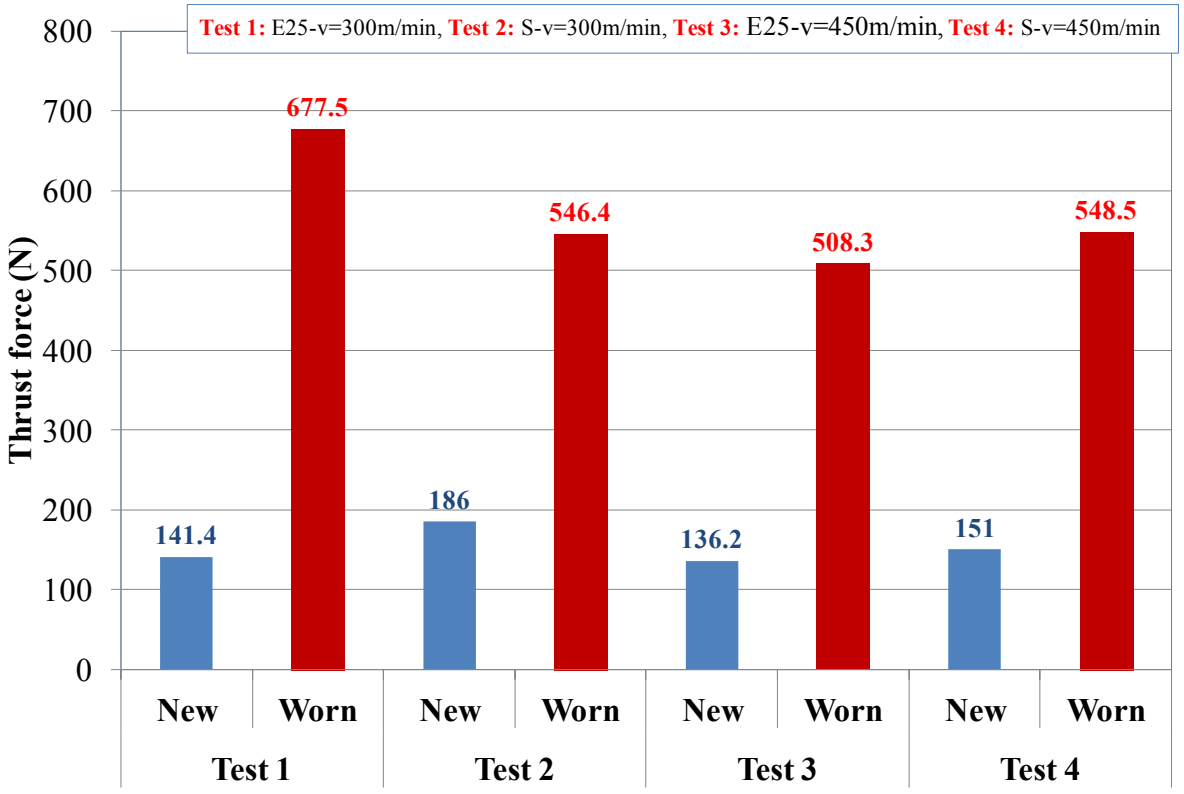

Figure 133: Thrust force at each test with new and worn tools

Main effects plots for thrust force with new and worn inserts are shown in Figures 134 and 135 respectively. In terms of ANOVA calculations, none of the factors were statistically significant irrespective of insert condition, although both edge preparation and cutting speed showed PCR's of ~30% when machining with worn inserts (Table 52). This was likely due to the cutting edge preparation (S-type and E25) employed in the current trials where thrust component acted parallel to the edge cross section and therefore remains unaffected. This was in agreement with the results reported by Pawade et al. [103] when employing chamfered only and chamfered plus honed PCBN tools in turning of Inconel 718. A schematic illustration of the turning operation using a chamfered edge cutting which highlighted the thrust and feed force components on the undeformed chip cross section was shown previously in Figure 45 in the literature review section.

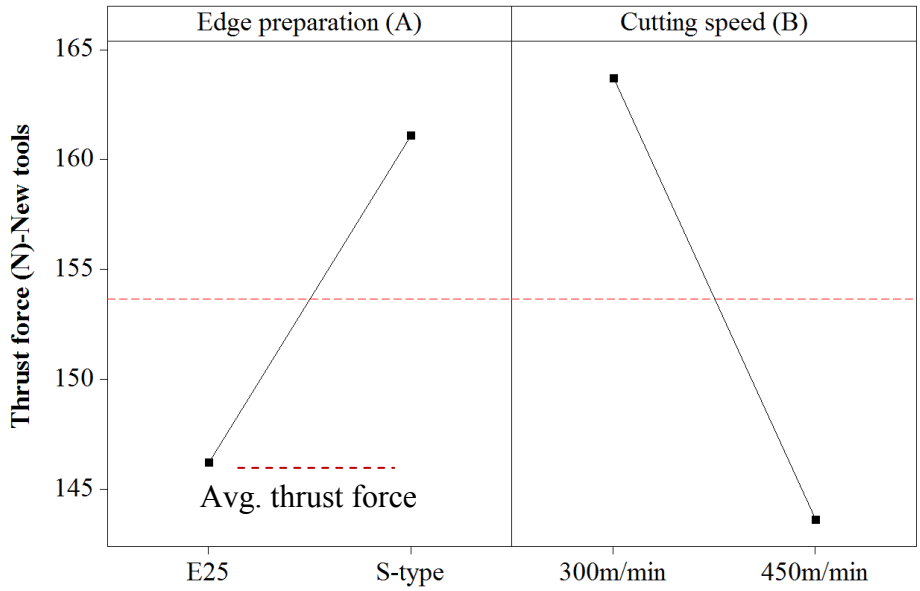

Figure 134: Main effects plots-means for thrust force with new tools (Phase 1D)

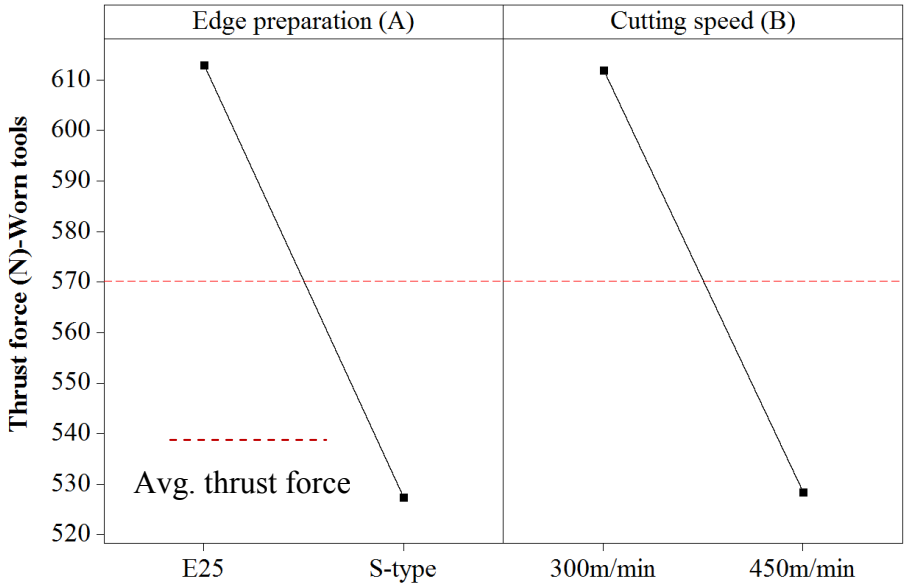

Figure 135: Main effects plots-means for thrust force with worn tools (Phase 1D)

Table 52: P-value and PCR's for thrust force with new and worn tools (Phase 1D)

Factors	**DF**	**New**		**Worn**	
		P	**PCR (%)**	**P**	**PCR (%)**
Edge preparation (A)	1	0.704	0	0.311	32.16
Cutting speed (B)	1	0.621	0	0.317	30
Error	1		***100***		***37.84***
Total	3	R-Sq(Adj)=0		R-Sq(Adj)=62.16	

Similar to cutting forces, a decrease in feed force was observed when cutting speed was increased from 300m/min to 450m/min using new inserts as shown in Figure 136. Conversely trends were reversed when utilising worn inserts, with feed force increasing by ~25-100N when operating at 450m/min.

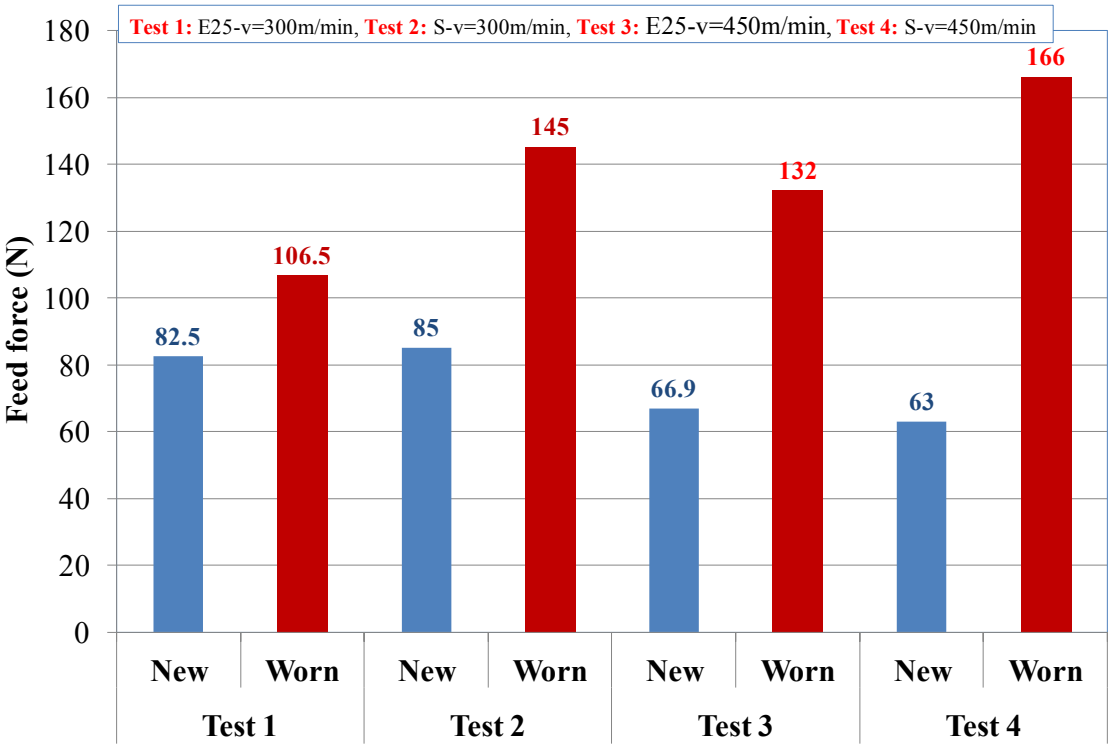

Figure 136: Feed force at each test with new and worn tools

Figures 137 and 138 detail the main effects plots for new and worn inserts respectively. Results from the ANOVA showed that the sole factor having a significant effect on feed force was cutting speed when employing new inserts, with an overwhelming PCR of ~97%. However, none of the factors were statistically significant relative to feed force using worn tools with 100% error level as observed for cutting force, see Table 53.

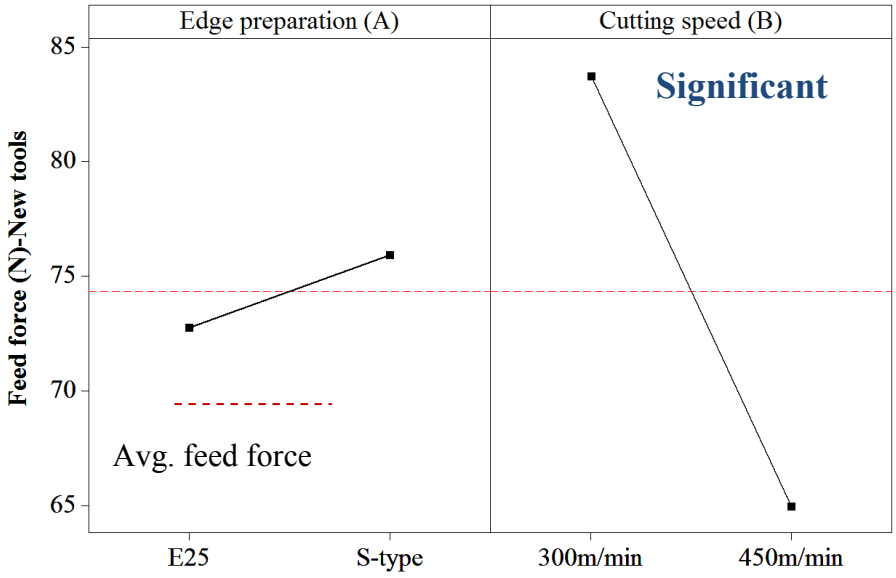

Figure 137: Main effects plots-means for feed force with new tools (Phase 1D)

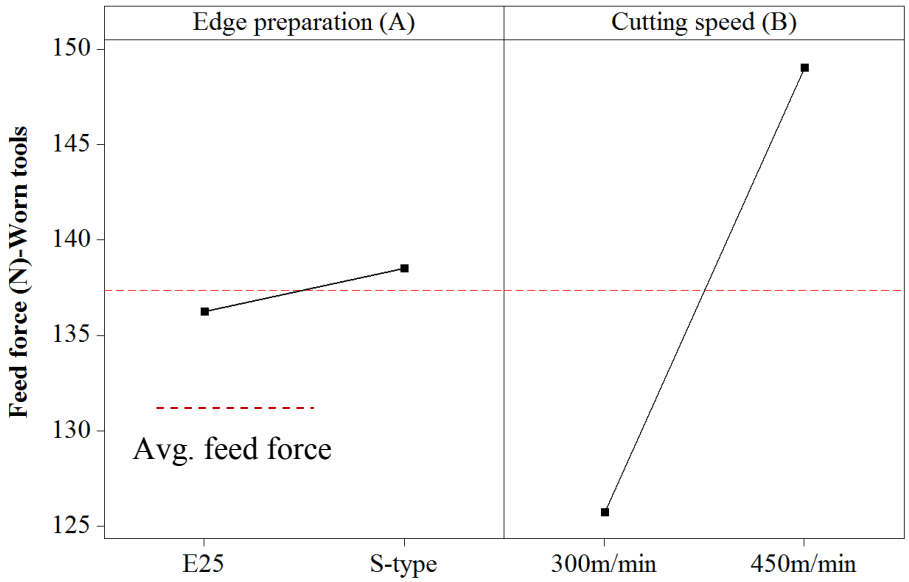

Figure 138: Main effects plots-means for feed force with worn tools (Phase 1D)

Table 53: P-value and PCR's for feed force with new and worn tools (Phase 1D)

Factors	DF	New		Worn	
		P	PCR (%)	P	PCR (%)
Edge preparation (A)	1	0.137	2.67	0.961	0
Cutting speed (B)	1	0.024*	96.9	0.637	0
Error	1		***0.43***		***100***
Total	3	R-Sq(Adj)=99.57		R-Sq(Adj)=0	

4.4.3 Workpiece surface damage

Feed marks were prevalent in all tests with no significant difference observed for surfaces produced with new inserts, irrespective of edge configuration and cutting speed level. Material side flow along the feed marks however was prevalent on the workpiece samples machined with worn S-type edge geometry, which increased the surface roughness as detailed previously in Section 4.4.1, see Figure C1 in Appendix C. In addition, grooves, microcracks of size ~7-15 µm and smeared material was apparent when machining with worn tools as shown in Figures 139 and 140 respectively. Pawade et al. [103] also recorded similar type of surface damage together with metal debris, re-deposited material and cracking of carbide particles in high speed (150 and 300 m/min) turning of Inconel 718 with PCBN tools when cutting dry. The latter surface flaws however, were not observed in the current work, most likely due to the use of cutting fluid, which in turn had reduced the friction and increased the heat removal from the surface.

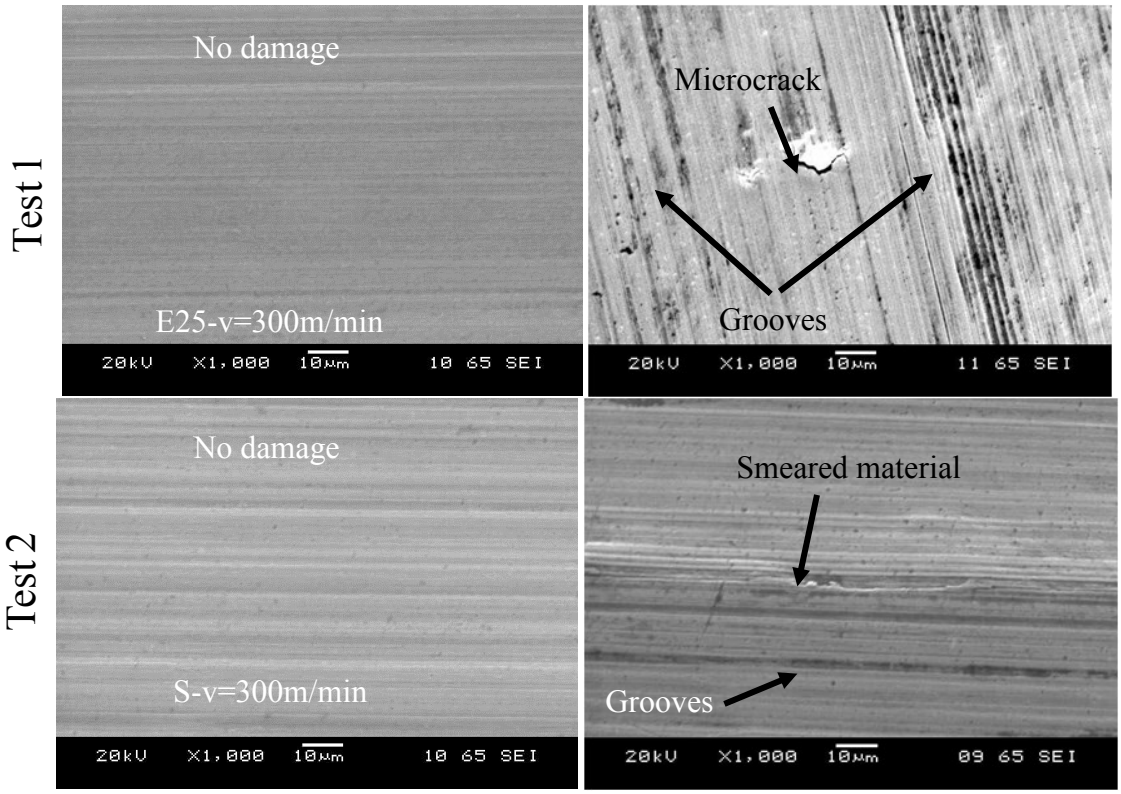

a) New b) Worn

Figure 139: Workpiece surfaces of Tests 1 and 2 following machining with a) new and b) worn inserts

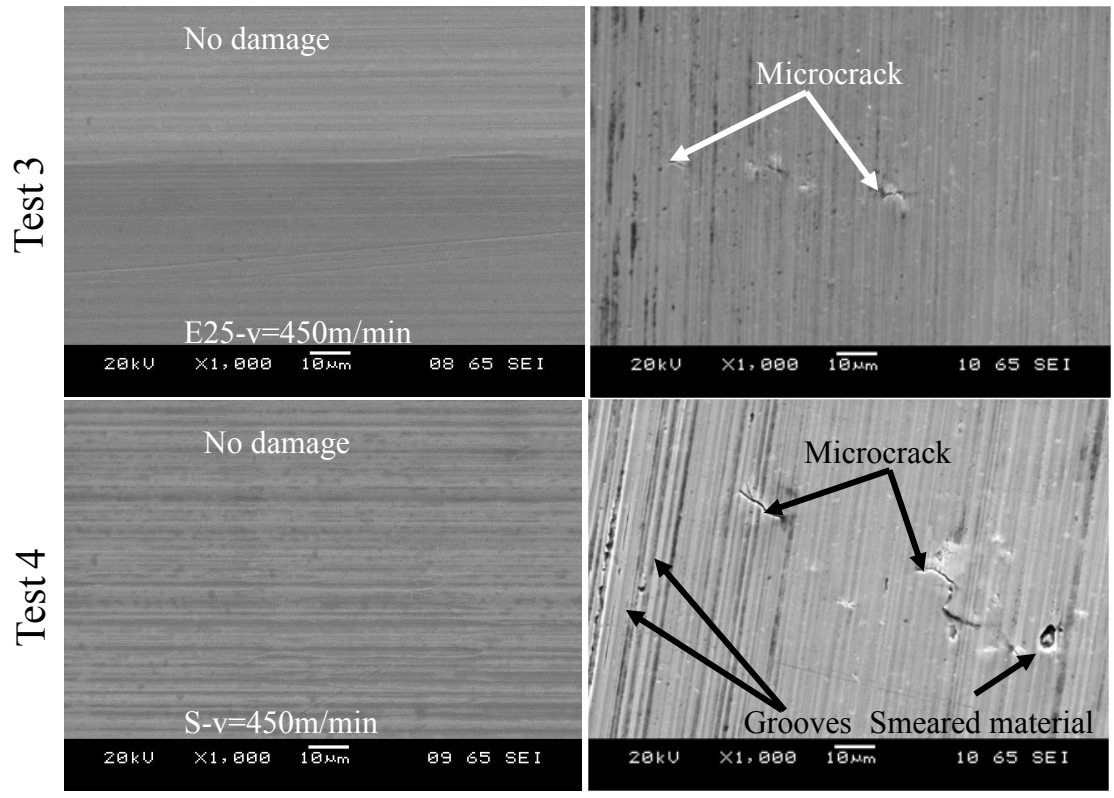

a) New b) Worn

Figure 140: Workpiece surfaces of Tests 3 and 4 following machining with a) new and a) worn inserts

4.4.4 Microhardness

Microhardness depth profiles measured parallel to the feed direction showed no significant strain hardening near the machined surface when utilising new tools in any of the trials, see Figure 141. Conversely, Figure 142 shows an increase in microhardness of up to ~100$HK_{0.025}$ above the bulk hardness and extending to a depth of 150µm was recorded following machining with worn inserts. The corresponding microhardness depth profiles measured perpendicular to the feed (radial/cutting speed direction) for samples machined with new and worn tools are detailed in Figures 143 and 144 respectively. With the former, an increase in hardness of ~50$HK_{0.025}$ to a depth of 50µm was observed in all cases. Workpiece hardening in the latter however was up to ~25% (612.7$HK_{0.025}$) above the bulk hardness and which prevailed to 500µm beneath the machined surface. The higher hardness levels (~30$HK_{0.025}$) extending to a greater depth (350µm) seen in the radial direction compared to the feed direction were attributed to the higher cutting speeds employed in the current trials. The drop in the microhardness level observed in the near surface region when cutting with worn tools was possibly due to some strain recovery as a result of high temperatures. Sharman et al. [145] also recorded a drop in microhardness level near the machined surface when turning Inconel 718 with worn (250µm flank wear) carbide tools at Vc of 40-120 m/min, feed rates of 0.15-0.25 mm/rev and employing constant depth of cut of 0.25mm in the presence of coolant.

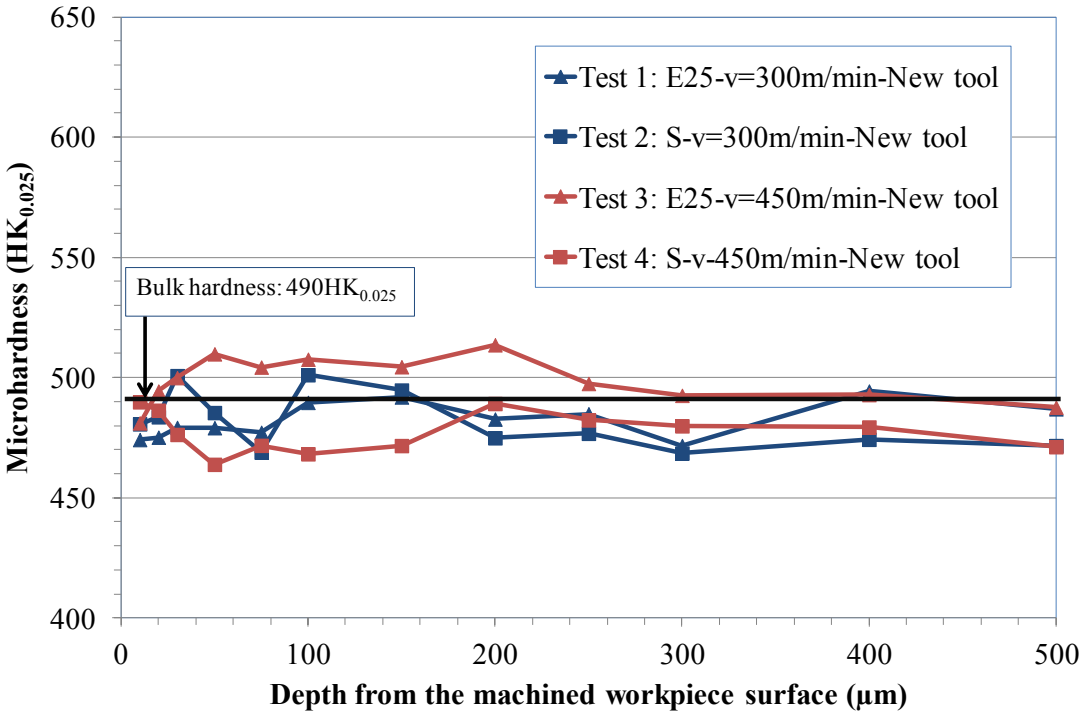

Figure 141: Workpiece microhardness depth profiles for new tools in a direction parallel to feed

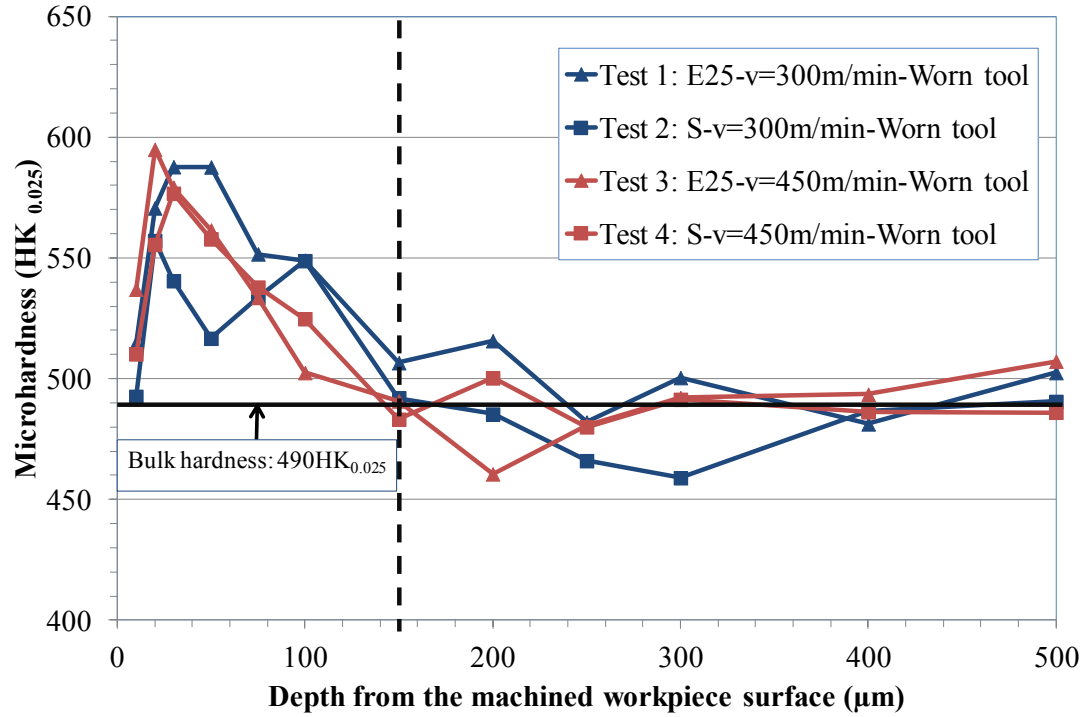

Figure 142: Workpiece microhardness depth profiles for worn tools in a direction parallel to feed

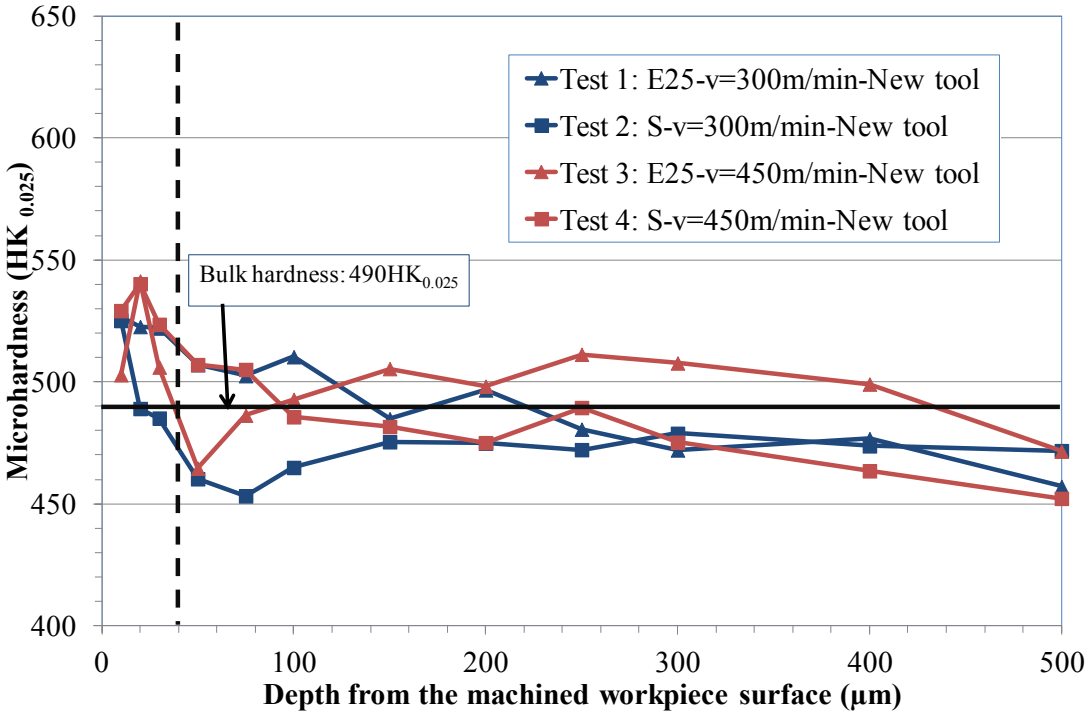

Figure 143: Workpiece microhardness depth profiles for new tools in a direction perpendicular to feed

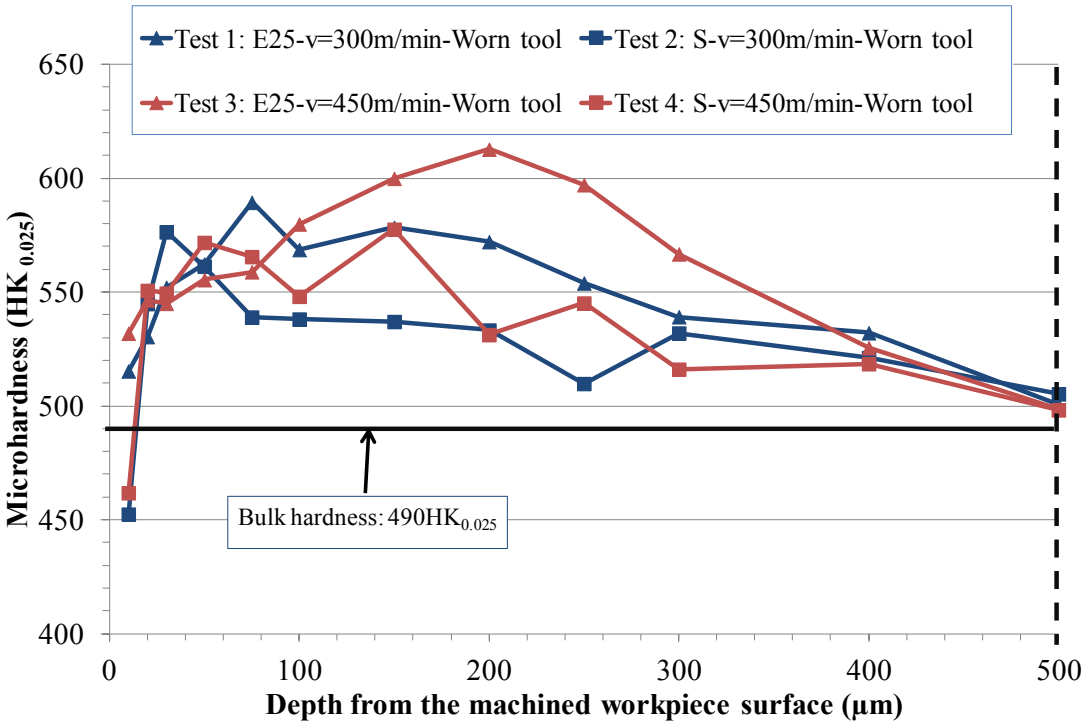

Figure 144: Workpiece microhardness depth profiles for worn tools in a direction perpendicular to feed

4.4.5 Microstructure

Figures 145-148 show cross-sectional optical micrographs of the machined workpiece subsurface both parallel and perpendicular to the feed direction in all tests. Since higher microhardness levels were observed perpendicular to the feed, machined workpiece subs-surfaces were examined in this direction under SEM at the cutting speed of 450m/min both with new and worn tools (Tests 3 and 4). No signs of microstructural damage, white layer formation or deformation of the workpiece grain boundaries were evident in any of the samples analysed, irrespective of tool condition, see Figure 149. Additionally, other common microstructural damage modes such as surface tearing, carbide cracking and material pull out when turning Inconel 718 using carbide [71, 145, 157] and ceramic [21, 95-96] cutting tools, however were not observed in the current work.

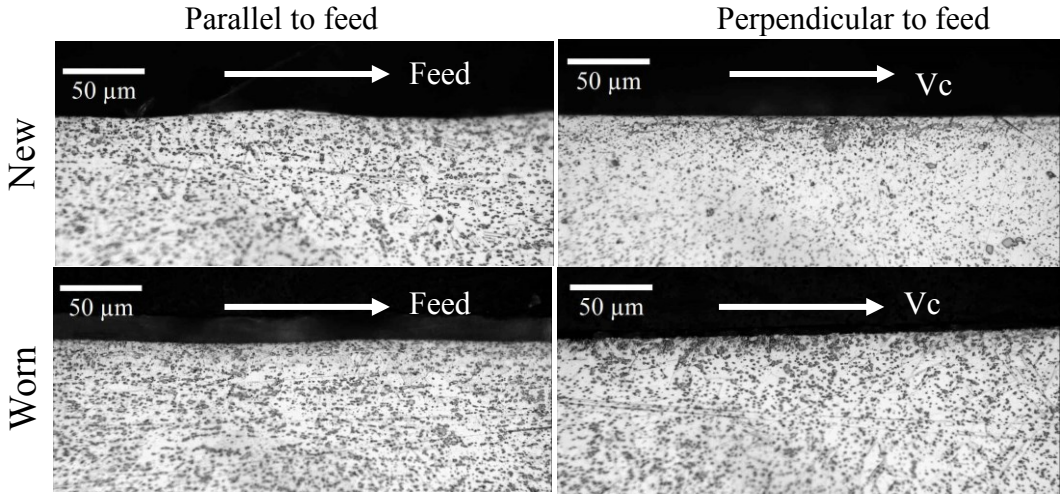

Figure 145: Cross sectional optical micrographs of machined workpiece sub-surface of Test 1 following machining with new and worn tools

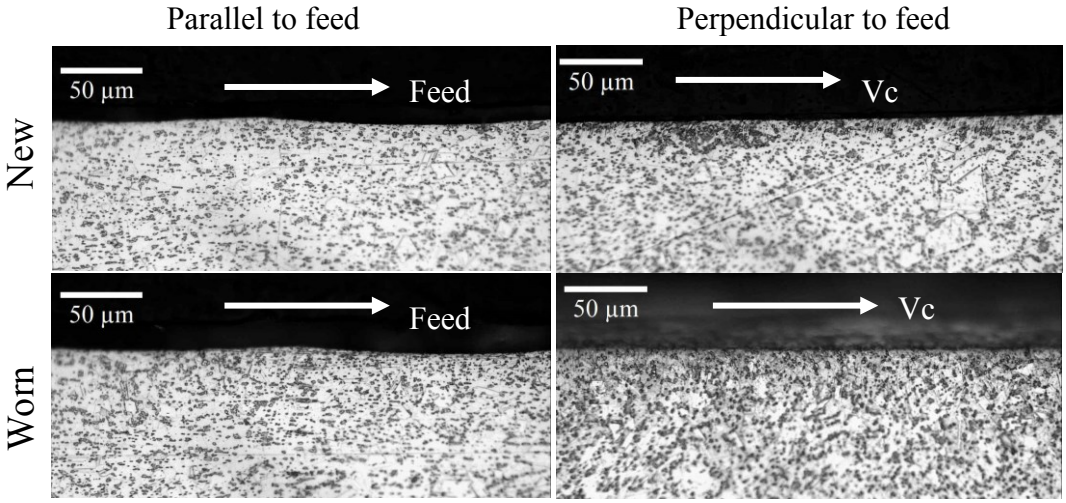

Figure 146: Cross sectional optical micrographs of machined workpiece sub-surface of Test 2 following machining with new and worn tools

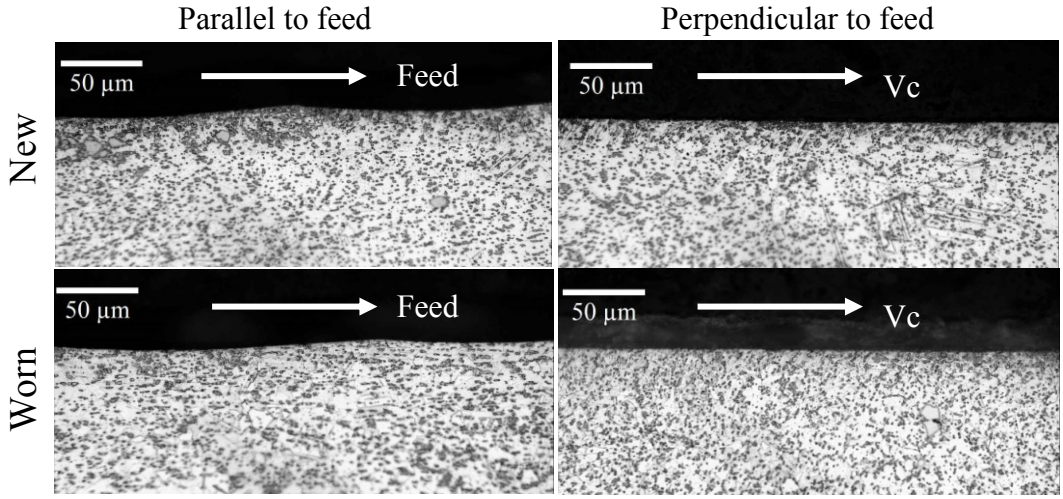

Figure 147: Cross sectional optical micrographs of machined workpiece sub-surface of Test 3 following machining with new and worn inserts

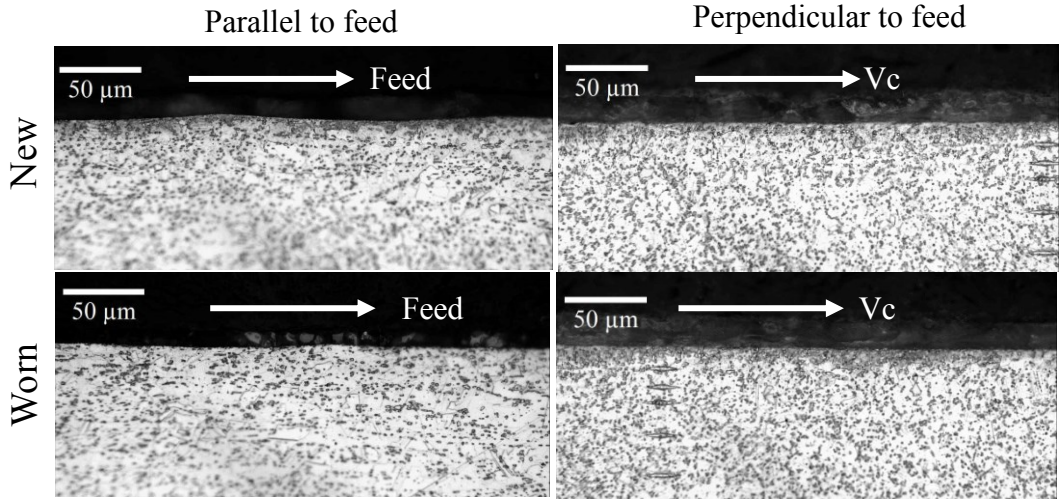

Figure 148: Cross sectional optical micrographs of machined workpiece sub-surface of Test 4 following machining with new and worn inserts

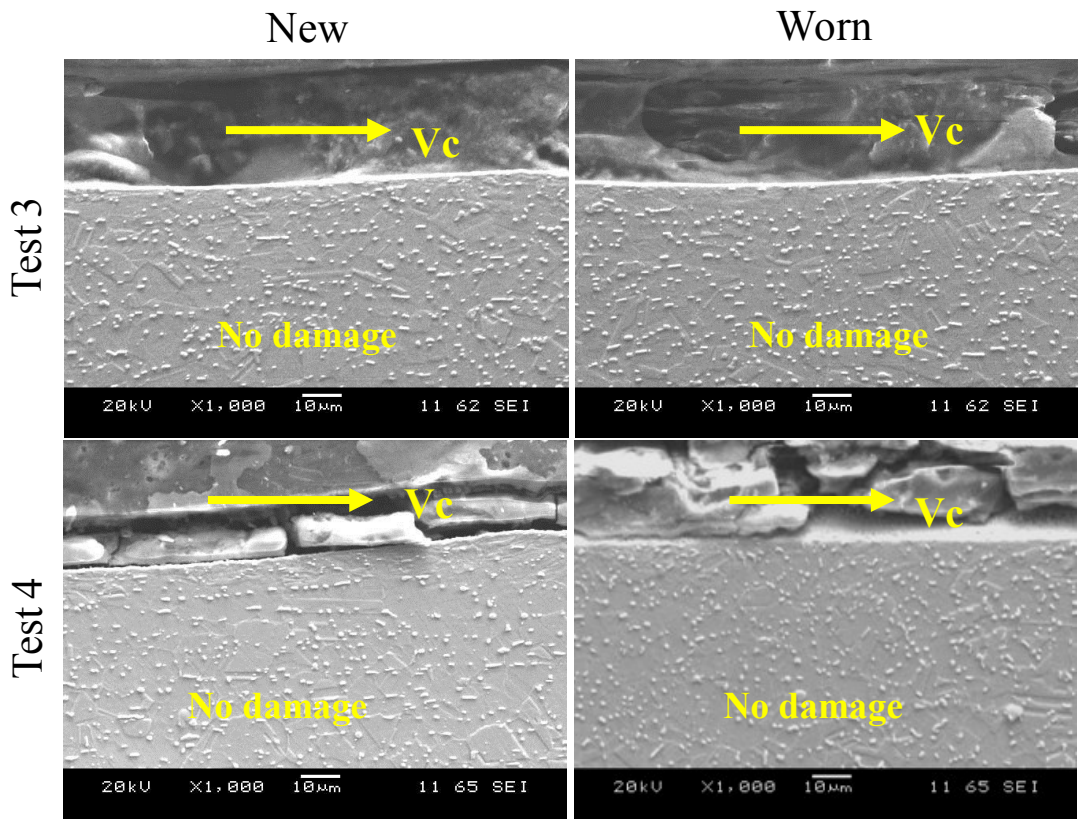

Figure 149: Cross sectional SEM images of machined workpiece sub-surface of Tests 3 and 4 in a direction perpendicular to feed

4.5 Phase 2A: Effect of cutting environment, cutting speed and feed rate on tool wear/life, surface roughness and cutting forces

4.5.1 Tool wear/life

Tool life ranged between 2.7 and 3.5 min when turning at a cutting speed of 300m/min, however this dropped to ~1min as Vc was increased to 450m/min, irrespective of the other parameters, see Figure 150. Results from Test 9 (replication of Test 1) were found to be within ~6% of Test 1. In terms of productivity, a cutting speed of 300m/min was preferred and maximum material of ~36.4cm^3 was removed in Test 7 (low speed, high feed rate and high pressure); see Figure D1 in Appendix D.

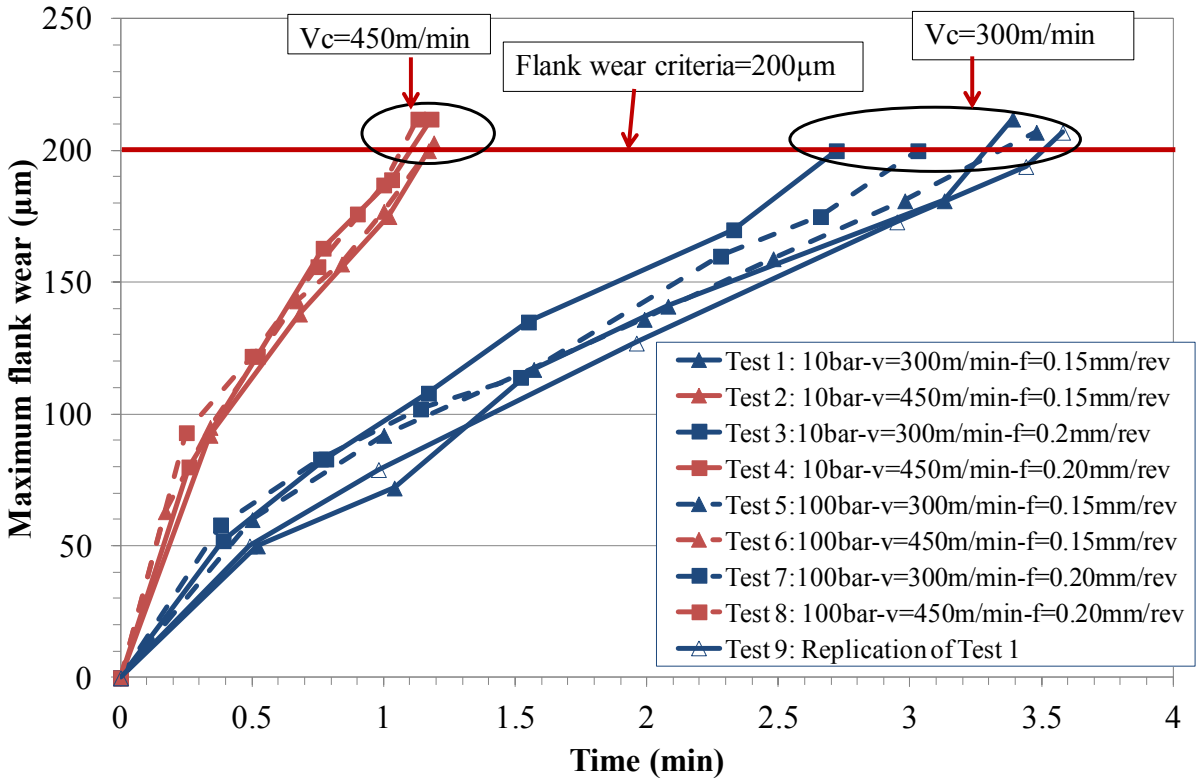

Figure 150: Evolution of flank wear against machining time

Figure 151 shows the main effects plots for tool life. A reduction in tool life was evident as cutting speed increased from 300m/min to 450m/min most likely due to larger temperatures and stresses. The factor was found to be statistically significant with an overwhelming PCR of ~94.80% while the influence of feed rate and cutting environment was negligible as shown in Table 54. Tool wear progression for Tests 1 (low cutting speed/feed rate/cutting fluid pressure) and 8 (high cutting speed/feed rate/cutting fluid pressure) are shown in Figure 152 while SEM micrographs of wear scars at the end of tool life from Tests 1, 3, 4 and 8 conducted at Vc of 300 and 450 m/min respectively, are detailed in Figure 153. The SEM micrographs at the end of tool life for the remaining tests (Tests 2, 5, 6 and 7) together with EDX analysis of Test 1 are shown in Figures D2 and D3 in Appendix D. Detection of Ni, Cr and Fe elements from the Inconel 718 on the insert surface confirmed the presence of workpiece material adhesion, as shown in Table D1 in Appendix D. No signs of chipping, notching or fracture were detected over the range of parameters evaluated with crater and flank wear observed as the dominant wear modes. Workpiece material adhesion was prevalent in all tests although abrasion was more apparent when operating at the higher Vc of 450m/min.

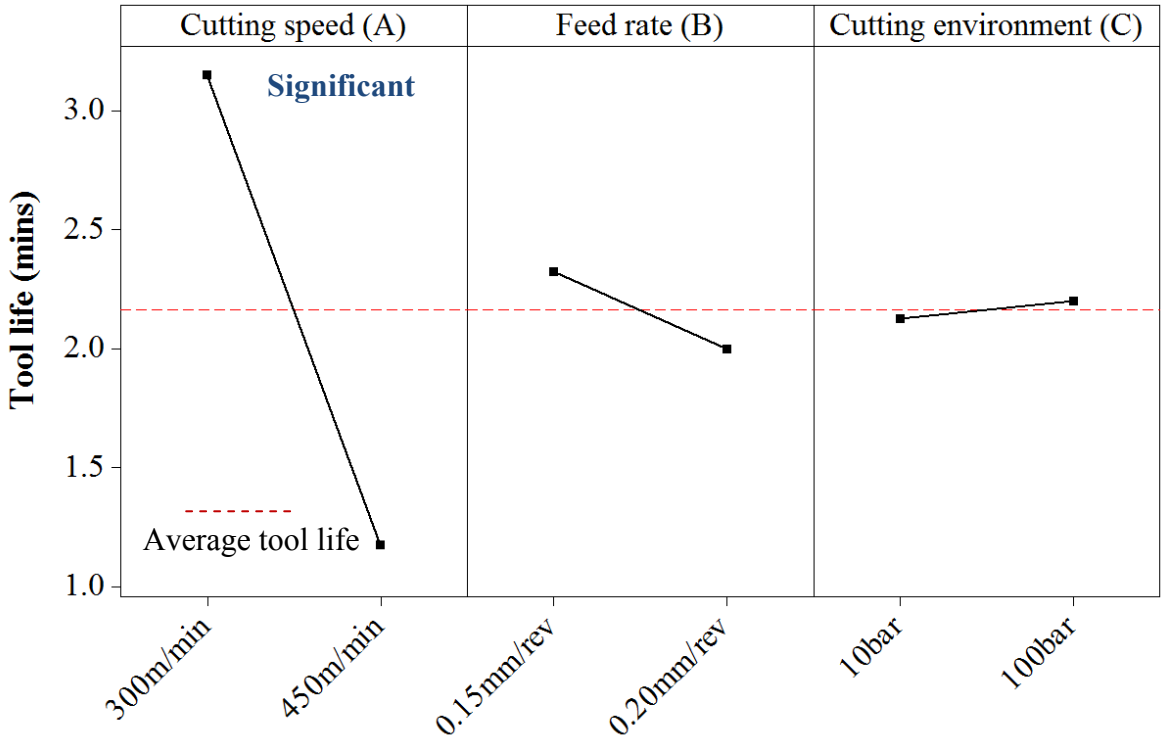

Figure 151: Main effects plots-means for tool life (Phase 2A)

Table 54: ANOVA table for tool life (Phase 2A)

Factors	DF	SS	MSS	F	P	PCR (%)
Cutting speed (A)	1	7.8012	7.8012	693.44	0.024*	94.78
Feed rate (B)	1	0.2112	0.2112	18.78	0.144	2.43
Cutting environment (C)	1	0.0112	0.0112	1.00	0.500	0.00
A*B	1	0.1512	0.1512	13.44	0.170	1.70
A*C	1	0.0312	0.0312	2.78	0.344	0.24
B*C	1	0.0012	0.0012	0.11	0.795	0.00
Error	1	0.0113	0.0113			***0.96***
Total	7	8.2187	R-Sq (Adj)=99.04			

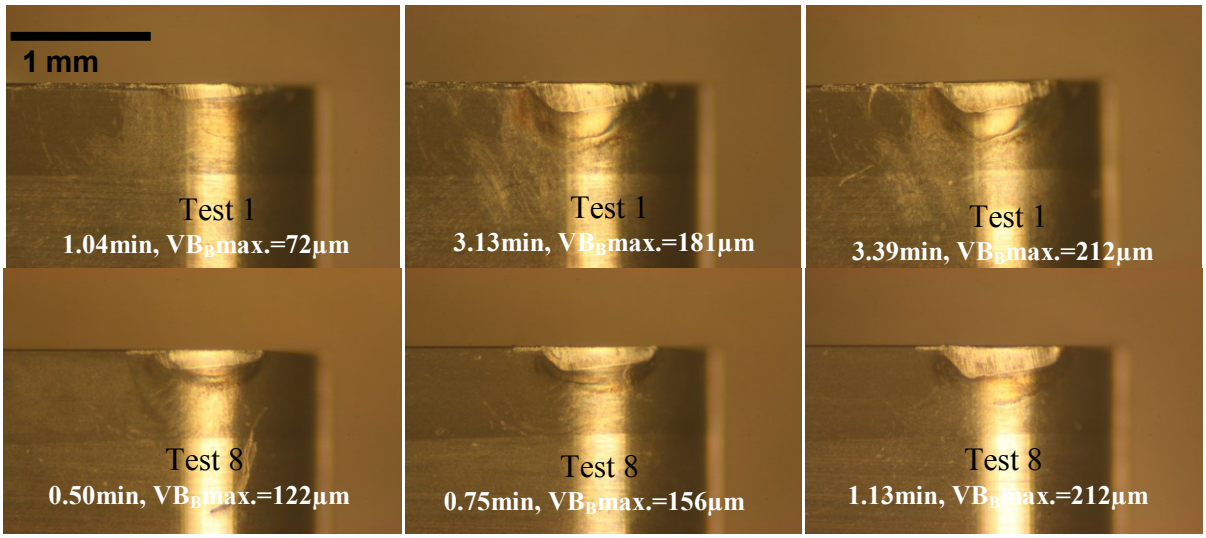

Figure 152: Wear progression of inserts in Tests 1 and 8

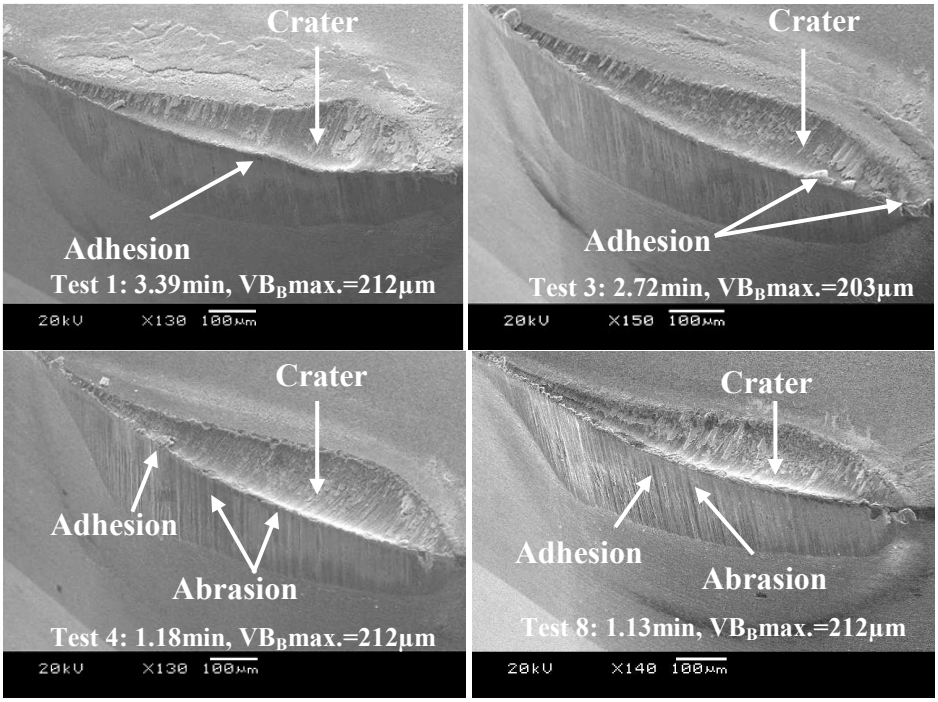

Figure 153: SEM micrographs of inserts wear scars at the end of tool life of Tests 1, 3, 4 and 8

A comparison of tool lives when machining the MHI and SI materials can be made by comparing the Test 23 of Phase 1C (Section 4.3.1) and Test 7 of the current phase. The test was performed at a cutting speed of 300m/min, feed rate of 0.20mm/rev and employing a cutting fluid pressure of 100bar. Despite having the same hardness (44-46HRC), tool life when turning the MHI material (4.5min) was ~45% higher compared to the SI product (3.1min) as shown in Figure 154 which suggests the former was easier to machine. Furthermore, the cutting and thrust forces were ~70% and 60% higher respectively with the SI supplied material, see Figure 155 which may indicate a higher shear strength/ductility level.

The discrepancy was most likely due to greater prevalence of γ″ precipitates at the grain boundaries of the SI material which forms the main strengthening mechanism in Inconel 718 alloy [18]. Furthermore, it is well documented that excessive formation of the δ-precipitates, found only in MHI workpiece microstructure cause degradation in properties [18]. Previous work involving the turning of Inconel 718 using uncoated carbide tools reported that notch wear was significantly higher for workpieces having a coarse grain size [23, 158-160].

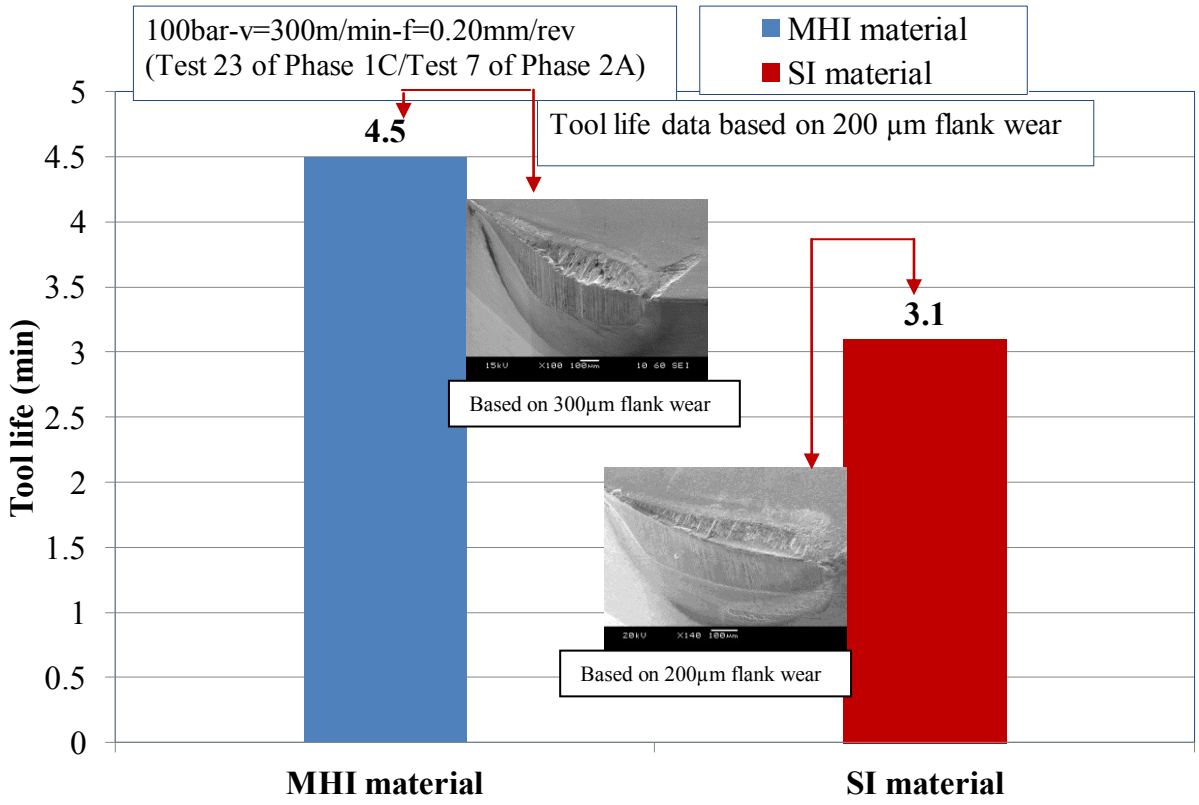

Figure 154: Tool life data for MHI and SI materials along with wear scar micrographs

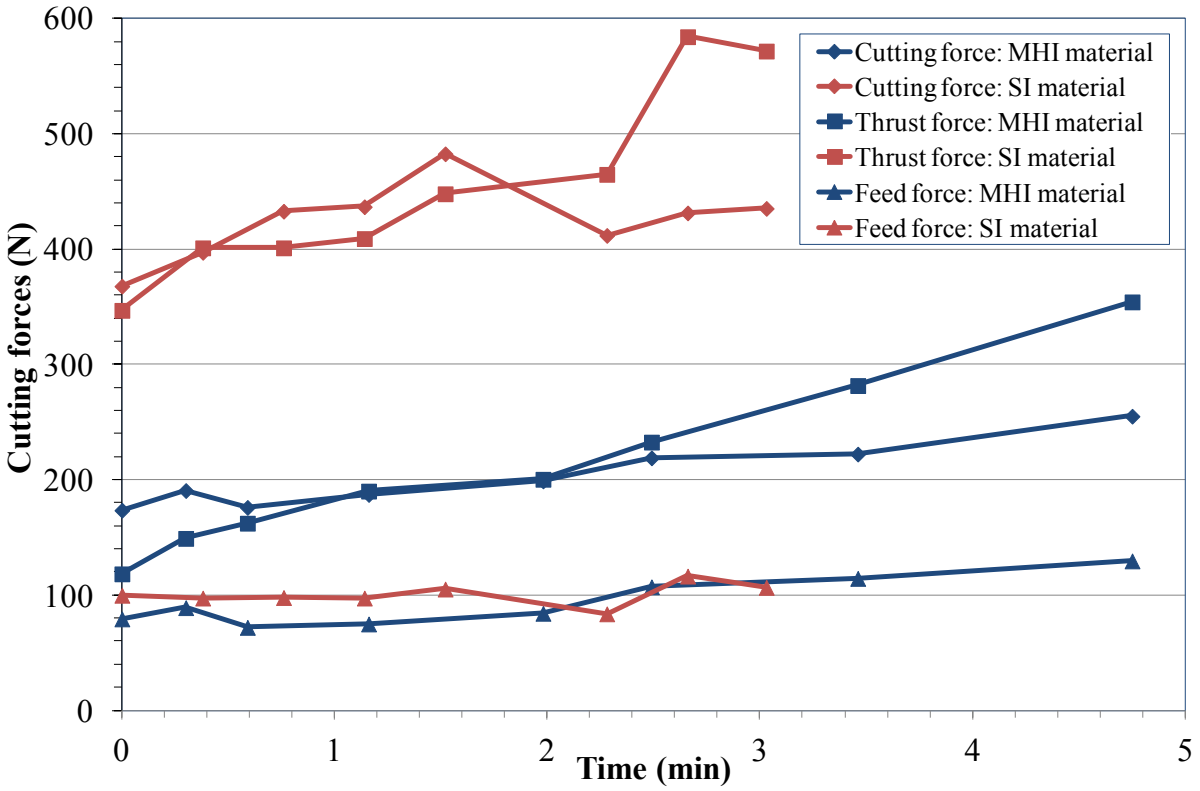

Figure 155: Cutting force data for MHI and SI products

4.5.2 Chip analysis

Machining with a cutting fluid pressure of 100bar resulted in short and discontinuous chips while long continuous helical chips were obtained in all experiments performed at 10bar, although no workpiece-swarf entanglement problems were encountered in the latter, see Figure 156. Figure 157 details SEM micrographs of serrated chip formation of Tests 1 and 2. This was most likely due to the intense rate of thermal softening caused by large strains along the shear plane, which weakened the material and led to failure initiation. In addition, chip serration depth and width was ~72.5µm and 127µm respectively at Vc of 450m/min which was 42% and 124% higher compared to 300m/min as the effect of thermal softening exceeded that of strain rate hardening. Similar chip morphologies were observed by Zheng et al. [92] and Dong et al. [161] when high speed turning Inconel 718 with Sialon and carbide tools respectively.

Figure 156: Typical chip morphology for tests at a) 10bar, b) 100bar and c) optical micrograph of continuous helical chips

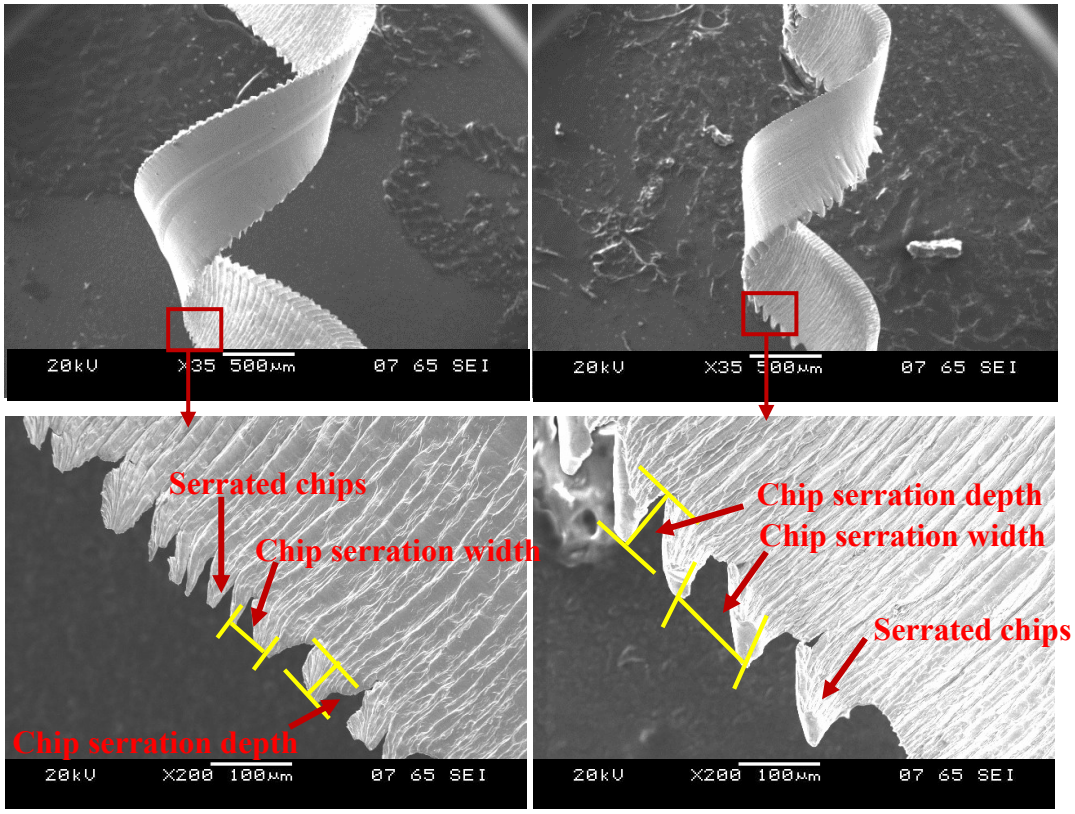

a) Test 1: 300m/min b) Test 2: 450m/min

Figure 157: SEM micrographs of chip morphology from Tests 1 and 2

4.5.3 Surface roughness

Not surprisingly, feed rate was found to have a considerable influence on workpiece surface roughness. While experiments performed at 0.15mm/rev feed rate (Tests 1, 2, 5 and 6) showed minor/gradual variation in surface roughness over the test duration (~0.70µm at the start to 0.40µm Ra at the end of tool life), a steep decrease from ~1.30µm to 0.50µm Ra was observed as flank wear increased to ~130µm (due to a corresponding increase in insert nose

radius) when operating at 0.20mm/rev (Tests 3, 4, 7 and 8), see Figure 158. The roughness subsequently deteriorated up to ~1µm Ra at test cessation.

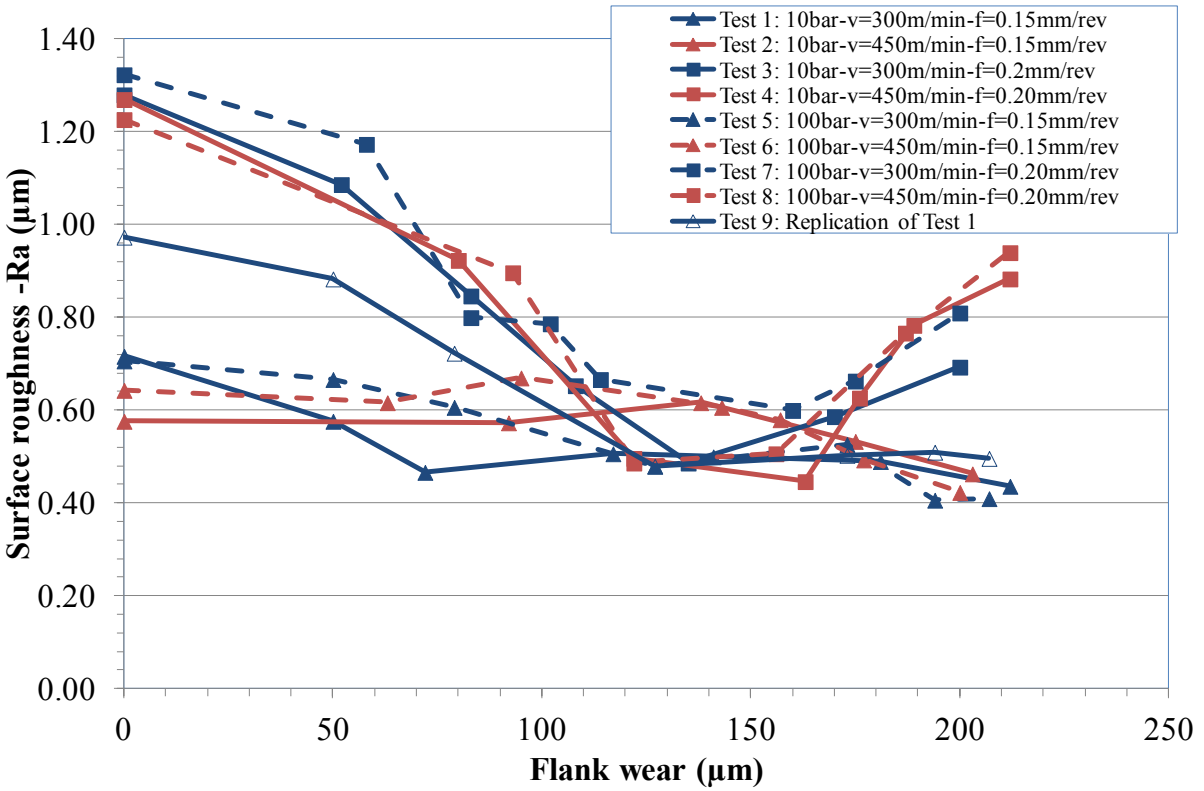

Figure 158: Workpiece surface roughness (Ra) against tool flank wear

While comparing the workpiece surface roughness, no discernible difference in Ra values were apparent when turning both MHI and SI Inconel 718 (at Vc=300m/min, f=0.20mm/rev, 100bar cutting fluid pressure), which was ~1.3µm Ra with inserts in the new condition and 0.80µm Ra at the end of tool life.

4.5.4 Cutting forces

4.5.4.1 Cutting force component

The cutting force component generally ranged from 270-370 N when using new inserts. When operating at the higher cutting speed of 450m/min (Tests 2, 4, 6 and 8), cutting force typically increased by ~35% over the test duration due to rapid tool wear. In contrast, trials performed at 300m/min (Tests 1, 3, 5 and 7) showed an increase in cutting force within the first 1-2min of machining but which later decreased towards the end of tool life, see Figure 159. This was attributed to initial rapid crater formation leading to greater frictional contact however, after the crater formation, subsequent better chip flow over the rake face causing a reduction in cutting force due to low friction. Figures 160 and 161 show the main effects plots for cutting force when employing new and worn inserts respectively. None of

the factors however were statistically significant in relation to cutting force for both new and worn tools, despite the latter showing a low error level of 9.31% respectively; see Table 55**.** This was possibly due to the level of cutting speeds employed in this phase of work. In these trials, Vc was on the higher side (300 and 450 m/min) and material was in the softening zone and could be deformed easily over the range of parameters tested, hence suppressed the effect of other variables. Due to the high error level from the statistical analysis for new tools, replication of Tests 2 and 6 were performed to validate results with similar values of cutting forces were obtained, see Table D2 in Appendix D. In case of worn tools, cutting environment had a relatively high PCR of 50.73%, most likely due to the greater mechanical force exerted at 100bar fluid pressure.

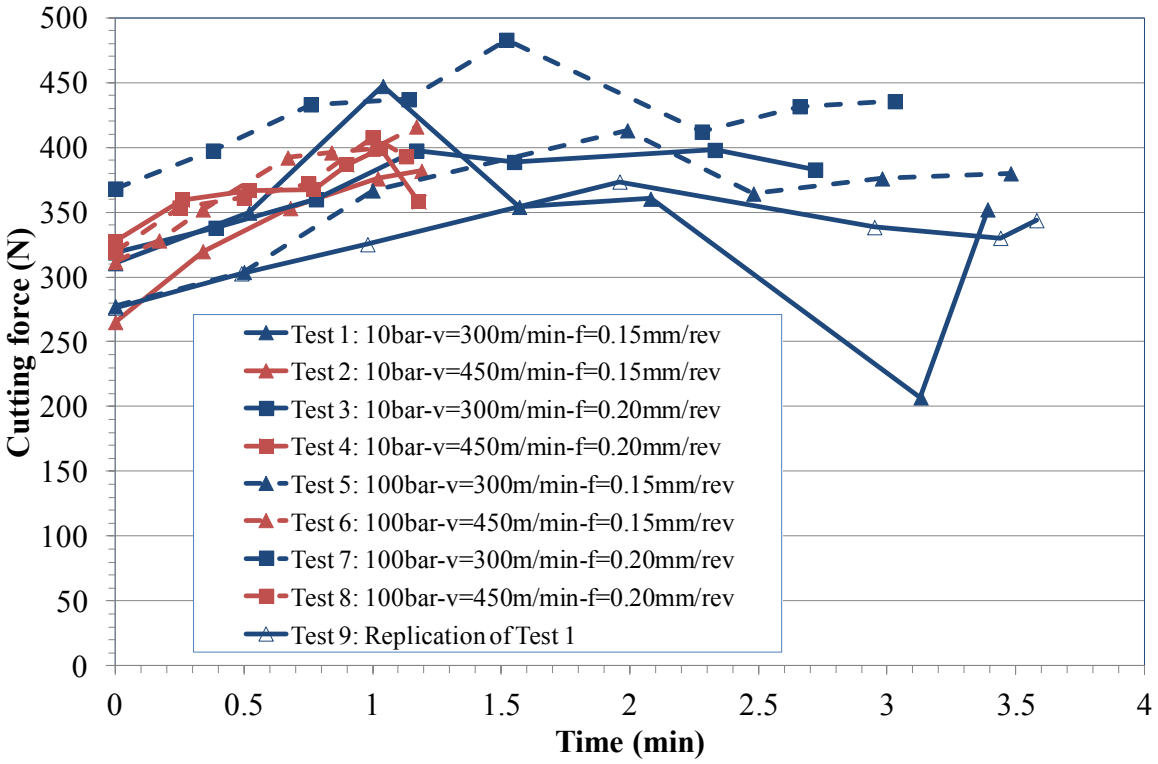

Figure 159: Cutting force against machining time

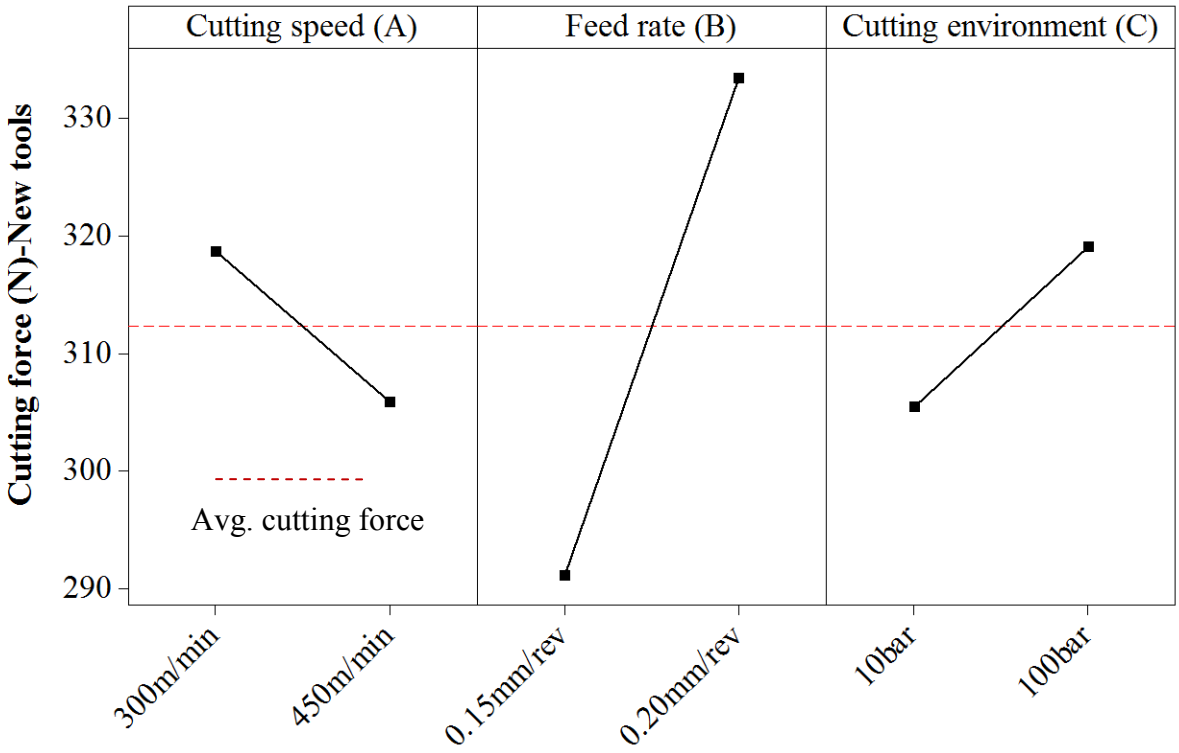

Figure 160: Main effects plots-means for cutting force with new tools (Phase 2A)

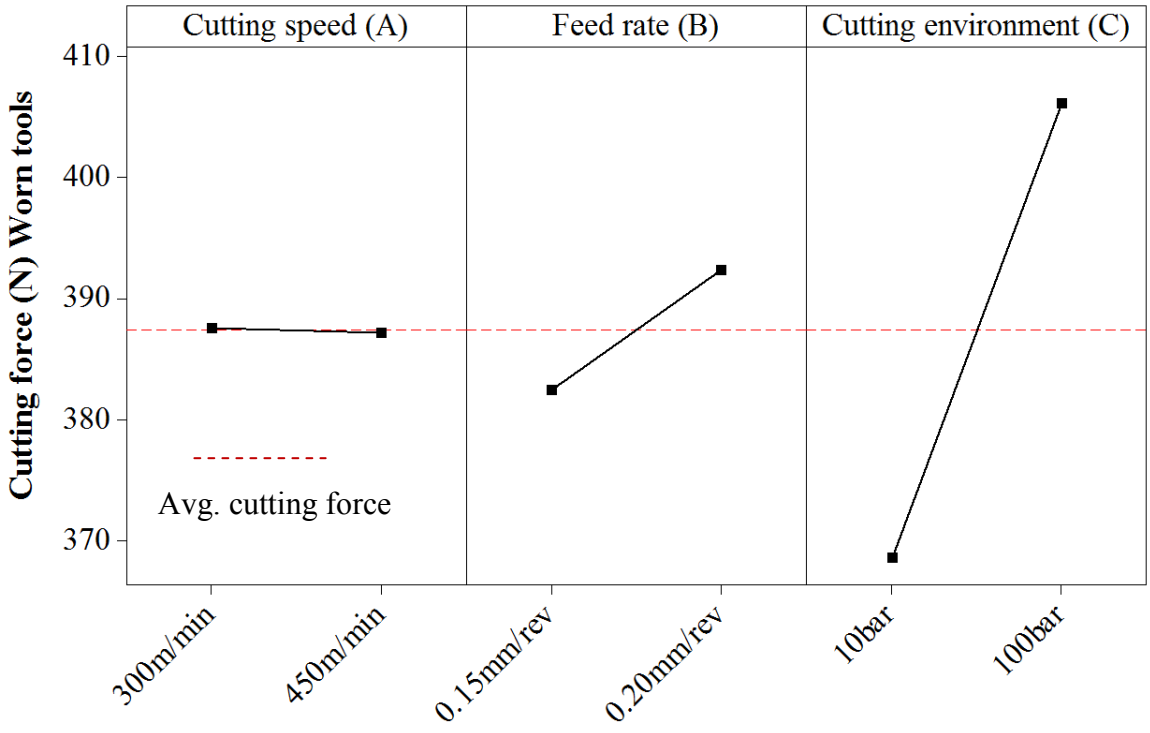

Figure 161: Main effects plots-means for cutting force with worn tools (Phase 2A)

Table 55: P-value and PCR's for cutting force with new and worn tools (Phase 2A)

Factors	DF	New		Worn	
		P	PCR (%)	P	PCR (%)
Cutting speed (A)	1	0.823	0.00	0.960	0.81
Feed rate (B)	1	0.465	9.73	0.347	2.29
Cutting environment (C)	1	0.735	0	0.101	50.73
A*B	1	0.934	0	0.113	39.79
A*C	1	0.992	0	0.722	1.04
B*C	1	0.991	0	0.476	0.21
Error	1		***90.3***		***9.31***
Total	7	R-Sq(Adj)=9.7		R-Sq(Adj)=90.69	

4.5.4.2 Thrust force component

The thrust forces at the start of the experiments were compareable to the cutting force component. The thrust force did not exceed 640N ever at the end of tool life irrespective of the other operating variables however, steep rise in thrust forces were recorded for the tests performed at 450m/min (Tests 2, 4, 6 and 8) over a duration of ~1min, see Figure 162.The main effects plots for new and worn tools are detailed in Figure 163 and 164 respectively. As with cutting forces, none of the factors were found to be statistically significant with respect to thrust force irrespective of tool condition with the analysis involving new inserts showed an error level of 100%. Conversely, cutting environment was found to have a PCR of 78.22% on thrust forces when utilising worn tools, with a corresponding lower error of ~18.4% (Table 56).

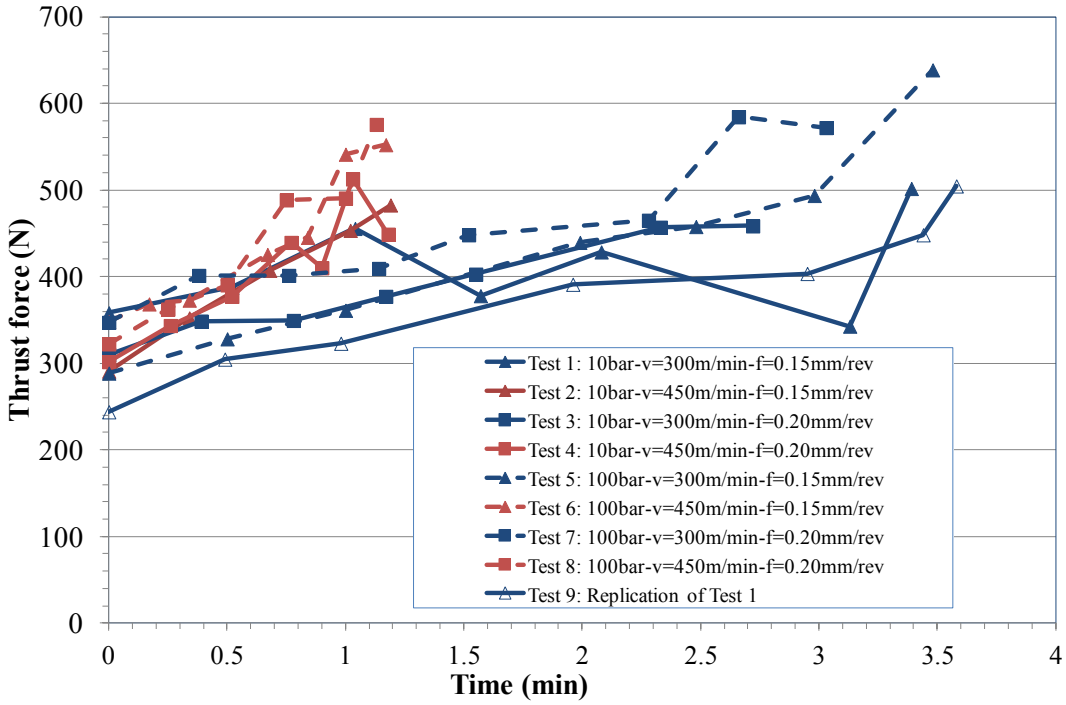

Figure 162: Thrust force against machining time

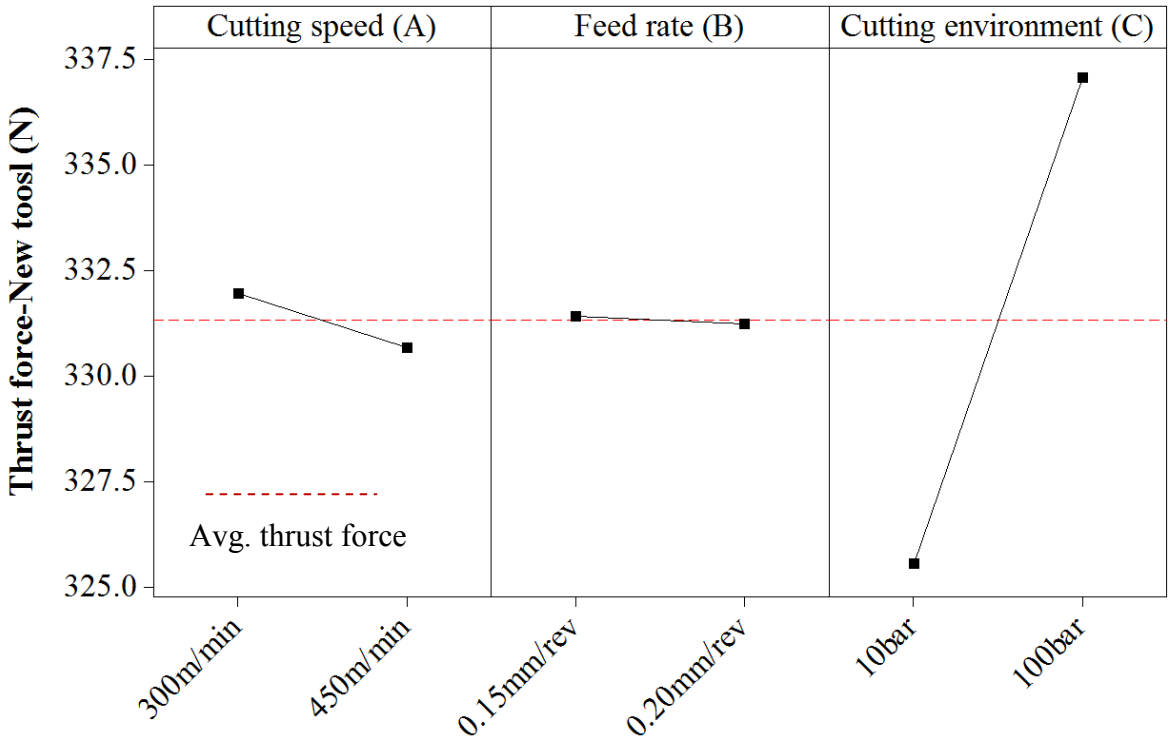

Figure 163: Main effects plots-means for thrust force with new tools (Phase 2A)

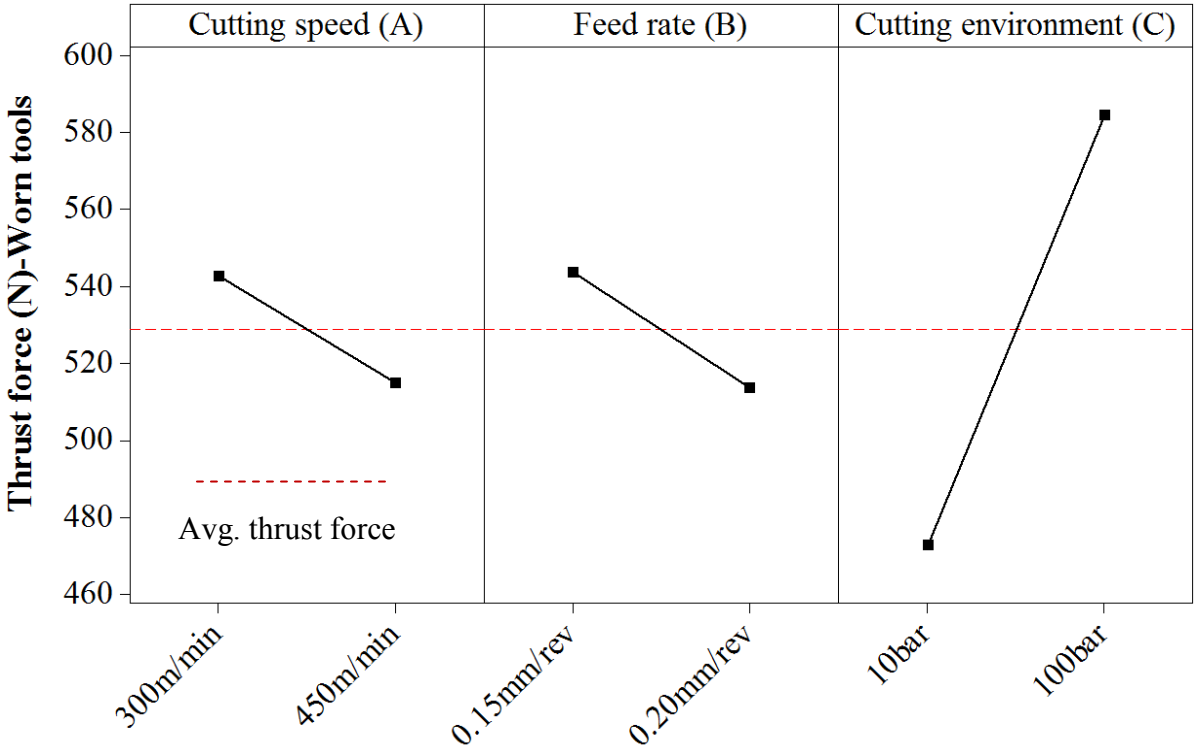

Figure 164: Main effects plots-means for thrust force with worn tools (Phase 2A)

Table 56: P-value and PCR's for thrust force with new and worn tools (Phase 2A)

Factors	**DF**	**New**		**Worn**	
		P	**PCR (%)**	**P**	**PCR (%)**
Cutting speed (A)	1	0.978	0	0.399	2.38
Feed rate (B)	1	0.997	0	0.376	3.21
Cutting environment (C)	1	0.805	0	0.114	78.20
A*B	1	0.889	0	0.433	1.38
A*C	1	0.662	0	0.623	0
B*C	1	0.793	0	0.748	0
Error	1		***100***		***18.42***
Total	7	R-Sq(Adj)=0.00		R-Sq(Adj)=81.58	

4.5.4.3 Feed force component

Figure 165 shows the progression of feed force for all tests, which did not exceed 125N even at test cessation. Figures 166 and 167 show the main effects plots for feed force when using new and worn tools respectively. As observed with the cutting and thrust force components, none of the factors were statistically significant relative to feed force for both new and worn tools as shown in Table 57. Feed force was however generally higher when machining using 100bar fluid pressure, with a PCR of 63.85% detailed for worn inserts.

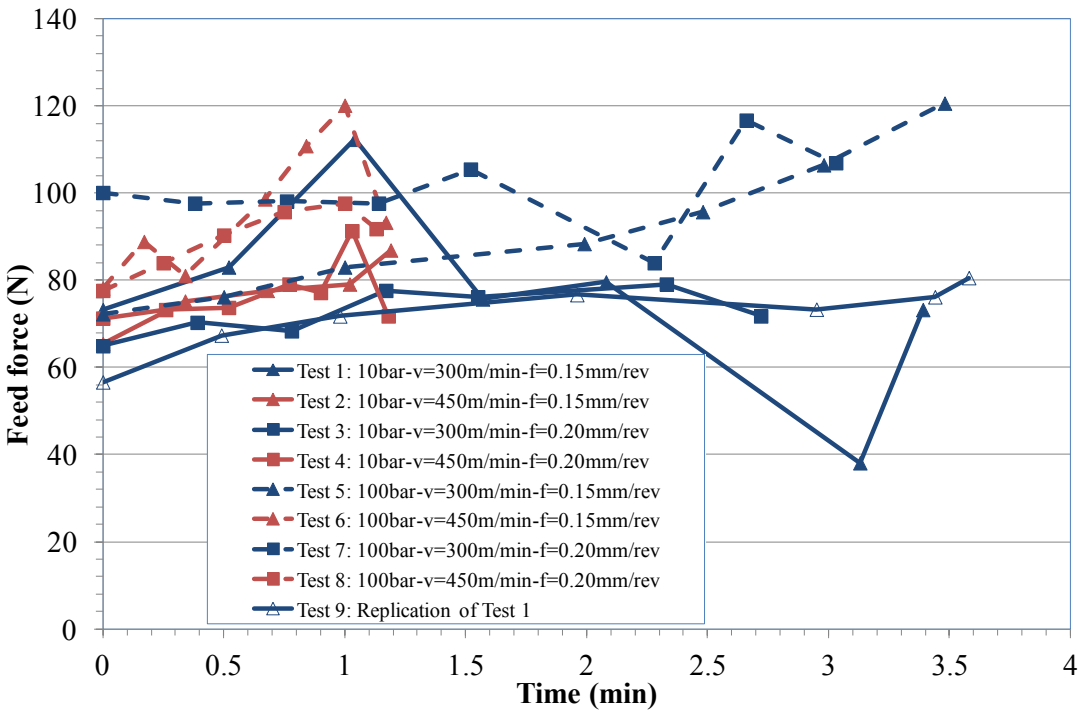

Figure 165: Feed force against machining time

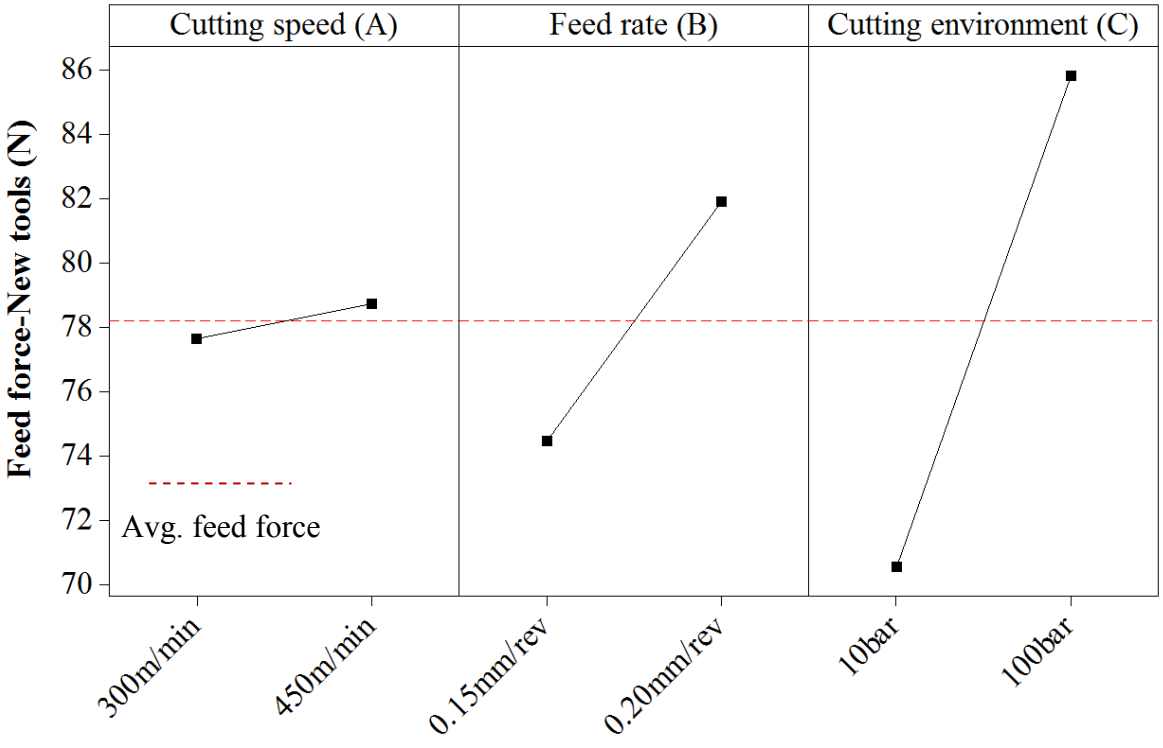

Figure 166: Main effects plots-means for feed force with new tools (Phase 2A)

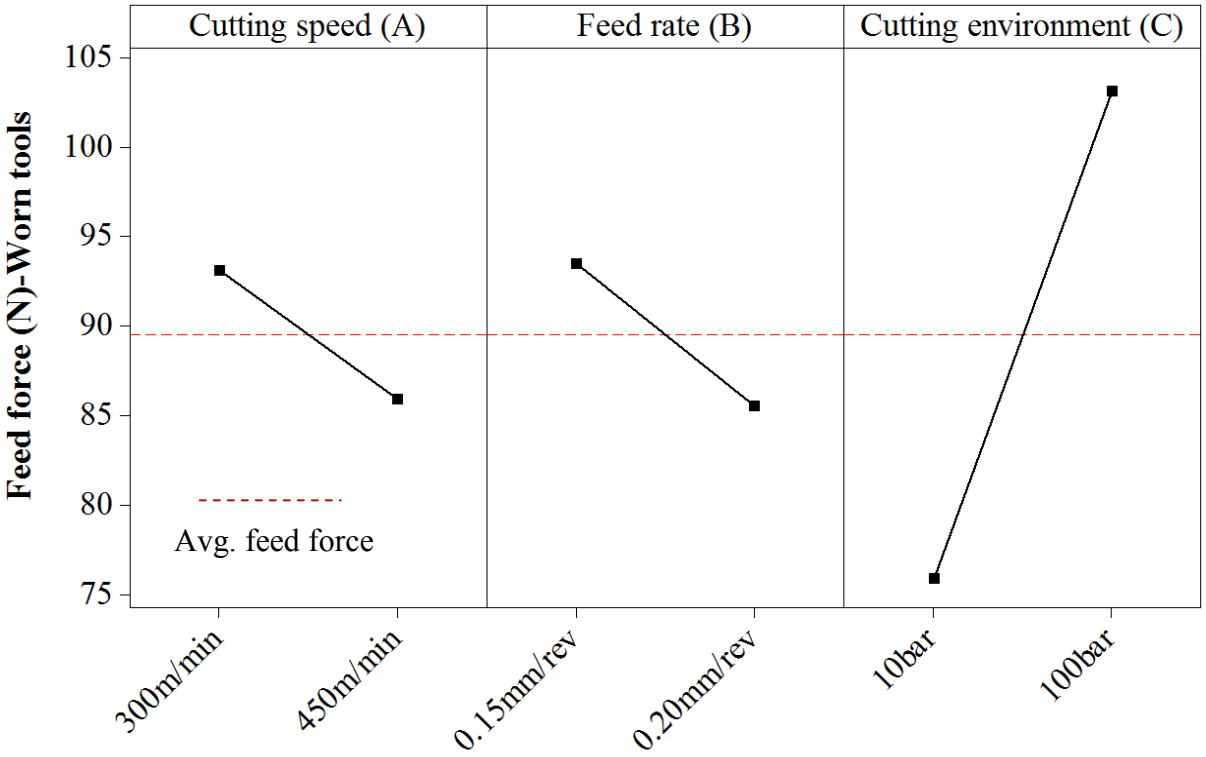

Figure 167: Main effects plots-means for feed force with worn tools (Phase 2A)

Table 57: P-value and PCR's for feed force with new and worn tools (Phase 2A)

Factors	DF	New		Worn	
		P	PCR (%)	P	PCR (%)
Cutting speed (A)	1	0.937	0.00	0.466	0.91
Feed rate (B)	1	0.624	0.00	0.436	1.92
Cutting environment (C)	1	0.401	0.00	0.149	63.85
A*B	1	0.869	0.00	0.964	0
A*C	1	0.896	0.00	0.275	14.16
B*C	1	0.644	0.00	0.964	0
Error	1		***100***		***26.77***
Total	7	R-Sq(Adj)=0		R-Sq(Adj)=73.23	

4.6 Phase 2B: Assessment of cutting environment, cutting speed and feed rate effects on workpiece surface integrity

4.6.1 Surface roughness and topography

Figure 168 shows that surface roughness was typically lower when using worn tools (<0.67µm), which was possibly due to the formation of a wear flat at the nose radius similar to that shown in Figure 169. With regard to new inserts, workpiece surface roughness was <0.90µm Ra for all tests performed at a feed rate of 0.20mm/rev (Tests 3, 4, 7 and 8), while this did not exceed 0.70µm Ra when operating at 0.15mm/rev (Tests 1, 2, 5 and 6). Examples of 3D surface topographic maps of Tests 3 and 4 when employing new and worn tools are shown in Figures 170 and 171 respectively. Typically, a ~40% reduction in Sa was observed

when using worn inserts compared to new tools. Main effects plots for both new and worn inserts are shown in Figures 172 and 173 respectively. Despite having a high PCR of 93.10%, the effect of feed rate on workpiece surface roughness was not statistically significant when turning with new inserts. This was likely due to the new inserts suppressing the influence of feed rate over the range of parameters tested. Conversely, feed rate had a significant impact on surface roughness with a corresponding PCR of 76.83% when utilising worn tooling, see Table 58. In addition, all of the interactions assessed had negligible influence, with error levels in the ANOVA not exceeding 7%, irrespective of tool condition.

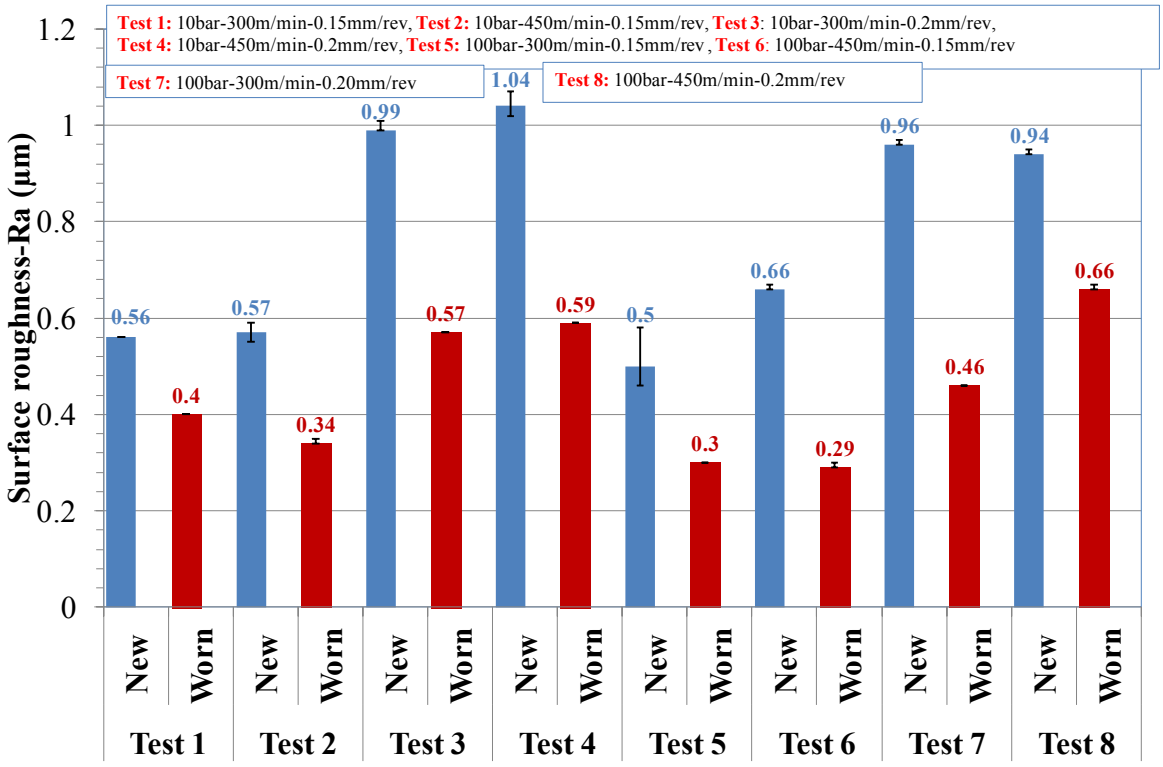

Figure 168: Surface roughness with new and worn tools

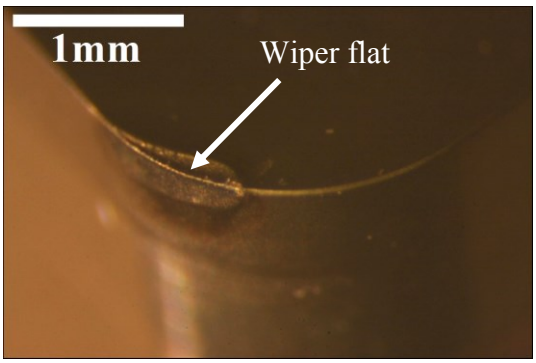

Figure 169: Optical micrograph of worn insert from Test 2

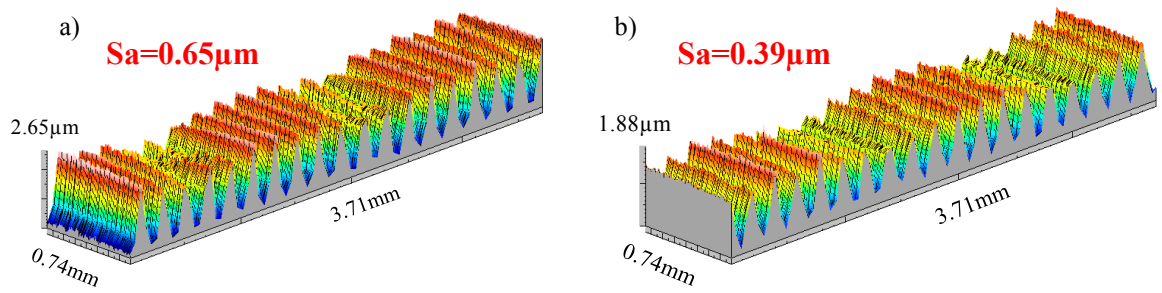

Figure 170: Workpiece surface topography produced with (a) new and (b) worn tools in Test 3

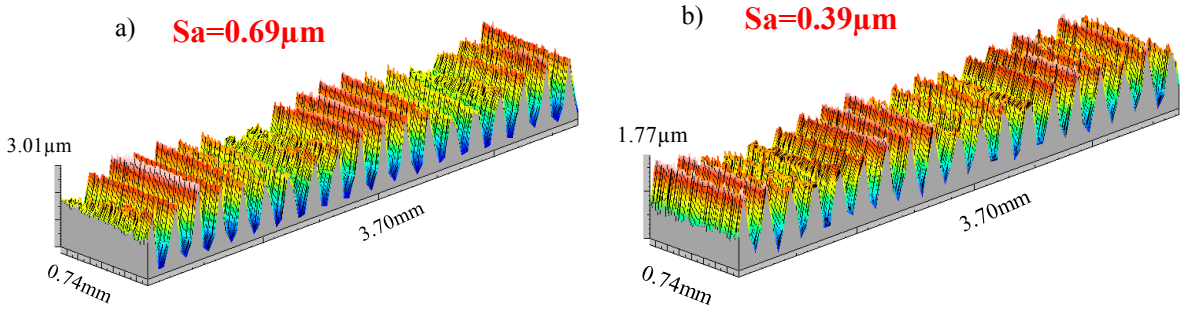

Figure 171: Workpiece surface topography produced with (a) new and (b) worn tools in Test 4

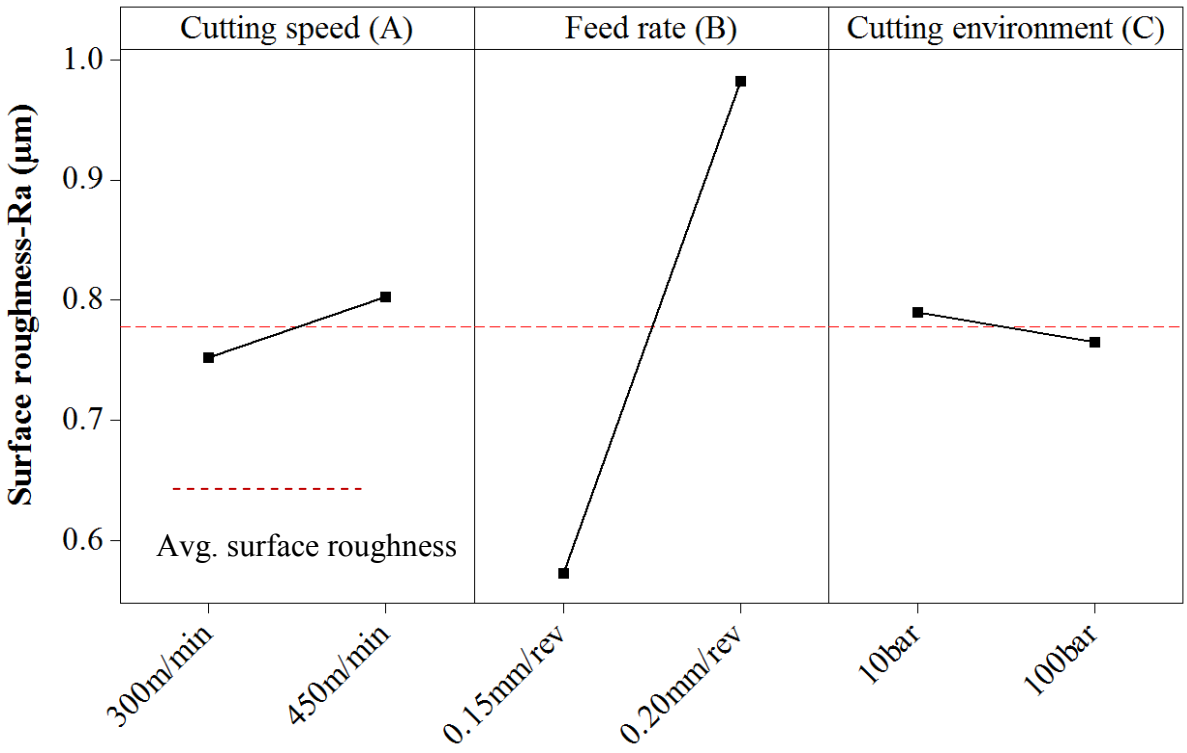

Figure 172: Main effects plots-means for surface roughness with new tools (Phase 2B)

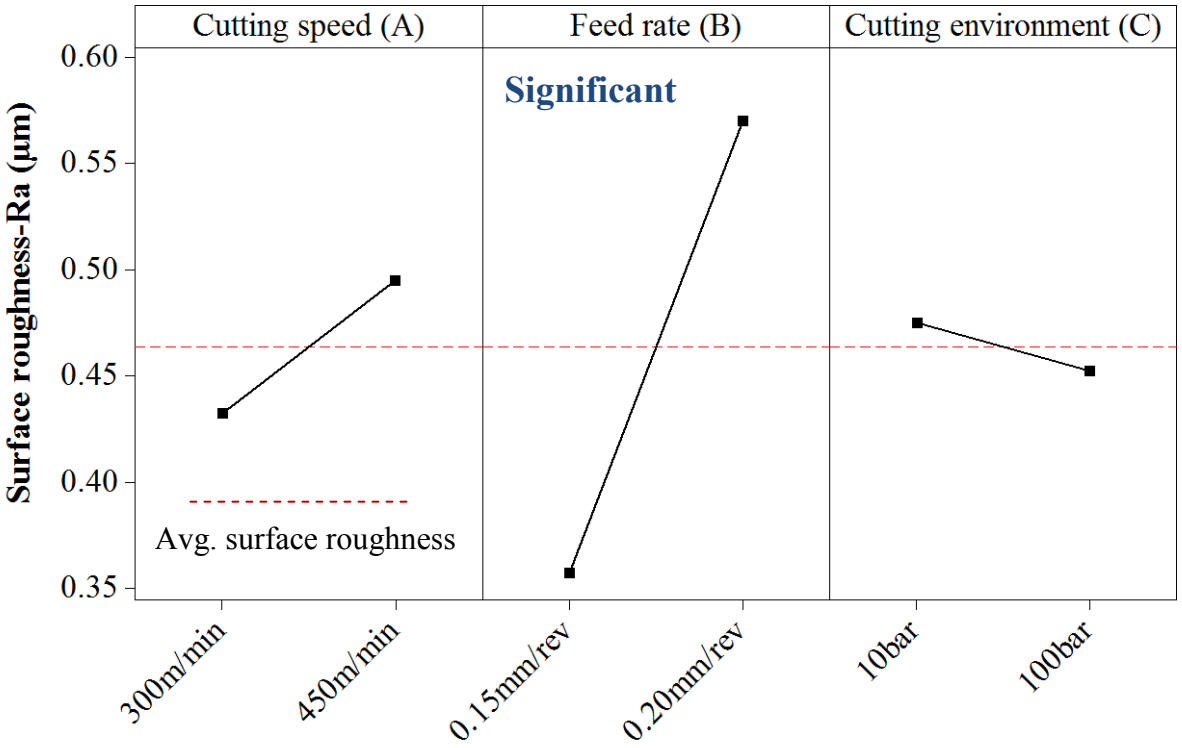

Figure 173: Main effects plots-means for surface roughness with worn tools (Phase 2B)

Table 58: P-value and PCR's for surface roughness with new and worn tools (Phase 2B)

Factors	DF	New		Worn	
		P	PCR (%)	P	PCR (%)
Cutting speed (A)	1	0.530	0.29	0.076	6.65
Feed rate (B)	1	0.085	93.10	0.022*	76.83
Cutting environment (C)	1	0.728	0	0.205	0.51
A*B	1	0.639	0	0.100	3.74
A*C	1	0.778	0	0.058	11.5
B*C	1	0.600	0	0.795	0
Error	1		***6.90***		***0.67***
Total	7	R-Sq(Adj)=93.1		R-Sq(Adj)=99.33	

4.6.2 Workpiece surface damage

Feed marks were visible on machined surfaces in all tests when employing new tools, irrespective of operating variables and cutting environment. However, the formation of grooves obscured the feed marks on the workpiece surfaces machined with worn tools as shown in Figure 174. The groove formation was likely due to rubbing between worn tool and workpiece as a result of reduction in clearance angle of cutting tool. Further analysis of higher magnification (1000x) SEM micrographs showed that surface microcracks of size 10-12 µm and grooves were evident in the samples machined with worn tools while no damage was recorded when employing new tools, examples of which are detailed in Figure 175. Typically, 1-2 microcracks were recorded in an area of ~10,000µm^2. These were in line with results

observed in Phase 1D (Section 4.4.3) involving the MHI Inconel 718 material. Workpiece surface damage including side flow, BUE, chip debris, cavity formation, plastic flow, surface tearing, breakage of niobium (NbC) and titanium carbides (TiC) observed when turning Inconel 718 using whisker ceramic inserts [21] however, were not seen in the current work.

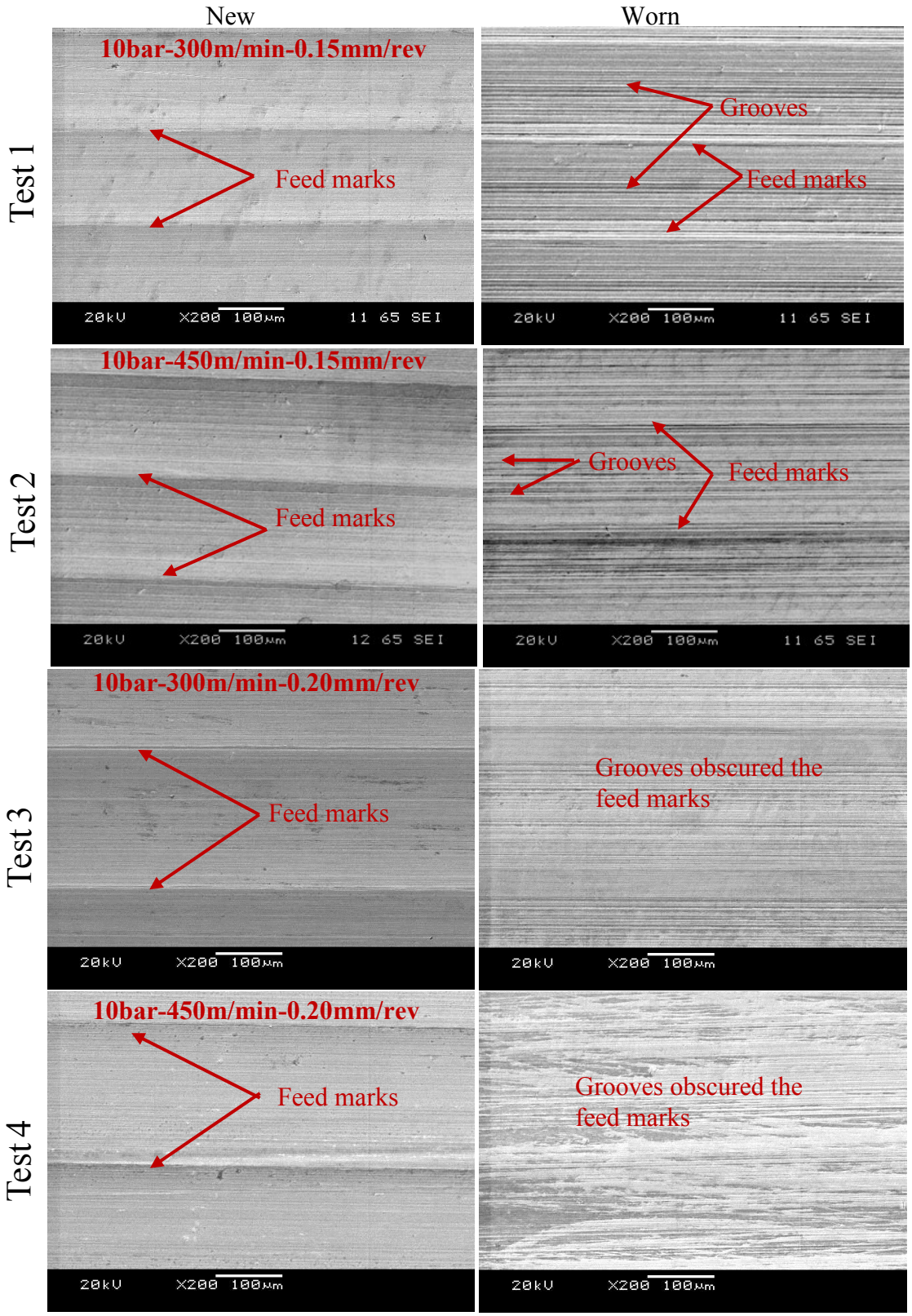

Figure 174: SEM micrographs of typical machined surfaces of Tests 1, 2, 3 and 4

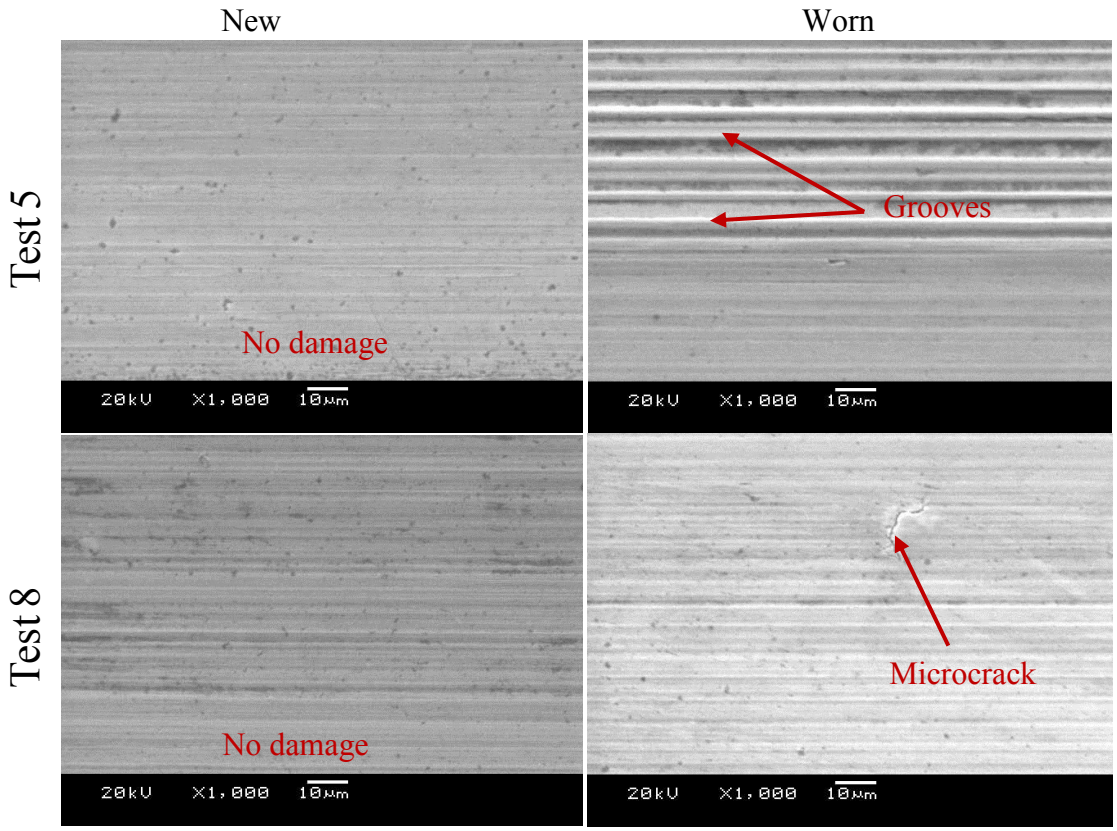

Figure 175: Higher magnification SEM micrographs of Tests 5 and 8

4.6.2 Microhardness

Microhardness depth profiles measured parallel to the feed direction with new and worn tools are shown in Figures 176 and 177 respectively. Minimal variation in sub-surface microhardness measurements were seen when utilising new inserts irrespective of operating parameters and cutting environment while surfaces machined with worn tools showed a strain hardened layer extending to a depth of ~50µm with a maximum value of 554.4$HK_{0.025}$ (~13%) above the bulk hardness (490$HK_{0.025}$). Figure 178 displays the depth profile measurements from samples produced with new tools in a direction perpendicular to the feed (radial/cutting speed), which showed no major changes in microhardness. In contrast, samples turned with worn inserts showed a rise of up to ~ 560$HK_{0.025}$ (perpendicular to feed direction) over a depth of ~100µm; see Figure 179.

When compared against microhardness results from tests with the MHI material detailed in Section 4.4.4, the depth of strain hardened region was ~3 to 4 times lower in both directions (parallel and perpendicular to the feed rate) in the SI workpiece. Furthermore, the maximum microhardness was ~50$HK_{0.025}$ higher in the former. This was likely due to the difference in microstructure discussed in Section 4.5.1.

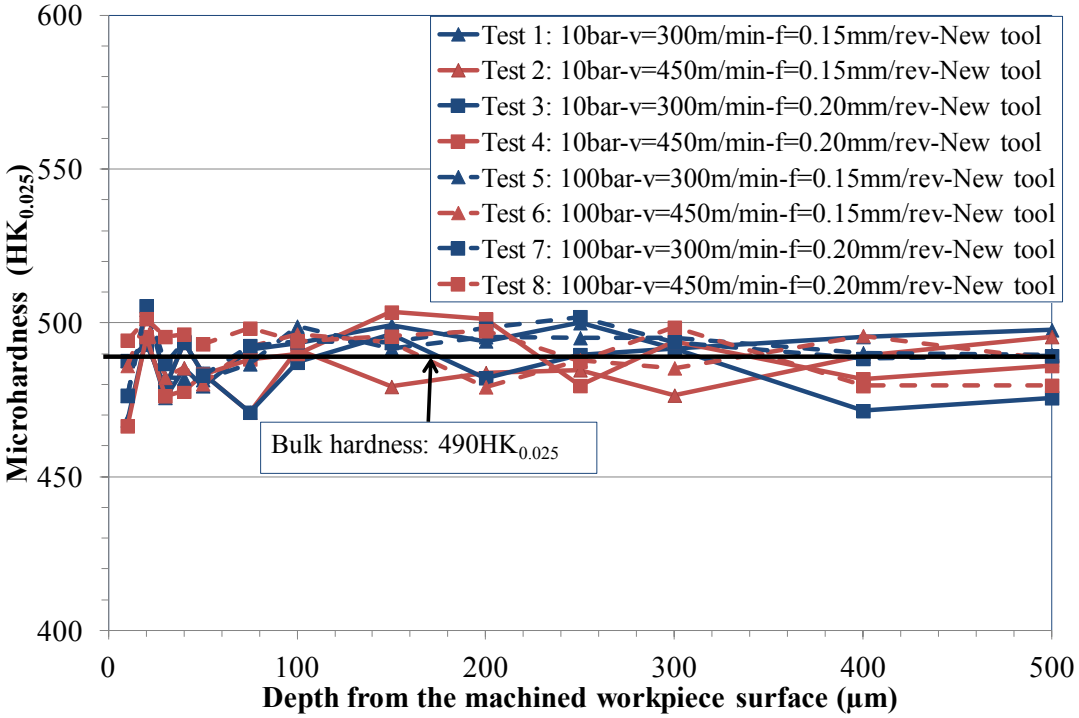

Figure 176: Workpiece microhardness depth profiles for new tools in a direction parallel to feed

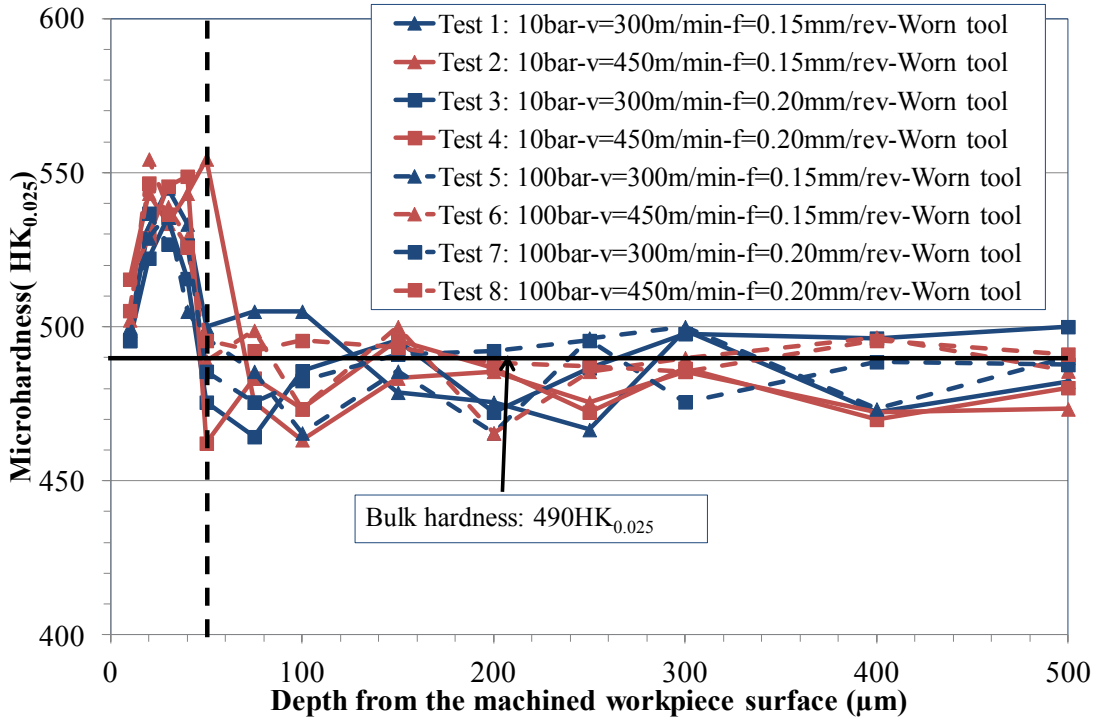

Figure 177: Workpiece microhardness depth profiles for worn tools in a direction parallel to feed

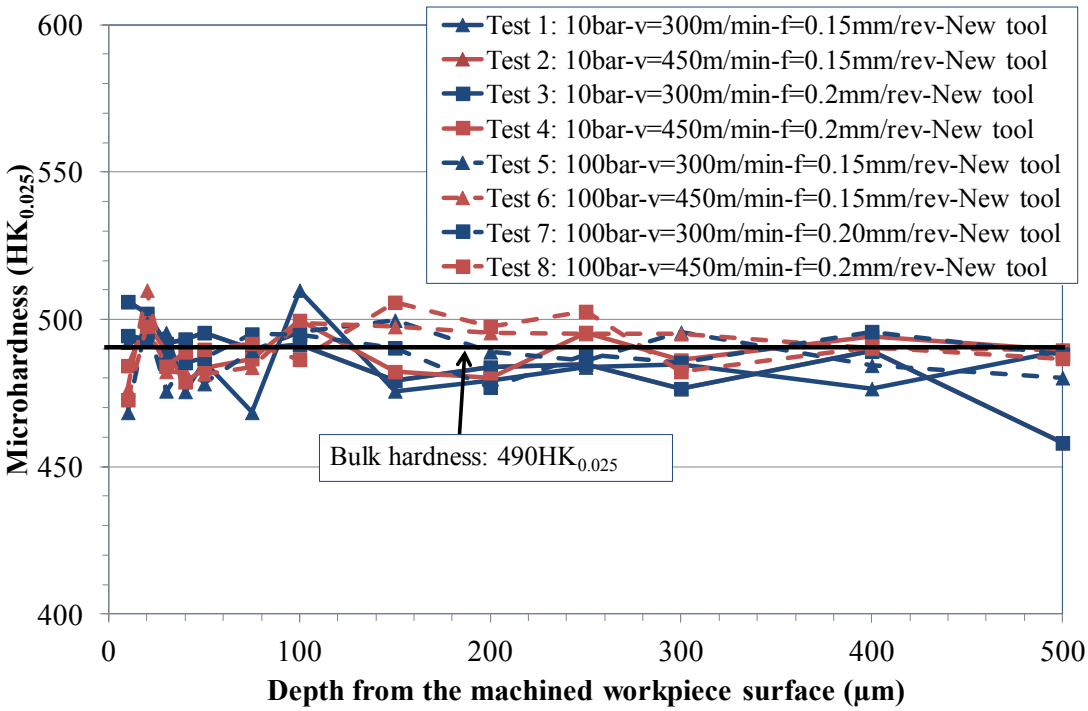

Figure 178: Workpiece microhardness depth profiles for new tools in a direction perpendicular to feed

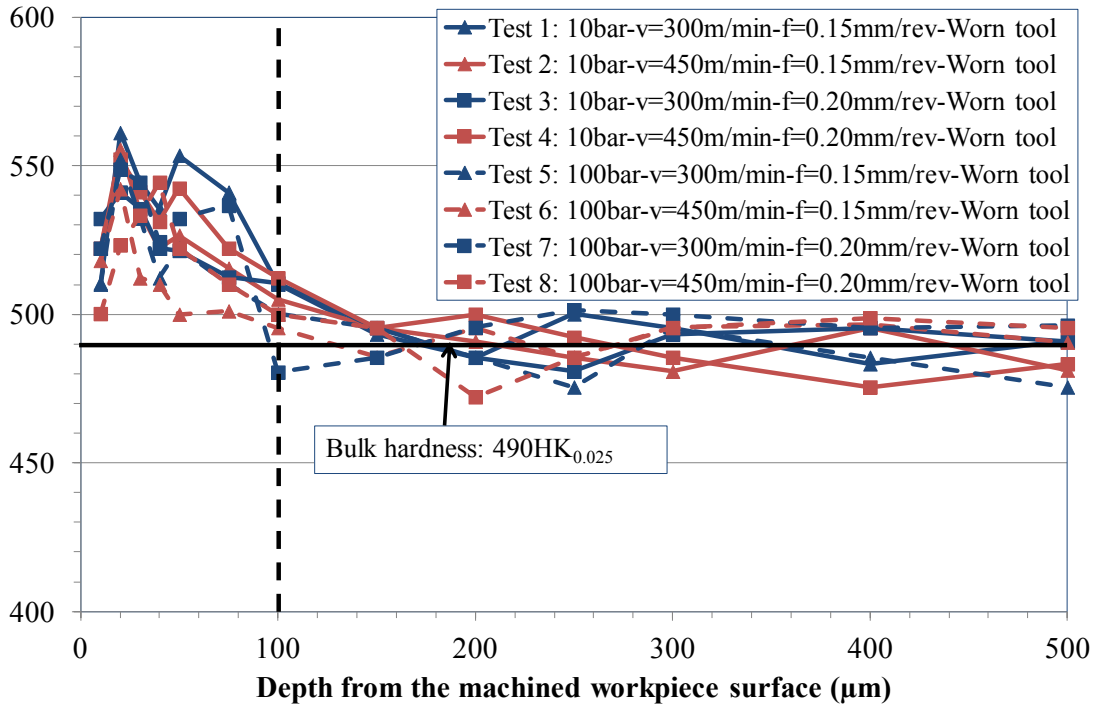

Figure 179: Workpiece microhardness depth profiles for worn tools in a direction perpendicular to feed

4.6.3 Microstructure

Figures 180-187 show the cross sectional optical micrographs of machined sub-surface both parallel and perpendicular to feed direction in all tests when employing new and worn inserts. In addition, selected workpiece samples were examined under SEM to analyse the effect of cutting speed (Test 1 vs Test 3), feed rate (Test 1 vs Test 3) and cutting environment (Test 3 vs Test 7), see Figures 188-191. In general, no white layers (WL's) were visible in any of the samples analysed irrespective of the tool condition and operating parameters. Similarly, no apparent damage beneath the machined surface was observed parallel to the feed direction. However, grain elongation/bending (~15-20µm) along the cutting speed direction was observed in all samples, viewed perpendicular to the feed direction which extended to a depth of ~25-30µm when using worn tools. This was in agreement with results reported by other researchers [111, 126, 145]. When compared with results in Phase 1D (Section 4.4.2), no significant grain deformation was apparent in the MHI material. This was most likely due to the lack of γ″ precipitates, which define the grain size in Inconel 718 alloy.

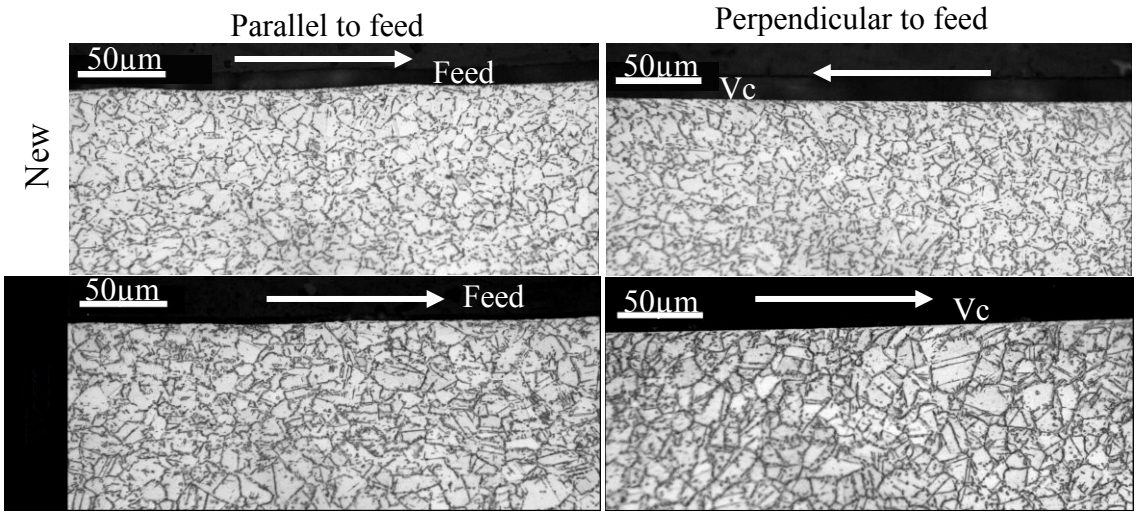

Figure 180: Cross sectional optical micrographs of machined workpiece sub-surface of Test 1 following turning with new and worn inserts

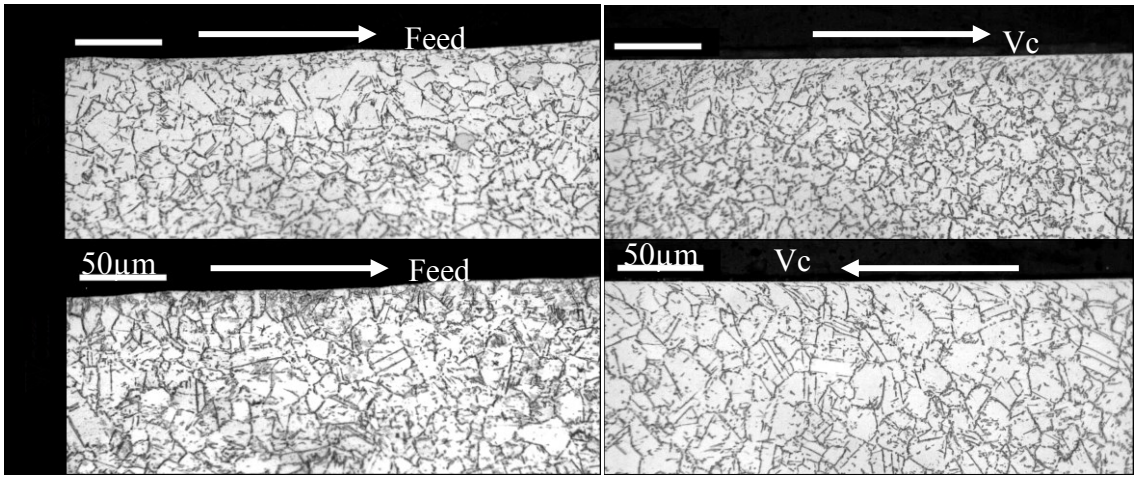

Figure 181: Cross sectional optical micrographs of machined workpiece sub-surface of Test 2 following turning with new and worn inserts

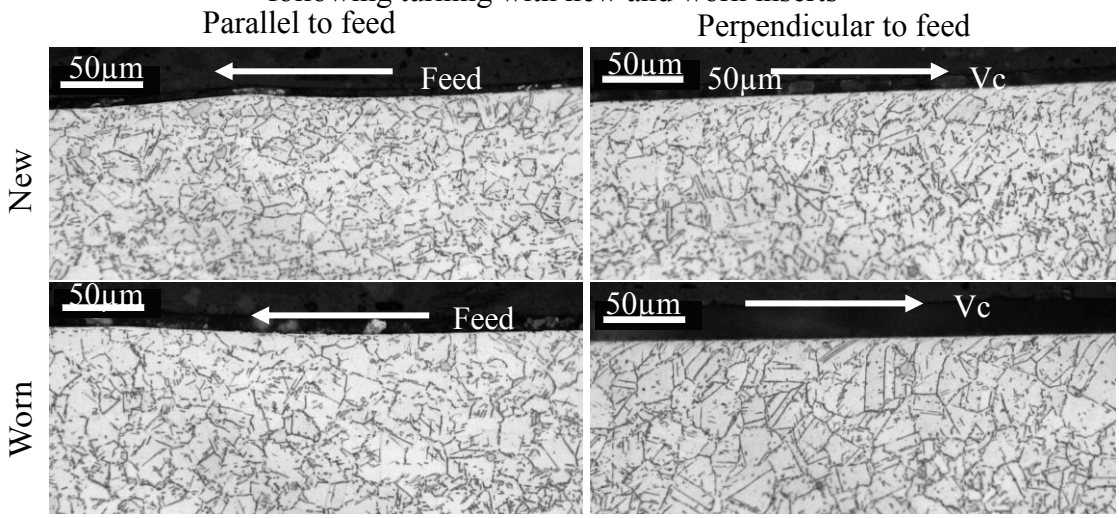

Figure 182: Cross sectional optical micrographs of machined workpiece sub-surface of Test 3 following turning with new and worn inserts

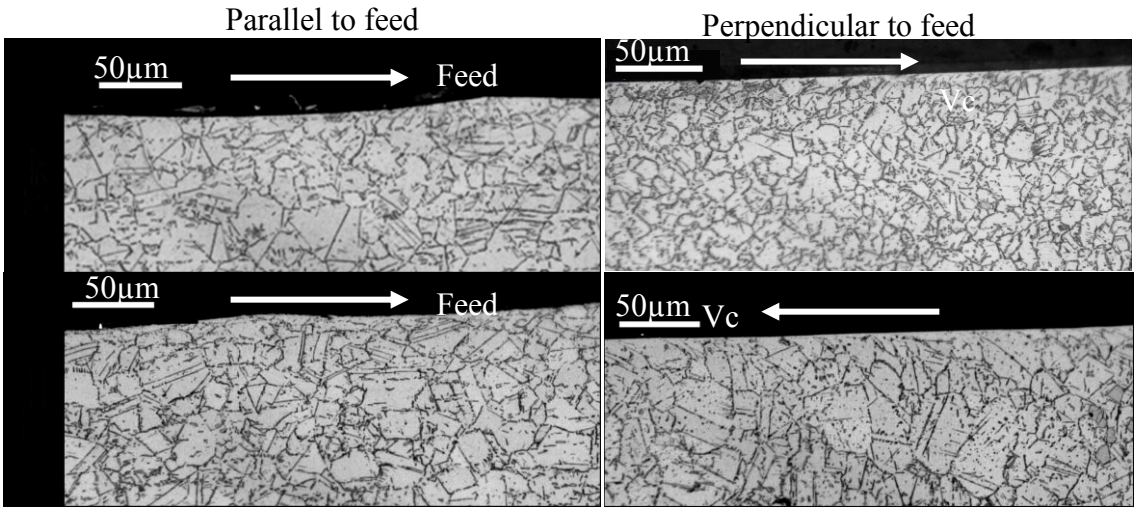

Figure 183: Cross sectional optical micrographs of machined workpiece sub-surface of Test 4 following turning with new and worn inserts

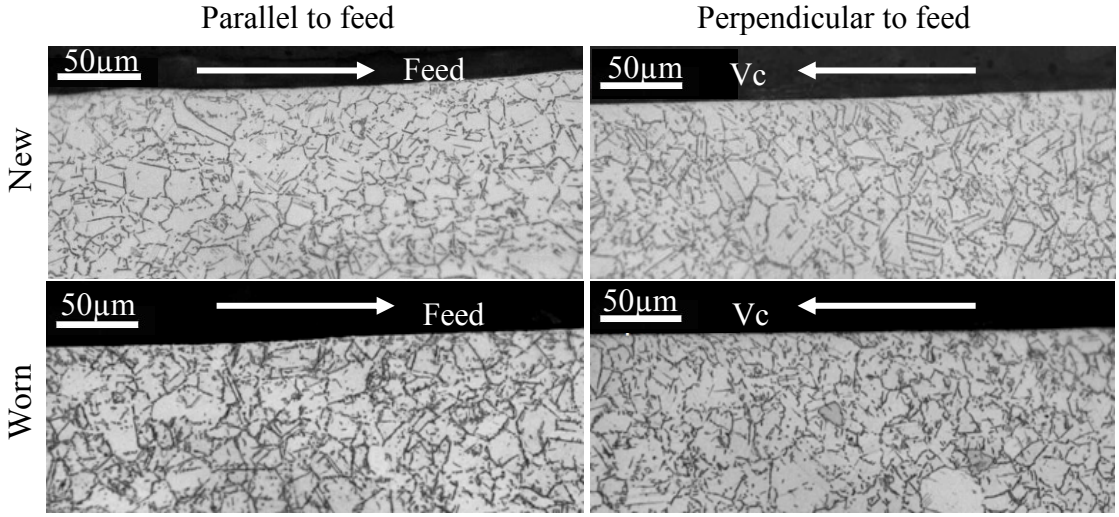

Figure 184: Cross sectional optical micrographs of machined workpiece of Test 5 following turning with new and worn inserts

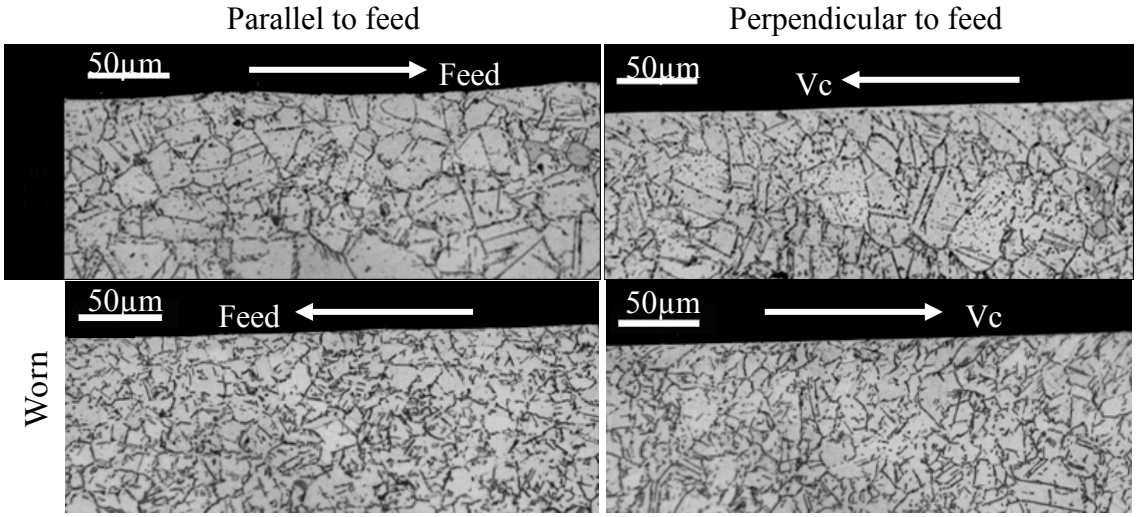

Figure 185: Cross sectional optical micrographs of machined workpiece of Test 6 following turning with new and worn inserts

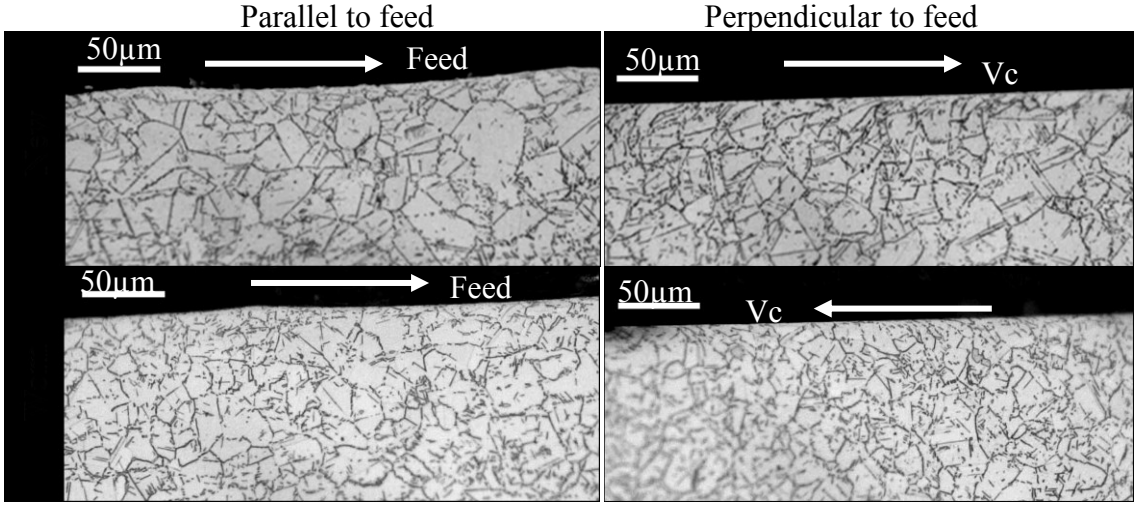

Figure 186: Cross sectional optical micrographs of machined workpiece sub-surface of Test7 following turning with new and worn inserts

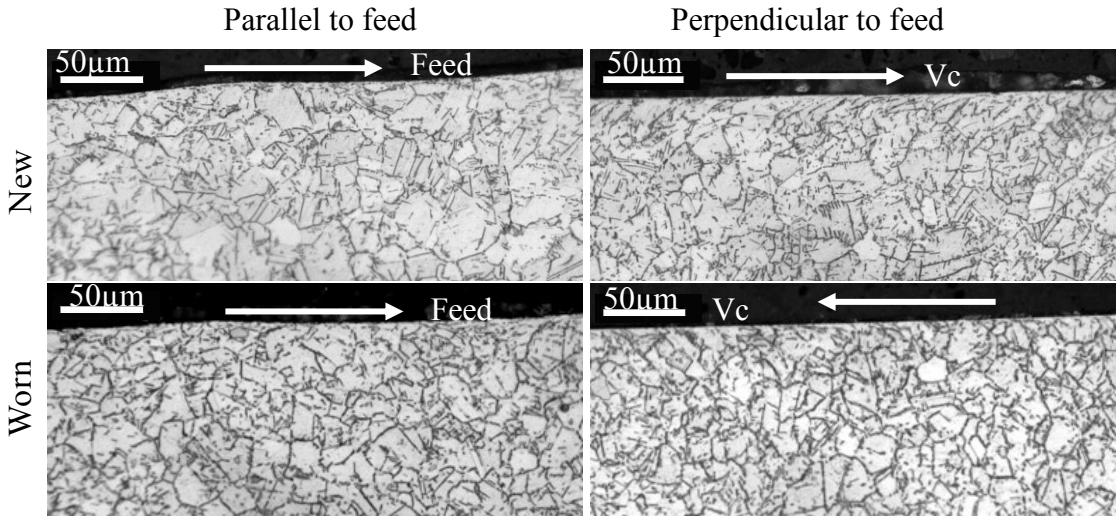

Figure 187: Cross sectional optical micrographs of machined workpiece sub-surface of Test 8 following turning with new and worn inserts

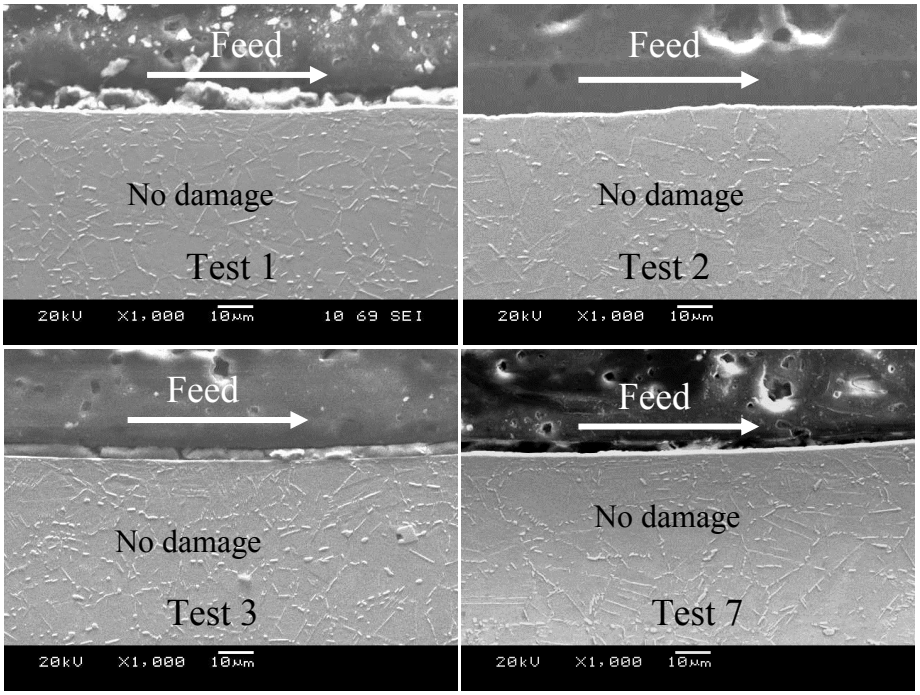

Figure 188: Cross sectional SEM images of workpiece sub-surface of Tests 1, 2, 3 and 7 produced with new tools in a direction parallel to feed

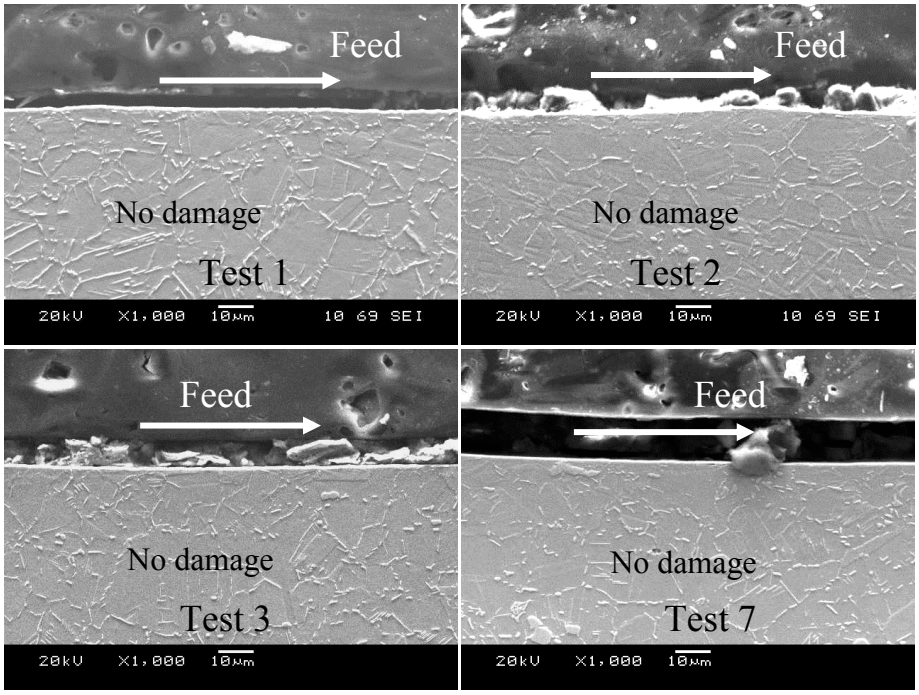

Figure 189: Cross sectional SEM images of workpiece sub-surface of Tests 1, 2, 3 and 7 produced with worn tools in a direction parallel to feed

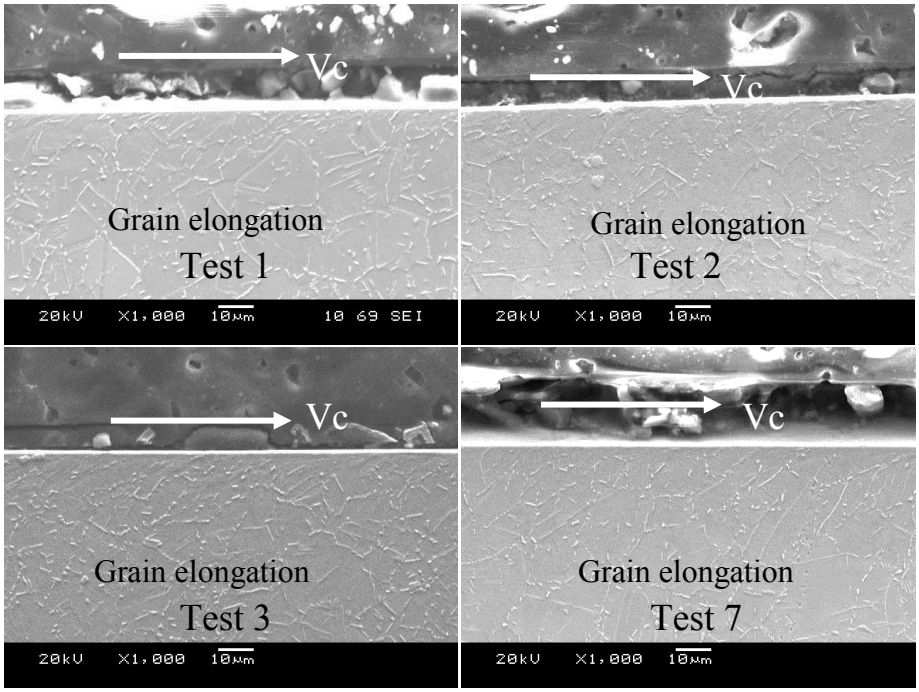

Figure 190: Cross sectional SEM images of workpiece sub-surface of Tests 1, 2, 3 and 7 produced with new tools in a direction perpendicular to feed

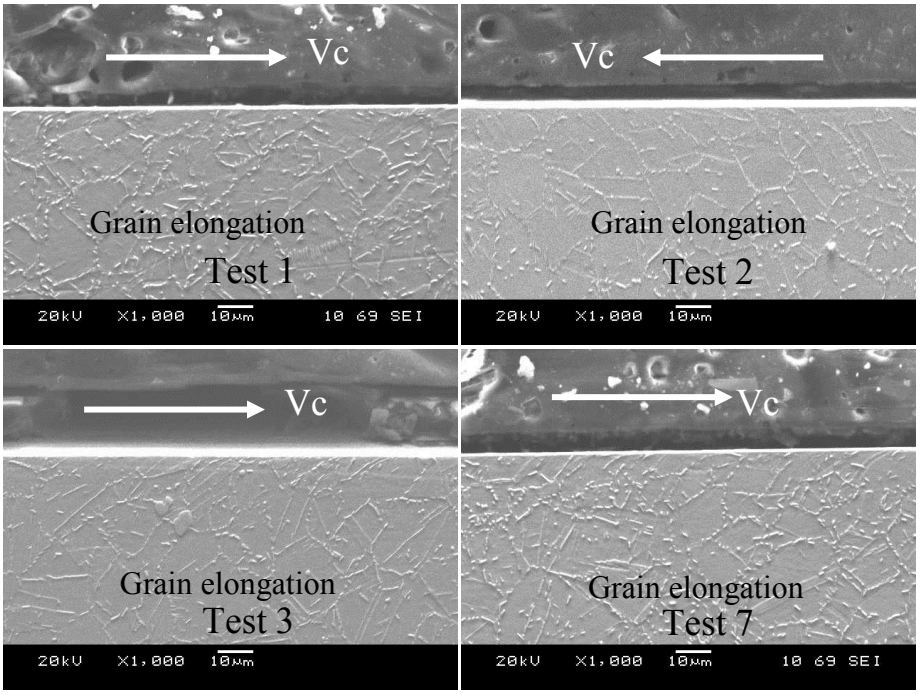

Figure 191: Cross sectional SEM images of workpiece sub-surface of Tests 1, 2, 3 and 7 produced with worn tools in a direction perpendicular to feed

4.7 Phase 3A: Evaluation of alternative PCBN grade and coatings on tool wear/life, surface roughness and cutting forces

4.7.1 Tool wear/life

Figure 192 shows the evolution of flank wear against machining time for the various coated/uncoated PCBN inserts at different cutting speeds. When turning at 200m/min, all of the inserts tested showed evidence of fracture together with BUE or adhered/welded chips on the rake face, see optical micrograph of tool wear progression of uncoated and TiSiN coated inserts and SEM micrographs of all inserts in Figures 193 and 194 respectively. Despite this, a maximum tool life of 8.8min was obtained in Test 2 with the TiSiN coated insert, which was ~35% longer compared to the uncoated tool in Test 1 (6.4min). All of the other coated inserts however failed due to the fracture mode with tool life less than 0.9min. Replication of Tests 5 and 6 yielded similar results. A possible reason for the poor performance of the various coated inserts (TiSiN/TiAlN, AlCrN and CrAlN) employed in Tests 3-6 was deterioration of cutting edge strength. This was due to the coating process or the surface preparation methods employed for the PCBN substrate, which weakened the cutting edges, hence unable to resist the ploughing effect, occurred in the presence of BUE.

Examination of the inserts prior to the machining using the SEM revealed poor cutting edge definition and coating adhesion, especially around the vicinity of the edge radius for the AlCrN and CrAlN (both 3 and 5.5µm thick) coated tools, see Figure 195. Conversely, the

TiSiN and TiSiN/TiAlN coated as well as uncoated PCBN inserts showed uniform cutting edges, although microspores were visible on the surfaces of the TiSiN/TiAlN coated tools which may indicate poor adhesion between the TiSiN/TiAlN layers. According to Bouzakis et al. [162], such condition may lead to premature removal of coating and hence decline in performance during machining. Additionally, the superior tool life obtained with the TiSiN product compared to the multilayer TiSiN/TiAlN coating was possibly due to the higher hardness ~4079HV, which is 500HV higher compared to the latter. Previous research has suggested that coating hardness is the principal criteria governing tool life in continuous turning operations [163-164].

Tool life when operating at cutting speeds of 300 and 450m/min typically resulted in tool lives of ~3 and 1 min respectively, with coatings providing no discernible benefits/difference in performance. Unlike trials at 200m/min cutting speed, insert wear progression was uniform in all experiments carried out at 300 and 450m/min, with no indication of tool fracture even at test cessation, see example of wear scar micrographs in Figure 196. Figure 197 shows SEM micrographs of uncoated and TiSiN/TiAlN coated inserts at the end of tool life after turning at a cutting speed of 300 and 450m/min. Crater wear and workpiece adhesion were prevalent in all of the inserts analysed, irrespective of cutting parameters or surface condition. Similar wear pattern were observed with the other 4 coating products as shown in Figures E1 (300m/min) and E2 (450m/min) of Appendix E.

Despite the poor edge integrity/adhesion, the performance of the TiSiN/TiAlN, AlCrN, CrAlN-3µm and CrAlN-5.5µm coated products were comparable to the uncoated and TiSiN coated inserts when operating at Vc of 300m/min and 450m/min. This suggests that at a cutting speed of 200m/min, all of the tools failed due to greater ploughing caused by the presence of BUE. However, although the BUE diminished at higher cutting speeds of 300 and 450m/min, the elevation in cutting temperature subsequently caused the removal of the coatings revealing the PCBN substrate, therefore no significant difference in the performance of coated and uncoated products were recorded.

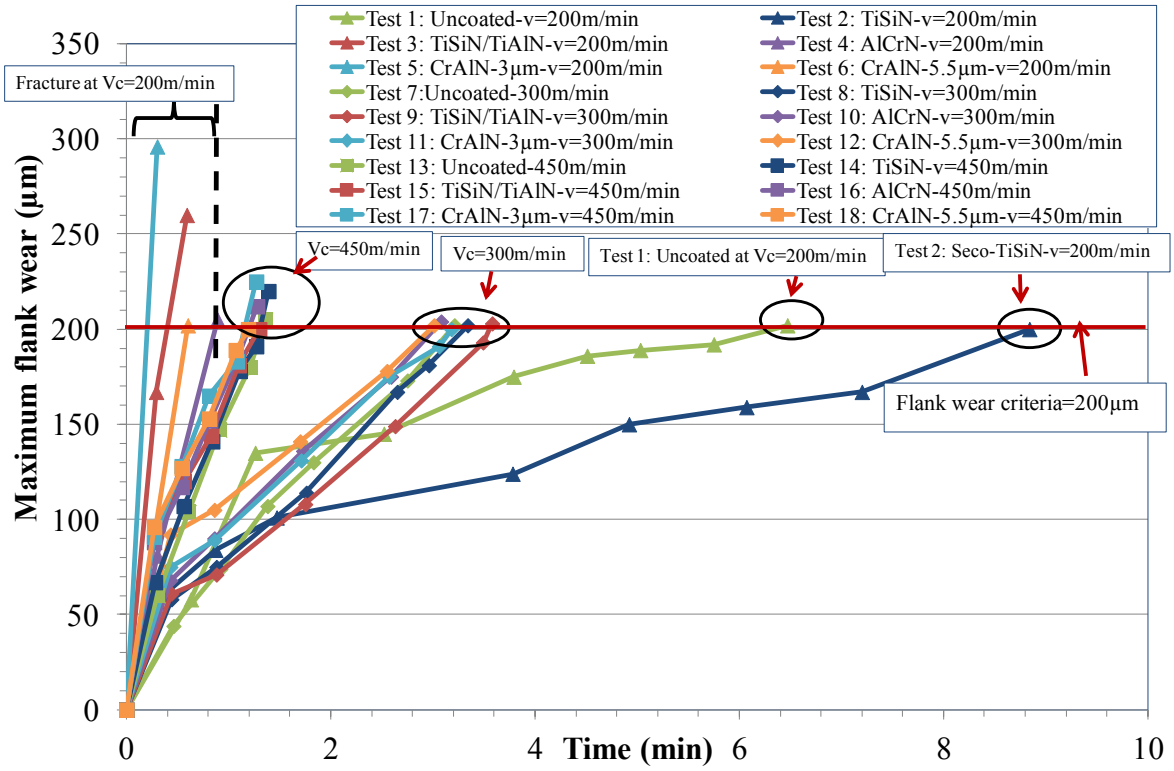

Figure 192: Maximum flank wear against machining time

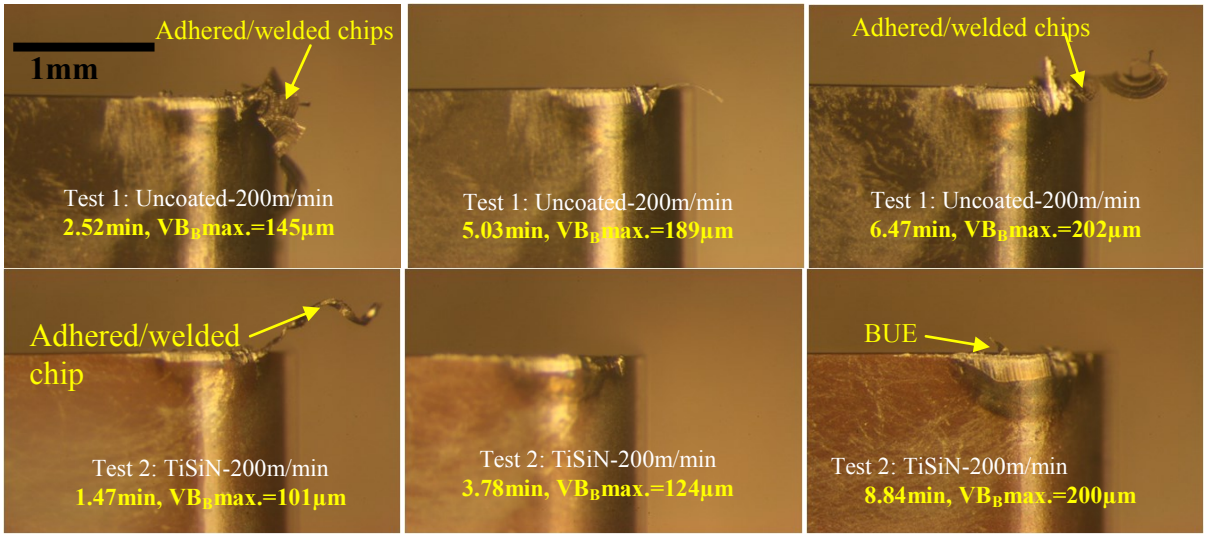

Figure 193: Wear scar progression of uncoated and TiSiN coated inserts at cutting speed of 200m/min

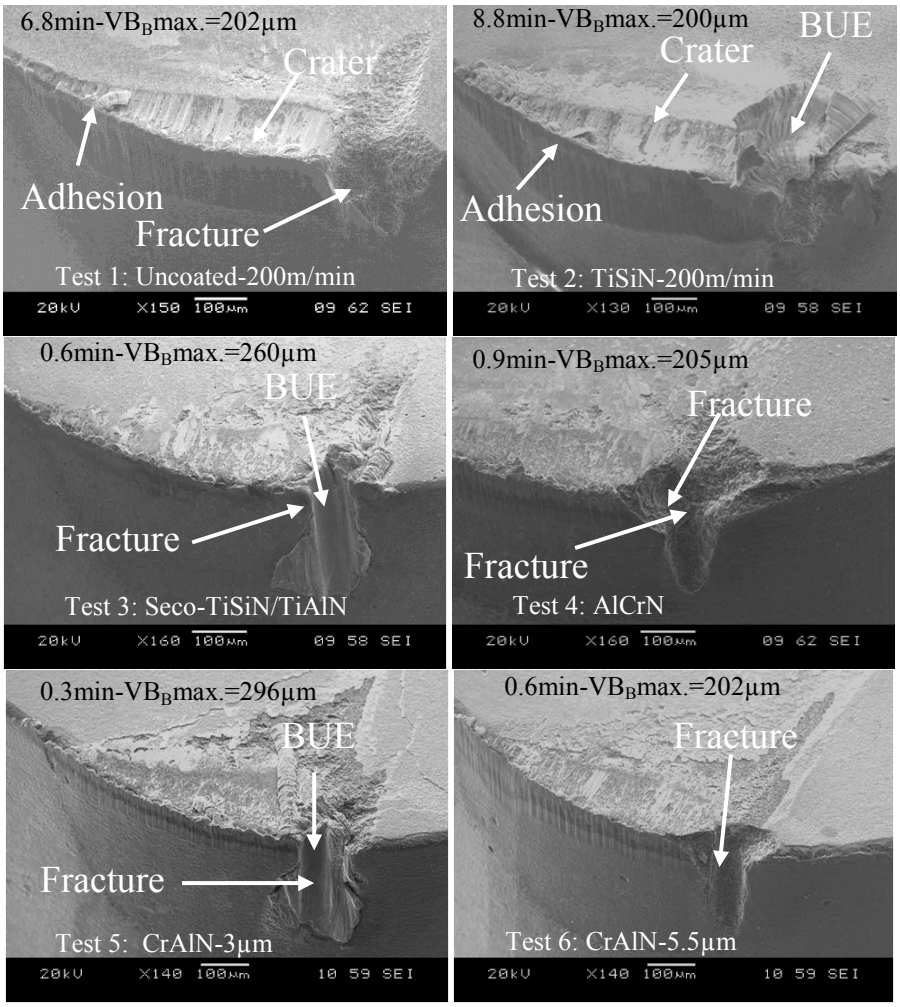

Figure 194: SEM micrographs at the end of tool life of Tests 1, 2, 3, 4, 5 and 6 at cutting speed of 200m/min

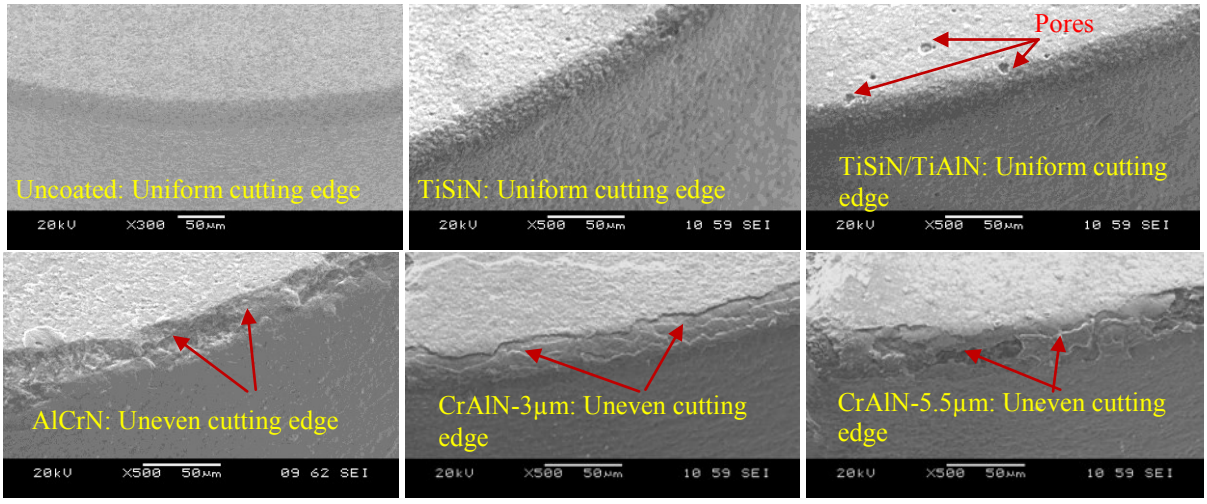

Figure 195: SEM micrographs of new cutting edges of uncoated/coated inserts

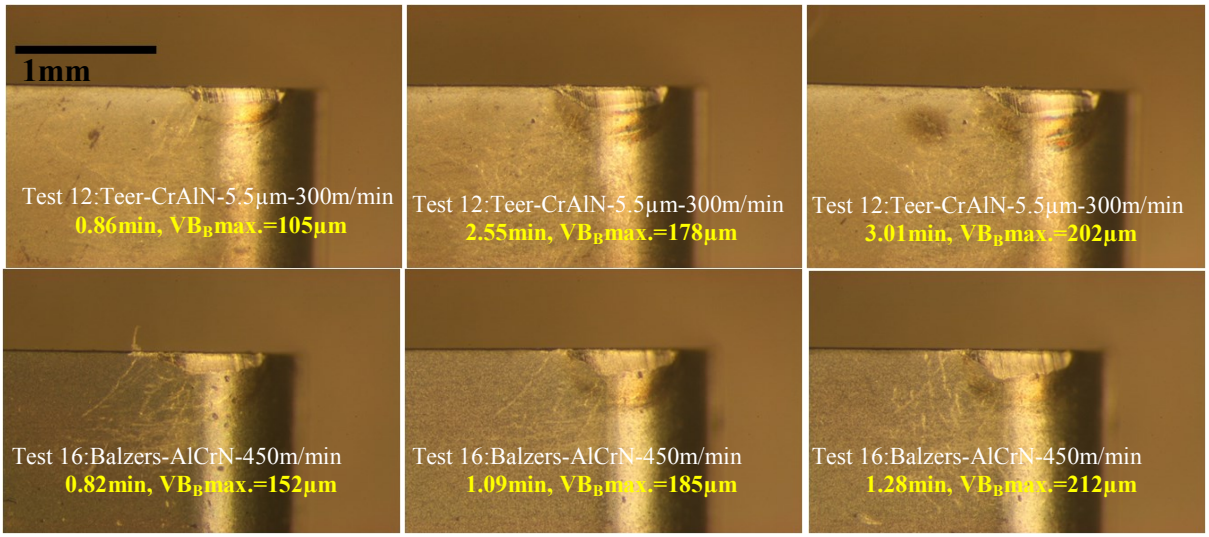

Figure 196: Wear scar progression of Tests 12 and 16 at cutting speeds of 300m/min and 450m/min

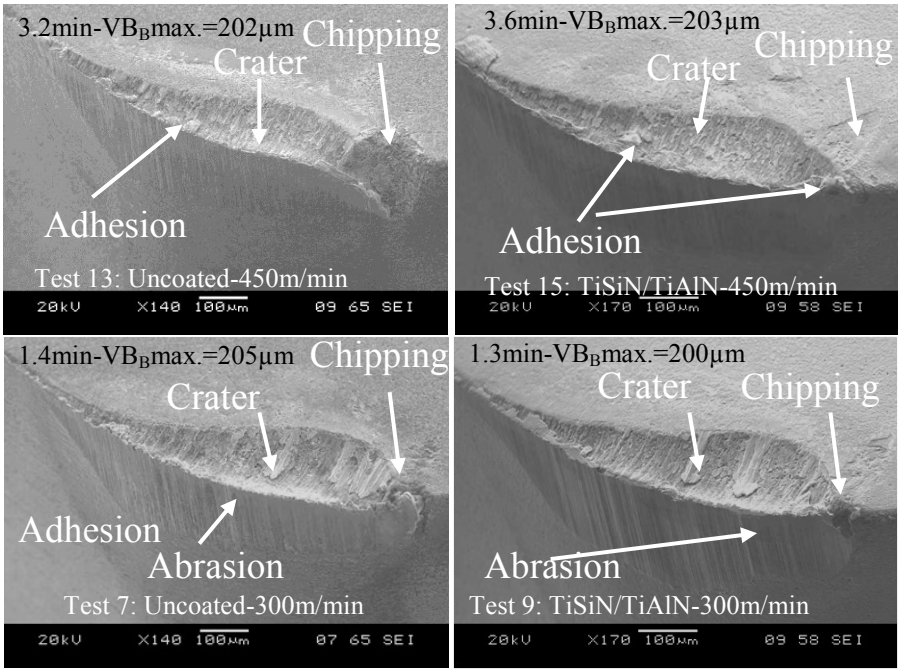

Figure 197: SEM micrographs at the end of tool life of uncoated and TiSiN/TiAlN coated inserts at cutting speeds of 300m/min and 450 m/min

When compared with experiments in Phase 2A (DCC 500 grade), no significant difference in tool lives were obtained for both PCBN grades as detailed in Figure 198. However, in terms of tool wear modes, minor chipping was visible in all of the CBN 170 inserts tested at 300 and 450m/min. This was probably due to smaller nose radius (0.8mm for CBN 170 and 1.2mm for DCC 500) which led to reduced insert edge strength. Corresponding the higher cutting and thrust forces (2-2.5 times) recorded when machining with DCC 500 inserts compared to CBN 170 was attributed to larger nose radius.

Table 35 in the experimental work section highlight the basis of comparison between the current phase and work by M'Saoubi et al. [126]. The tool life based on 200µm flank wear was extrapolated from the latter work as shown in Figure E3 of Appendix E. The tool life and wear mode results from the uncoated inserts employed at 300m/min were similar in both investigations irrespective of tool geometry. Although tool life with C-type configuration was marginally higher (6.4min) compared to triangular inserts (5.5min) when operating at a cutting speed of 200m/min but no fracture or BUE was seen with the latter, which was possibly due to the difference in tool geometry.

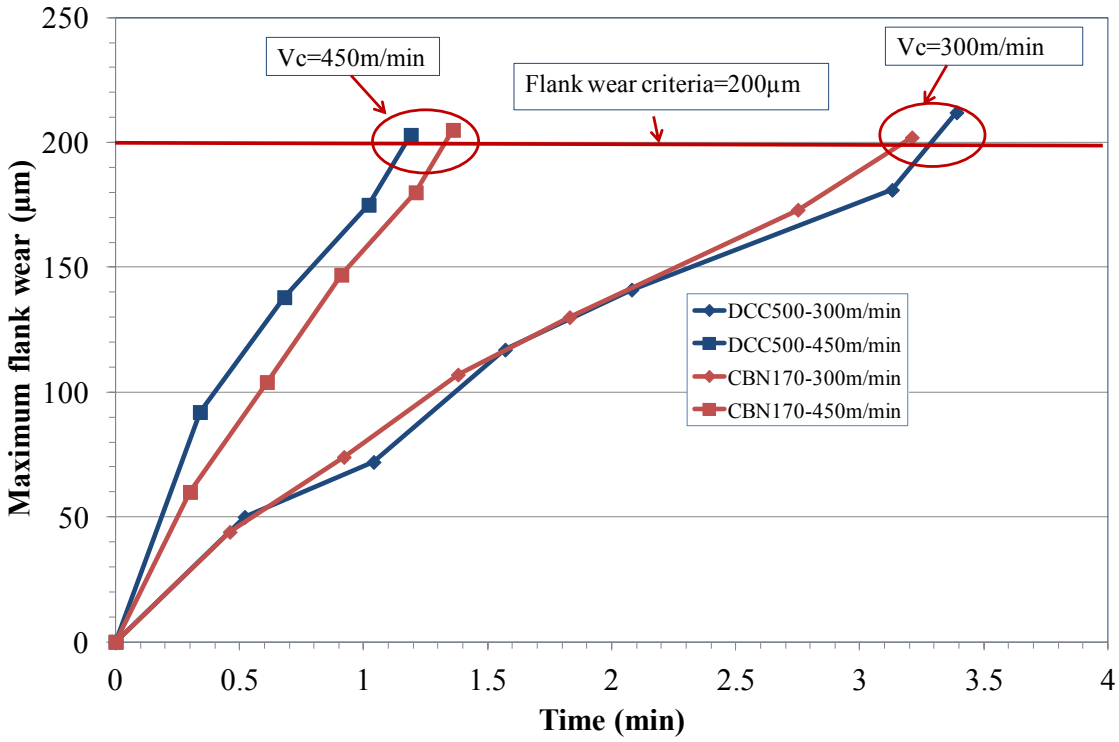

Figure 198: Comparison of tool life between two PCBN grades at 300m/min and 450m/min

Figure 199 shows the main effects plots for tool life with respect to cutting speed and surface condition while the associated ANOVA results are detailed in Table 59. None of the factors were found to be statistically significant with both cutting speed and surface condition showing negligible PCR's of 4.90% and 2.25% respectively. An extremely high error of 92.85% was obtained, which was either due to interactions between factors or the fracture seen in Tests 3, 4, 5 and 6. Unfortunately, the interaction between cutting speed and surface condition could not be included in the ANOVA model due to the lack of degrees of freedom (10) available in the experimental design. If the interaction was included in the analysis, then there will be no degrees of freedom for estimating the experimental error. Full interaction plots of tool life are shown in Figure E4 of Appendix E.

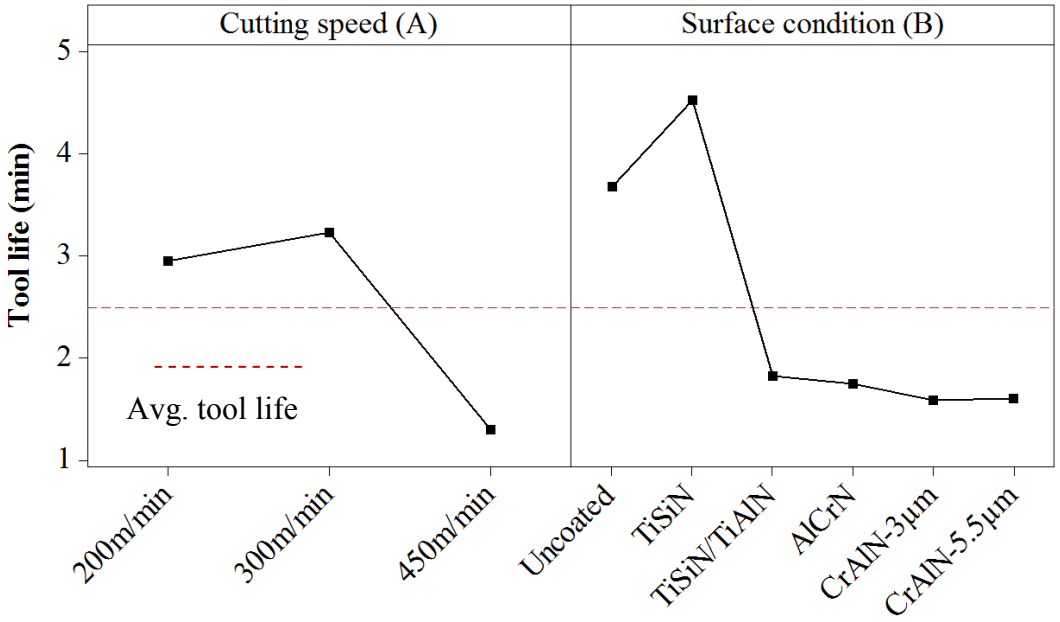

Figure 199: Main effects plots-means for tool life (Phase 3A)

Table 59: ANOVA table for tool life (Phase 3A)

Factors	DF	SS	MSS	F	P	PCR (%)
Cutting speed (A)	2	13.096	6.584	1.45	0.280	4.90
Surface condition (B)	5	24.470	4.894	1.08	0.426	2.25
Error	10	45.204	4.520			***92.85***
Total	17	82.770	R-Sq(Adj)=7.15			

4.7.2 Chip analysis

Despite the generation of helical chips (see Figure 200), no swarf entanglement problem with the workpiece material occurred in any of the performed trials. Figure 201 details SEM micrographs of chip morphology from various tests. Serrated chip formation was observed in all trials which was likely due to catastrophic thermoplastic shear at the primary deformation zone, similar to results in Phase 2A.

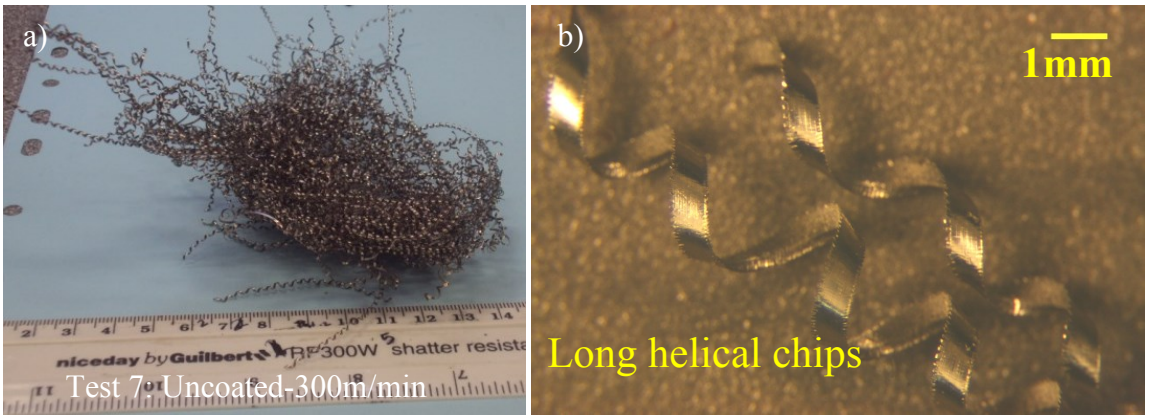

Figure 200: Chip morphology from (a) Test 7 and (b) optical micrograph of long helical chips

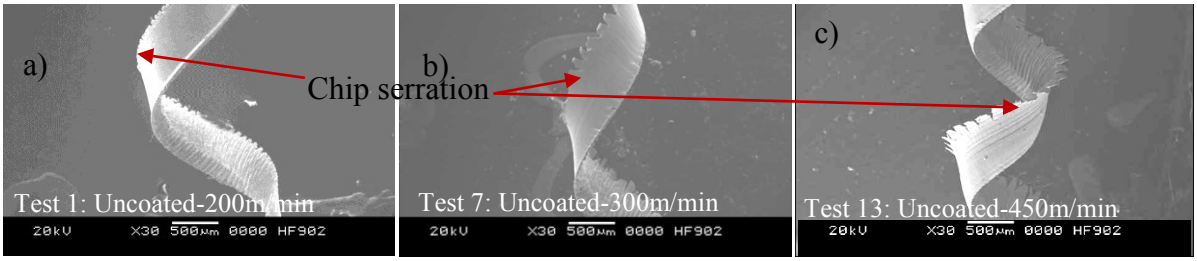

Figure 201: SEM micrographs of chip morphology from (a) Test 1, (b) Test 7 and (c) Test 13

4.7.3 Surface roughness

In general, a decreasing trend in workpiece surface roughness was observed up to a flank wear of ~130µm due to formation of a wiper flat radius (Figure 202), which subsequently remained stable in the range of 0.25-0.50 µm Ra until the end of tool life, except for Tests 3, 4, 5 and 6 where tool fracture occurred; see Figure 203. Figures 204 and 205 show the main effects plots for surface roughness with both new and worn tools respectively. None of the factors were statistically significant over the range of parameters tested irrespective of the tool condition with an error PCR of 100% and 76.03% calculated for new and worn inserts respectively as detailed in Table 60. This was most likely due to the surface roughness being influenced by feed rate and tool nose radius, which were kept constant in the present phase of experiments.

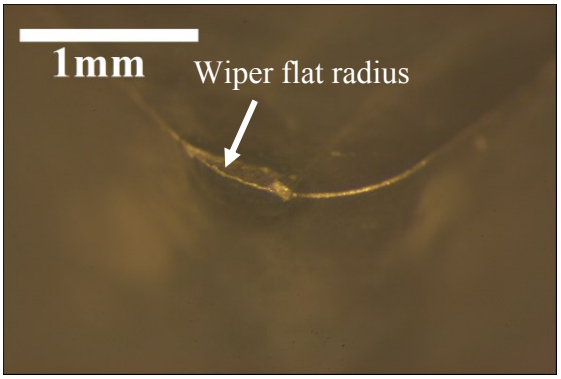

Figure 202: Optical micrograph of worn insert from Test 9

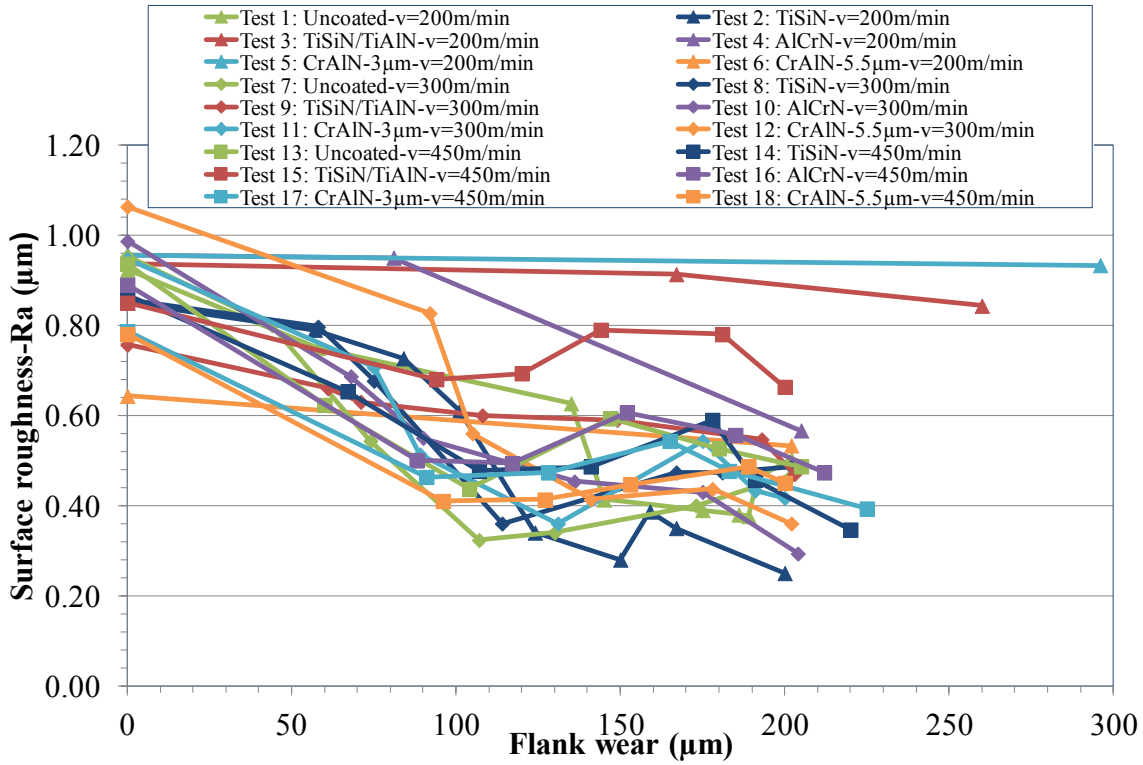

Figure 203: Evolution of workpiece surface roughness against tool flank wear

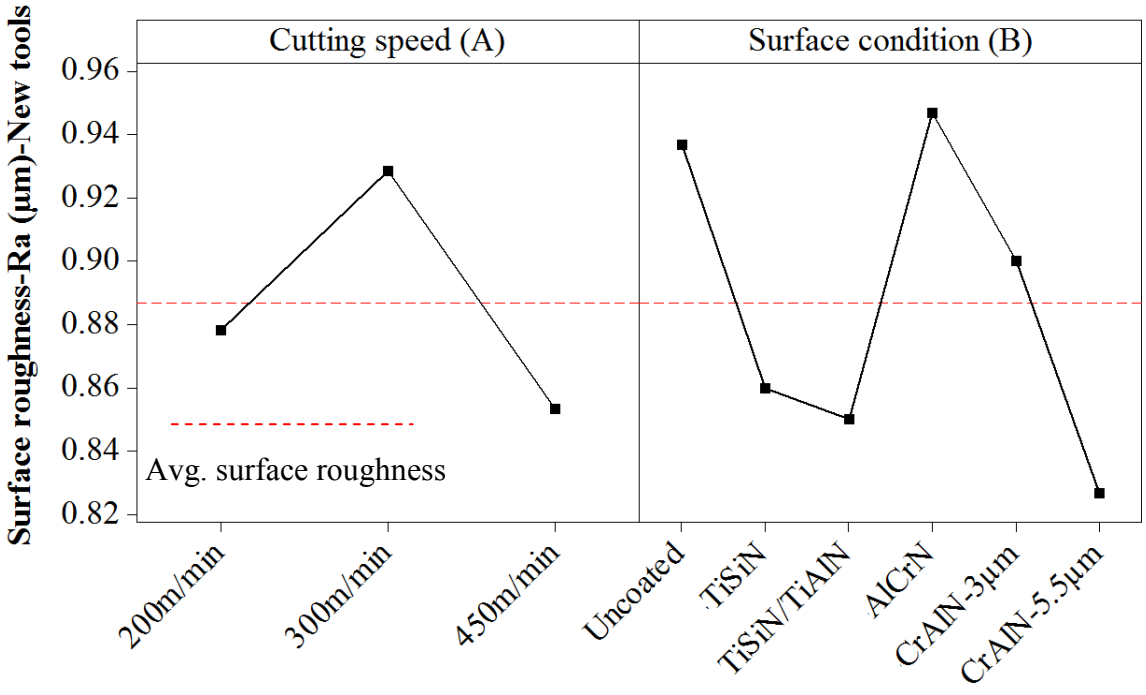

Figure 204: Main effects plots-means for surface roughness with new tools (Phase 3A)

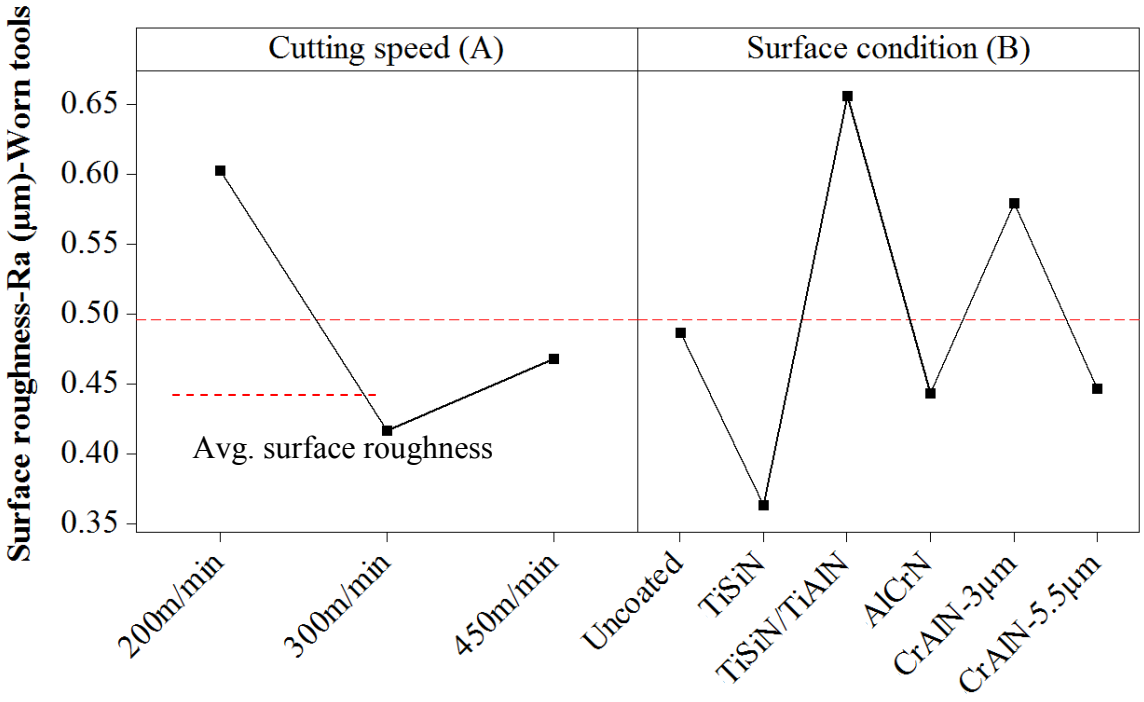

Figure 205: Main effects plots-means for surface roughness with worn tools (Phase 3A)

Table 60: P-value and PCR's for surface roughness with new and worn tools (Phase 3A)

Factors	DF	New		Worn	
		P	PCR (%)	P	PCR (%)
Cutting speed (A)	2	0.491	0	0.134	13.16
Surface condition (B)	5	0.684	0	0.278	10.81
Error	10		***100***		***76.03***
Total	17	R-Sq(Adj)=0		R-Sq(Adj)=23.97	

4.7.4 Cutting forces

4.7.4.1 Cutting force component

Cutting forces were observed to rise steadily (up to 170N) with machining time, particularly in trials where tool wear progression was uniform (Vc=300m/min and 450m/min). In addition, forces did not exceed 175N at the end of tool life in Tests 3, 4, 5 and 6 despite the inserts fracturing shortly after cutting commenced (<1min tool life); see Figure 206. Corresponding main effects plots are detailed in Figures 207 and 208 for new and worn inserts respectively, but with none of the factors having a statistically significant influence on cutting force, see Table 61. The high error levels seen for both new (76.8%) and worn (95.73%) tools were either due to the premature tool failures or interactions between the factors, which was not accounted for in the ANOVA model.

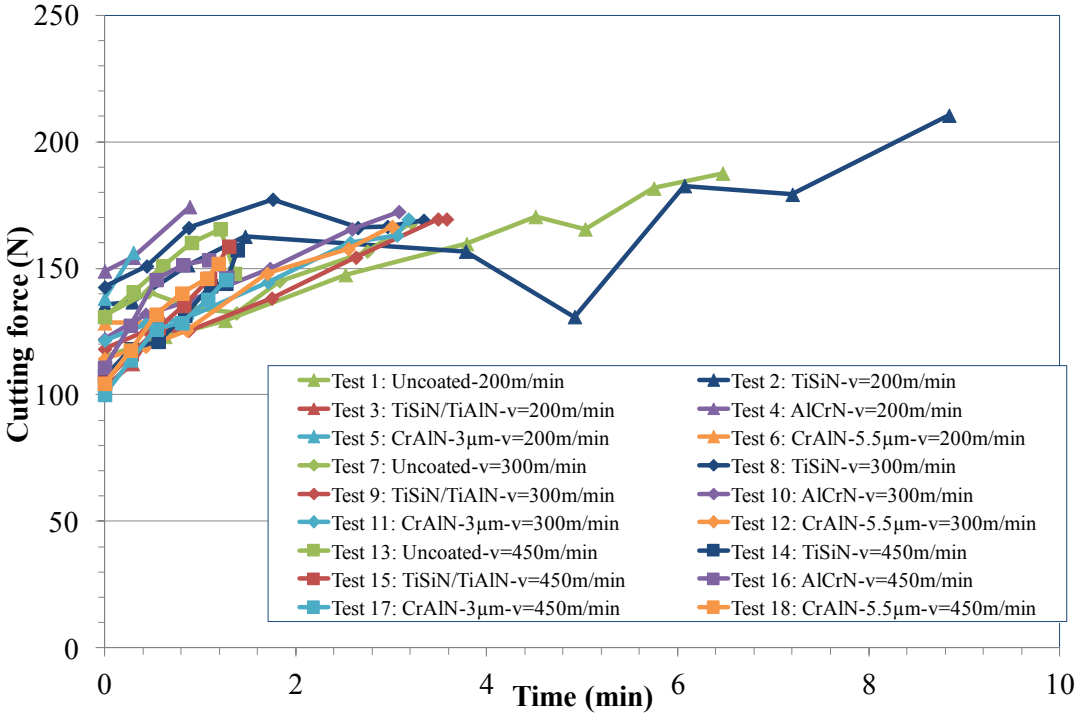

Figure 206: Cutting force against machining time

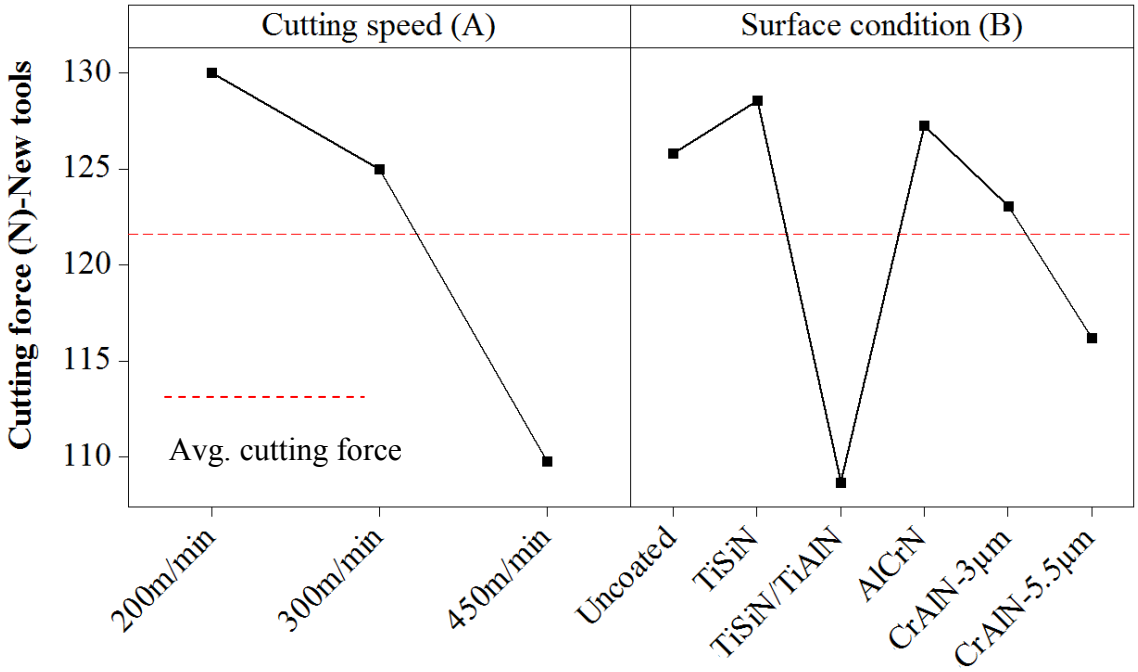

Figure 207: Main effects plots-means for cutting force with new tools (Phase 3A)

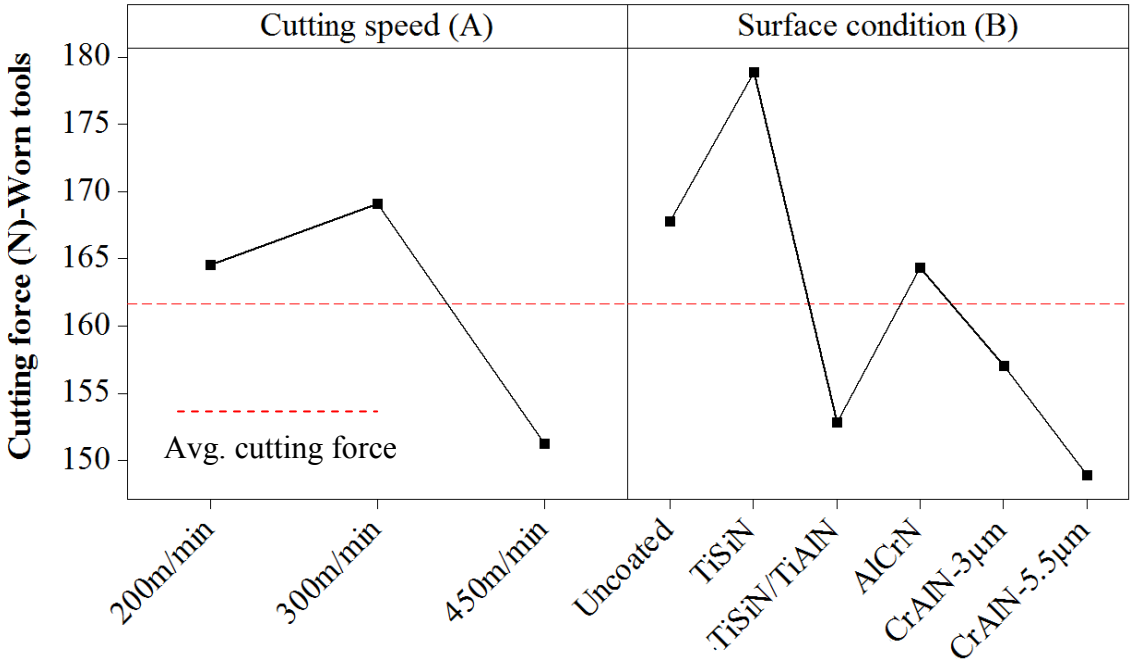

Figure 208: Main effects plots-means for cutting force with worn tool (Phase 3A)

Table 61: P-value and PCR's for cutting force with new and worn tools

Factors	**DF**	**New**		**Worn**	
		P	**PCR (%)**	**P**	**PCR (%)**
Cutting speed (A)	2	0.069	23.2	0.288	4.63
Surface condition (B)	5	0.494	0	0.468	0
Error	10		***76.8***		***95.37***
Total	17	R-Sq(Adj)=23.2		R-Sq(Adj)=4.63	

4.7.4.2 Thrust force component

Figure 209 shows the evolution of thrust forces against machining time for all trials. For Tests 3, 4, 5 and 6 (where fracture occurred with tool life <0.90min), the rise in thrust force over the test duration was < 35N while the levels ranged between 190-284N at test cessation for trials where tool wear progression was uniform. Main effects plots for thrust force are highlighted in Figures 210 and 211 for new and worn tools respectively. Similar to the cutting force component, neither cutting speed nor surface condition was found to be statistically significant when employing either new or worn tools with errors of 58% and 64.49% respectively, see Table 62, although surface condition showed a moderately high PCR of 34% for new inserts.

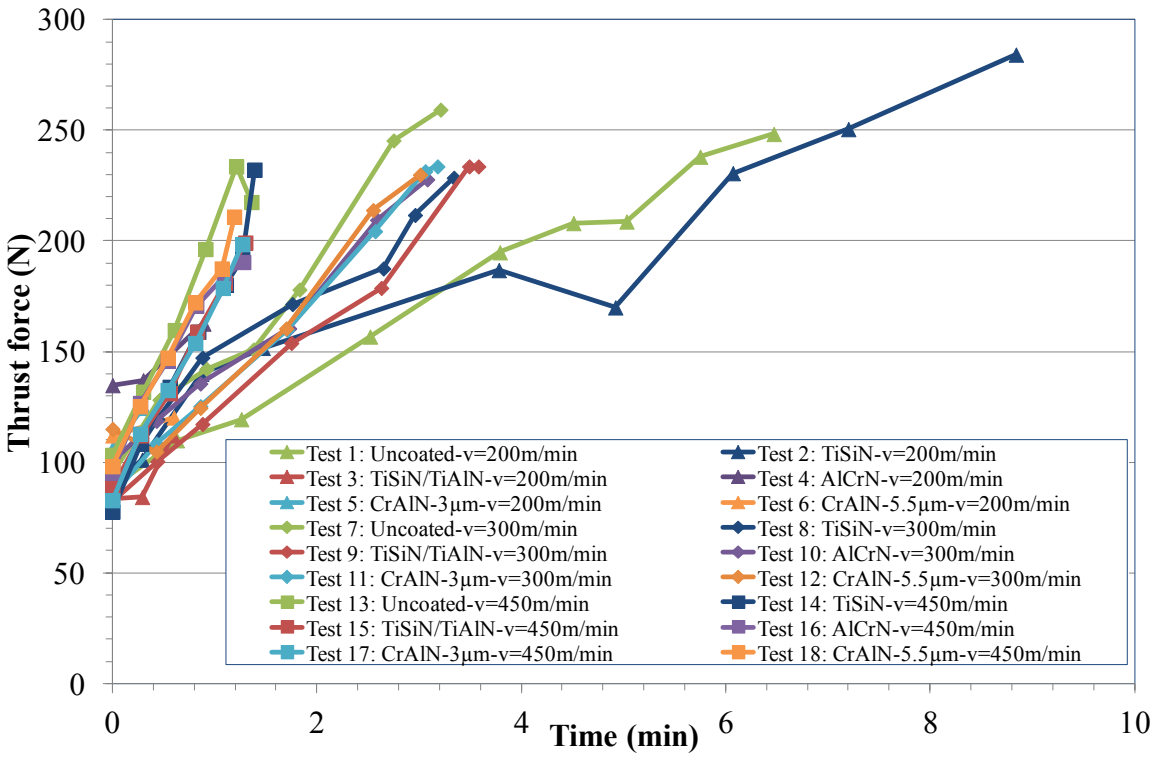

Figure 209: Thrust force against machining time

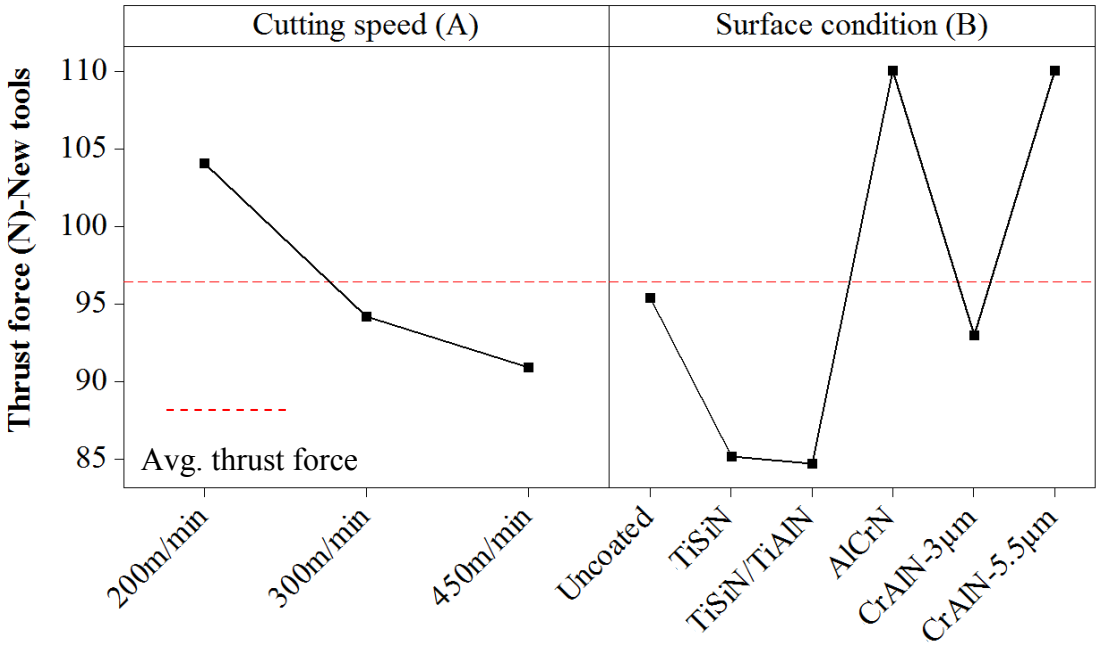

Figure 210: Main effects plots-means for thrust force with new tools (Phase 3A)

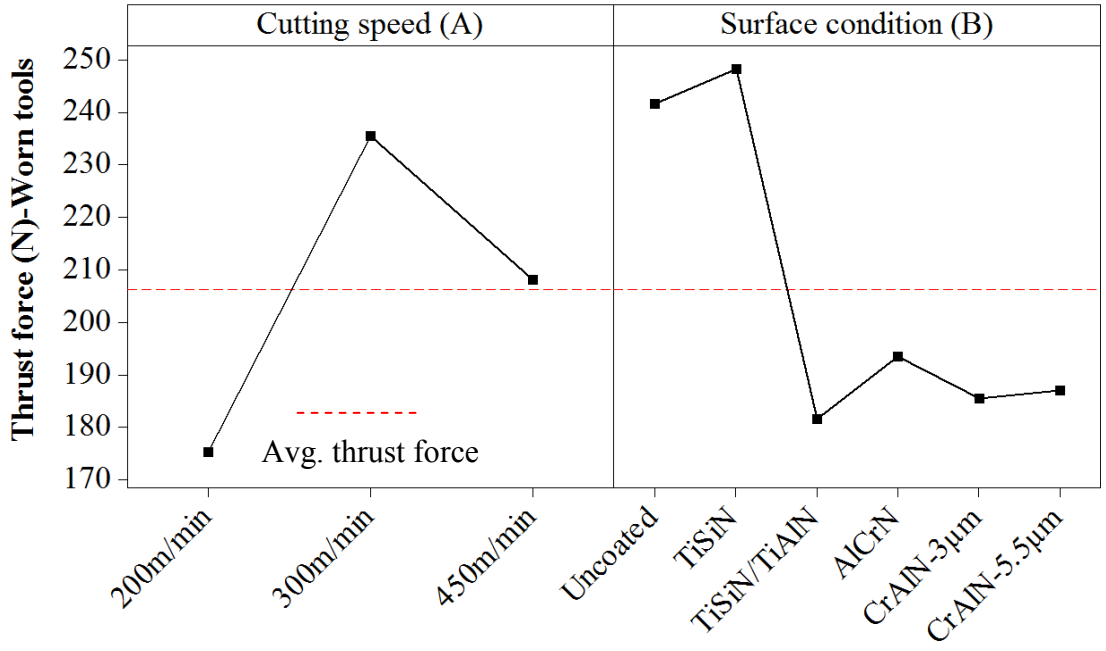

Figure 211: Main effects plots-means for thrust force with worn tools (Phase 3A)

Table 62: P-value and PCR's for thrust force with new and worn tools

Factors	**DF**	**New**		**Worn**	
		P	**PCR (%)**	**P**	**PCR (%)**
Cutting speed (A)	2	7.98	7.98	0.066	19.82
Surface condition (B)	5	0.066	34.02	0.195	15.69
Error	10		***58***		***64.49***
Total	17	R-Sq(Adj)=42		R-Sq(Adj)=35.51	

4.7.4.3 Feed force component

In general, feed force was found to increase two-fold over the test duration but did not exceed 125N even at the end of tool life, see Figure 212. Figures 213 and 214 show the main effects plots with new and worn tools respectively. As seen with the cutting and thrust force component, ANOVA calculations showed that none of the factors were statistically significant relative to feed force. Large error levels for both new and worn inserts were obtained with corresponding PCR's 98.9% and 77.3% respectively, as shown in Table 63. Not being statistically significant, surface condition had a moderate PCR of 16.69% with worn tools.

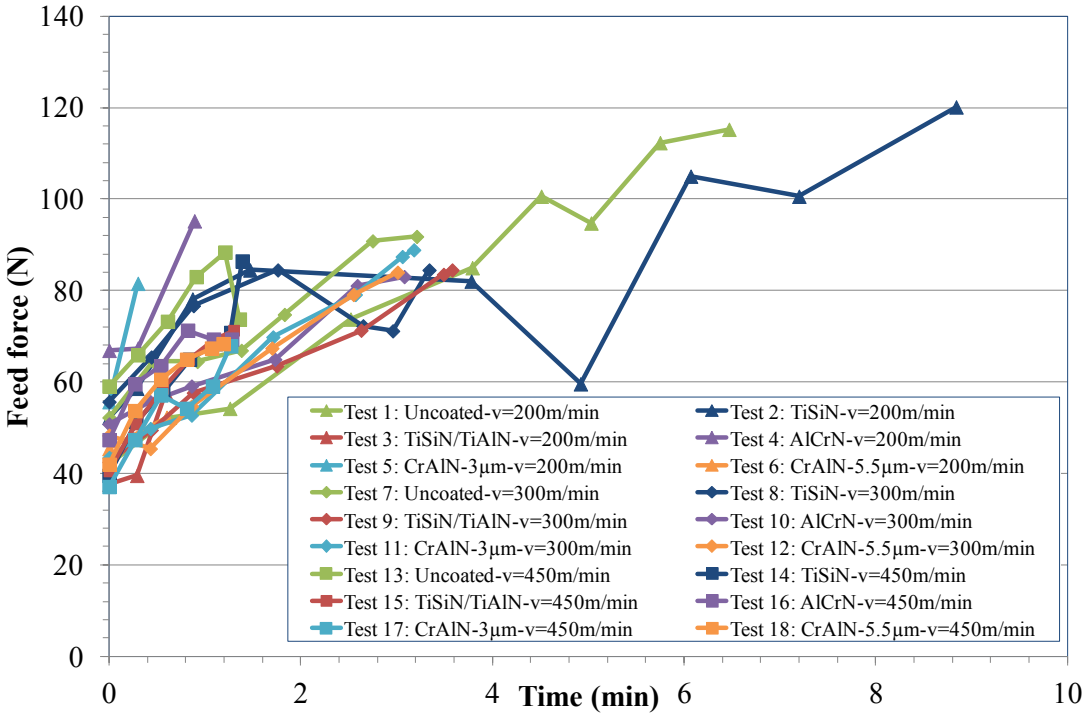

Figure 212: Feed force against machining time

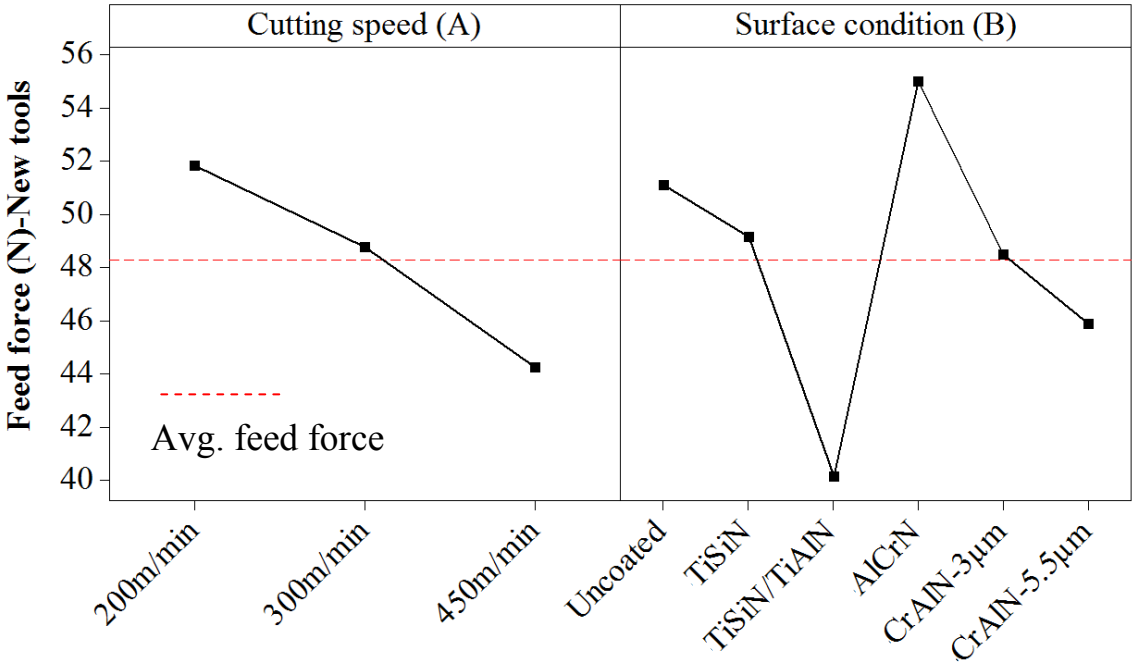

Figure 213: Main effects plots-means for feed force with new tools (Phase 3A)

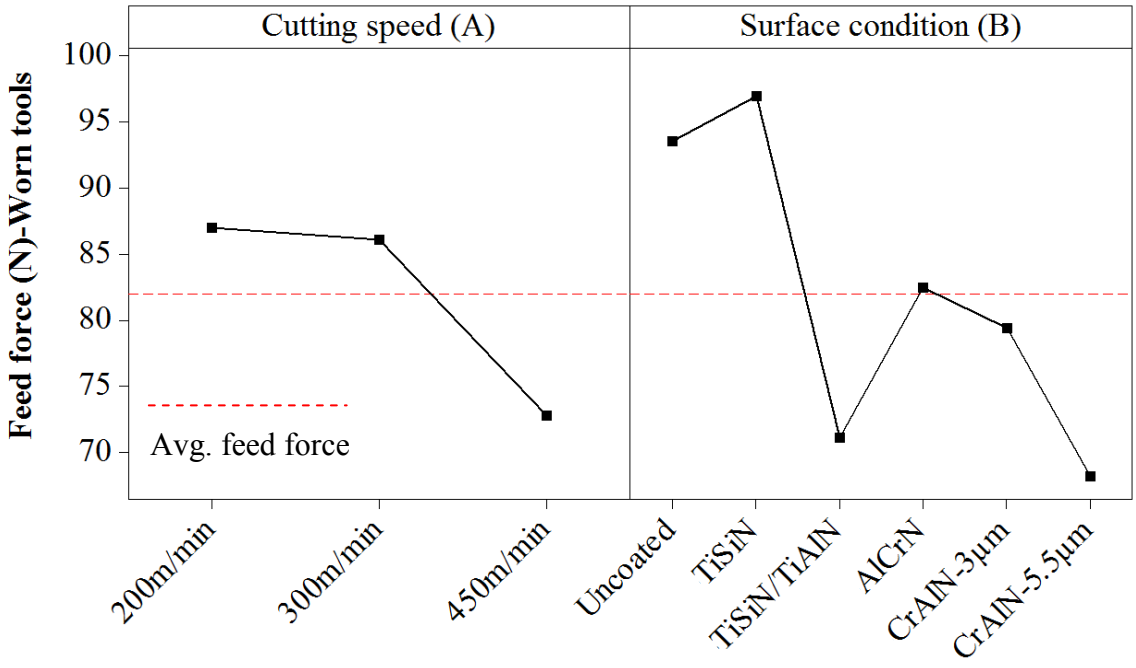

Figure 214: Main effects plots-means for feed force with worn tools (Phase 3A)

Table 63: P-value and PCR's for feed force with new and worn tools

Factors	DF	New		Worn	
		P	PCR (%)	P	PCR (%)
Cutting speed (A)	2	0.372	1.10	0.247	5.58
Surface condition (B)	5	0.490	0	0.215	16.69
Error	10		***98.9***		***77.73***
Total	17	R-Sq(Adj)=1.1		R-Sq(Adj)=22.27	

4.8 Phase 3B: Effect of alternative PCBN grade and tool coatings on workpiece surface integrity

4.8.1 Workpiece surface damage

Examples of machined surfaces produced using uncoated and TiSiN coated PCBN inserts which were examined using the SEM, are shown in Figures 215 and 216. Feed marks were observed on all machined surfaces, however it was difficult to distinguish between grooves and feed marks, particularly on surfaces machined with worn inserts. Higher magnification SEM inspection further revealed the presence of 1-2 microcracks per ~10,000µm^2 on specimens machined with worn tools irrespective of the operating parameter and surface condition, however no damage was recorded with new tools as shown in Figure 217. The results however were comparable to surfaces obtained in Phase 2B (machined with DCC grade inserts).

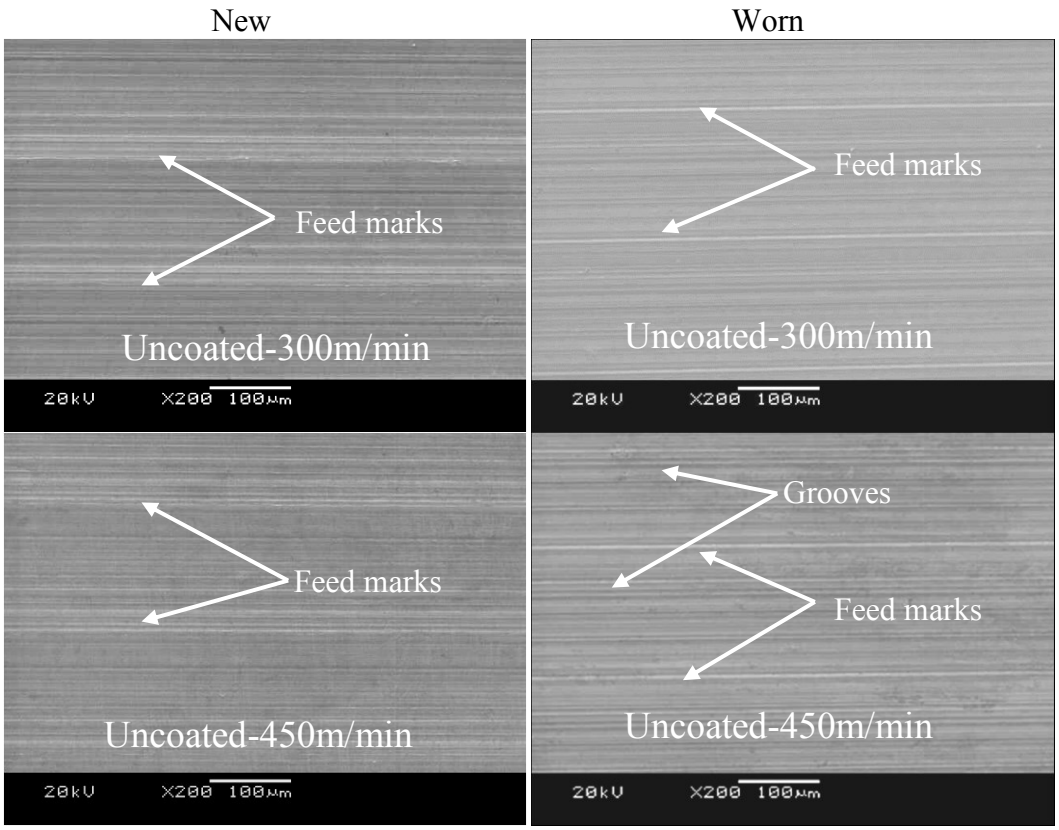

Figure 215: Workpiece surfaces following machining with new and worn uncoated inserts at 200X magnification

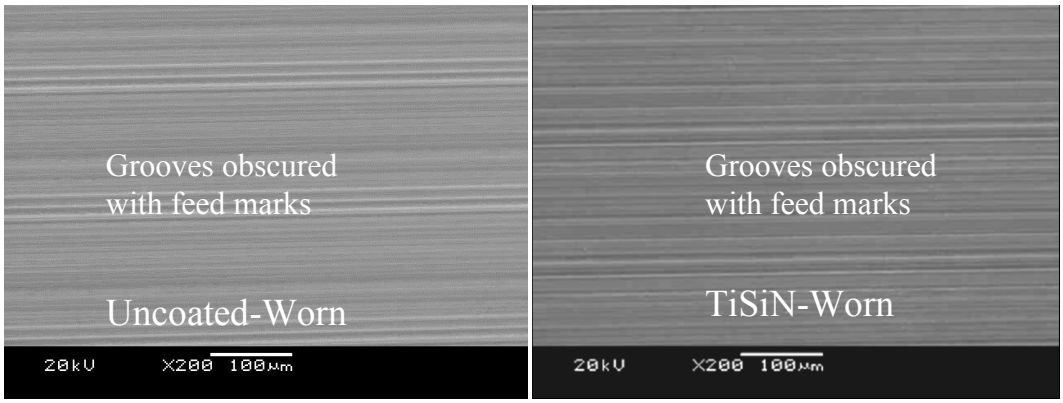

Figure 216: Workpiece surfaces following machining with worn uncoated and TiSiN coated inserts at cutting speed of 200m/min at 200X magnification

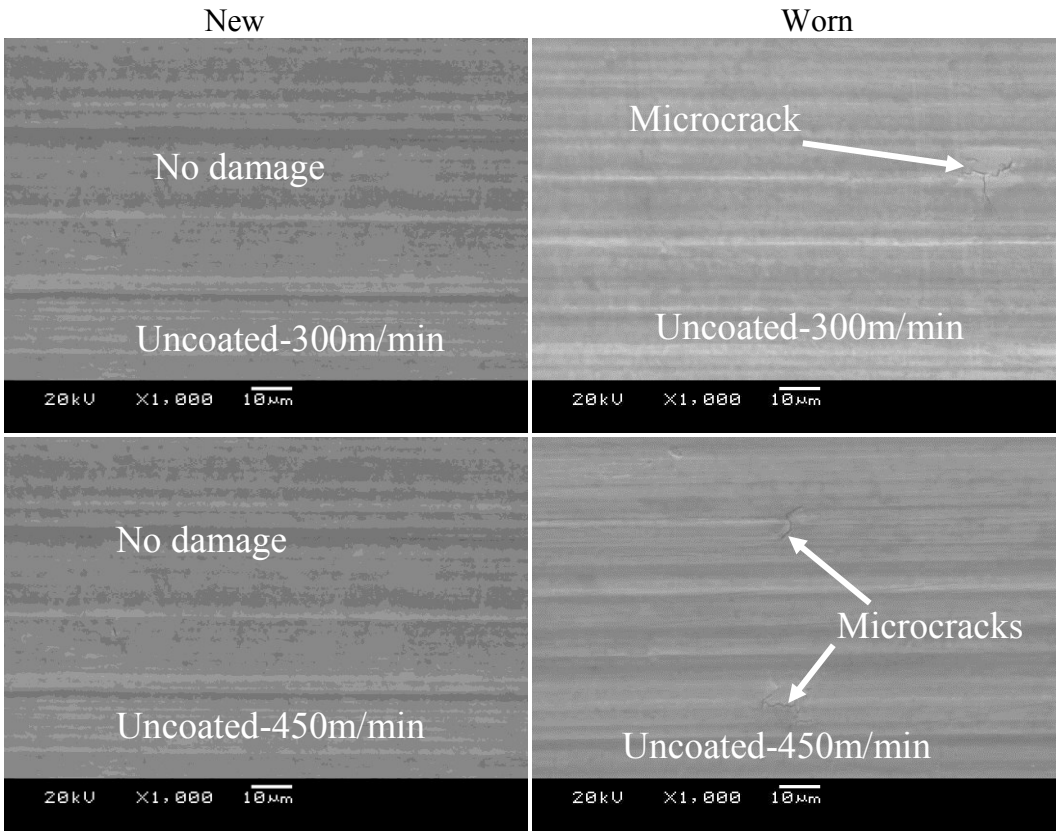

Figure 217: Higher magnification SEM micrographs of workpiece surfaces following machining with new and worn uncoated PCBN inserts

4.8.2 Microhardness

Figure 218 and 219 shows the microhardness depth profile of surfaces machined with new and worn inserts respectively, measured parallel to the feed direction. In general, no significant strain hardening was observed when utilising new tools, irrespective of the insert surface condition and cutting speed. An increase in workpiece hardness of up to ~60$HK_{0.025}$ above the bulk value and to a depth of ~50µm was however apparent in the experiment employing the worn TiSiN coated insert at 200m/min cutting speed. This was attributed to BUE formation as well as insert fracture, which occurred under these test condition. Lower levels of strain hardening up to ~35$HK_{0.025}$ over the bulk hardness extending to a depth of ~40µm was also seen when using uncoated worn inserts at cutting speeds of 300 and 450 m/min.

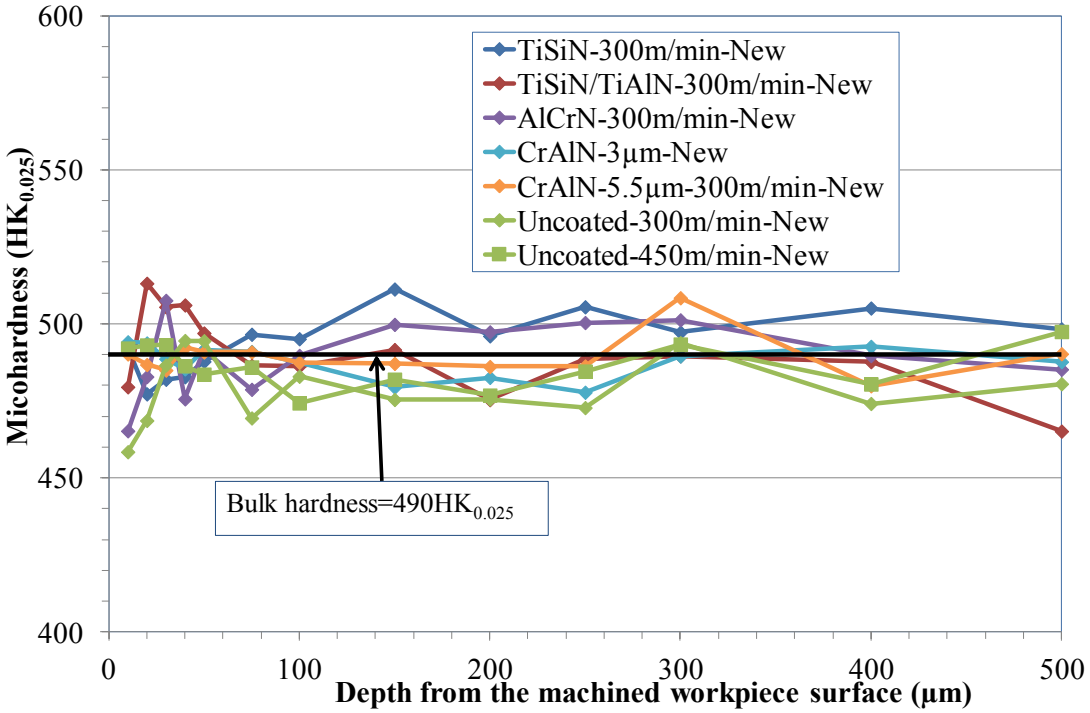

Figure 218: Microhardness depth profiles of surfaces machined using new tools in a direction parallel to the feed

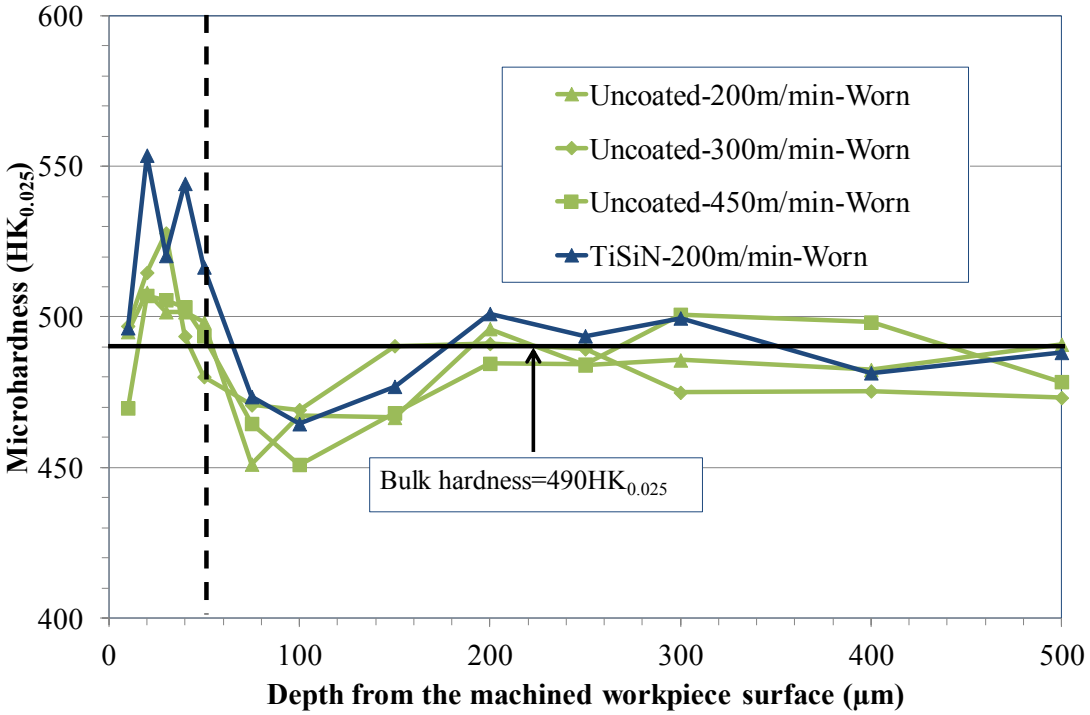

Figure 219: Microhardness depth profiles of surfaces machined using worn tools in a direction parallel to the feed

Microhardness depth profiles of workpiece surfaces machined with new and worn tools measured perpendicular to the feed direction are shown in Figures 220 and 221 respectively. In the case of new inserts, no significant strain hardening was apparent when turning at

300m/min except when employing the CrAlN-5.5µm coating, which resulted in hardened layer to a maximum of 544$HK_{0.025}$ within 50µm below the machined surface. This was possibly due to the greater coating thickness of the insert (5.5µm) compared to other coating where thicknesses were in the range of 1-3µm. The greater coating thickness was thought to increase the edge radius, which enhanced ploughing due to the larger contact area, hence induced the greater mechanical deformation beneath the machined surface. Workpiece surfaces machined with worn TiSiN coated insert were strain hardened near machined surface up to a maximum value of 565$HK_{0.025}$ and which extended to a depth of ~200µm. An increase in workpiece hardness of up to ~80$HK_{0.025}$ above the bulk value and to a depth of ~100µm was recorded when employing worn uncoated inserts.

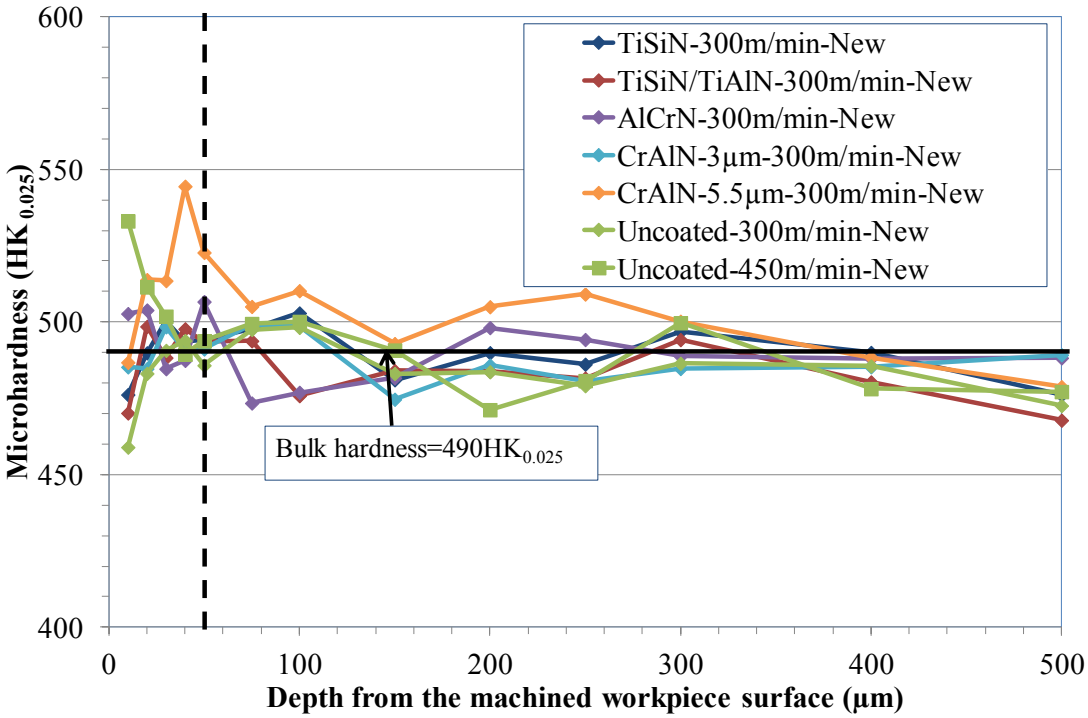

Figure 220: Microhardness depth profiles of surfaces machined using new tools in a direction perpendicular to the feed

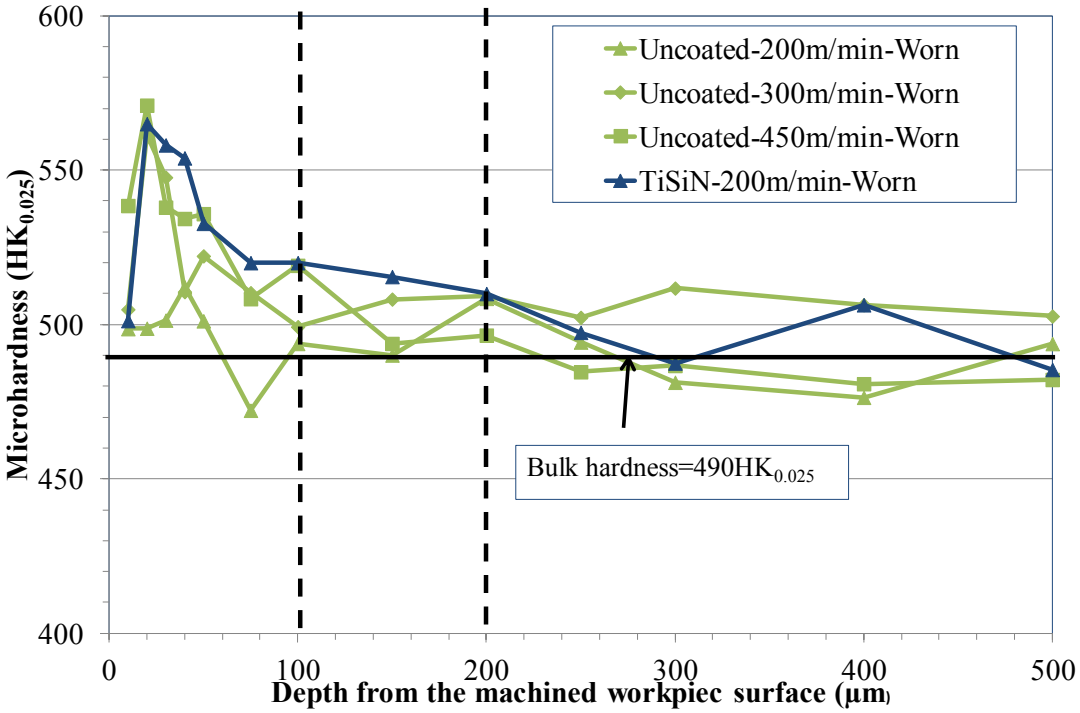

Figure 221: Microhardness depth profile of surfaces machined using worn tools in a direction perpendicular to the feed

4.8.3 Microstructure

Grain elongation directly beneath the machined surface in the direction perpendicular to the feed was evident up to a depth of ~15-20µm in specimens turned with new tools except the CrAlN-5.5µm coated insert, where it extended to ~30µm beneath the machined surface due to the larger contact area associated with it. The extent of microstructural deformation was also ~30µm beneath the machined surface when employing worn inserts due to the greater contact area between the tool and workpiece resulting in higher levels of ploughing and rubbing. In contrast, no obvious signs of sub-surface microstructural damage were observed in any of the samples viewed parallel to the feed direction as shown in Figures 222-229. Further inspection of all surfaces machined with worn tools examined under the SEM revealed no evidence of white layer formation irrespective of surface condition and cutting speed for workpieces sectioned parallel and perpendicular to the feed direction respectively, see Figures 230 and 231.

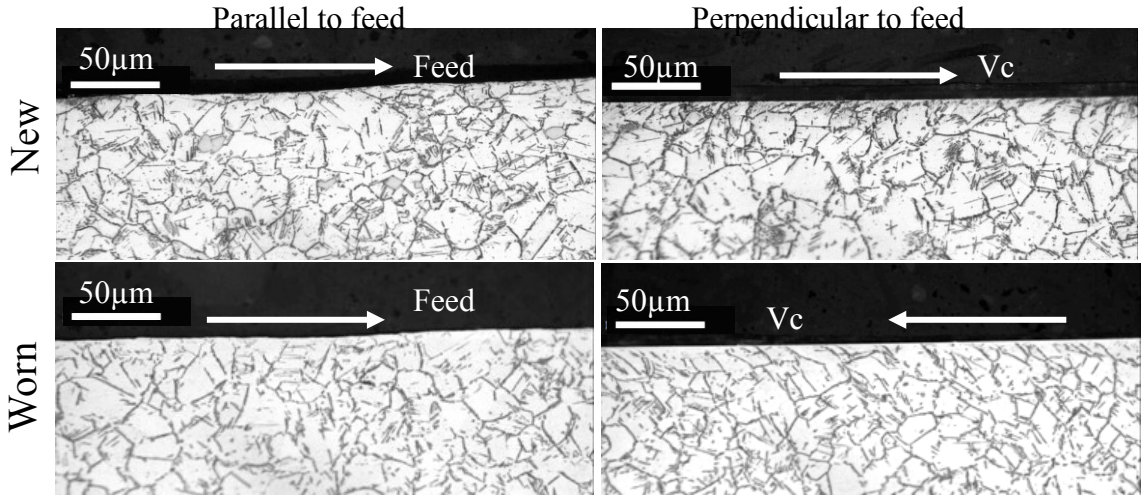

Figure 222: Cross-sectional optical micrographs of machined workpiece sub-surface produced with uncoated tools at cutting speed of 300m/min

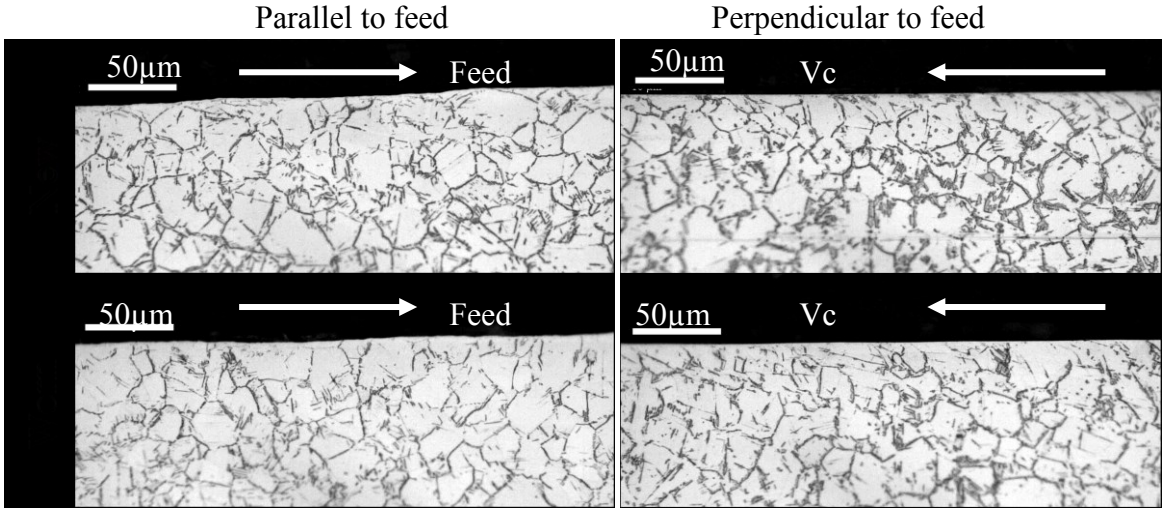

Figure 223: Cross-sectional optical micrographs of machined workpiece sub-surface produced with uncoated tools at cutting speed of 450m/min

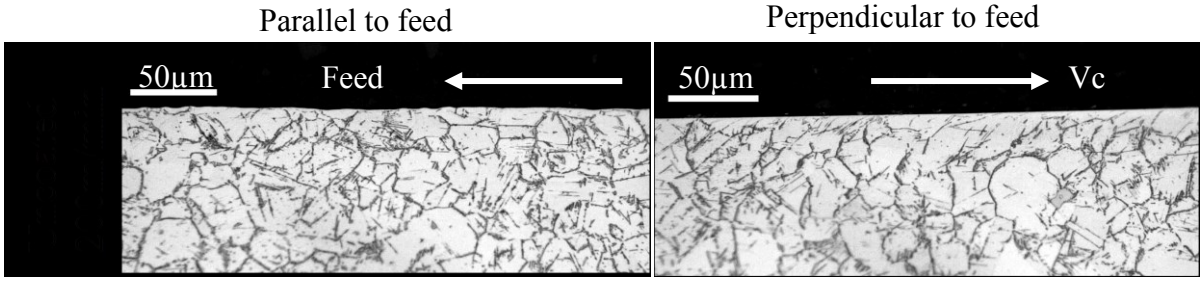

Figure 224: Cross-sectional optical micrographs of machined workpiece sub-surface produced with worn uncoated tool at cutting speed of 200m/min

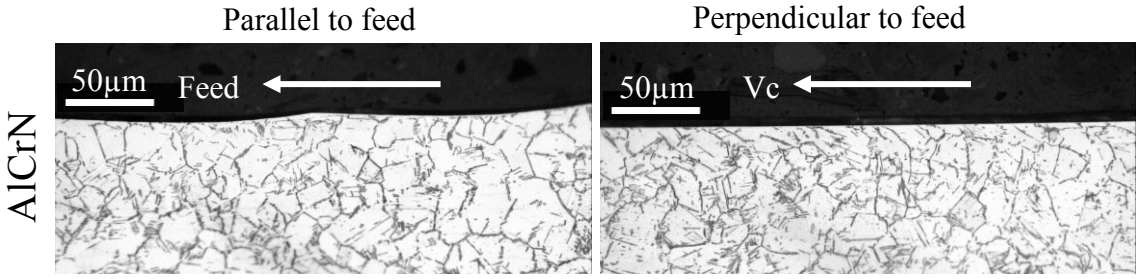

Figure 225: Cross-sectional optical micrographs of machined workpiece sub-surface produced with new AlCrN coated tool at cutting speed of 300m/min

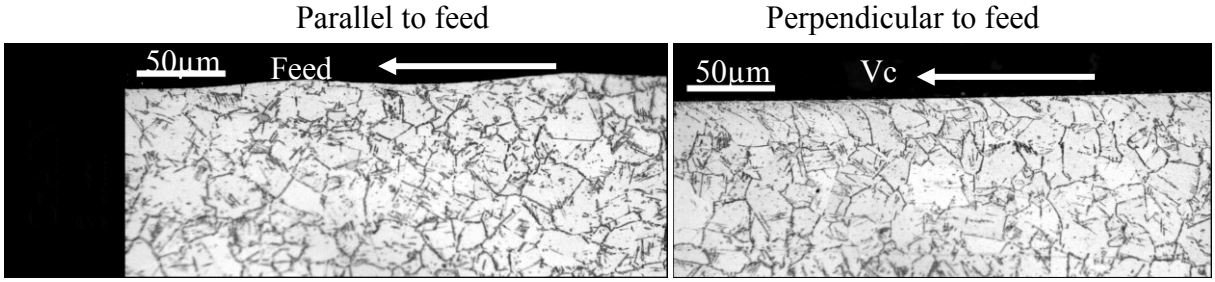

Figure 226: Cross-sectional optical micrographs of machined workpiece sub-surface produced with new CrAlN-3µm coated tool at cutting speed of 300m/min

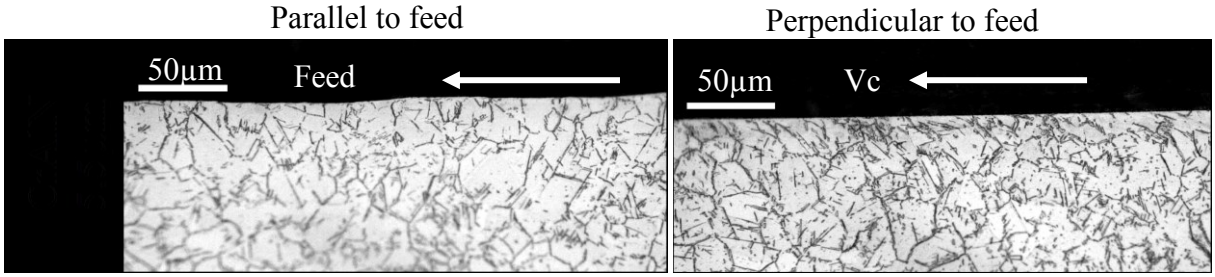

Figure 227: Cross-sectional optical micrographs of machined workpiece sub-surface produced with new CrAlN-5.5µm coated tool at cutting speed of 300m/min

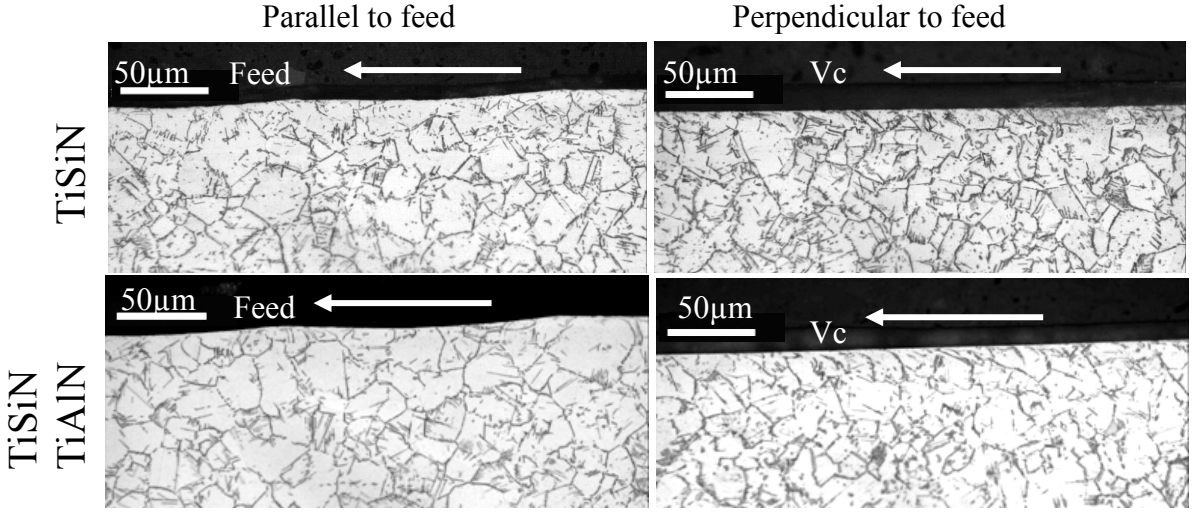

Figure 228: Cross-sectional optical micrographs of machined workpiece sub-surface produced with new TiSiN and TiSiN/TiAlN coated tool at cutting speed of 300m/min

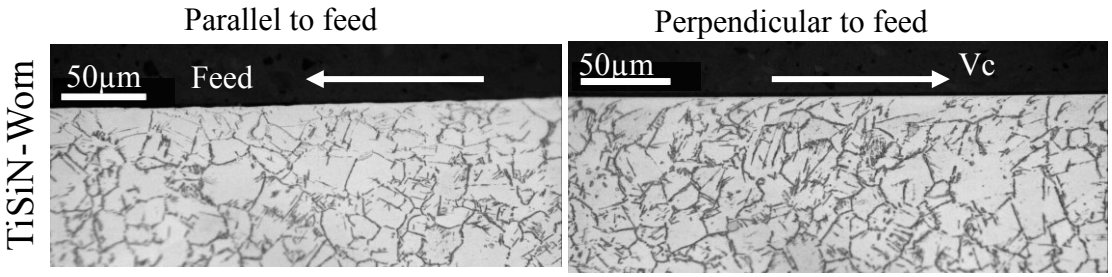

Figure 229: Cross-sectional optical micrographs of machined workpiece sub-surface produced with worn TiSiN coated tool at cutting speed of 200m/min

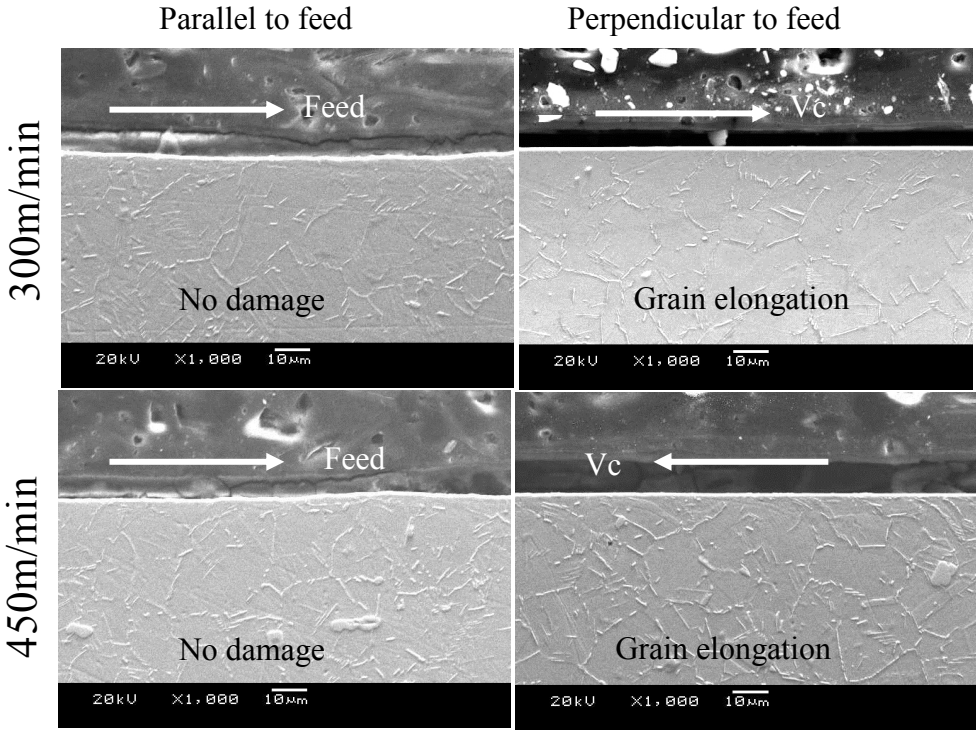

Figure 230: Cross-sectional SEM images of machined workpiece sub-surface produced with worn uncoated tools at cutting speeds of 300 and 450 m/min

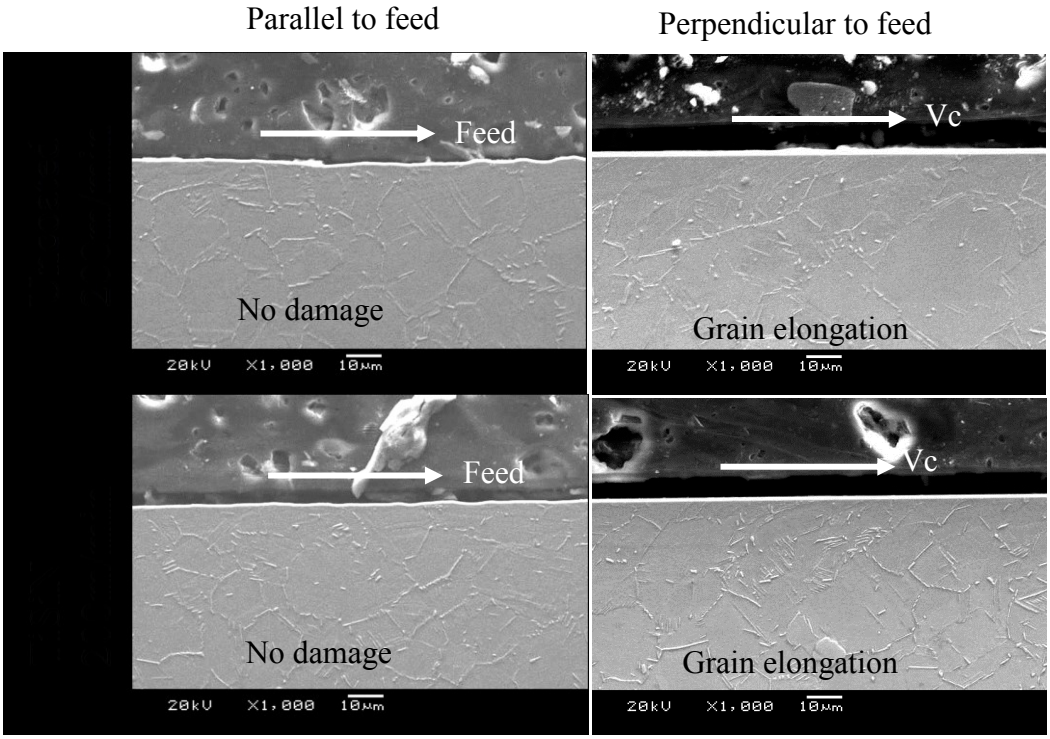

Figure 231: Cross-sectional SEM images of machined workpiece sub-surface produced with worn uncoated and TiSiN coated tools at cutting speed of 200m/min

4.9 Phase 3C: Effect of PCBN grades and cutting environment on residual stresses

Typically, 'hook' shaped residual stress depth profiles were observed for each of the machined surfaces investigated, irrespective of the test conditions. This corresponded to published data by Bushlya et al. [111] who recorded similar trends when high speed turning Inconel 718 using PCBN tools. In general, compressive surface residual stresses were obtained in all of the samples evaluated parallel to the feed direction, conversely corresponding results perpendicular to the feed (cutting speed direction) were predominantly tensile, see Figures 232 and 233. The latter was possibly due to the relatively high cutting speed (300m/min) employed, which likely had an overriding influence on resulting residual stress patterns. Sharman et al. [71, 145] similarly reported that residual stresses when turning Inconel 718 were marginally less tensile/more compressive in surfaces parallel to the feed direction.

The sub-surface residual stresses measured both parallel and perpendicular to the feed direction were compressive in all experiments. The use of the worn insert in Test 2 induced the highest residual stress levels (-1268MPa in the feed direction and -930MPa perpendicular to the feed) with the depth of penetration extending to ~450µm before recovering to the near

neutral stress condition of the bulk material. This was due to the larger area of tool-workpiece contact as a result of insert wear, with mechanical loads most likely being dominated over temperature effects. In contrast, sub-surface compressive residual stresses only extended to a depth of ~100µm below the machined surface when utilising new inserts for the specimens measured in the feed direction. The application of high pressure cutting fluid at 100bar in Test 3 was found to almost double the maximum sub-surface compressive residual stress (-410MPa) compared to 10bar in Test 1 (-240MPa) due to its greater mechanical impact, see Figure 232. An increase in compressive residual stresses of up to 75% was recorded with the CBN 170 (Test 4) compared to the DCC 500 grade (Test 1) and was attributed to the likely higher thermal conductivity in the former as tools with higher CBN content generally exhibit higher thermal conductivity [141].

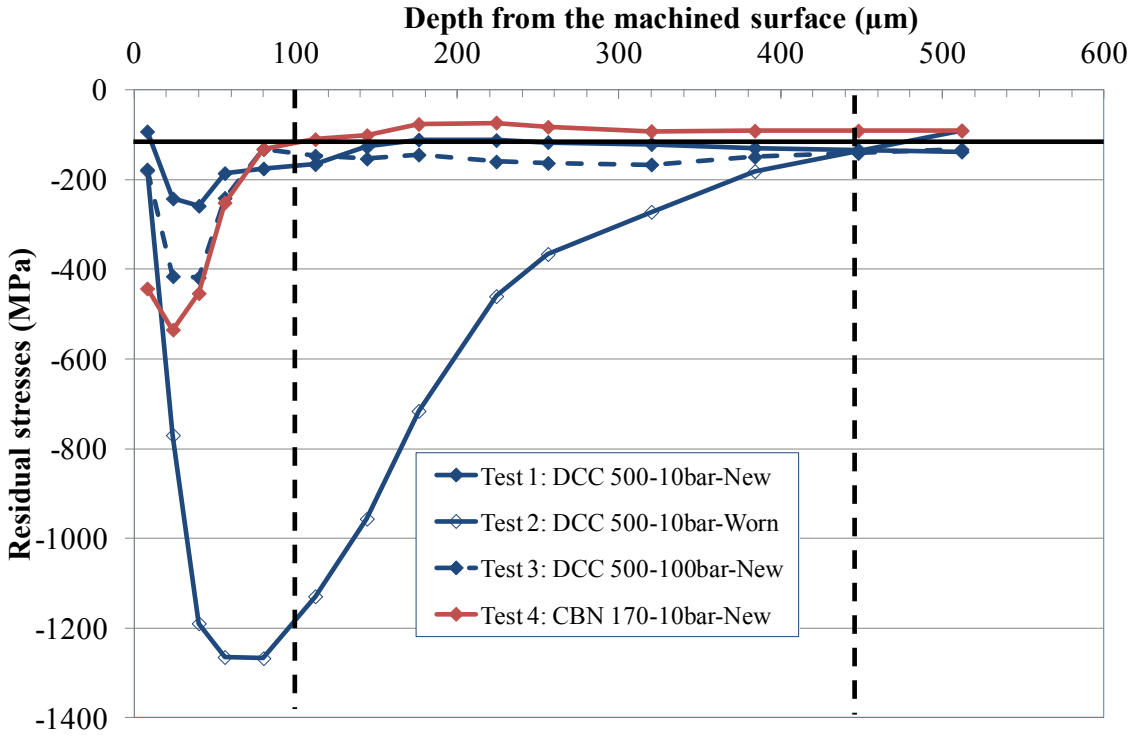

Figure 232: Residual stresses depth profiles measured parallel to the feed direction (σ//)

A similar trend was observed for specimens measured perpendicular to the feed direction where the depth of compressive residual stress penetration was limited to ~140m when machining with new inserts (Test 1, 2 and 4); see Figure 233. In addition, workpieces which exhibited surface tensile residual stresses all crossed over to a compressive regime at ~15-20µm below the machined surface. Maximum sub-surface compressive residual stress was also seen to increase by ~120MPa when employing 100bar fluid pressure (with DCC 500) or using the alternative CBN 170 grade, which was similar to the results for specimens evaluated parallel to the feed direction. However contrary to previously published work [71,

146], there was no appreciable difference in the magnitude of surface residual stresses due to the variation in cutting fluid pressure (Test 1 vs Test 3).

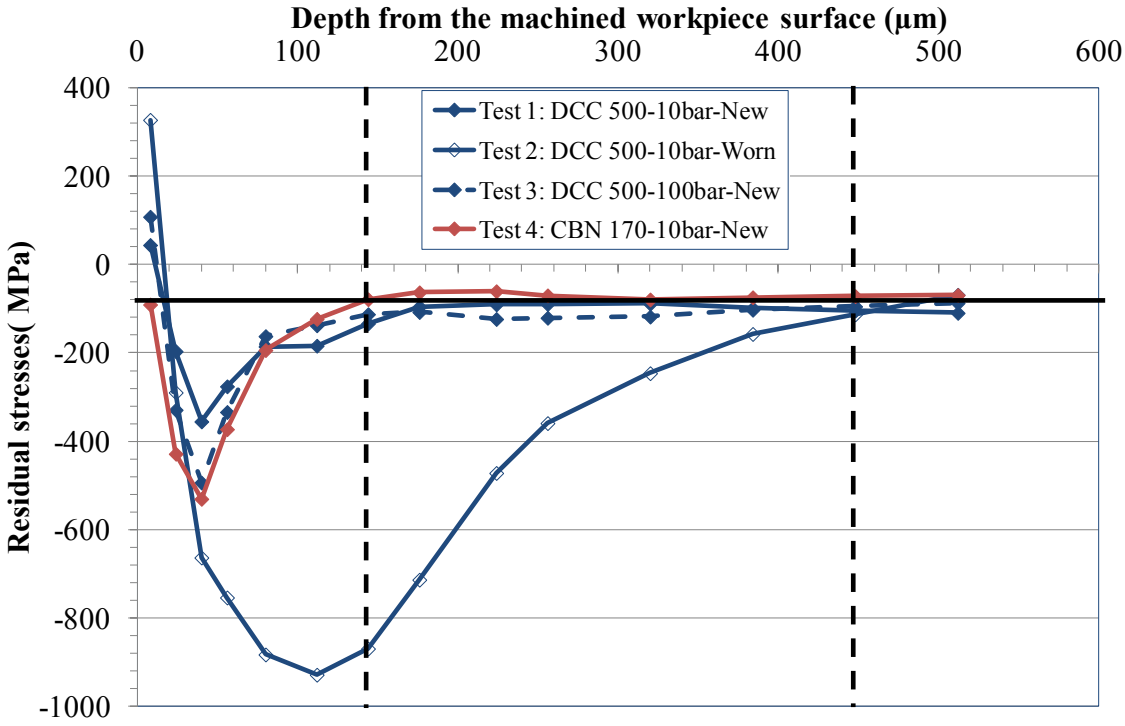

Figure 233: Residual stresses depth profiles measured perpendicular to the feed direction (σ⊥)

5. CONCLUSIONS

5.1 Literature review

- While work is cited on the use of CVD coated carbide, it appears that more extensive research has been carried out on the development and evaluation of novel PVD hard metal/ceramic coating products when turning different nickel based superalloys using carbide tooling. Up to a 2-fold improvement in tool life was observed with the CBN coating compared to a TiAlN coated insert. While the addition of Cr, Si and Y in (Ti,Al)N based PVD coatings in a multilayered structure outperformed the recent state of the art AlTiN coating product where ~65% improvement in tool life was recorded. These coatings were evaluated both in roughing and finishing cutting regimes where the maximum cutting speed was limited to 140m/min while feed rates were generally within the range of 0.10-0.30 mm/rev. In terms of surface integrity, the coatings failed to provide any benefit over their uncoated counterparts.

- Different types of cutting environment were assessed when turning Inconel 718 using carbide inserts. The benefits of high pressure fluid cooling were limited to roughing and operation at lower cutting speed (53m/min) and higher tool life (~30%) being achieved with air jet assisted machining compared to conventional wet cutting. In comparison to dry and MQL, lower workpiece surface roughness (~13-22%) and greater thickness (~75%) of the compressed layer beneath the machined surface were recorded with cryogenic machining while deformation of the grain boundaries was up to 1-2μm with the latter but this increased up to 5-fold in the former case. The literature survey highlighted that comparable performance between dry and wet cutting is possible in terms of surface integrity using CVD TiCN/Al_2O_3/TiN coating at a cutting speed of 60m/min.

- Mixed alumina ceramic tools are generally not suitable when turning Inconel 718 due to high flank and notch wear but nano-ceramic tools have shown potential in terms of tool life. Rapid failure of Sandvik Sialon grade 6080 was reported in turning of Inconel 718 and powder manufactured nickel based superalloy however, Kennametal Sialon grades KY 2000 and KY 2100 are recommended both for roughing and semi-finishing

applications. Recently developed functionally graded nano-composite Sialon ceramic was generally found to be suitable for finishing applications when turning Inconel 718 without coolant where ~8min tool life was recorded at a cutting speed of 200m/min, feed rate of 0.10mm/rev and depth of cut of 0.10mm.

- Improved productivity is reported when using Sandvik CC670 whisker reinforced alumina to machine nickel based superalloys (Inconel 718 and Nimonic C 263) where cutting speeds within the range of 250-300 m/min, feed rates of 0.05-0.20 mm/rev and depths of cut of 0.30-0.50 mm were employed but the occurrence of white layer and high tensile residual stresses (725-850 MPa) is also detailed. Coated whisker ceramic inserts, effect of high pressure cooling and hybrid machining are detailed as providing benefits in terms of tool life (~50-70 %) when turning Inconel 718 but still published data is limited.

- In high speed turning of nickel based superalloys using PCBN tools;
  - The use of chamfered and honed edge is reported as generating compressive residual stresses and a higher degree of work hardening compared to a chamfered only tool.
  - Better performance in terms of higher tool life, lower workpiece surface roughness and compressive residual stresses has been recorded with round inserts.
  - Titanium nitride (TiN) coated PCBN inserts have been evaluated and their advantage relative to tool life was limited to a cutting speed of 250m/min, however no significant differences in terms of surface integrity were reported using coated and uncoated inserts.
  - Use of coolant is recommended in order to improve tool life and workpiece surface integrity.
  - PCBN tools having low CBN content (50%) with a ceramic binder (TiC or TiN) and fine grain size (1-2μm) outperformed high concentration PCBN inserts with a metallic binder phase where ~300% improvement in tool life was recorded.
  - High concentration (90% CBN) PCBN tools with a metallic binder have been evaluated both for roughing and finishing applications with a maximum cutting speed of 250m/min. Notch wear dictated the tool life and was less than 3min. Low to medium (50-65%) CBN content PCBN tools with a ceramic binder have been tested in finishing. In the latter case, cutting speeds within the range of 200-300

m/min were found to be the optimal giving a tool life of 5-6 min. Additionally, a reduction in cutting forces, better workpiece surface roughness, less surface damage and compressive residual stresses are reported at Vc of 475m/min indicated the potential for employing PCBN tools at higher cutting speeds.

- Abrasion and diffusion of the binder phase were the main tool wear mechanisms reported, therefore binderless PCBN has been suggested for evaluation.

- Significant benefits in term of higher tool life (38-200%) and lower workpiece surface roughness (33-41%) were recorded with coated PCBN inserts in comparison to uncoated tools when turning hardened steels and cast iron.

5.2 Experimental work

5.2.1 Phases 1A: Preliminary experimental trials when turning Inconel 718

- Grooving at the tool nose and notch on the flank face was observed in all trials however, fracture was more prevalent in tests performed at the higher cutting speeds of 300 and 450 m/min. Here tool life was extremely low with a maximum value of 1.63min while surface roughness was generally within the range of 1.28-2.52 μm Ra.

5.2.2 Phase 1B: Benchmarking of Mitsubishi Inconel 718 workpiece using production approved carbide/PCBN inserts and operating parameters

- Tool wear progression was 'steady' in all tests with a maximum tool life of ~25min observed with the coated carbide insert. In terms of productivity, PCBN tools outperformed uncoated and coated carbide inserts where ~587% and ~65% more material was removed respectively after 5min of machining. Uncoated carbide produced the same level of tool wear when machining the RR and MHI materials.
- In contrast to the uncoated carbide, workpiece surface roughness was found to decrease for the increasing flank wear with coated insert which reduced to 0.82μm Ra at the end of tool life, however Ra increased to 2.50μm with the former at test cessation. Workpiece surface roughness showed limited variability with PCBN inserts, which was less than 1.3μm Ra over the duration of the experiments.
- Compared to PCBN and uncoated carbide inserts, cutting forces were higher (2 to 3 times) with coated WC insert. Although the same feed rate and depth of cut were utilised both with PCBN and uncoated WC insert, 3 times higher thrust force was recorded with the former due to the presence of chamfer geometry.

5.2.3 Phase 1C: Influence of tool geometry, edge preparation, cutting environment, surface condition and operating parameters on tool wear/life, surface roughness and cutting forces

- At a cutting speed of 150m/min, intensive grooving and BUE was observed with the C-type inserts, whereas wear progression was uniform with the round inserts which provided a maximum tool life of 44.8min in Test 4. When cutting speed was increased to 300 and 450 m/min, no significant difference in tool life was recorded for both types of insert. At Vc of 300m/min, uniform tool wear was observed with round and C-type tool geometries. However thermal cracks, chipping and fracture was seen at a cutting speed of 450m/min with a minimum tool life of 1.3min (Test 9).

- Flank wear was the dominant wear mode. Workpiece material adhesion was present in all trials and abrasion was identified to be the main wear mechanism.

- Surface roughness (Ra) was generally less than 1μm in the majority of the tests performed with round inserts at a cutting speed of 150m/min while a significant rise of up to 4.00μm Ra was recorded using C-type inserts due to intensive grooving and BUE formation. At intermediate (300m/min) and higher cutting speeds (450m/min), Ra did not exceed 1.5μm over the duration of experiments irrespective of tool geometry and operating variables.

- Thrust forces were up to ~185% and ~450% higher than the corresponding cutting and feed forces respectively with a maximum of 936N recorded in Test 12.

- In terms of productivity, a cutting speed of 300m/min and feed rate of 0.20mm/rev were the preferred operating parameters. Although a direct comparison between the round and C-type tool geometries was not possible due to the difference in edge geometry however, better performance was observed with the C-type inserts where ~50% higher material was removed compared to the round tools, therefore it was selected for future trials.

- Tool geometry and cutting speed was significant on all responses however, feed rate was significant on tool life, cutting and thrust force only. Higher cutting and thrust forces were recorded with round tool geometry but feed force was generally higher with C-type tool configuration.

- Although edge preparation did not appear to be statistically significant relative to tool life in terms of standard ANOVA calculation, it appeared to be statistically significant with feed rate on tool life based on the stepwise routine, as longer tool life was typically obtained when using inserts having an E25 edge preparation at a feed rate of 0.05mm/rev. Higher values of cutting forces and surface roughness were observed when utilising S-type edge preparation compared to E25.

- Cutting environment was not found to be statistically significant in terms of tool life in standard ANOVA calculation but high cutting fluid pressure of 100bar was detrimental to tool life at low material removal rate (150m/min and 0.05mm/rev). Cutting forces were generally higher when employing 100bar fluid supply compared to 10bar pressure.

- Coatings failed to provide any benefit in terms of tool life which suggests that then selected composition may not suitable under the conditions investigated in the current trials. However a marginal reduction in thrust force was observed with the coated PCBN tooling.

5.2.4 Phase 1D: Evaluation of edge preparation and cutting speed on workpiece surface integrity

- Surface roughness (Ra) was within the range of 0.67µm to 1.56µm for the conditions tested. With E25 edge preparation, a decrease in the value of surface roughness (Ra) was recorded when using worn tools. The opposite was true for the S-type edge configuration where ~30 to 40% increase in Ra was observed. In addition, none of the factors were statistically significant at the 5% level relative to surface roughness.

- In terms of statistical analysis, cutting speed had a significant influence on cutting and feed forces when utilising new tools. Typically, cutting force decreased as cutting speed increased from 300m/min to 450m/min. With worn tools, none of the factors were statistically significant for any of the force components and none of the variable parameters appeared to have any effect on the thrust force irrespective of the tool condition.

- In terms of surface damage, feed marks were prevalent in all tests however grooves, microcracks and smeared material were apparent when utilising worn tools.

- All workpiece samples were strain hardened to a depth of 500µm from the machined surface with a maximum value of 612.7$HK_{0.025}$ in the perpendicular to the feed when turning with worn tools (300µm flank wear level).

- No significant microstructural damage was seen in the any of the workpiece samples evaluated.

5.2.5 Phase 2A: Effect of cutting environment, cutting speed and feed rate on tool wear/life, surface roughness and cutting forces

- Flank wear was the dominant wear mode and uniform tool wear progression was recorded in all trials.

- Cutting speed was the main contributing factor affecting tool life with a PCR of 94.80%. In terms of productivity, a cutting speed of 300m/min was preferred with a tool life of ~3min.

- Adhesion was observed in all tests and abrasion was prevalent particularly at high cutting speed of 450m/min.

- Lower tool life (~31%) and higher cutting (~60%) and thrust (~70%) forces were recorded when turning SI workpiece material compared to the MHI product. This was possibly either due to the coarser grain or due to the presence of γ″ precipitates in the former.

- Better chip breaking was observed when employing the higher cutting fluid pressure of 100bar compared to 10bar while no workpiece swarf entanglement problems was encountered in any trial

- In general, Ra<0.80µm was observed over the entire test duration for all tests employing a feed rate of 0.15mmm/rev.

- In terms of cutting forces, none of the factors/interactions were statistically significant over the range of parameters/conditions used irrespective of tool condition, likely due to material softening. Although not statistically significant, cutting environment showed

high PCR's (50-78%) on cutting force components when utilising worn tools. Cutting forces were generally higher when employing 100bar fluid pressure.

5.2.6 Phase 2B: Assessment of cutting environment, cutting speed and feed rate effects on workpiece surface integrity

- In terms of surface roughness (Ra), a decreasing trend was seen when utilising worn tools over new inserts. Workpiece surface roughness was greater than 0.90µm Ra for the trials performed at a feed rate of 0.20mm/rev, however this was <0.70µm Ra at a feed rate of 0.15mm/rev. Feed rate showed high PCR's of 93.10% and 76.83% relative to surface roughness with new and worn tools respectively.

- Feed marks were found on all machined surfaces when employing new tools irrespective of operating variables and cutting environment; however grooves obscured the feed marks for the samples machined with worn tools. At high magnification (1000x), microcracks of size 10-12µm were recorded over an area of 10,000µm^2 for the samples machined with worn tools.

- No major changes in microhardness was observed for the samples machined with new tools however, a strain hardened region with a maximum value of 560$HK_{0.025}$ over a depth of 100µm was observed for the samples machined with worn tools in a direction perpendicular to the feed.

- No significant sub-surface damage was observed parallel to the feed direction while grain elongation/bending up to a depth of 30µm was recorded perpendicular to the feed direction.

- Depth of strain hardened region was ~3 to 4 times higher in both directions (Parallel and perpendicular to the feed) in the MHI material compared to the SI workpiece and the maximum microhardness was ~50$HK_{0.025}$ higher in the former.

5.2.7 Phase 3A: Evaluation of alternative PCBN grade and coatings on tool wear/life, surface roughness and cutting forces

- At a cutting speed of 200m/min, fracture and BUE were observed in all tests and was detrimental to tool life for the TiSiN/TiAlN, AlCrN, CrAlN 3µm and CrAlN5.5µm

coated inserts due to poor edge integrity/coating adhesion. A maximum tool life of ~8.8min was obtained with TiSiN coated insert followed by uncoated tool (lasted 6.4min).

- When Vc was increased to 300 and 450 m/min, wear progression of all tools was uniform, however no improvement in tool life was obtained with any of the coated products compared with the uncoated inserts.

- No significant difference in terms of tool life was observed with either of the PCBN grades used (DCC 500 and CBN 170).

- Long cylindrical helical serrated chips were seen in all tests however there were no swarf entanglement problems with the workpiece.

- Workpiece surface roughness was found to decrease with increasing flank wear (130µm) but then remained stable within the range of 0.25-0.50µm Ra at the end of tool life.

- Cutting, thrust and feed force components did not exceed 300N irrespective of surface condition and cutting speed.

- None of the variable factors were found to be statistically significant in terms of tool life, cutting forces and surface roughness.

5.2.8 Phase 3B: Effect of alternative PCBN grade and tool coatings on workpiece surface integrity

- Feed marks were observed on all machined surfaces when employing new tools however, it was difficult to distinguish between grooves and feed marks for the samples machined with worn inserts. High magnification SEM inspection showed the same trend as observed in Phase 2B.

- With new tools, no significant workpiece strain hardening was recorded irrespective of the cutting speed and surface condition at Vc of 300m/min except with the CrAlN-5.5µm coating, which showed a hardened layer of up to ~544$HK_{0.025}$ extending to a depth of 50µm from the machined surface. An increase in workpiece hardness of up to

~80$HK_{0.025}$ above the bulk value was recorded when employing worn tools irrespective of the surface condition however, depth of strain hardened layer was ~200µm with the TiSiN coated insert, which was ~100µm higher than its uncoated counterparts.

- Grain elongation/bending (~15-20µm) in the direction of cutting speed was observed in all workpiece samples machined with new tools irrespective of tool surface condition except with the CrAlN-5.5µm coating where it extended to ~30µm beneath the machined surface due to the higher level of ploughing as a result of the larger contact area associated with it.

5.2.9 Phase 3C: Effect of PCBN grades and cutting environment on residual stresses

- Surface residual stresses were compressive (typically up to -443MPa.) in all samples measured parallel to the feed while the opposite was true in the perpendicular feed direction where corresponding results were predominantly tensile (up to 320MPa.), however CBN 170 PCBN grade generated compressive residual stresses in both directions.
- The use of worn inserts induced the highest level of sub-surface compressive residual stresses (-1268MPa in the feed direction and -930MPa perpendicular to the feed) extending to a depth of ~450µm.
- The depth of compressive residual stresses was limited to ~140µm when machining with new inserts measured perpendicular to the feed direction, which was 40µm lower in the parallel direction.

5.2.10 Overall conclusions and recommended operating parameters

Table 59 below lists the recommended/preferred operating parameter conditions when turning Inconel 718 using PCBN tools under finishing condition (0.20mm depth of cut);

Table 59: Recommended/preferred operating parameters

Parameter	Value
Cutting speed	300m/min
Feed rate	0.15 mm/rev
Edge preparation	E25
Tool geometry	CNGA 120412
Tool grade	CBN 170
Cutting environment	100bar

At these operating parameters, tool wear progression was uniform with a tool life of ~3min (VB_Bmax.=200µm) and workpiece surface roughness was <0.70µm over the entire duration of the experiment. In general, no significant benefit in terms of tool life, workpiece surface/sub-surface damage was observed with the new PCBN grade CBN 170 compared to DCC 500 however, workpiece surface residual stresses were compressive with the former, therefore selected over the latter PCBN grade. A cutting fluid pressure of 100bar failed to provide any benefit in terms of tool life and workpiece surface integrity in comparison to 10bar, however sub-surface residual stresses were more compressive at high cutting fluid pressure.

6. RECOMMENDATIONS FOR FUTURE WORK

Based on results from the present research, the following areas have been identified which warrant further investigation.

- In depth evaluation of recently developed binderless PCBN materials for the machining of nickel based superalloys, which are manufactured by sintering hexagonal boron nitride crystals at high temperatures (1800˚C) and pressures (10GPa) into cubic boron nitride (CBN) having very fine grain sizes (100-500 nm). The thermal conductivity and hardness of binderless PCBN are quoted to be 3 and 1.5 times higher respectively in comparison to conventional PCBN tooling. In addition, significant benefits in terms of tool life and surface roughness have been reported when using binderless PCBN tools for machining titanium alloys, alloyed and stainless steel as well as cast iron workpiece materials.

- Performance evaluation of PCBN inserts with wiper tool geometry to potentially further increase material removal rate and productivity by operating at feed rates without affecting the workpiece surface roughness.

- Investigation of PCBN tool performance and establishment of preferred operating parameter windows for the machining of alternative nickel based superalloy materials such as Nimonics, Udimets, RR 1000 etc.

- Evaluation of state-of-the art superlattice and nano-structured AlTiN and TiAlCrSiYN multilayer coatings when turning Inconel 718 using PCBN inserts in order to increase tool life. These coating products are typically more stable at high temperatures and possess superior mechanical and tribological properties.

- Further in depth assessment involving the influence of round CBN 170 PCBN inserts on tool life and workpiece surface integrity when turning Inconel 718 as benefits such as higher tool life, lower workpiece surface roughness and compressive residual stresses over C-type configuration have been reported in the literature.

- Performance evaluation of PCBN tooling for the milling and drilling of nickel based superalloys at high cutting speeds in order to increase productivity over conventional carbide cutters.

- Performance evaluation of standard tool coatings (TiAlN/TiN, TiN etc.) by increasing their temperature resistance and chemical inertness.

- Measurement of cutting temperature when turing Inconel 718 using PCBN tooling.

- Fatigue performance evaluation of Inconel 718 workpiece samples following machining with PCBN tools.

- Further in depth residual stress measurement using XRD method

REFERENCES

[1] E. O. Ezugwu, Z. M. Wang and A. R. Machado, *The machinability of nickel based alloys: a review*, Journal of Materials Processing Technology, 1999. (86): 1-16.

[2] E. O. Ezugwu, J. Bonney and Y. Yamane, *An overview of the machinability of aeroengine alloys*, Journal of Materials Processing Technology, 2003. (134): 233-253.

[3] E. O. Ezugwu, *Key improvements in the machining of difficult-to-cut aerospace superalloys*, International Journal of Machine Tools and Manufacture, 2005. (45): 1353-1367.

[4] R. M'Saoubi, J. C. Outeiro, H. Chandrasekaran, O. W. D. Jr. and I. S. Jawahir, *A review of surface integrity in machining and its impact on functional performance and life of machined products*, International Journal of Sustainable Manufacturing, 2008. (1): 203-235.

[5] W. Grzesik, *Advanced Machining Processes of Metallic Materials*, Elsevier, 2008, Oxford, UK: ISBN: 978-0-08-044534-2.

[6] D. G. Thakur, B. Ramamoorthy and L. Vijayaraghavan, *Study on the machinability characteristics of superalloy Inconel 718 during high speed turning*, Materials & Design, 2009. (30): 1718-1725.

[7] Y. Kamata and T. Obikawa, *High speed MQL finish-turning of Inconel 718 with different coated tools*, Journal of Materials Processing Technology, 2007. (192–193): 281-286.

[8] C. Courbon, D. Kramar, P. Krajnik, F. Pusavec, J. Rech and J. Kopac, *Investigation of machining performance in high-pressure jet assisted turning of Inconel 718: An experimental study*, International Journal of Machine Tools and Manufacture, 2009. (49): 1114-1125.

[9] L. Settineri, M. G. Faga and B. Lerga, *Properties and performances of innovative coated tools for turning inconel*, International Journal of Machine Tools and Manufacture, 2008. (48): 815-823.

[10] G. Kappmeyer, C. Hubig, M. Hardy, M. Witty and M. Busch, *Modern Machining of Advanced Aerospace Alloys - Enabler for Quality and Performance*, Procedia CIRP, 2012. (1): 28-43.

[11] T. Harada, S. Kukino, Y. Kanada, T. Fukaya, T. Wakabayashi, T. Sahashi, M. Goto and T. Nakai, *Development of a coated PCBN tool*, SEI Technical Review, 2001. (52): 81-86.

[12] G. Poulachon, A. Moisan and I. S. Jawahir, *Tool-wear mechanisms in hard turning with polycrystalline cubic boron nitride tools*, Wear, 2001. (250): 576-586.

[13] A. E. Diniz, J. R. Ferreira and F. T. Filho, *Influence of refrigeration/lubrication condition on SAE 52100 hardened steel turning at several cutting speeds*, International Journal of Machine Tools and Manufacture, 2003. (43): 317-326.

[14] G. d. S. Galoppi, M. S. Filho and G. F. Batalha, *Hard turning of tempered DIN 100Cr6 steel with coated and no coated CBN inserts*, Journal of Materials Processing Technology, 2006. (179): 146-153.

[15] R. T. Coelho, E.-G. Ng and M. A. Elbestawi, *Tool wear when turning hardened AISI 4340 with coated PCBN tools using finishing cutting conditions*, International Journal of Machine Tools and Manufacture, 2007. (47): 263-272.

[16] W. F. Sales, L. A. Costa, S. C. Santos, A. E. Diniz, J. Bonney and E. O. Ezugwu, *Performance of coated, cemented carbide, mixed-ceramic and PCBN-H tools when turning W320 steel*, The International Journal of Advanced Manufacturing Technology, 2009. (41): 660-669.

[17] E. F. Bradley, *Superalloys A Technical Guide*, ASM International, Metals Park, 1989, OH: ISBN: 0-87170-327.
[18] R. C. Reed, *The Superalloys, Faundamentals and Applications*, Cambridge University Press, 2006, Cambridge, UK: ISBN: 978-0-521-85904-2.
[19] M. J.Donachie and S. J. Donachie, *Superalloys A Technical guide*, ASM International, 2002. Edition: 2nd: ISBN: 0-87170-749-7.
[20] D. S. Mackenzie and G. E.Totten, *Analytical characterization of Aluminum, Steel and Superalloys*, Taylor & Francis, 2005: ISBN: 978-0-82475843-1.
[21] J. M. Zhou, V. Bushlya and J. E. Stahl, *An investigation of surface damage in the high speed turning of Inconel 718 with use of whisker reinforced ceramic tools*, Journal of Materials Processing Technology, 2012. (212): 372-384.
[22] T. M.Pollock and S. Tin, *Nickel Based Superalloys for Advanced Turbine Engines: Chemistry, Microstructure and Properties*, Journal of Propulsion and Power, 2006. (22)
[23] S. Olovsjö, A. Wretland and G. Sjöberg, *The effect of grain size and hardness of wrought Alloy 718 on the wear of cemented carbide tools*, Wear, 2010. (268): 1045-1052.
[24] G. Totten, *Fatigue crack propagation*, Advanced Materials & Processes, 2008. 39-41.
[25] S. Kalpakjian and S. R.Schmid, *Manufacturing Engineering and Technology*, 2004. 4th Edition, Delhi, India: ISBN: 81-7808-157-1.
[26] H. El-Hofy, *Machining Processes: Conventional and non-conventional processes*, Taylor & Francis Group, 2007, Boca Raton: ISBN: 0-8493-7288-7.
[27] *Sandvik Coromant, Modern Metal Cutting, A Practical Handbook, AB Sandvik Coromant*, 1994, ISBN: 91-972299-0-3.
[28] H. El-Hofy, *Faundamentals of Machining Processes*, Taylor & Francis Group, 2007, Boca Raton, Florida, USA: ISBN: 0-8493-7288-7.
[29] G. T.Smith, *Cutting tool technology, Industrial Handbook*, Springer-Verlag London Limited, 2008, London: ISBN: 978-1-84800-204-3.
[30] *Metalworking product, New tools from Sandvik coromant, supplement to turning tool catalogue and rotating tools catalogue*, AB Sandvik Coromant, 2005,
[31] E. M. Trent and P. K. Wright, *Metal Cutting*, Butterworth-Heinemann, 2000. 4th Edition, Woburn: ISBN: 0-7506-7069-X.
[32] M.C.Shaw, *Metal Cutting Principles*, Oxford Science Publications, 1997: ISBN: 0-7506-1068-9.
[33] J. P. Davim, *Surface Integrity in Machining*, Springer-Verlag London Limited, 2009, Aveiro, Portugal: ISBN: 978-1-84882-873-5.
[34] M.Field and J. F. Kahles, *The surface integrity of machined and ground high strength steels, DMIC Report 210*, 1964.
[35] M. Field and J.F.Kahles, *Review of surface integrity of machined components*, Annals of CIRP, 1971. (20): 153-162.
[36] M.Fied, J.F.Kahles and J.T.Cammett, *Review of measuring methods for surface integrity*, Annals of the CIRP, 1972. (21): 219-238.
[37] *Geometric product specifications (GPS). Surface texture: Profile method. Surfaces having stratified functional properties, height characterization using the linear material ration curve: BSEN ISO 13565-2: 1997: ISBN: 0580 27534 5*.
[38] *Seco Turning Catalog, Seco Tools AB, 73782 Fagersta*, Sweden. 2011,
[39] *Machining Data Handbook*, Techsolve In;, 1980. 2nd Edition, Volume 2: ISBN: 978-0936974002.

[40] D. Ulutan and T. Ozel, *Machining induced surface integrity in titanium and nickel alloys: A review*, International Journal of Machine Tools and Manufacture, 2011. (51): 250-280.

[41] D. A. Axinte, P. Andrews, W. Li, N. Gindy, P. J. Withers and T. H. C. Childs, *Turning of advanced Ni based alloys obtained via powder metallurgy route*, CIRP Annals - Manufacturing Technology, 2006. (55): 117-120.

[42] R. S. Pawade, S. S. Joshi and P. K. Brahmankar, *Effect of machining parameters and cutting edge geometry on surface integrity of high-speed turned Inconel 718*, International Journal of Machine Tools and Manufacture, 2008. (48): 15-28.

[43] J. P. Davim, *Machining of Hard Materials*, Springer-Verlag London Limited, 2010, Aveiro, Portugal: ISBN: 978-1-84996-449-4.

[44] A. R. C. Sharman, J. I. Hughes and K. Ridgway, *An analysis of the residual stresses generated in Inconel 718™ when turning*, Journal of Materials Processing Technology, 2006. (173): 359-367.

[45] C. H. Che-Haron and A. Jawaid, *The effect of machining on surface integrity of titanium alloy Ti–6% Al–4% V*, Journal of Materials Processing Technology, 2005. (166): 188-192.

[46] C. H. Che-Haron, *Tool life and surface integrity in turning titanium alloy*, Journal of Materials Processing Technology, 2001. (118): 231-237.

[47] E. Brinksmeier, J. T. Cammett, W. König, P. Leskovar, J. Peters and H. K. Tönshoff, *Residual Stresses — Measurement and Causes in Machining Processes*, CIRP Annals - Manufacturing Technology, 1982. (31): 491-510.

[48] D. Walker, *Residual Stress Measurement Techniques*, Advanced Materials & Processes, 2001. 30-33.

[49] B. D. Cullity, *Elements of X-ray diffraction*, Addison-Wesley publishing company, INC., 1978. 2nd Edition, Massachusetts, United States of America: ISBN: 0-201-01174-3.

[50] *Measurement of residual stresses by the hole drilling strain gage method*, Micro measurement, Vishay precision group, Document number: 11053, 2010.

[51] D. Novovic, R. C. Dewes, D. K. Aspinwall, W. Voice and P. Bowen, *The effect of machined topography and integrity on fatigue life*, International Journal of Machine Tools and Manufacture, 2004. (44): 125-134.

[52] B.A.Cowles, *High cycle fatigue in aircraft gas turbines—an industry perspective*, International Journal of Fracture, 1989. (80): 147-163.

[53] R. M. Arunachalam and M. A. Mannan, *Machinability of nickel based high temperature alloys*, Machining Science and Technology, 2000. (4): 127-168.

[54] J. L. Cantero, J. Díaz-Álvarez, M. H. Miguélez and N. C. Marín, *Analysis of tool wear patterns in finishing turning of Inconel 718*, Wear, 2013. (297): 885-894.

[55] D. Dudzinski, A. Devillez, A. Moufki, D. Larrouquère, V. Zerrouki and J. Vigneau, *A review of developments towards dry and high speed machining of Inconel 718 alloy*, International Journal of Machine Tools and Manufacture, 2004. (44): 439-456.

[56] P. C. Jindal, A. T. Santhanam, U. Schleinkofer and A. F. Shuster, *Performance of PVD TiN, TiCN, and TiAlN coated cemented carbide tools in turning*, International Journal of Refractory Metals and Hard Materials, 1999. (17): 163-170.

[57] H. G. Prengel, P. C. Jindal, K. H. Wendt, A. T. Santhanam, P. L. Hegde and R. M. Penich, *A new class of high performance PVD coatings for carbide cutting tools*, Surface and Coatings Technology, 2001. (139): 25-34.

[58] A. Devillez, F. Schneider, S. Dominiak, D. Dudzinski and D. Larrouquere, *Cutting forces and wear in dry machining of Inconel 718 with coated carbide tools*, Wear, 2007. (262): 931-942.

[59] C. Ducros and F. Sanchette, *Multilayered and nanolayered hard nitride thin films deposited by cathodic arc evaporation. Part 2: Mechanical properties and cutting performances*, Surface and Coatings Technology, 2006. (201): 1045-1052.

[60] G. S. Fox-Rabinovich, K. Yamamoto, M. H. Aguirre, D. G. Cahill, S. C. Veldhuis, A. Biksa, G. Dosbaeva and L. S. Shuster, *Multi-functional nano-multilayered AlTiN/Cu PVD coating for machining of Inconel 718 superalloy*, Surface and Coatings Technology, 2010. (204): 2465-2471.

[61] A. Biksa, K. Yamamoto, G. Dosbaeva, S. C. Veldhuis, G. S. Fox-Rabinovich, A. Elfizy, T. Wagg and L. S. Shuster, *Wear behavior of adaptive nano-multilayered AlTiN/MexN PVD coatings during machining of aerospace alloys*, Tribology International, 2010. (43): 1491-1499.

[62] G. K. Dosbaeva, S. C. Veldhuis, K. Yamamoto, D. S. Wilkinson, B. D. Beake, N. Jenkins, A. Elfizy and G. S. Fox-Rabinovich, *Oxide scales formation in nano-crystalline TiAlCrSiYN PVD coatings at elevated temperature*, International Journal of Refractory Metals and Hard Materials, 2010. (28): 133-141.

[63] G. S. Fox-Rabinovich, B. D. Beake, K. Yamamoto, M. H. Aguirre, S. C. Veldhuis, G. Dosbaeva, A. Elfizy, A. Biksa and L. S. Shuster, *Structure, properties and wear performance of nano-multilayered TiAlCrSiYN/TiAlCrN coatings during machining of Ni-based aerospace superalloys*, Surface and Coatings Technology, 2010. (204): 3698-3706.

[64] E. Uhlmann, J. A. O. Fuentes and M. Keunecke, *Machining of high performance workpiece materials with CBN coated cutting tools*, Thin Solid Films, 2009. (518): 1451-1454.

[65] A. Bhatt, H. Attia, R. Vargas and V. Thomson, *Wear mechanisms of WC coated and uncoated tools in finish turning of Inconel 718*, Tribology International, 2010. (43): 1113-1121.

[66] J. C. Outeiro, J. C. Pina, R. M'Saoubi, F. Pusavec and I. S. Jawahir, *Analysis of residual stresses induced by dry turning of difficult-to-machine materials*, CIRP Annals - Manufacturing Technology, 2008. (57): 77-80.

[67] R. M. Arunachalam, M. A. Mannan and A. C. Spowage, *Surface integrity when machining age hardened Inconel 718 with coated carbide cutting tools*, International Journal of Machine Tools and Manufacture, 2004. (44): 1481-1491.

[68] T. Özel and D. Ulutan, *Prediction of machining induced residual stresses in turning of titanium and nickel based alloys with experiments and finite element simulations*, CIRP Annals - Manufacturing Technology, 2012. (61): 547-550.

[69] W. Li, P. J. Withers, D. Axinte, M. Preuss and P. Andrews, *Residual stresses in face finish turning of high strength nickel-based superalloy*, Journal of Materials Processing Technology, 2009. (209): 4896-4902.

[70] I. A. Choudhury and M. A. El-Baradie, *Machinability of nickel-base super alloys: a general review*, Journal of Materials Processing Technology, 1998. (77): 278-284.

[71] A. R. C. Sharman, J. I. Hughes and K. Ridgway, *Surface integrity and tool life when turning Inconel 718 using ultra-high pressure and flood coolant systems*, Proceedings of the Institution of Mechanical Engineers Part B-Journal of Engineering Manufacture, 2008. (222): 653-664.

[72] E. O. Ezugwu and J. Bonney, *Effect of high-pressure coolant supply when machining nickel-base, Inconel 718, alloy with coated carbide tools*, Journal of Materials Processing Technology, 2004. (153-154): 1045-1050.

[73] T. Obikawa, M. Yamaguchi, K. Funai, Y. Kamata and S. Yamada, *Air jet assisted machining of nickel-base superalloy*, International Journal of Machine Tools and Manufacture, 2012. (61): 20-26.

[74] M. Z. A. Yazid, C. H. CheHaron, J. A. Ghani, G. A. Ibrahim and A. Y. M. Said, *Surface integrity of Inconel 718 when finish turning with PVD coated carbide tool under MQL*, Procedia Engineering, 2011. (19): 396-401.

[75] F. Pusavec, H. Hamdi, J. Kopac and I. S. Jawahir, *Surface integrity in cryogenic machining of nickel based alloy--Inconel 718*, Journal of Materials Processing Technology, 2011. (211): 773-783.

[76] D. Thakur, B. Ramamoorthy and L. Vijayaraghavan, *Investigation and optimization of lubrication parameters in high speed turning of superalloy Inconel 718*, The International Journal of Advanced Manufacturing Technology, 2010. (50): 471-478.

[77] T. Obikawa, Y. Kamata, Y. Asano, K. Nakayama and A. W. Otieno, *Micro-liter lubrication machining of Inconel 718*, International Journal of Machine Tools and Manufacture, 2008. (48): 1605-1612.

[78] D. Thakur, B. Ramamoorthy and L. Vijayaraghavan, *Effect of cutting parameters on the degree of work hardening and tool life during high-speed machining of Inconel 718*, The International Journal of Advanced Manufacturing Technology, 2012. (59): 483-489.

[79] A. Devillez, G. Le Coz, S. Dominiak and D. Dudzinski, *Dry machining of Inconel 718, workpiece surface integrity*, Journal of Materials Processing Technology, 2011. (211): 1590-1598.

[80] K. Weinert, I. Inasaki, J. W. Sutherland and T. Wakabayashi, *Dry Machining and Minimum Quantity Lubrication*, CIRP Annals - Manufacturing Technology, 2004. (53): 511-537.

[81] E. O. Ezugwu, J. Bonney and R. B. d. Silva, *Evaluation of the performance of different nano-ceramic tool grades when machining nickel based, Inconel 718 alloy*, Journal of the Brazilian Society of Mechanical Sciences and Engineering, 2004. (26): 12-16.

[82] T. Kitagawa, A. Kubo and K. Maekawa, *Temperature and wear of cutting tools in high-speed machining of Inconel 718 and Ti-6Al-6V-2Sn*, Wear, 1997. (202): 142-148.

[83] N. Richards and D. K. Aspinwall, *Use of ceramic tools for machining nickel based alloys*, International Journal of Machine Tools and Manufacture, 1989. (29): 575-588.

[84] E. O. Ezugwu and S. H. Tang, *Surface abuse when machining cast iron (G-17) and nickel-base superalloy (Inconel 718) with ceramic tools*, Journal of Materials Processing Technology, 1995. (55): 63-69.

[85] R. M. Arunachalam, M. A. Mannan and A. C. Spowage, *Residual stress and surface roughness when facing age hardened Inconel 718 with CBN and ceramic cutting tools*, International Journal of Machine Tools and Manufacture, 2004. (44): 879-887.

[86] R. T. Coelho, L. R. Silva, A. Braghini and A. A. Bezerra, *Some effects of cutting edge preparation and geometric modifications when turning INCONEL 718(TM) at high cutting speeds*, Journal of Materials Processing Technology, 2004. (148): 147-153.

[87] L. R. Silva and C. B. Soares, *Performance of the minimum quantity lubrication technique in turning Inconel 718 at high cutting speed* International Journal of Machining and Machinability of Materials, 2009. (5): 401-416.

[88] Z. Vagnorius and K. Sørby, *Effect of high-pressure cooling on life of SiAlON tools in machining of Inconel 718*, The International Journal of Advanced Manufacturing Technology, 2011. (54): 83-92.

[89] M. Nalbant, A. Altın and H. Gökkaya, *The effect of cutting speed and cutting tool geometry on machinability properties of nickel-base Inconel 718 super alloys*, Materials & Design, 2007. (28): 1334-1338.

[90] A. Altin, M. Nalbant and A. Taskesen, *The effects of cutting speed on tool wear and tool life when machining Inconel 718 with ceramic tools*, Materials & Design, 2007. (28): 2518-2522.

[91] L. Li, N. He, M. Wang and Z. G. Wang, *High speed cutting of Inconel 718 with coated carbide and ceramic inserts*, Journal of Materials Processing Technology, 2002. (129): 127-130.

[92] G. Zheng, J. Zhao, Z. Gao and Q. Cao, *Cutting performance and wear mechanisms of Sialon; graded nano-composite ceramic cutting tools*, The International Journal of Advanced Manufacturing Technology, 2012. (58): 19-28.

[93] G. Zheng, J. Zhao and Y. Zhou, *Friction and wear behaviors of Sialon–Si3N4 graded nano-composite ceramic materials in sliding wear tests and in cutting processes*, Wear, 2012. (290–291): 41-50.

[94] A. Gatto and L. Iuliano, *Advanced coated ceramic tools for machining superalloys*, International Journal of Machine Tools and Manufacture, 1997. (37): 591-605.

[95] J. M. Zhou, V. Bushlya, R. L. Peng, S. Johansson, P. Avdovic and J. E. Stahl, *Effects of Tool Wear on Subsurface Deformation of Nickel-based Superalloy*, Procedia Engineering, 2011. (19): 407-413.

[96] V. Bushlya, J. M. Zhou, F. Lenrick, P. Avdovic and J. E. Ståhl, *Characterization of White Layer Generated when Turning Aged Inconel 718*, Procedia Engineering, 2011. (19): 60-66.

[97] C. Ezilarasan, V. S. Senthil kumar and A. Velayudham, *An experimental analysis and measurement of process performances in machining of nimonic C-263 super alloy*, Measurement, 2013. (46): 185-199.

[98] C. Ezilarasan, V. S. Senthil kumar and A. Velayudham, *Effect of Machining Parameters on Surface Integrity in Machining Nimonic C-263 Super Alloy Using Whisker-Reinforced Ceramic Insert*, Journal of Materials Engineering and Performance, 2012. 1-10.

[99] E. O. Ezugwu, J. Bonney, D. A. Fadare and W. F. Sales, *Machining of nickel-base, Inconel 718, alloy with ceramic tools under finishing conditions with various coolant supply pressures*, Journal of Materials Processing Technology, 2005. (162-163): 609-614.

[100] Z. Y. Wang, K. P. Rajurkar, J. Fan, S. Lei, Y. C. Shin and G. Petrescu, *Hybrid machining of Inconel 718*, International Journal of Machine Tools and Manufacture, 2003. (43): 1391-1396.

[101] H. Ding and Y. Shin, *Improvement of machinability of Waspaloy via laser-assisted machining*, The International Journal of Advanced Manufacturing Technology, 2013. (64): 475-486.

[102] E. Uhlmann and G. Ederer, *High speed turning of Inconel 718*, Industrial Diamond Review, 2001. (3): 169-174.

[103] R. S. Pawade, S. S. Joshi, P. K. Brahmankar and M. Rahman, *An investigation of cutting forces and surface damage in high-speed turning of Inconel 718*, Journal of Materials Processing Technology, 2007. (192-193): 139-146.

[104] H. Kato, K. Shintani, A. Ohshima and Y. Kohno, *Cutting performance of PCBN end mill on the machining of nickel based superalloys*, International Conference on Progress in Cutting and Grinding, Osaka, Japan, 1996: 19-22.

[105] R. Arunachalam and M.A.Mannan, *Performance of CBN cutting tools in facing of age hardned Inconel 718*, Transactions of NAMRI, 2006: 87-94.

[106] M. Lee, J. G. Horne and D. Tabor, *The mechanism of notch Formation at the depth of cut line of ceramic tools machining nickel based superalloys*

Proceedings of 2nd International Conference, Wear Materials, Dearborn, MI, 1979: 460-469.

[107] F. Klocke, W. Konig and K. Gerschwiler, *Advanced machining of titanium and nickel-based alloys*, Advanced Manufacturing Systems and Technology, 1997. (372): 7-21.

[108] W. Konig and K. Gerschwiler, *Machining Nickel based superalloys,* Manufacturing Engineering, 1999. 102-108.

[109] V. Bushlya, J. Zhou, P. Avdovic and J.-E. Ståhl, *Performance and wear mechanisms of whisker-reinforced alumina, coated and uncoated PCBN tools when high-speed turning aged Inconel 718*, The International Journal of Advanced Manufacturing Technology: 1-9.

[110] J. Zhou, V. Bushlya, P. Avdovic and J. Ståhl, *Study of surface quality in high speed turning of Inconel 718 with uncoated and coated CBN tools*, The International Journal of Advanced Manufacturing Technology, 2011. 1-11.

[111] V. Bushlya, J. Zhou and J. E. Ståhl, *Effect of Cutting Conditions on Machinability of Superalloy Inconel 718 During High Speed Turning with Coated and Uncoated PCBN Tools*, Procedia CIRP, 2012. (3): 370-375.

[112] H. Sadao, *Finish cutting of Inconel 713 (1st Report)-Lubricating effects of cutting fluid*, Progress of cutting and grinding, China, 1998: 223-228.

[113] S. Takatsu, H. Shimoda and K. Otani, *Effect of CBN content on the cutting performance of polycrystalline CBN tools*, International Journal of Refractory and Hard Metal, 1983. (2): 175-178.

[114] T. K. Harris, E. J. Brookes and C. J. Taylor, *The effect of temperature on the hardness of polycrystalline cubic boron nitride cutting tool materials*, International Journal of Refractory Metals and Hard Materials, 2004. (22): 105-110.

[115] Y. Kono, A. Hara, S. Yazu, T. Uchida and Y. Mori, *Cutting performance of sintered CBN tools*, 'Cutting Tool Materials' proceedings of an International Conference Ft. Mitchell, September 1980: 281-295.

[116] C. Wick, *Machining with PCBN tools,* Manufacturing Engineering 1988. 73-78.

[117] K. Shintani, H. Kato, T. Maeda, Y. Fujimura and A. Yamamoto, *Cutting performance of CBN tools in machining of nickel based superalloys*, Journa of the Japan Society of Precision Engineering, 1992. (58): 1685-1690.

[118] J. P. Costes, Y. Guillet, G. Poulachon and M. Dessoly, *Tool-life and wear mechanisms of CBN tools in machining of Inconel 718*, International Journal of Machine Tools and Manufacture, 2007. (47): 1081-1087.

[119] W. Sun, *Effects on tool wear in Inconel 718 turning with coated and uncoated PCBN inserts*, M.Sc thesis, School of Mechanical Engineering, University of Birmingham, UK, 2009/2010.

[120] A. E. Focke, F. E. Westermann, J. Kemphaus, W. T. Shih and M. Hoch, *Wear of superhard materials when cutting super-alloys*, Wear, 1978. (46): 65-79.

[121] N. Richards, A. M. Currie, D. K. Aspinwall, D. J. M. Smith and R. C. Dewes, *Tool life data when machining nickel based alloys with ceramic cutting tools*, Proceedings of the Thirteenth Conference of the Irish Manufacturing Committee:, 1996: 13-22.

[122] S. M. Darwish, *The impact of the tool material and the cutting parameters on surface roughness of supermet 718 nickel superalloy*, Journal of Materials Processing Technology, 2000. (97): 10-18.

[123] S. M. Darwish, *Machining of difficult-to-cut materials with bonded tools*, International Journal of Adhesion and Adhesives, 2000. (20): 279-289.

[124] J. Angseryd, E. Coronel, M. Elfwing, E. Olsson and H. O. Andrén, *The microstructure of the affected zone of a worn PCBN cutting tool characterised with SEM and TEM*, Wear, 2009. (267): 1031-1040.

[125] E. L. Emerson, *Wear performance of cubic boron nitride*, B.Sc thesis, Department of Mechanical Engineering, Massachusetts Institute of Technology, United States of America, 1981.
[126] R. M'Saoubi, T. Larsson, J. Outeiro, Y. Guo, S. Suslov, C. Saldana and S. Chandrasekar, *Surface integrity analysis of machined Inconel 718 over multiple length scales*, CIRP Annals - Manufacturing Technology, 2012.
[127] R. Pawade and S. Joshi, *Multi-objective optimization of surface roughness and cutting forces in high-speed turning of Inconel 718 using Taguchi grey relational analysis (TGRA)*, The International Journal of Advanced Manufacturing Technology, 2011. (56): 47-62.
[128] R. S. Pawade, A. H. Sonawane and S. S. Joshi, *An analytical model to predict specific shear energy in high-speed turning of Inconel 718*, International Journal of Machine Tools and Manufacture, 2009. (49): 979-990.
[129] K. Jemielniak, *Finish turning of Inconel 718*, Advances in Manufacturing Science and Technology, 2009. (33): 59-69.
[130] M. Ota, T. Fukaya, J. Shiraishi, T. Nakai, H. Ohara and H. Fukui, "Coated PCBN cutting tools," United states Patent, 2001.
[131] Z. Ban and Y. Liu, "Coated PCBN cutting insert, coated PCBN cutting tool using such coated PCBN cutting insert and method for making the same," United States Patent, 2010.
[132] R. M'Saoubi, M. P. Johansson and J. M. Andersson, *Wear mechanisms of PVD-coated PCBN cutting tools*, Wear, 2013. (302): 1219-1229.
[133] D. C. Montgomery, *Design and Analysis of Experiments*, Wiley, 2005. 6th Edition, New York: ISBN: 047148735X.
[134] P. J.Ross, *Taguchi techniques for quality engineering*, McGraw Hill, 1996. 2nd Edition, New York: ISBN: 0-07-053958-8.
[135] J. Pignatiello and J. Ramberg, *Top ten triumphs and tragedies of Genichi Taguchi*, Quality engineering, 1991-92. (4): 211-225.
[136] G. Taguchi, *Taguchi Quality Engineering*, Wiley, 2005, New Jersy: ISBN: 0471413348.
[137] J. Fox, *Applied Regression analysis, Linear Models, and Related Methods*, SAGE Publications, Inc., 1997, California: ISBN: 0-8039-4540-X.
[138] N. R. Draper and H. Smith, *Applied Regression Analysis*, John Wiley & Sons, 1981. 2nd Edition, New York: ISBN: 0-471-02995-5.
[139] J. Neter, M. H. Kutner, C. J. Nachtsheim and W. Wasserman, *Applied Linear Regression Models*, The McGraw-Hill Companies, Inc., 1996. 3rd Edition: ISBN: 0-256-08601-X.
[140] S. L. Soo, *Three dimensional finite element modelling when end milling Inconel 718*, PhD thesis, School of Mechanical Engineering, University of Birmingham, UK, 2003.
[141] *PCBN Metalworking, E6 Advanced Materials*, Shannon, Ireland.
[142] P. Harden, *Personal communication with Element Six (E6)*, 2010.
[143] S. Newton, *Personal communication with Rolls Royce*, 2011.
[144] B. Griffith, *Manufacturing Surface Technology-Surface Integrity and Functional Performance*, Penton Press, 2001, London
[145] A. R. C. Sharman, J. I. Hughes and K. Ridgway, *An analysis of the residual stresses generated in Inconel 718(TM) when turning*, Journal of Materials Processing Technology, 2006. (173): 359-367.
[146] M. Habak and J. L. Lebrun, *An experimental study of the effect of high-pressure water jet assisted turning (HPWJAT) on the surface integrity*, International Journal of Machine Tools and Manufacture, 2011. (51): 661-669.

[147] R. Arunachalam, M.A.Mannan and A.C.Spowage, *Comparison of surface roughness and residual stresses induced by coated carbide, ceramic and CBN cutting tools in high speed facing of Inconel 718*, Transaction of NAMRI, 2006: 87-94.

[148] M. C. Shaw, A. L. Thurman and H. J. Ahlgren, *A plasticity problem involving plane strain and plane stress simultaneously: Groove formation in the machining of high temeprature alloys* Transactions of the ASME, Journal of Engineering for Industry, 1966. (88): 142-146.

[149] V. Solaja, *Wear of carbide tools and surface finish generated in finish turning of steel*, Wear, 1958. (2): 40-58.

[150] C. T. Ansell and J. Taylor, *The surface finishing properties of a carbide and ceramic cutting tool*, Proceedings of the Third International Conference of Advances in Machine tool Design and Research, 1962: 225-243.

[151] M. J. Bermingham, S. Palanisamy, D. Kent and M. S. Dargusch, *A comparison of cryogenic and high pressure emulsion cooling technologies on tool life and chip morphology in Ti–6Al–4V cutting*, Journal of Materials Processing Technology, 2012. (212): 752-765.

[152] Z. Vagnorius and K. Sørby, *Effect of high-pressure cooling on life of SiAlON tools in machining of Inconel 718*, The International Journal of Advanced Manufacturing Technology, 2011. (54): 83-92.

[153] M. Dogra, V. S. Sharma and J. Dureja, *Effect of tool geometry variation on finish turning – A Review*, Journal of Engineering Science and Technology Review, 2011. (4): 1-13.

[154] H. A. Kishawy and M. A. Elbestawi, *Effects of process parameters on material side flow during hard turning*, International Journal of Machine Tools and Manufacture, 1999. (39): 1017-1030.

[155] W. Chen, *Cutting forces and surface finish when machining medium hardness steel using CBN tools*, International Journal of Machine Tools and Manufacture, 2000. (40): 455-466.

[156] G. Bartarya and S. K. Choudhury, *State of the art in hard turning*, International Journal of Machine Tools and Manufacture, 2012. (53): 1-14.

[157] J. I. Hughes, A. R. C. Sharman and K. Ridgway, *The effect of tool edge preparation on tool life and workpiece surface integrity*, Proceedings of Institutions of Mechanical Engineers; Part B: Journal of Engineering Manufacture, 2004. (218): 1113-1123.

[158] S. Olovsjö, A. Wretland and G. Sjöberg, *The effect of grain size and hardness of Waspaloy on the wear of cemented carbide tools*, The International Journal of Advanced Manufacturing Technology, 2010. (50): 907-915.

[159] S. Cedergren, S. Olovsjö, G. Sjöberg and L. Nyborg, *The effects of grain size and feed rate on notch wear and burr formation in wrought Alloy 718*, The International Journal of Advanced Manufacturing Technology, 2012. 1-7.

[160] S. Olovsjö and L. Nyborg, *Influence of microstructure on wear behaviour of uncoated WC tools in turning of Alloy 718 and Waspaloy*, Wear, 2012. (282–283): 12-21.

[161] G. Dong, H. Zhaopeng, H. Rongdi, C. Yanli and J. N. Muguthu, *Study of cutting deformation in machining nickel-based alloy Inconel 718*, International Journal of Machine Tools and Manufacture, 2011. (51): 520-527.

[162] K. D. Bouzakis, G. Skordaris, S. Gerardis, G. Katirtzoglou, S. Makrimallakis, M. Pappa, E. LilI and R. M'Saoubi, *Ambient and elevated temperature properties of TiN, TiAlN and TiSiN PVD films and their impact on the cutting performance of coated carbide tools*, Surface and Coatings Technology, 2009. (204): 1061-1065.

[163] L. Chen, Y. Du, P. H. Mayrhofer, S. Q. Wang and J. Li, *The influence of age-hardening on turning and milling performance of Ti–Al–N coated inserts*, Surface and Coatings Technology, 2008. (202): 5158-5161.
[164] L. Chen, S. Q. Wang, Y. Du, S. Z. Zhou, T. Gang, J. C. Fen, K. K. Chang, Y. W. Li and X. Xiong, *Machining performance of Ti–Al–Si–N coated inserts*, Surface and Coatings Technology, 2010. (205): 582-586.

APPENDIX A

Collaborators contact details

The project was conducted in collaboration with Rolls Royce, Element Six Ltd., Seco Tools, University of Birmingham and University of Engineering and Technology Lahore, Pakistan. The contact persons for the respective industrial collaborators are included in Table A1.

Table A1: Industrial collaborators' contacts

Company	**Contact details**
Rolls-Royce	Colin Sage Turbines Rolls-Royce plc. Bristol UK. Dr. Gregor Kappmeyer Global Machining Process Owner Rolls-Royce Deutschland Ltd & Co KG Hohemarkstrasse 60-70 D-61440 Oberursel, Germany.
Element Six Ltd.	Dr. Wayne Leahy Element Six Ltd., Global Innovation Centre, Fermi Avenue, Harwell Oxford, OX11 0QR.
Seco Tools	Dr. Rachid M'Saoubi Senior Research Scientist Grades and Cutting Metallurgy Seco Tools AB, SE-737 82 Fagersta, Sweden. David Pearson Business Development Manager - Aerospace Seco Tools (UK) Ltd. Springfield Business Park, Alcester, Warks, B49 6PU. Michael Fleming Technical and Marketing Manager Seco Tools (UK) Ltd. Springfield Business Park, Alcester, Warks, B49 6PU.

APPENDIX B

Optical micrographs of tool wear progression/SEM micrographs of worn inserts and interaction lots for tool life, surface roughness and cutting force of Phase 1C

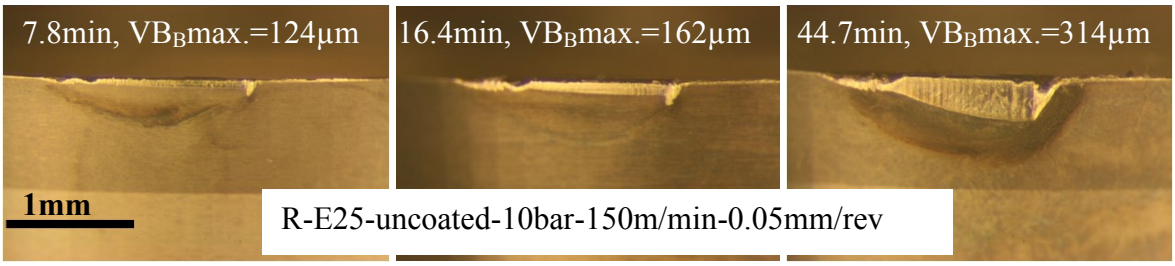

Figure B1: Wear progression of Test 4

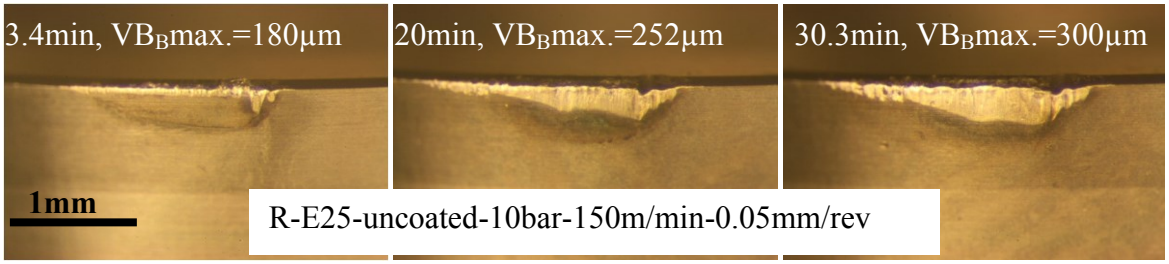

Figure B2: Wear progression of Test 13

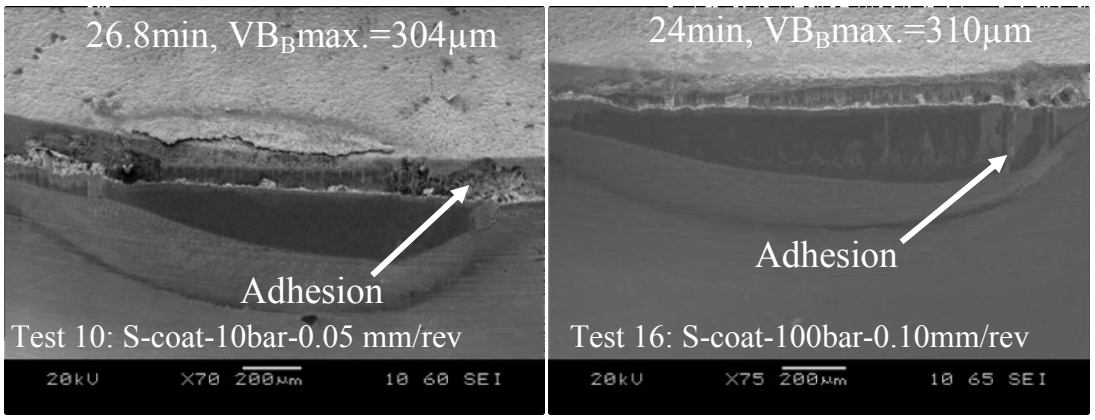

Figure B3: SEM wear scar micrographs of Tests 10 and 16 at the end of tool life at 150m/min

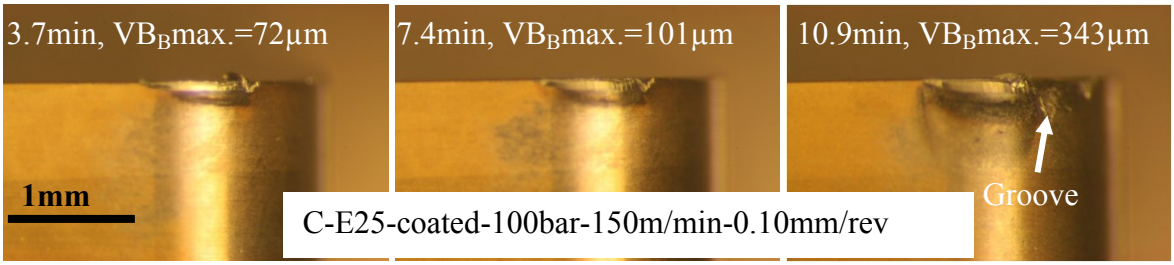

Figure B4: Wear progression of Test 19

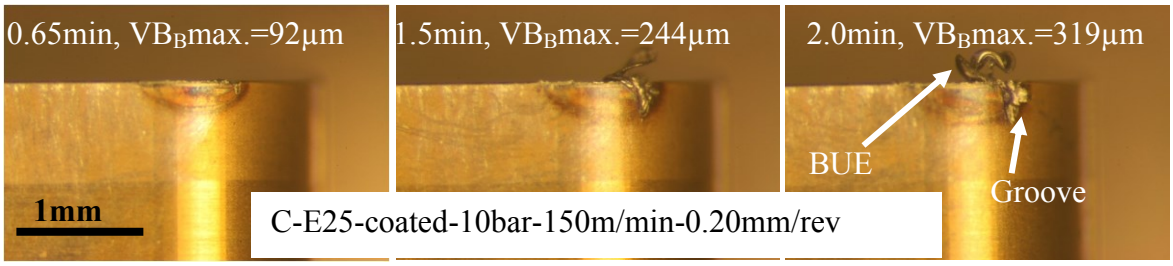

Figure B5: Wear progression of Test 25

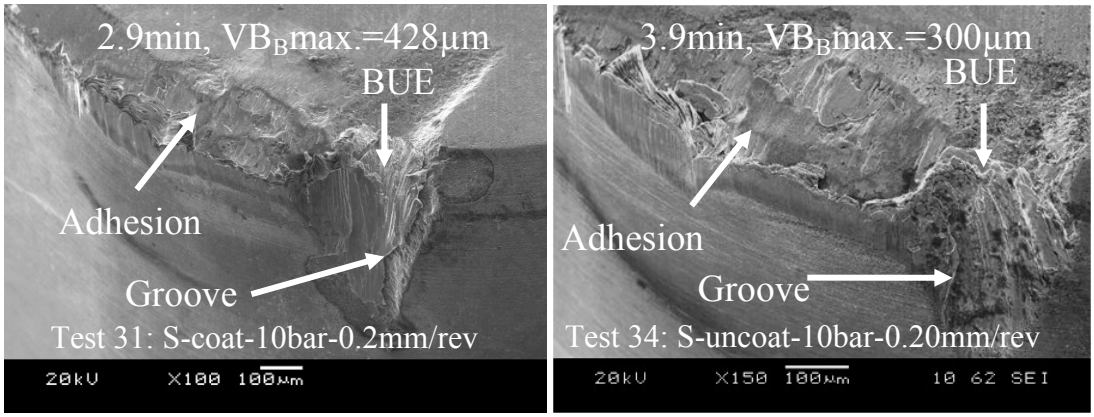

Figure B6: SEM wear scar micrographs of Tests 31 and 34 at the end of tool life at 150m/min

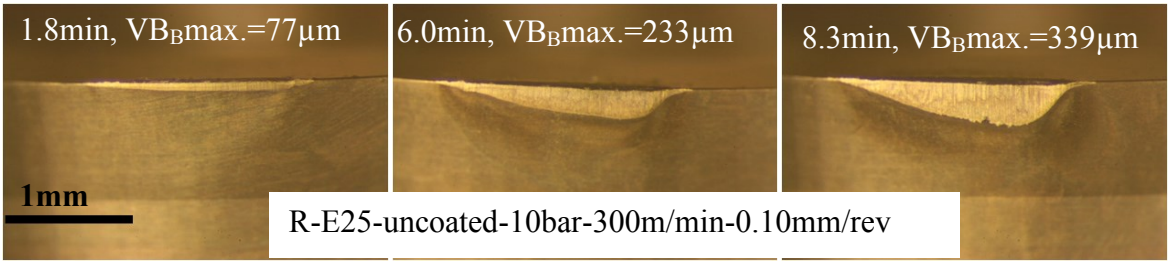

Figure B7: Wear progression of Test 2

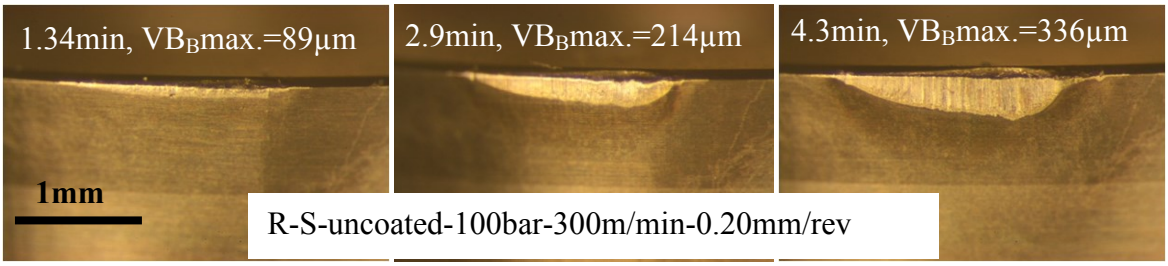

Figure B8: Wear progression of Test 14

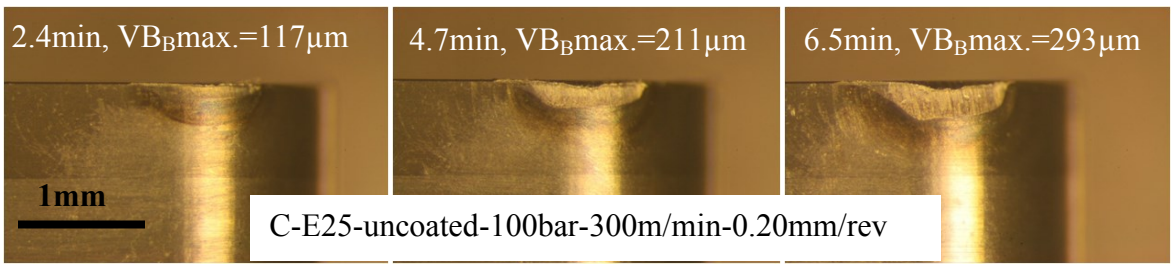

Figure B9: Wear progression of Test 23

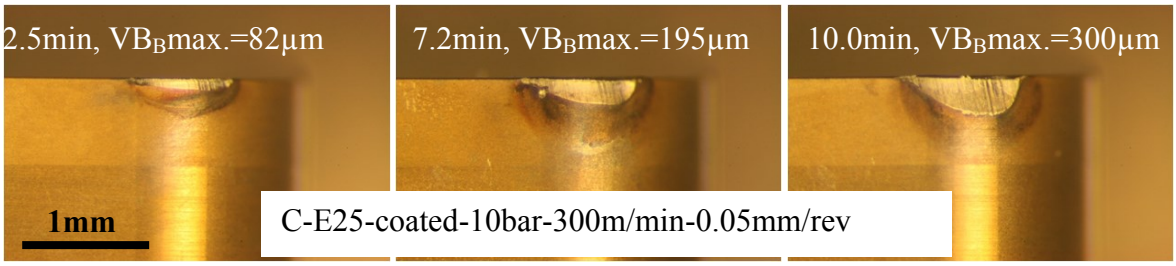

Figure B10: Wear progression of Test 26

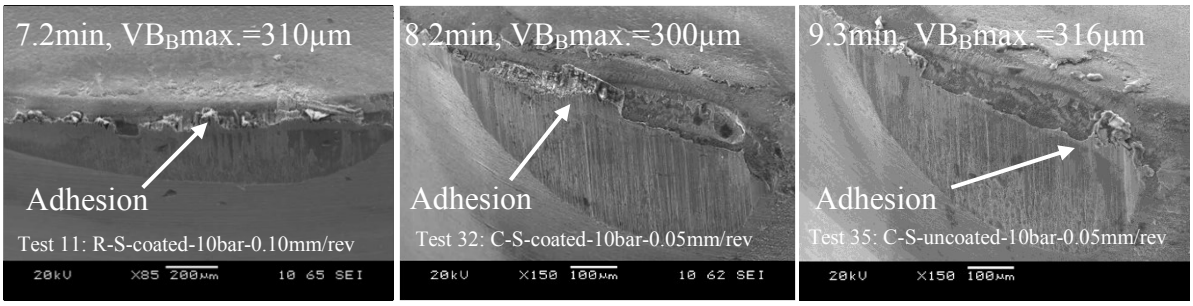

Figure B11: SEM micrographs at the end of tool life of Tests 11, 32 and 35 at 300m/min

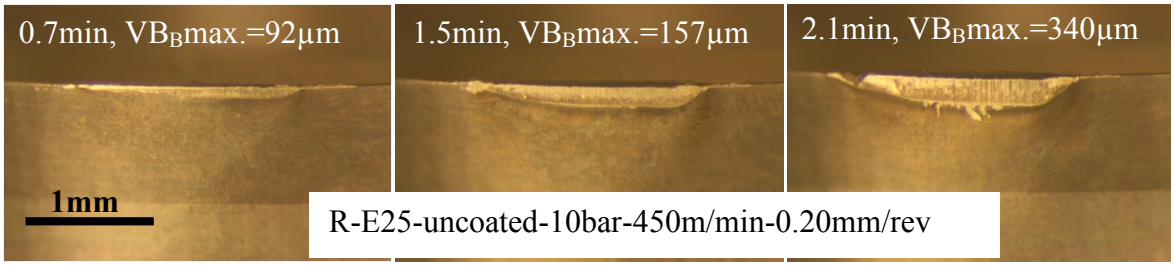

Figure B12: Wear progression of Test 3

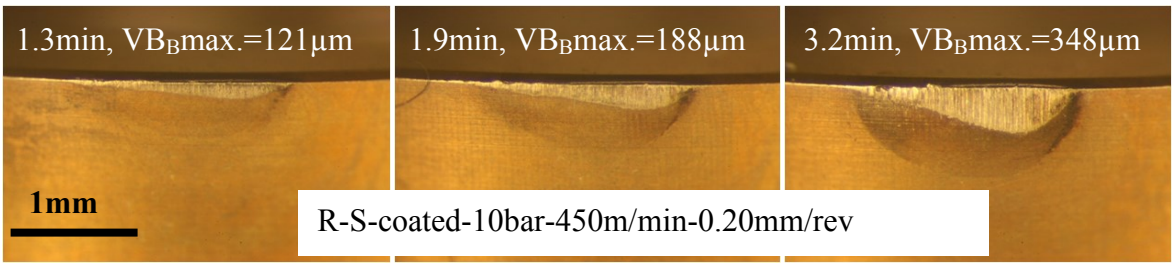

Figure B13: Wear progression of Test 18

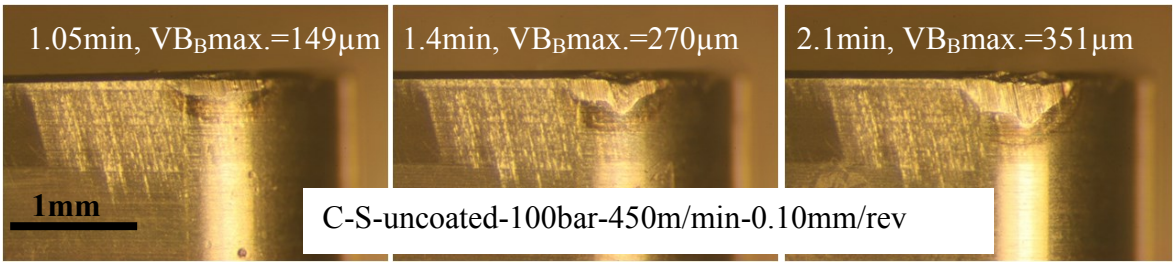

Figure B14: Wear progression of Test 30

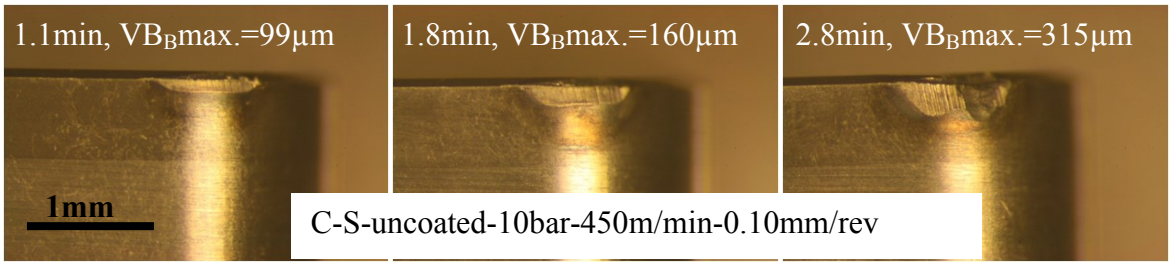

Figure B15: Wear progression of Test 36

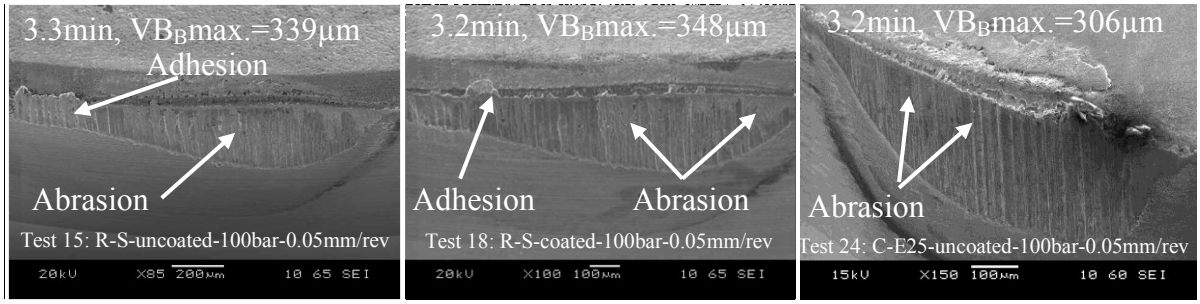

Figure B16: SEM micrographs of Tests 15, 18 and 24 at the end of tool life at 450m/min

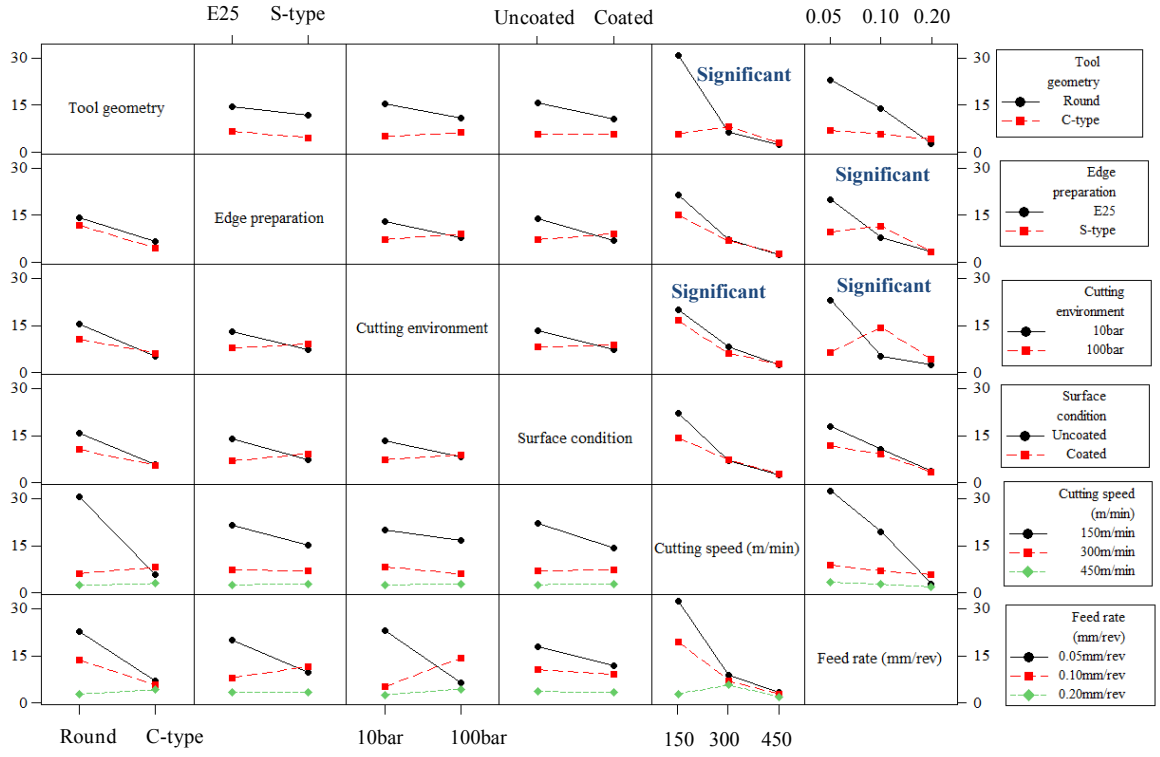

Figure B17: Interaction plots for tool life

Regression equation for tool life based on stepwise backward elimination (SBE) procedure

Tool life= 9.34 - 3.74 A - 7.54 LE + 5.64 ALE + 1.72 AQE + 1.13 AQF + 2.32 DLE + 1.19 AC - 2.01 LF + 1.13 CQF + 1.28 AD + 1.49 DLF - 0.895 D B (1)

Regression equations for tool life based on stepwise forward entry (SFE) procedure

Tool life = 9.34 - 3.74 A - 1.13 B - 0.908 C - 1.29 D - 7.82 LE - 2.01 LF - 1.11 QE + 0.469 QF + 5.12 ALE + 2.24 AQE B (2)

Tool life = 9.34 - 3.74 A - 1.13 B - 0.908 C - 1.29 D - 8.23 LE - 5.69 LF - 0.581 QE + 0.204 QF + 0.37 BLF + 1.98 BQF B (3)

Tool life = 9.34 - 3.74 A - 1.13 B - 0.908 C - 1.29 D - 7.82 LE - 7.15 LF - 1.11 QE + 0.543 QF - 0.44 CLE + 1.80 CQE B (4)

Tool life = 9.34 - 3.74 A - 1.13 B - 0.908 C - 1.29 D - 6.11 LE - 5.69 LF- 2.09 QE + 0.204 QF + 4.67 CLF + 0.728 CQF B (5)

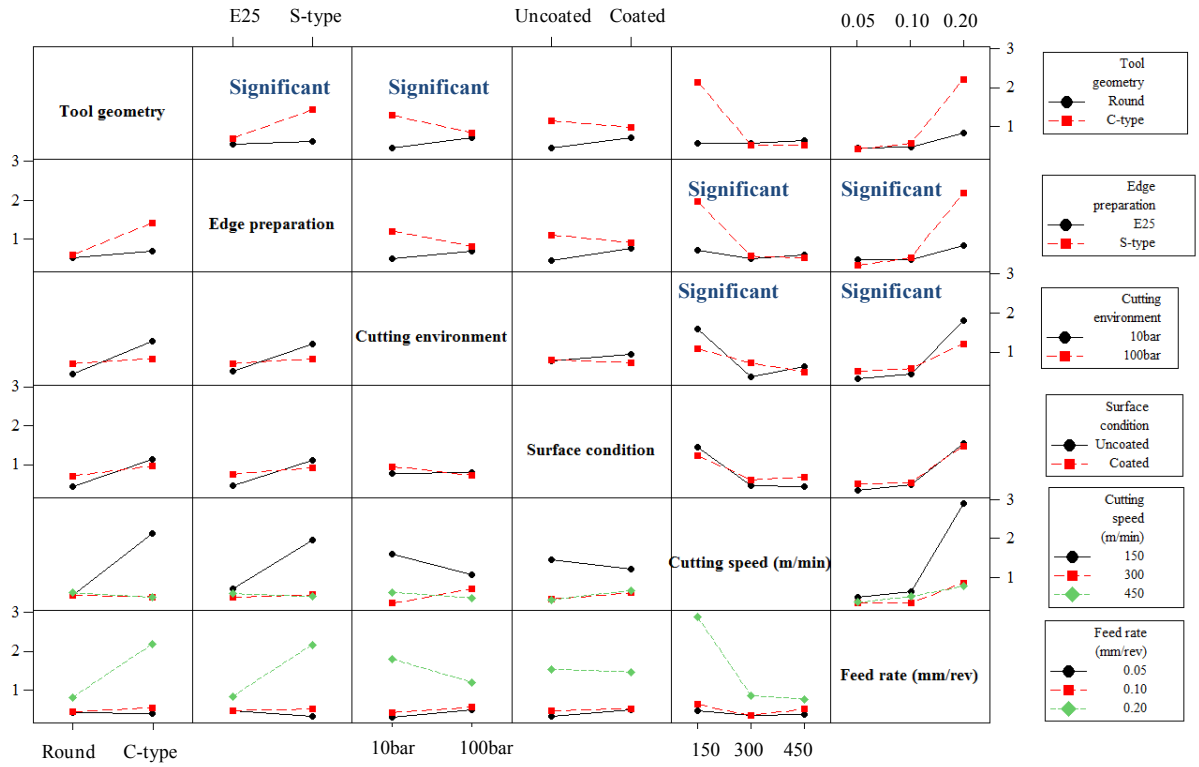

Figure B18: Interaction plots for surface roughness

Regression equation for surface roughness based on stepwise backward elimination (SBE) procedure

Surface roughness = 0.807 + 0.241 A + 0.172 B + 0.0162 C + 0.0580 D - 0.423 LE + 0.582 LF - 0.104 QE - 0.142 QF + 0.189 AB - 0.0981 AC - 0.149 BLE + 0.245 BLF - 0.0727 BQE - 0.0830 BQF + 0.131 CLE - 0.222 CLF - 0.0659 CQE - 0.0739 CQF B (6)

Regression equations for surface roughness based on stepwise forward entry (SFE) procedure

Surface roughness = 0.807 + 0.241 A + 0.205 B + 0.0209 C + 0.0953 D - 0.394 LE + 0.555 LF - 0.140 QE - 0.153 QF + 0.203 AB B (7)

Surface roughness = 0.807 + 0.241 A + 0.163 B - 0.0469 C - 0.0142 D - 0.394 LE + 0.555 LF - 0.140 QE - 0.153 QF - 0.125 AC B (8)

Surface roughness = 0.807 + 0.241 A + 0.205 B - 0.0469 C + 0.0275 D - 0.394 LE

+ 0.492 LF - 0.140 QE - 0.160 QF - 0.167 BLE - 0.0846 BQE B (9)

Surface roughness = 0.807 + 0.241 A + 0.205 B - 0.0469 C + 0.0275 D - 0.302 LE
+ 0.555 LF - 0.144 QE - 0.153 QF + 0.265 BLF - 0.103 BQF B (10)

Surface roughness = 0.807 + 0.241 A + 0.205 B - 0.0469 C + 0.0275 D - 0.394 LE B (11)
+ 0.656 LF - 0.140 QE - 0.134 QF + 0.155 CLE - 0.0825 CQE

Surface roughness = 0.807 + 0.241 A + 0.205 B - 0.0469 C + 0.0275 D - 0.532 LE B (12)
+ 0.555 LF - 0.103 QE - 0.153 QF - 0.249 CLF - 0.101 CQF B (13)

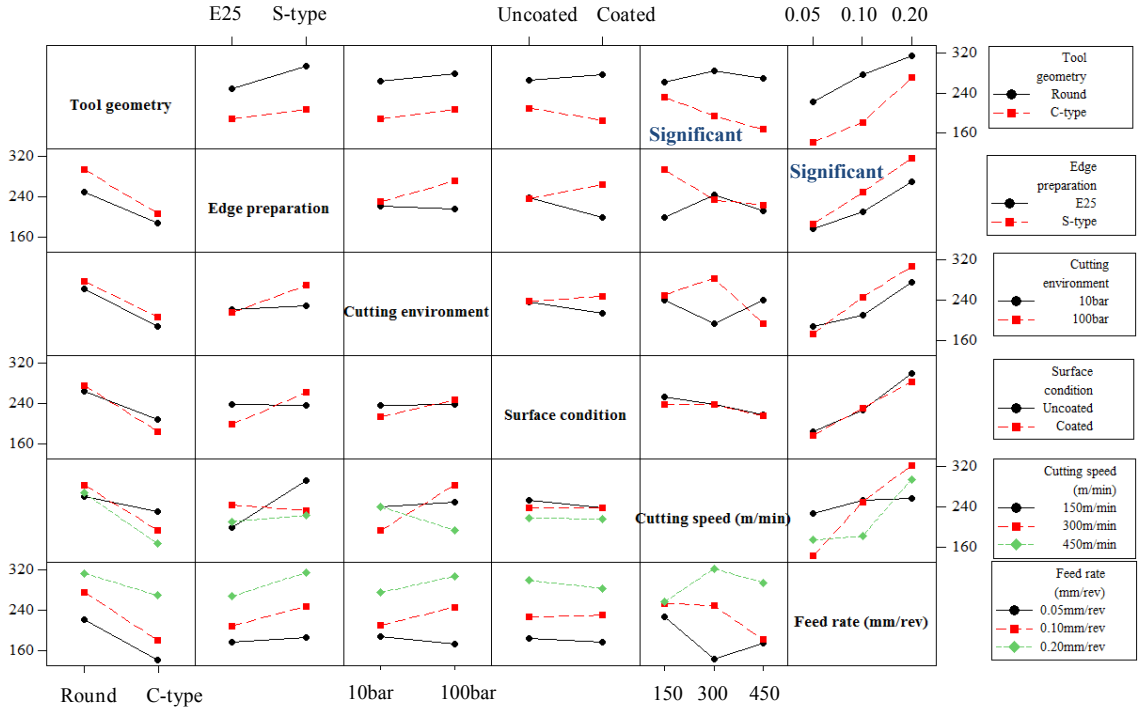

Figure B19: Interaction plots for cutting force

Regression equation for cutting force based on stepwise backward elimination (SBE) procedure

Cutting force = 234 - 34.1 A + 15.9 B + 12.1 C - 3.29 D - 14.5 LE + 67.4 LF + 2.40
QE- 2.58 QF + 17.2 ALE + 5.92 AQE + 9.33 BD B (14)

Regression equations for surface cutting force based on stepwise forward entry (SFE) procedure

Cutting force= 234 - 37.2 A + 15.9 B + 9.01 C - 3.29 D - 14.5 LE + 67.4 LF + 2.40
QE- 2.58 QF + 17.2 ALE + 5.92 AQE B (15)

Cutting force= 234 - 34.1 A + 15.9 B + 12.1 C - 3.29 D - 14.5 LE + 55.9 LF + 2.40
QE- 2.68 QF + 9.33 BD B (16)

APPENDIX C

ANOVA tables for surface roughness/cutting forces and SEM micrographs of workpiece surfaces following machining with new and worn inserts

Table C1: ANOVA table for surface roughness with new tools

Factors	DF	SS	MSS	F	P	PCR (%)
Edge preparation (A)	1	0.121	0.0121	0.11	0.795	0
Cutting speed (B)	1	0.0036	0.0036	0.03	0.886	0
Error	1	0.1089	0.1089			***100***
Total	3	0.1246	R-Sq(Adj)=0.00			

Table C2: ANOVA table for surface roughness with worn tools

Factors	DF	SS	MSS	F	P	PCR (%)
Edge preparation (A)	1	0.0182	0.0182	0.06	0.853	0
Cutting speed (B)	1	0.0930	0.0930	0.28	0.690	0
Error	1	0.3306	0.3306			***100***
Total	3	0.4419	R-Sq(Adj)=0.00			

Table C3: ANOVA table for cutting force with new tools

Factors	DF	SS	MSS	F	P	PCR (%)
Edge preparation (A)	1	213.16	213.16	108.76	0.061	27.69
Cutting speed (B)	1	547.56	547.56	279.37	0.038*	71.53
Error	1	1.96	1.96			***0.78***
Total	3	762.68	R-Sq(Adj)=99.10			

Table C4: ANOVA table for cutting force with worn tools

Factors	DF	SS	MSS	F	P	PCR (%)
Edge preparation (A)	1	112.36	112.36	2.50	0.359	29.60
Cutting speed (B)	1	70.56	70.56	1.57	0.429	11.20
Error	1	44.89	44.89			***59.20***
Total	3	227.81	R-Sq(Adj)=40.80			

Table C5: ANOVA table for thrust force with new tools

Factors	DF	SS	MSS	F	P	PCR (%)
Edge preparation (A)	1	222.00	222.0	0.25	0.704	0
Cutting speed (B)	1	404.00	404.0	0.46	0.621	0
Error	1	882.10	882.10			***100***
Total	3	1508.10	R-Sq(Adj)=0			

Table C6: ANOVA table for thrust force with worn tools

Factors	DF	SS	MSS	F	P	PCR (%)
Edge preparation (A)	1	7336	7336	3.55	0.311	32.16
Cutting speed (B)	1	6981	6981	3.38	0.317	30
Error	1	2066	2066			***37.84***
Total	3	16382	R-Sq(Adj)=62.16			

Table C7: ANOVA table for feed force with new tools

Factors	DF	SS	MSS	F	P	PCR (%)
Edge preparation (A)	1	10.24	10.24	20.90	0.137	2.67
Cutting speed (B)	1	353.44	353.44	721.31	0.024*	96.9
Error	1	0.49	0.49			***0.43***
Total	3	364.17	R-Sq(Adj)=99.57			

TableC8: ANOVA table for feed force with worn tools

Factors	DF	SS	MSS	F	P	PCR (%)
Edge preparation (A)	1	5	5	0.00	0.961	0
Cutting speed (B)	1	541	541	0.41	0.637	0
Error	1	1314	1314			***100***
Total	3	1860	R-Sq(Adj)=100			

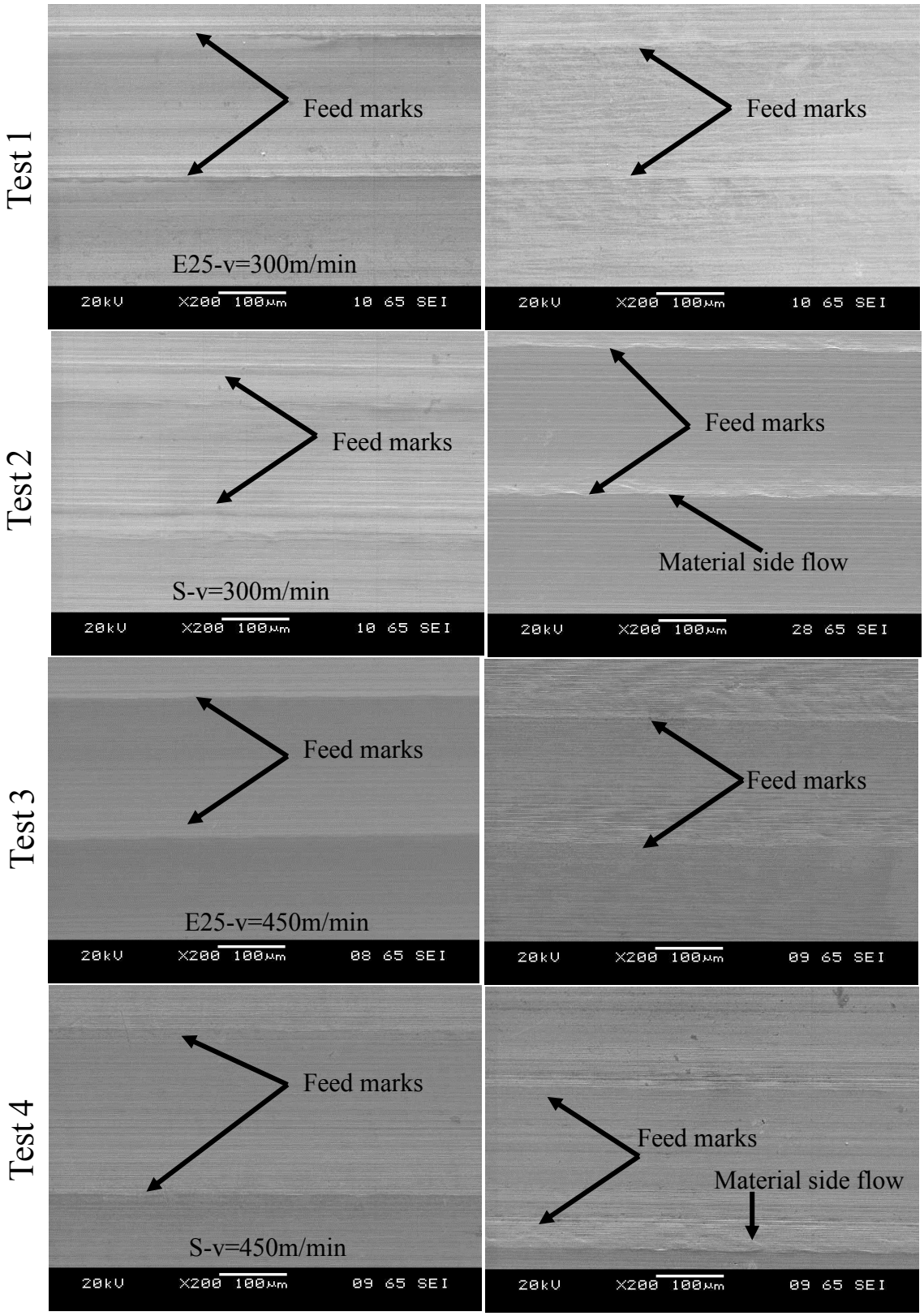

a) New b) Worn

Figure C1: Workpiece surfaces following machining with (a) new and (b) worn inserts

APPENDIX D

Tool life and material removed in each test, SEM micrographs of worn inserts

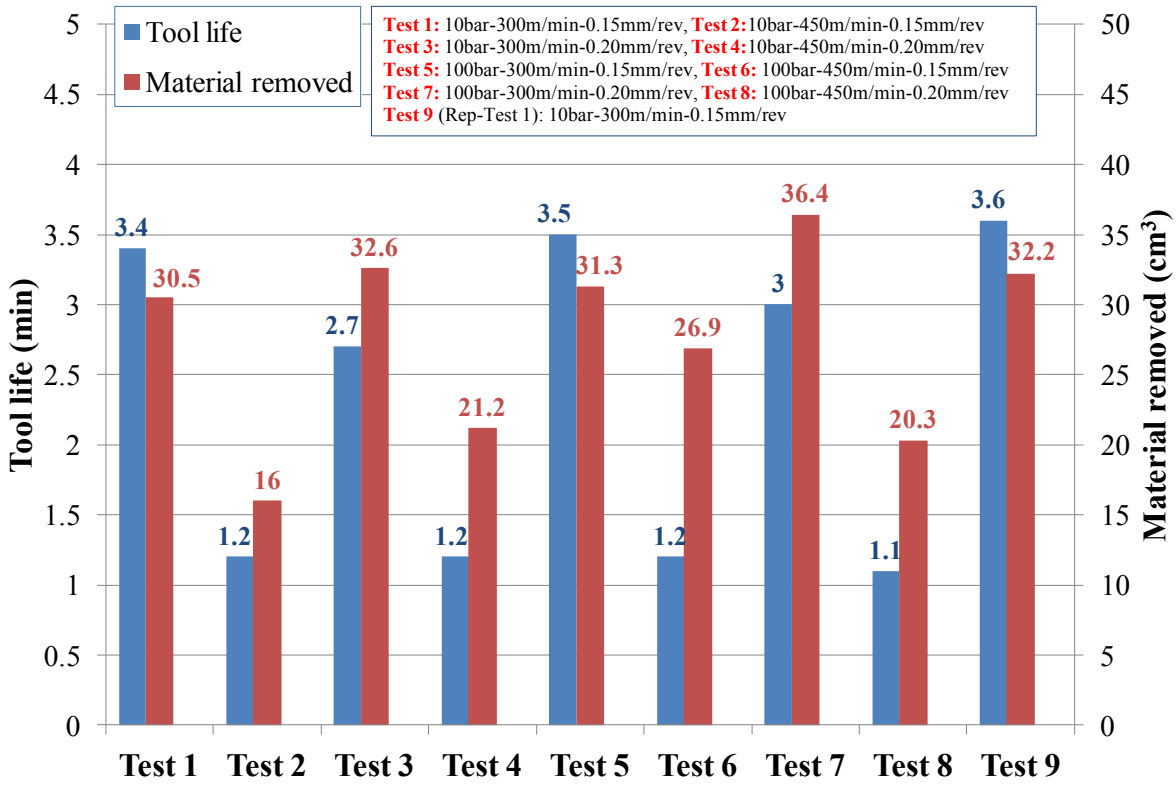

Figure D1: Tool life and material removed at each test

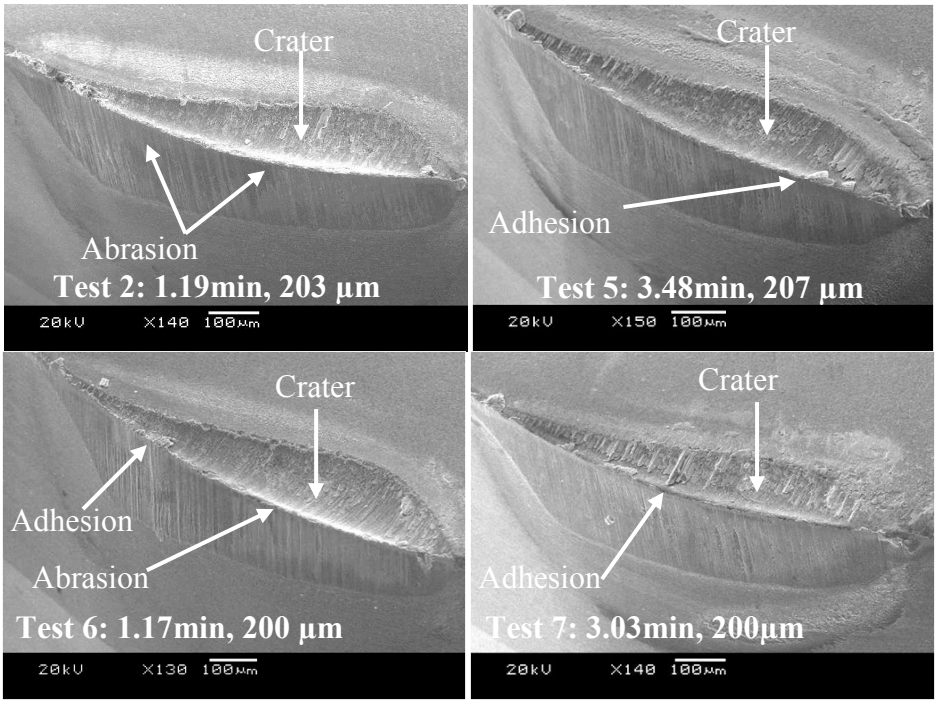

Figure D2: SEM images of Tests 2, 5, 6 and 7 at the end of tool life

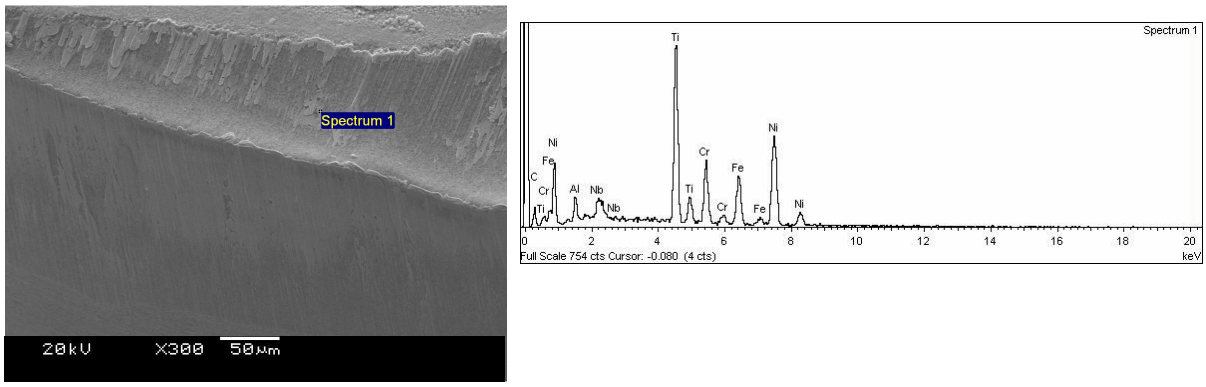

Figure D3: EDX analysis of Test 1 along with spectrum

Table D1: Element analysis of Test 1 with weight and atomic percentage

Elements	Wt.(%)	Atomic (%)
Ni	36.83	25.57
Nb	2.67	1.17
Fe	12.46	9.09
Cr	11.47	8.99
Ti	24.63	20.96
Al	3.34	5.05
C	8.59	29.16

Table D2: Comparison of cutting force components for replication of Tests 2 and 6

	Test 2	Replication of Test 2	Test 6	Replication of Test 6
Cutting force	265.14	269.90	311.52	313.53
Thrust force	290.77	296.6	347.9	352.60
Feed force	65.43	69.43	78.16	81.60

APPENDIX E

SEM micrographs of worn inserts and Interaction plots of tool life from Phase 3A

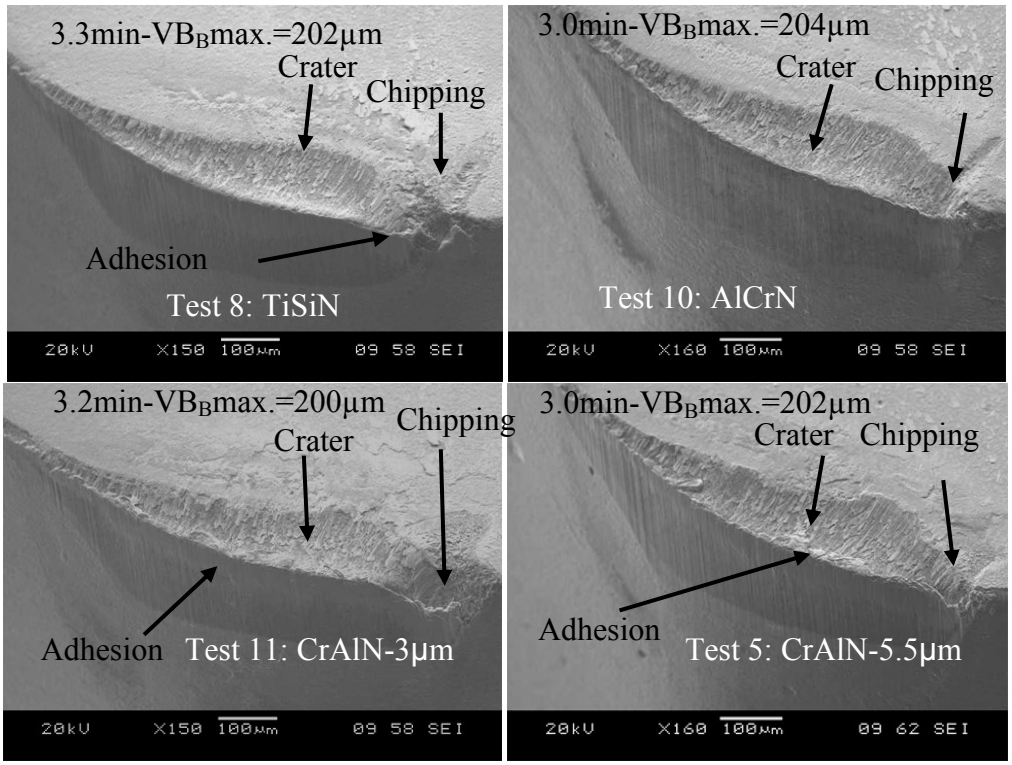

Figure E1: SEM micrographs of TiSiN, AlCrN, CrAlN-3µm and CrAlN5.5µm coated inserts at the end of tool life at cutting speed of 300m/min

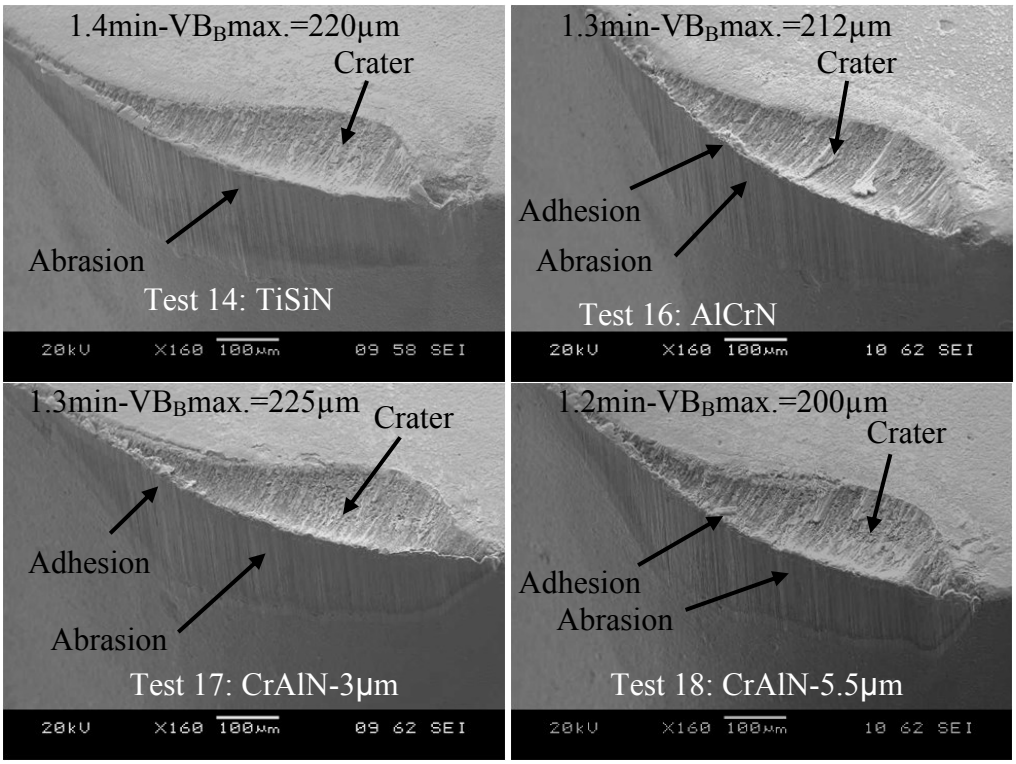

Figure E2: SEM micrographs of TiSiN, AlCrN, CrAlN-3µm and CrAlN5.5µm coated inserts at the end of tool life at cutting speed of 450m/min

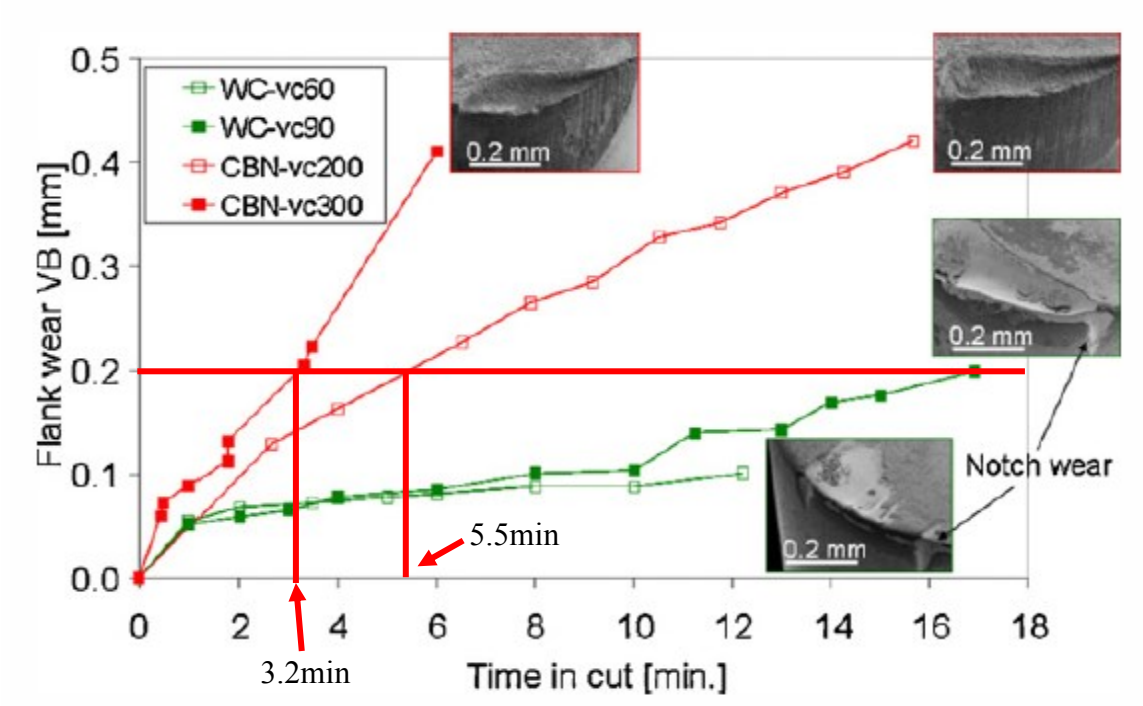

Figure E3: Flank wear against machining time, results from M'Saoubi et al. [126]

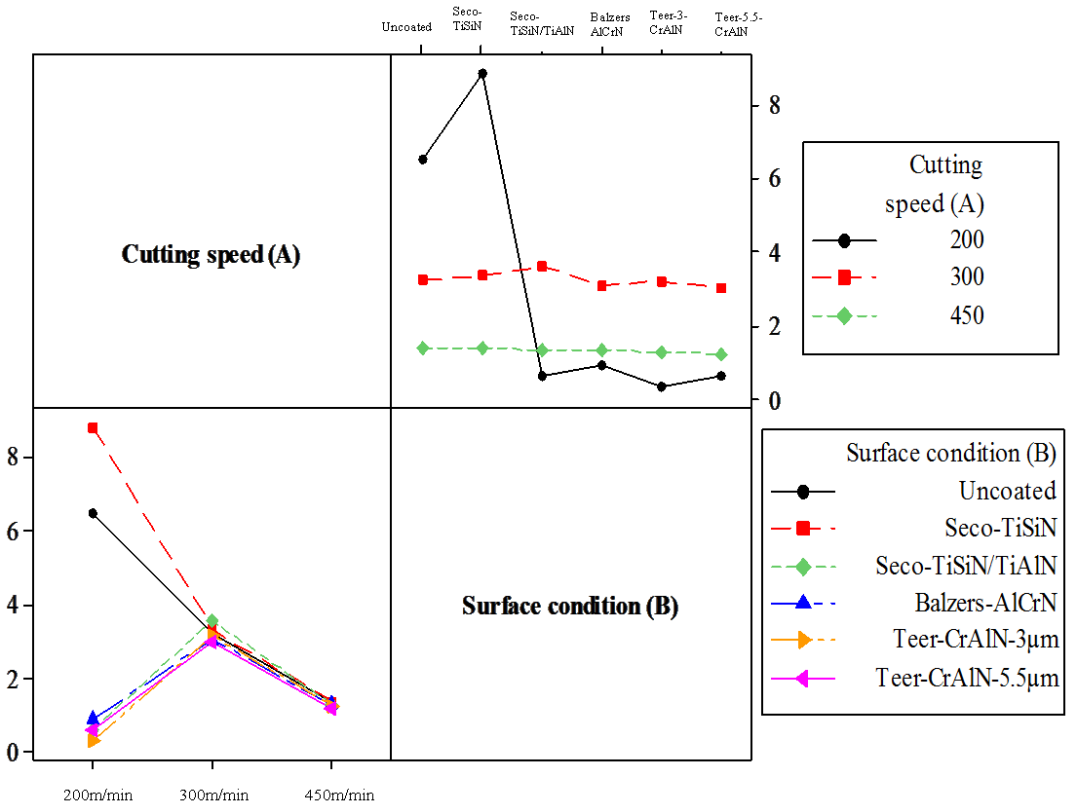

Figure E4: Interaction plots for tool life

APPENDIX F

List of publications

Paper published

S.A. Khan, S.L. Soo, D.K. Aspinwall, C. Sage, P. Harden, M. Fleming, A. White and R. M'Saoubi, Tool wear/life evaluation when finish turning Inconel 718 using PCBN tooling, Fifth CIRP Conference on High Performance Cutting, 2012, Zurich, Switzerland, 4-7th June 2012, pp. 283-288.

Papers under preparation

S.A. Khan, S.L. Soo, D.K. Aspinwall, C. Sage and R. M' Saoubi, An investigation of tool life, cutting forces and surface roughness when turning Inconel 718 with PCBN tools using statistically based experimental design
To be submitted to International Journal of Machine tools and Manufacture
S.A. Khan, S.L. Soo, D.K. Aspinwall, C. Sage and R. M' Saoubi, Effect of edge geometry, cutting speed and tool condition on workpiece integrity when turning Inconel 718 using PCBN tools
To be submitted to The International Journal of Advanced Manufacturing Technology
S.A. Khan, S.L. Soo, D.K. Aspinwall, C. Sage and R. M' Saoubi, Assessment of cutting environment and operating parameters on tool wear/life and workpiece surface integrity in high speed turning of Inconel 718 using PCBN tooling
To be submitted to Journal of Materials Processing and Technology
S.A. Khan, S.L. Soo, D.K. Aspinwall, C. Sage and R. M' Saoub, Performance evaluation of coated PCBN inserts in high speed turning of Inconel 718
To be submitted to The International Journal of Advanced Manufacturing Technology

S.A. Khan, S.L. Soo, D.K. Aspinwall, Machinability of nickel based superalloys using PCBN, a review
To be submitted to Journal of Materials Processing and Technology